UNIVERSITY OF SOUTHAMPTON
FACULTY OF PHYSICAL AND APPLIED SCIENCES
ELECTRONICS AND COMPUTER SCIENCE

Energy-Efficient Cooperative Single-Carrier Frequency-Division Multiple-Access

by

Jiayi Zhang
BEng, MSc

A thesis submitted for the degree of Doctor of Philosophy
at the University of Southampton

May 2012

Supervisor: *Professor Lajos Hanzo*
Dipl Ing, MSc, PhD, DSc, FIET, FIEEE, FREng
Chair in Telecommunications, Head of Group

Supervisor: *Professor Lie-Liang Yang*
BEng, MEng, PhD, FIET, SMIEEE
Chair in Wireless communications
Communications, Signal Processing and Control Group
Electronics and Computer Science
University of Southampton
Southampton, SO17 1BJ
United Kingdom

Dedicated to my family.

UNIVERSITY OF SOUTHAMPTON

ABSTRACT

FACULTY OF PHYSICAL AND APPLIED SCIENCES
Electronics and Computer Science

Doctor of Philosophy

ENERGY-EFFICIENT COOPERATIVE SINGLE-CARRIER FREQUENCY-DIVISION MULTIPLE-ACCESS

by Jiayi Zhang

A variety of cooperative relaying schemes are designed for the *single-carrier frequency-division multiple-access* (SC-FDMA) uplink, when communicating over broadband wireless channels. Our goal is to reduce the battery power dissipated both by transmission and signal processing, so that the overall energy-efficiency may be increased. We assume that there are a number of inactive mobile terminals acting as potential relays, which have either fixed or time-variant positions in a cell. Our investigations are focused on the optimum exploitation of all the resources, when considering relay selection, power allocation and channel-quality-aided adaptive subband allocation. We exploit the benefits of combining the path-loss reduction and diversity gains arising from both fixed and opportunistic relaying, user cooperation and from all the propagation paths, as well as from multiple antennas. Novel frequency-domain equalisation and diversity combining approaches are also conceived.

Specifically, we firstly conceive two single-relay assisted topologies for the sake of exploiting the achievable cooperative diversity, namely the *single-dedicated-relaying* (SDR), where each relay is dedicated to a single user, and the *single-shared-relaying* (SSR), when a single relay assists multiple users. In order to eliminate both the multi-user interference and for the sake of mitigating the noise-amplification imposed by *amplify-and-forward* (AF) relaying, we propose an efficient subband-based AF scheme, which is benchmarked against the conventional AF regime in the context of both the SDR and SSR topologies. Furthermore, by assuming that the *channel state information* (CSI) is available at the *base station* (BS)'s receiver, a joint frequency-domain equalisation and diversity-combining scheme is proposed for the sake of increasing the achievable cooperative diversity gain. In this case, when considering the different number of available relays that are geographically dispersed across a large-scale environment subject to both path-loss and shadowing, we propose three different dynamic relay selection schemes, namely *single-user relay selection* (SU-RS), *multi-user relay selection* (MU-RS), and *multiple-access relay selection* (MA-RS), combined with source/relay

power allocation in the context of *opportunistic cooperation* (OC) for the sake of increasing the multi-user system's throughput. By contrast, when the *source-to-destination* (S-D) direct links are of low quality and hence are deemed to be unavailable, we exploit the relays which are roaming within each other's vicinity in geographically localised manner in a cluster. Therefore, by assuming that these cooperating relays are capable of exchanging their *channel quality information* (CQI), we propose two *first-hop-quality-aware* (FHQA) joint *dynamic resource allocation* (DRA) schemes for *opportunistic relaying* (OR) based SC-FDMA uplink, which beneficially combines channel-quality-aware subband allocation with efficient relay selection. The FHQA joint DRA schemes optimise the multi-user multi-relay networks relying on whether it is the *source-to-relay* (S-R) or the *relay-to-destination* (R-D) link, which dominates the attainable performance, when the BS's receiver employs either single or multiple antennas. Additionally, the benefits of OR are quantified in the context of interleaver-aided *decode-and-forward* (DF) relaying for transmission over correlated fading channels. Therefore, the length of the interleavers combined with channel coding may be shortened. As a result, we benefit from a reduced interleaving delay and/or from a total transmit power reduction.

In comparison to the benchmark schemes considered in the literature, the reliability and energy-efficiency of our proposed systems are significantly improved.

Declaration of Authorship

I, **Jiayi Zhang**, declare that the thesis entitled

Energy-Efficient Cooperative Single-Carrier Frequency-Division Multiple-Access

and the work presented in it are my own and has been generated by me as the result of my own original research. I confirm that:

1. This work was done wholly or mainly while in candidature for a research degree at this University;
2. Where any part of this thesis has previously been submitted for a degree or any other qualification at this University or any other institution, this has been clearly stated;
3. Where I have consulted the published work of others, this is always clearly attributed;
4. Where I have quoted from the work of others, the source is always given. With the exception of such quotations, this thesis is entirely my own work;
5. I have acknowledged all main sources of help;
6. Where the thesis is based on work done by myself jointly with others, I have made clear exactly what was done by others and what I have contributed myself;
7. Parts of this work have been published, as seen in the list of publications.

Signed:

Date:

Acknowledgements

There are many people I would like to acknowledge for making my experience in the University of Southampton one of the most important and rewarding periods of my life.

First of all, I would like to express my heartfelt gratitude to my first supervisor Professor Lajos Hanzo for his outstanding supervision. It would simply not have been possible to produce this thesis without his extremely generous and friendly support throughout my PhD career. His guidance, inspiration and encouragement have greatly benefited me; especially his generous investment of time and energy deserve my utmost acknowledgement. Most importantly, I would like to thank him for his invaluable friendship.

Meanwhile, I especially appreciate my second supervisor Professor Lie-Liang Yang for his friendly support and engaging in intensive and inspiring discussions throughout my research. I deeply grateful to him for nurturing me with great patience and enthusiasm on the long path to fruition. I also wish sincerely to thank him for his encouragement and for his kindness to cultivate me not only in research but also in life.

Furthermore, I am also greatly beholden to other colleagues within our Communications Lab. Many thanks to Professor Sheng Chen, Dr. Soon Xin Ng, Dr. Robert Maunder, Dr. Nan Wu, Dr. Wei Liu, Dr. Wei Fang, Dr. Mohammed El-Hajjar, Dr. Rong Zhang, Dr. Lingkun Kong, Dr. Li Wang, Dr. Du Yang, Dr. Dongxiao Wu, Dr. Tingting Liu, Dr. Peng Pan, Dr. Wang Yao, Dr. Hong Chen, Chen Dong, Shaoshi Yang, Jiankang Zhang, Jing Zuo and Kent Cheung, etc., for their discussions during my research, all of their warm and sincere help will not be forgotten. I am also deeply indebted to my friends both in and outside Southampton, too many to mention. Their sincere friendship makes my life in the UK become rich and colourful.

Additionally, financial support from the *Virtual Centre of Excellence in Mobile and Personal Communications, Ltd.* (Mobile VCE), including that of *Engineering and Physical Sciences Research Council, United Kingdom* (EPSRC, UK) is gratefully acknowledged.

Finally, I want to express my immense and never-ending gratefulness to my admirable parents Min Zhang and Hong Zhang as well as my grandparents for their endless love and unconditional support. Special thanks also to my relatives in China for their care and love to me.

List of Publications

Journal Papers:

1. **Jiayi Zhang**, Lie-Liang Yang and Lajos Hanzo, "Energy-Efficient Dynamic Resource Allocation for Opportunistic Relaying Assisted SC-FDMA Using Turbo Equaliser Aided Soft Decode-and-Forward", submitted to *IEEE Transactions on Vehicular Technology*.

2. Mohammad Kadir, Shinya Sugiura, **Jiayi Zhang**, Sheng Chen and Lajos Hanzo, "OFDMA/SC-FDMA Aided Space-Time Shift Keying for Dispersive Multi-User Scenarios", submitted to *IEEE Transactions on Vehicular Technology*.

3. C. Han, T. Harrold, I. Krikidis, I. Ku, T. A. Le, S. Videv, **Jiayi Zhang**, S. Armour, P. M. Grant, H. Haas, Lajos Hanzo, M. R. Nakhai, J. S. Thompson and C. X. Wang, "Green Radio: Radio Techniques to Enable Energy Efficient Wireless Networks", in *IEEE Communications Magazine Special Issue: Green Communications*, vol. 49, no. 6, pp. 46-54, Jun. 2011.

4. **Jiayi Zhang**, Lie-Liang Yang and Lajos Hanzo, "Energy-Efficient Channel-Dependent Cooperative Relaying for the Multiuser SC-FDMA Uplink", in *IEEE Transactions on Vehicular Technology*, vol. 60, no. 3, pp. 992-1004, Mar. 2011.

Conference Papers:

1. **Jiayi Zhang**, Lie-Liang Yang and Lajos Hanzo, "Frequency-Domain Turbo Equalisation in Coded SC-FDMA Systems: EXIT Chart Analysis and Performance", accepted by *Proceedings of 2012 IEEE 76th Vehicular Technology Conference (VTC 2012-Fall)*, 3-6 September, 2012, Québec City, Canada.

2. **Jiayi Zhang**, Lie-Liang Yang and Lajos Hanzo, "First-Hop-Quality-Aware Dynamic Resource Allocation for Amplify-and-Forward Opportunistic Relaying Assisted SC-FDMA", accepted by *Proceedings of 2012 IEEE Interference Conference on Communications (ICC 2012)*, 10-15 June 2012, Ottawa, Canada.

3. **Jiayi Zhang**, Lie-Liang Yang and Lajos Hanzo, "Power-Efficient Opportunistic Amplify-and-Forward Single-Relay Aided Multi-User SC-FDMA Uplink", in *Proceedings of 2010 IEEE 71st Vehicular Technology Conference (VTC 2010-Spring)*, 16-19 May 2010, Taipei, Taiwan.

4. **Jiayi Zhang**, Lie-Liang Yang and Lajos Hanzo, "Multi-User Performance of the Amplify-and-Forward Single-Relay Assisted SC-FDMA Uplink", in *Proceedings of 2009 IEEE 70th Vehicular Technology Conference (VTC 2009-Fall)*, 20-23 September, 2009, Anchorage, Alaska, USA.

List of Symbols

General notation

- The superscript * is used to indicate complex conjugation.
- The superscript ^{T} is used to indicate matrix transpose operation.
- The superscript ^{H} is used to denote the complex conjugate transpose operation.
- The superscripts $^{\mathrm{t}}$ and $^{\mathrm{f}}$ are used to denote the signal processed in the time-domain (TD) and frequency-domain (FD), respectively.
- The superscripts $^{\mathrm{i}}$ and $^{\mathrm{o}}$ are used to indicate the inner and outer bit streams in concatenated channel coded systems, respectively.
- The superscripts $^{\mathrm{S}}$, $^{\mathrm{R}}$ and $^{\mathrm{D}}$ are used to represent the signal at the source, the relay and the destination, respectively.
- The superscripts $^{\mathrm{SD}}$, $^{\mathrm{SR}}$ and $^{\mathrm{RD}}$ are used to indicate the transmisstions from the source to destination, source to relay and relay to destination, respectively.
- The notation $\tilde{\boldsymbol{x}}$ denotes the U-length symbol vector of $\boldsymbol{x}$.
- The notation $\breve{\boldsymbol{x}}$ denotes the cyclic prefix (CP) aided symbol vector of $\boldsymbol{x}$.
- The notation $\hat{\boldsymbol{x}}$ represents the estimate of $\boldsymbol{x}$.
- The notation $\overline{\boldsymbol{x}}$ indicates the mean of $\boldsymbol{x}$.
- The notation $\breve{j}$ represents the selected relay j.
- The notation $\underline{k}$ represents user k waiting for resource assignment.
- The notation $\mathring{\mathcal{K}}$, $\mathring{\mathcal{J}}$ and $\mathring{\mathcal{M}}$ represents the ordered set of the user, the relay and the subband group, respectively.
- The notation $\mathring{k}_i$, $\mathring{m}_i$ denotes the user k and subband group m in the sets $\mathring{\mathcal{K}}$ and $\mathring{\mathcal{M}}$ with ordering index i, respectively.
- The notation $\Re\{\cdot\}$ represents the real part of a complex symbol.
- The notation $\Im\{\cdot\}$ is the imaginary part of a complex symbol.

Special symbols

$\boldsymbol{A}$, a Circulant influence matrix and element of desired signal.

$\boldsymbol{b}$ Source bit stream.

$\boldsymbol{c}$ Encoded bit stream.

$E_{\mathbf{b}}$ Bit energy.

$E_{\mathbf{s}}$ Symbol energy.

$\boldsymbol{e}$, e Estimated error vector and the minimum mean-square error (MMSE).

$\boldsymbol{e}_n$ A vector in which the i-th element is 0 for $i \neq n$, while the n-th element of the $(\cdot)$-part is 1.

$F(\cdot)$, $f(\cdot)$ Cumulative distribution function (CDF) and probability density fuction (PDF), respectively.

$\boldsymbol{\mathcal{F}}_N$ Normalised N-point discrete Fourier transform (DFT) matrix.

$\boldsymbol{H}$, $\boldsymbol{h}$, h Channel fading coefficient matrix, vector and one of its element.

G Instantaneous relaying gain including shadowing.

$\mathcal{G}$, g Set of average channel attenuations and one of its elements.

$\boldsymbol{I}_N$ The $(N \times N)$-element indentity matrix.

I The number of iterations of turbo frequency-domain equalisation (FDE).

i The ordering index.

J, j Number of (candidate) relays and the index of (candidate) relay.

$\mathcal{J}$ Set of relays.

K, k Number of active users and the index of a specific user.

$\mathcal{K}$ Set of users.

L, l Number of paths and the index of a path in the channel impulse response.

$\boldsymbol{\mathcal{L}}$, $\mathcal{L}$ Log-likelihood ratio (LLR).

M, m Bandwidth expansion factor (the number of subband groups) and the index of a subband group.

$\mathcal{M}$ Set of subband groups.

$\mathcal{M}$ Number of constellation points in quadrature amplitude modulation (QAM)

N_0 Noise power spectral density.

N, n Size of DFT (the number of symbol elements per SC-FDMA symbol) and the index of an element.

$N_{\mathbf{r}}$, $n_{\mathbf{r}}$ Number of antennas at the BS and the antenna index.

$N_{\mathbf{b}}$, $n_{\mathbf{b}}$ Number of information bits per frame and the bit index.

$N_{\mathbf{c}}$, $n_{\mathbf{c}}$ Number of encoded bits per frame and the index of an encoded bit.

$N_{\mathbf{s}}$, $n_{\mathbf{s}}$ Number of modulated symbols per frame and the symbol index.

$N_{\mathbf{v}}$, $n_{\mathbf{v}}$ Number of SC-FDMA symbols per frame and the SC-FDMA symbol index.

$N_{\mathbf{rb}}$, $n_{\mathbf{rb}}$ Number of resource blocks (RB) per frame and the RB index.

$N_{\mathbf{rv}}$ Number of resource vectors (RV) (SC-FDMA symbols in the FD) per RB.

$n(t)$ The continuous-time representation of the complex-valued additive white Gaussian noise (AWGN) contaminating the received signal.

$\boldsymbol{n}$ The discrete-time expression of complex-valued AWGN contaminating the received signal.

$\mathcal{N}$ Noise power.

$\mathcal{O}$ Computational complexity function expressed in terms of the order of the number of operations/comparisons

$\boldsymbol{\mathcal{P}}$, $\mathcal{P}$ Subband allocation matrix and its element.

P Transmitted power.

$P_{\mathbf{des}}$ Desired signal power.

$P_{\mathbf{est}}$ Combined estimated signal power.

$P_{\mathbf{ISI}}$ Inter-symbol-interference (ISI) power.

Q Bits per symbol.

$\boldsymbol{R}_y$ Auto-correlation matrix of $\boldsymbol{y}$.

$\boldsymbol{R}_{yx}$ Cross-correlation matrix of $\boldsymbol{y}$ and $\boldsymbol{x}$.

$\boldsymbol{R}_{\mathbf{IN}}$ Auto-correlation matrix of the interference-plus-noise.

$\boldsymbol{R}_{\mathbf{N}}$ Auto-correlation matrix of the noise.

$\boldsymbol{r}$ Received symbol vector.

$\boldsymbol{s}$ Transmitted symbol vector.

t Time index.

U The number of subcarriers/subbands in the system.

W Total transmission bandwidth.

$\boldsymbol{W}$**,** $\boldsymbol{w}$ **and** w Weight matrix, vector and coefficient.

$\boldsymbol{x}$**,** x Symbol vector and one of its elements processed in the transmitter.

$\boldsymbol{y}$**,** y Symbol vector and one of its elements processed in the receiver.

$\boldsymbol{z}$**,** z Symbol vector and one of its elements after equalsation or detection in the receiver.

α Power sharing factor.

$\boldsymbol{\beta}$**,** β Amplification matrix and factor.

γ Signal-to-noise ratio (SNR) or signal-plus-interference-to-noise ratio (SINR).

Γ Set of SINRs.

$\gamma_{\mathbf{b}}^{\Delta}$ The power reduction of SNR per bit.

δ Normalised distance fraction.

ϵ Power control error (PCE).

ε Energy consumption per bit.

η Pathloss exponent.

θ Phase shift imposed by the fading.

κ Ricean fading factor.

ξ Log-normal shadowing effect.

σ Standard deviation.

σ_{ξ} Standard deviation of shadowing.

σ_{ϵ} Standard deviation of PCE.

$\sigma_{\mathbf{N}}^2$ Variance of AWGN.

τ Channel's multipath delay.

Contents

Chapter 1

Introduction

1.1 Motivation - A Green Radio Perspective

During the last decade, the worldwide growth in both the number of mobile subscribers and their demand for increased data-rate mobile broadband services provided further impetus for the mobile telecommunication operators to improve both the capacity and the reliability of cellular networks. Hence, they have been upgraded from the second generation (2G) to the third generation (3G) globally. As a result, the operating expenditure (OPEX) has been substantially increased owing to the increase price and quantity of electricity and diesel fuel [1]. Hence the operators have to pay an increased energy bill, which additionally results in excessive carbon dioxide (CO_2) emissions. New air interfaces, such as the *Third Generation Partnership Project's* (3GPP) *Long Term Evolution* (LTE) [2] have also been rolled out in several countries. However, the subscribers are rather unwilling to accept the increased operating costs of smart phones and tablet personal computers, let alone a reduced battery pre-charge time [3, 4]. Ultimately, the information and communication technology (ICT) sector has its responsibility in terms of both environmental protection and sustainable development. The '*Green Radio*' concept, which is also referred to as '*Green Communications*', leads to a new avenue of research towards energy-efficient mobile wireless communication architectures and techniques in both the academic and industrial communities [1, 4, 5].

Energy-efficient solutions have been investigated in terms of many different components of wireless communication systems, such the base station (BS) cell cite as well as the entire network architecture. However, since the issues of BS site energy savings are beyond the scope of our study, we focus our attention on the power reduction at the equipment level and across the network level. To elaborate a little further, innovation at the mobile terminal

(MT) and BS equipment level is related not only to the *radio frequency* (RF) front-end and to the power supply, but also to the *digital signal processing* at the baseband. Hence, we focus our attention on designing power efficient signal processing solutions conceived for various air interface techniques [6–14]. Furthermore, in the classic *radio access networks*, a direct link is constructed for both the uplink and downlink. Naturally, the wireless signal is subjected to path-loss, shadow fading as well as to fast fading. The deleterious effects of these propagation phenomena may be mitigated with the aid of distributed antennas, relay-assisted user cooperation as well as BS cooperation [15–20].

1.2 Overview - A Cooperative Communication Framework

1.2.1 Multiple-Input Multiple-Output Systems

Since the pioneering work of Shannon [21] in 1948, researchers have endeavoured to improve the capacity integrity, and quality-of-service (QoS) of wireless communications. However, the channel capacity of conventional *single-input single-output* systems is severely limited by the logarithmic low of $C = B\log_2(1+SNR)$. As a remedy, multiple-antenna aided systems have been conceived [22, 23]. The *single-input multiple-output* (SIMO) architecture employs a single transmit antenna and multiple receive antennas for uplink transmission, while the *multiple-input single-output* (MISO) architecture invokes multiple transmit antennas and a single receive antenna for downlink transmission. Upon combining the SIMO and MISO architectures, we arrive at the *multiple-input multiple-output* (MIMO) concept relying on diverse multi-antenna aided systems [24–31].

The most valuable bandwidth used for mobile communications lies in the range of 700 MHz to 3.8 GHz [32]. In order to guarantee the independent fading of the physical wireless channels at multiple antennas, a sufficiently high minimum distance has to be maintained between the adjacent antennas, which is not practically feasible, given the limited size of the MT. However, most of the benefits of MIMO techniques, such as the provision of a *transmit diversity* gain attained by space-time coding [26, 27, 29] or the *space-frequency coding* [30], as well as the multiplexing gain provided by the *Bell Laboratories Layered Space-Time* (BLAST) architecture [25], are beyond our reach in the context of the MTs..

1.2.2 Relay-Assisted Transmission and Cooperation

The conventional relaying technique known from the classic telegraph simply repeats a weak signal received at the end of a long wire-section in order to extend the coverage. Similarly, the relay of a wireless backhaul is capable of amplifying a weak signal in order to compensate

TABLE 1.1: Illustration of TDD relaying protocols for the three-terminal fading relay channel of [40] over two time-slots (TSs), constituted by the source (S), relay (R) and destination (D), each of which employs a single antenna. The notation 'A→B' denotes the signals transmitted from terminal A to terminal B.

	Protocol I	Protocol II	Protocol III
TS-1: broadcast phase	S→R, D	S→R, D	S→R
TS-2: relay/cooperation phase	S→D, R→D	R→D	S→D, R→D
Equivalent model	MIMO	SIMO	MISO

for the path-loss effects during radio propagation. A three-terminal communication channel model was introduced by van der Meulen *et al.* in [33,34], which includes a source node that transmits information, a destination node receiving the signal, and a relay node which both receives and transmits information for the sake of enhancing the attainable performance of communications between the source and destination nodes. Forty years later, this concept of relay-assisted transmission has been adopted by the *3GPP-LTE Advanced* standard for commercial employment [35, 36].

With the aid of relaying, the so-called '*user cooperation*' concept relying on 'antenna sharing' and relaying was proposed by Sendonaris *et al.* in 1998 [37], which was then further developed by Laneman and Wornell in 2000 [38]. The basic idea in the context of cellular systems is that a MT may be assigned by the BS to assist another MT as a cooperating partner, where the cooperating MT may relay the source information and additionally it may also transmit its own information to the destination [39]. Note that the source and the destination might be the BS or another MT, depending on whether uplink or downlink transmissions are considered.

Furthermore, user cooperation allows the collaborative MTs to be distributed across the terrain and may be able to achieve a power reduction by reducing the path-loss. Furthermore, it is capable of eliminating the spatial correlation of shadow fading, since the cooperative MTs are typically selected to be at geographically separated locations. Ultimately, user cooperation is capable of achieving substantial gains by providing the following benefits [39]: (1) achieving an improved energy/power efficiency; (2) increasing the attainable system throughput; (3) improving the cell-edge coverage; (4) guaranteeing a given QoS; etc.

1.2.3 Cooperative Relaying Protocols

As mentioned in Section 1.2.1, user cooperation may be regarded as a specific manifestation of a *virtual* or *distributed* MIMO scenario, where the cooperating single-antenna-aided MTs may be treated as the external antennas of cooperating partners [40,41]. Therefore, user cooperation is capable of providing a *cooperative diversity* gain in the form of *spatial diversity*,

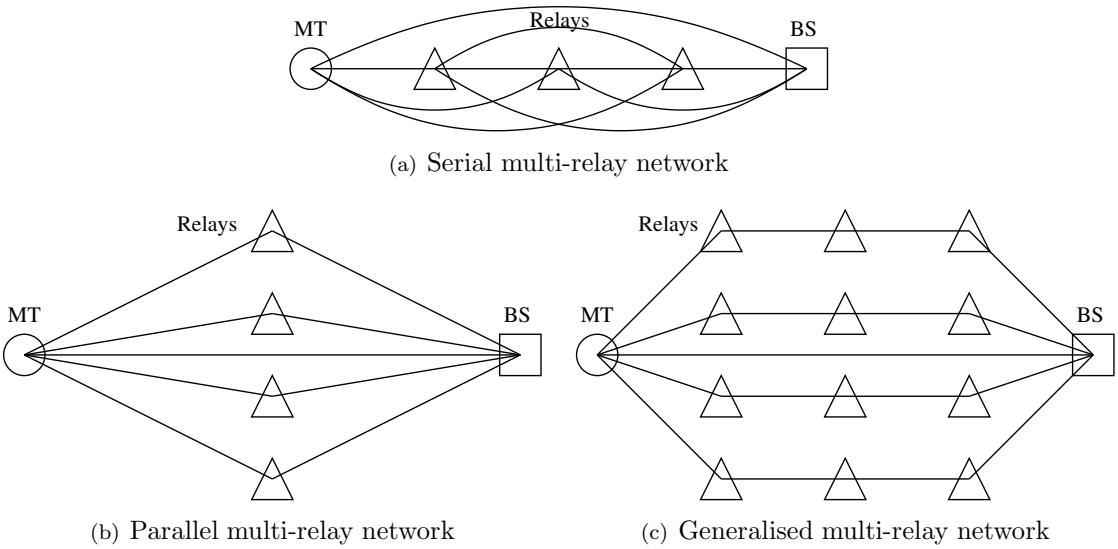

(a) Serial multi-relay network

(b) Parallel multi-relay network

(c) Generalised multi-relay network

FIGURE 1.1: Topologies of multi-relay aided cooperative networks for single-user uplink transmissions

since the destination may receive the replicas of signal via both the direct- and relay-aided links. According to [40], the classic three-terminal fading relay channels may be converted into equivalent MIMO, SIMO and MISO channel models with the aid of the different *time-division-duplex* (TDD) *relaying protocols* of Table 1.1, respectively. For example, a typical virtual SIMO channel may be constructed, where the source broadcasts the signal both to the relays and to the destination during the first time slot, namely *broadcast* phase; then the relays may forward the signal during the second slot, namely during *relay/cooperation* phase. The outage probability results of [40] indicated that the maximum attainable spacial diversity can be achieved by certain protocols, when employing appropriate power control amongst the cooperating MTs.

1.2.4 Multi-Relay Aided Cooperative Networks

Based on the number of relays invoked by the system, cooperative relaying schemes may be classified as follows.

Serial multi-relay network: In [42], serial multi-relay aided transmissions as shown in Figure 1.1(a) were investigated by forwarding the source's signals with the aid of either *multi-hop relaying* or *multi-hop cooperation*, depending on the absence or presence of cooperative diversity combining at each hop. Clearly, the advantage of multi-hop cooperation is the additional diversity gain attained as a benefit of having several independently fading signal paths, which further improves the path-loss reduction induced relying gains.

Parallel multi-relay network: By contrast, in the context of parallel multi-relay assisted transmissions as shown in Figure 1.1(b), the signals are forwarded with the aid of *multi-branch cooperation* for the sake of maximising the achievable diversity order [43, 44].

Generalised multi-relay network: Observe in Figure 1.1(c), a combination of both multi-hop relaying and multi-branch cooperation was examined in [45] as a generalised co-operative scheme aiming for both relaying-aided path-loss reduction and for diversity gain.

Considering the system implementation, the serial multi-relay network is suitable for further extending the cellular coverage, however this is done on the expense of increasing the delay and decreasing the throughput. By contrast, the parallel multi-relay network may be use to beneficially increase the network capacity without coverage extension. Although the generalised multi-relay network inherits the advantages of both serial and parallel multi-relay networks, the network architecture design is complicated.

1.2.5 Signal Processing at the Relay

Furthermore, there are two main transmission modes operated at the relays, namely the *amplify-and-forward* (AF) mode and the *decode-and-forward* (DF) mode [46].

Amplify-and-forward: The AF relays simply normalise and amplify the signals received from the source prior it is transmission to the destination.

Decode-and-forward: In parallel, the DF relays firstly detect, demodulate and decode the source's signals; after hard- or soft-decision the bit stream is then encoded and re-transmitted.

Other types of relaying, such as the so-called *compress-and-forward* [47], *detect-and-forward* or *demodulate-and-forward* [48] techniques may be regarded as modified transmission modes of the AF and DF modes. Generally, the AF relays jointly increase both the signal power and the noise power. By contrast, DF relays are capable of eliminating the effects of noise, provided that the source's signals are decoded without error. However, at low signal-to-noise-ratio (SNR), they often result in decoding error propagation, which degrades the *bit-error rate* (BER) performance at the destination. In order to mitigate the effects of error propagation, the DF relays are also capable of carrying out soft-decisions rather than hard-decisions, where the soft-information is forwarded [49]. A more sophisticated solution is constituted by *coded-cooperation* [50–52] as a form of enhanced DF relaying, which allows the joint design of *forward-error-correction* (FEC) coding of both the source's and the relay's

information [53]. In this scenario, the presence of the direct link in the distributed coding aided cooperative network may provide additional gains by improving the error-correction capability for the sake of near capacity operation [54].

1.2.6 Relay-Assisted Resource Allocation

The *orthogonal frequency-division multiplexing* (OFDM) [55] based 3GPP-LTE air-interface, such as the *orthogonal frequency-division multiple-access* (OFDMA) downlink scheme and the *single-carrier frequency-division multiple-access* (SC-FDMA) uplink [2,35], conveniently facilitate near-instantaneous adaptive *multi-user scheduling* and *subcarrier allocation*, depending on the *channel state information* (CSI) of the subcarriers, when communicating over frequency-selective fading channels [56–59]. Compared to classic single-hop transmissions, optimising radio resource allocation for relay-assisted dual-hop transmissions involves more substantial technical challenges, especially, when considering both multiple users and multiple relays sharing the resource in terms of *time*, *frequency*, *space* and *power*, leading to the cross-layer operation problems [60–62].

Naturally, the availability of inactive mobiles as candidate relays has the potential of mitigating the effects of fading. The activation of multiple relays results in *cooperative* or *selection diversity* in the *spatial-domain*, which transforms the *relay selection* problem into a *multi-relay scheduling* scenario reminiscent of *multi-user scheduling*. Relay selection may be carried out in numerous ways.

Static relay selection assigns the relays for the entire duration of a session, hence the achievable gains depend on the velocity of the cooperating nodes[1].

Random relay selection appoints the relays stochastically without relying on any channel knowledge, but in this case only a limited gain may be attained.

Distance-dependent relay selection is capable of maximising the relaying-aided path-loss reduction by appointing relays in the optimum locations [63, 64].

Channel-dependent relay selection monitors the instantaneous channel conditions, including the associated path-loss, shadowing and multi-path fading effects. Therefore, both relaying-aided path-loss reduction and a diversity gain may be achieved. This kind of relaying scheme is also known as *opportunistic relaying* (OR) [16, 65–67].

[1]The relays having higher velocity communicate over the fading channel with lower time-correlation. In this case, the SRS within a session benefits from time-diversity gain over a high correlated fading channel but it may also suffer from poor channel quality over a low correlated fading.

Furthermore, the selection diversity may be achieved also in the *frequency-domain* (FD) with the aid of beneficial *subcarrier allocation* and *power allocation* schemes. The optimisation cost-function, may be the channel gain, the SNR, the spectral efficiency, etc.

Subcarrier allocation allows the different users' signals to be assigned to the most appropriate subcarriers or to a subcarrier-group in the LTE system [68–72]. In the context of relay-assisted OFDM systems, the joint optimisation of the subcarrier allocation of all hops is desirable, namely that of the *source-to-relay* (S-R) link, of the *source-to-destination* (S-D) link and of the *relay-to-destination* (R-D) link in the dual-hop scenario. This was also referred to as *subcarrier pairing* in [73–79].

Power allocation determines the total transmit power of the individual users' signals shared by the source and the multiple relays subject to the total power constraint [80–82]. In [74–76], the power allocation was also jointly optimised with the subcarrier allocation subject to a specific maximum power constraint at the individual nodes, while striking a trade-off between the cost, the complexity and the achievable performance.

1.2.7 Relay Access Types in LTE-Advanced

In the LTE-Advanced system, which is also known as LTE Release 10, the relays may be operated in two different access modes [35, 83]. The so-called Type-I relays, which possess their own cell identifier, are capable of supporting the MTs with the aid of similar functions to those of the BS in order to improve the cell-edge coverage, when the direct link between the BS and the MTs is of low quality. By contrast, the Type-II relays do not have their own cell identifier and hence do not offer BS-like functions. Their main function is that of creating cooperative relaying links between the BS and the MTs for the sake of achieving cooperative diversity. However, the relays satisfied by the current LTE-Advanced standard were designed to form part of the fixed infrastructure, hence they are stationary.

1.3 Organisation of the Thesis

As part of the LTE Release 8 air-interface [2], SC-FDMA inherits numerous advantages of OFDMA when communicating over broadband wireless channels. However, as a single-carrier modulation scheme, SC-FDMA signalling is capable of additionally maintaining a low *peak-to-average power ratio* (PAPR) in comparison to the OFDM-style multi-carrier modulation schemes. Because of the advantage relying on low PAPR, the SC-FDMA is suitable for the uplink transmission. The above-mentioned user cooperation schemes may

be also introduced into the relay-assisted SC-FDMA systems. We generally assume the inactive or idle MTs are capable of acting as candidate relays. In this thesis, we conceive a range of energy-efficient cooperative SC-FDMA uplink solutions.

1.3.1 Key Aspects

For the sake of achieving a power reduction, our solutions consider three main aspects.

Cooperative networking: The cooperative SC-FDMA uplink will be evaluated in the context of diverse network topologies in comparison to the conventional single-hop scenario. In Chapter 3, we will conceive the so-called *single-dedicated-relaying* (SDR) topology, where each relay is dedicated to a single user. By contrast, when a single relay assists multiple users, we refer to the network as a *single-shared-relaying* (SSR) topology. Furthermore, these single-relaying topologies may be invoked in diverse application scenarios, depending on the number of potential cooperative relay candidates within the network. In Chapter 4, we will investigate the family of *opportunistic cooperation* (OC) systems, both with and without sufficient relays for supporting all the actively communicating users. A generalised OR network will be introduced in Chapter 5, for exploiting the benefits provided by flexible relay resource allocation.

Resource allocation: The family of cooperative SC-FDMA systems will be studied in order to achieve either frequency-selection diversity, as discussed in Chapter 3 and Chapter 4 or for attaining multi-user diversity, as explored in Chapter 5. When the relays are geographically distributed, Chapter 4 considers both the relay selection and power allocation issues in the presence of path-loss, shadowing and multi-path fading. By contrast, when the relays are assumed to be geographically localised, in Chapter 5, we will jointly optimise the dynamic subband allocation and relay selection of dual-hop SC-FDMA transmissions by exploiting the knowledge of both the first-hop channel quality and of the buffering delay of the channel decoder.

Signal processing: In Chapter 3, various *subband-based* AF schemes are designed for SC-FDMA for supporting multiple users. In Chapter 4, *diversity combining* will be intrinsically amalgamated with *frequency-domain equalisation* (FDE) for both the direct and the relay channels. In Chapter 5, opportunistic relays operating either in the AF or the DF mode will be designed, which rely on frequency-domain turbo equalisation.

1.3.2 Outline and Contributions

Figure 1.2 illustrates the dependencies among all chapters in terms of the above-mentioned aspects. The outline and novel contributions of this thesis are summarised as follows:

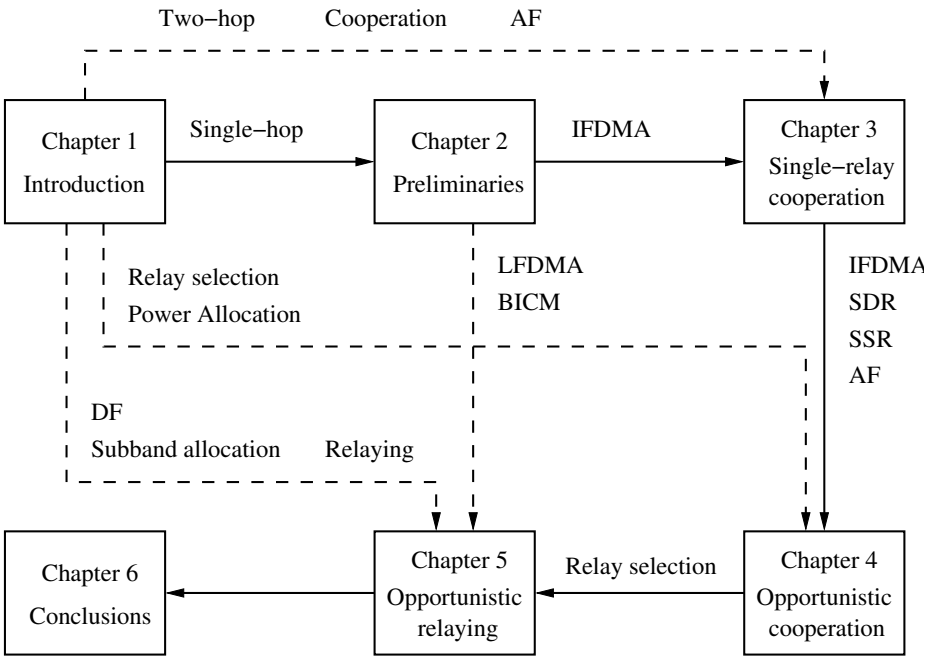

FIGURE 1.2: Structure of the thesis

Chapter 2: In this chapter, the underlying fundamentals of this thesis are introduced. In Section 2.1, we commence with the basic principles of OFDM as the preliminaries of SC-FDMA. Furthermore, we present a rudimentary introduction to SC-FDMA, commencing by introducing the *single-carrier* modulation philosophy invoking FDE. Based on the SC-FDE scheme, the conventional time-domain (TD) signal generation of SC-FDMA is studied in Section 2.2.1. Then in Section 2.2.2 we introduce the time-frequency-domain (TFD) signal generation scheme of SC-FDMA, referred to as *discrete Fourier transform* (DFT)-spread OFDMA. Then in Section 2.2.3, the signal reception and equalisation techniques of SC-FDMA are detailed. Additionally, the *bit-interleaved coded modulation* (BICM) philosophy using iterative decoding (ID) will be briefly introduced.

Contribution 1: *An unied treatment of the principle of SC-FDMA is offered. The relationship between the TD and the TFD signal generation of SC-FDMA is detailed, by considering both the localised FDMA (LFDMA) [84] and the interleaved FDMA (IFDMA) [85] schemes. Finally, the similarities and dissimilarities, advantages and weaknesses of the LFDMA, IFDMA and OFDMA systems are compared.*

Chapter 3: This chapter characterises two single-relay assisted SC-FDMA AF based cooperative strategies employed for multi-user uplink transmissions over multi-path fading channels. For the sake of exploiting the benefits of cooperative diversity, we investigate both the above-mentioned SDR as well as SSR topologies, and propose a subband-based AF scheme combined with subband remapping, which is benchmarked against the conventional AF regime in the context of both the above-mentioned relay-

ing topologies. Our simulation results show that cooperative diversity is beneficial for both SDR and SSR, both in the absence as well as in the presence of multi-path diversity. More importantly, the proposed subband-based AF scheme is capable of attaining a multi-user performance, which is better than that of the conventional single-user AF protocol operating in a multi-path environment.

Contribution 2: *Two single-relay assisted cooperative SC-FDMA network topologies are proposed for different application scenarios. The power-efficient subband-based AF relay scheme is designed for the SC-FDMA. The proposed solutions are capable of achieving a beneficial multi-path diversity gain, while eliminating the multi-user interference and suppressing the effects of AF-induced noise imposed on the multi-user multi-relay networks.*

Chapter 4: In this chapter we exploit the benefits of combining the diversity gains arising from cooperation, multiple propagation paths and from the OC of multiple users. Our goal is to improve the energy-efficiency of the AF relay-assisted SC-FDMA uplink, where the opportunistic cooperating relay considered may support a single user or may be shared by multiple users communicating over dispersive channels subject to large-scale fading. Based on the proposed amalgam of single-tap FDE and a diversity combining aided receiver relying on the *minimum mean-square error* (MMSE) criterion, three different relay selection schemes, namely *single-user relay selection* (SU-RS), *multi-user relay selection* (MU-RS), and *multiple-access relay selection* (MA-RS), are investigated, when combined with source/relay power allocation, which employ imperfect power control.

Contribution 3: *A joint frequency-domain equalisation and combining scheme is proposed and analysed, when combining the signals from both the direct and relaying links.*

Contribution 4: *When encountering both the ubiquitous propagation path-loss and shadowing, both significant relaying-aided path-loss reductions and selection diversity gains are attainable by the proposed optimal power allocation (OPA) aided relay selection schemes. The practicability and feasibility of various power allocation schemes are discussed in the light of their computational complexity.*

Contribution 5: *An energy-efficiency analysis of cooperative SC-FDMA system is offered. The proposed systems are capable of reducing the required signal-to-interference-plus-noise ratio (SINR), which in turn results in a significantly increased multi-user throughput. As a result, the attainable energy-efficiency is improved, when the relays are geographically dispersed in a shadowing environment.*

Chapter 5: In this chapter, we exploit the benefits of the diversity gains arising from a cluster of opportunistic relays and from the independently fading subcarriers of multi-

ple users. Our goal is to improve the energy-efficiency of the AF or DF aided OR based SC-FDMA uplink, where the direct transmission link is unavailable. We proposed two joint *dynamic resource allocation* (DRA) schemes, operating under the assumption that the pilot aided *channel quality information* (CQI) of all the users may be exchanged. Furthermore, we take two important aspects into account, namely what we refer to as *first-hop quality awareness* (FHQA), which improves the attainable gain of DRA aided OR and *buffering delay awareness*, which is particularly important in the context of interleaver-aided FEC coded systems.

Contribution 6: *Any potential extra selection diversity is explored for the sake of reducing the transmit power required and/or for improving the attainable system performance, while assuming that all the multiple relays are geographically localised in a cluster. The FHQA aided joint DRA schemes optimise the multi-user multi-relay networks depending on whether it is the S-R or the R-D channel quality, which dominates the attainable performance, when the system invokes either single or multiple antennas at the BS receiver.*

Contribution 7: *The benefits of opportunistic relaying combined with DSA are quantified in the context of interleaver-aided DF relaying for transmission over correlated fading channels. Therefore, the length of the interleavers combined with FEC may be shortened. As a result, the reduced interleaving delay and/or the total transmit power also provide additional energy savings.*

Contribution 8: *Our investigations of opportunistic relaying involve two advanced FDE schemes. The MMSE based FDE in the principle of successive interference cancellation (SIC) [86, 87] is invoked for uncoded SC-FDMA transmissions relying on AF relays, while the MMSE turbo FDE relying on the turbo equalisation in [88–90] is employed for BICM aided SC-FDMA systems invoking either AF or DF relays. The performance benefits of both single- and multi-antenna aided BS receivers are quantified.*

Chapter 6: In this final chapter, the conclusions of our investigations are presented, followed by a variety of suggestions for future research.

Chapter 2

Preliminaries

In this chapter, the underlying fundamentals of this thesis are introduced. These cover three major aspects, namely *orthogonal frequency-division multiplexing* (OFDM) [55], *single-carrier frequency-division multiple-access* (SC-FDMA) [91] as well as *bit-interleaved coded modulation* (BICM) [92] schemes.

Initially, the OFDM fundamentals will be briefly introduced in Section 2.1. We will demonstrate that by invoking the *discrete Fourier transform* (DFT) and the *inverse discrete Fourier transform* (IDFT), as well as *cyclic prefix* (CP), etc the OFDM receiver's complexity may be beneficially reduced, despite communicating over frequency-selective fading channels.

Furthermore, in Section 2.2 we will present a rudimentary introduction to SC-FDMA, commencing by introducing the *single-carrier modulation* philosophy, invoking *frequency-domain equalisation* (FDE) [93, 94]. Then, the approaches conceived for generating SC-FDMA signals are addressed in Section 2.2.1. Both the *localised* FDMA (LFDMA) scheme relying on a specific contiguous frequency-domain (FD) subband of carriers and the *interleaved* FDMA (IFDMA), which maps a specific user's bits to subcarriers that are far apart, are analysed [95]. Both the LFDMA and IFDMA have their advantages and disadvantages. Simultaneously achieving the advantages of LFDMA and IFDMA constitutes a challenge, unless two different transmitter structures are implemented in parallel, hence increasing the cost. We will carefully map the modulated symbols to the most appropriate subband in the FD. This *subband mapping* technique is similar to the corresponding process of *orthogonal frequency-division multiple-access* (OFDMA) [56]. This results in an efficient hybrid scheme, referred to as DFT-spread OFDMA [96], which will be introduced in Section 2.2.2. We will demonstrate that DFT-spread OFDMA is capable of generating the SC-FDMA signals both LFDMA and IFDMA signals, or even their combination with the aid of appropriate subband

mapping. Furthermore, the signal reception and equalisation techniques of SC-FDMA will be studied in Section 2.2.3.

In Section 2.3, we will study BICM, which is a joint channel coding and modulation scheme. Specifically, BICM using *iterative decoding* (ID) [97, 98] will be introduced in Section 2.3.2. Finally, we will summarise this chapter in Section 2.4.

2.1 Orthogonal Frequency-Division Multiplexing

When communicating over broadband channels imposing frequency-selective fading, conventional *single-carrier modulation* based systems require high-complexity *time-domain* (TD) equalisers having a large number of taps, in order to suppress the *inter-symbol interference* (ISI) due to time-dispersion. However, this disadvantage can be overcome by the family of *multi-carrier modulation* techniques, such as OFDM which was originally introduced in [99]. In the context of multi-carrier communications, the original *bit stream* is divided into numerous low-rate *substreams* transmitted in parallel, which are mapped to *subcarriers* or *subchannels*. When using a high number of substreams, each subchannel becomes sufficiently narrow compared to the *coherence bandwidth* of the channel. Therefore, the signal transmitted over each non-dispersive subchannel experiences frequency-flat fading. As a result, the ISI of each FD substream becomes lower and a low-complexity FD equaliser having a single tap may be employed [100]. However, this parallel transmission scheme would potentially require a bank of modulators and demodulators operating in parallel. Fortunately, it was shown in [101] that this problem may be circumvented by employing the DFT and the IDFT operations, which carry out the modulation/demodulation in a single step. More explicitly, the implementation complexity of OFDM is significantly lower than that of the parallel banks of modulators and the demodulators/equalisers. A plethora of further OFDM system improvements, such as various combinations of OFDM and *code-division multiple-access* (CDMA), leading to multi-carrier CDMA systems have been investigated in [55, 102]. In this section, we briefly review the basic principles of OFDM as the preliminaries of SC-FDMA.

2.1.1 OFDM System Structure

We consider a single-user OFDM system employing N subcarriers. The block diagrams of the OFDM transmitter/receiver are shown in Figure 2.1. Let us describe each block as follows.

BICM and BICM-ID: The principles of BICM and BICM-ID will be provided in Section

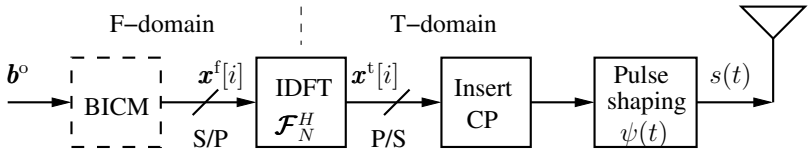

(a) Signal path in the transmitter

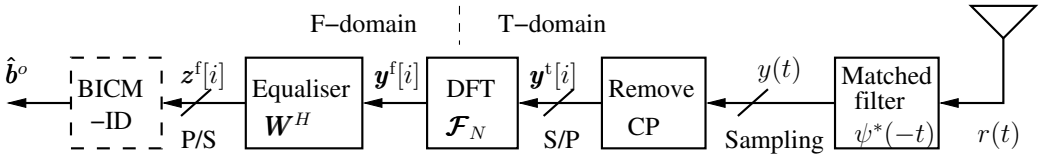

(b) Signal path in the receiver

FIGURE 2.1: Block diagram of baseband OFDM system

2.3.2. Specifically, the bit stream $\boldsymbol{b}^{\mathrm{o}}$ is encoded, interleaved and modulated to generate the *quadrature amplitude modulation* (QAM) based symbol frame in the transmitter of Figure 2.1(a). Let the symbols to be transmitted by the i-th symbol block be expressed as $\boldsymbol{x}^{\mathrm{f}}[i]$, which is a N-length vector. At the receiver, the BICM decoder carries out the symbol-to-bit demapping, deinterleaving and channel decoding, in order to generate the bit stream $\hat{\boldsymbol{b}}^{\mathrm{o}}$ from the equalised symbol frame containing the i-th equalised symbol vector $\boldsymbol{z}^{\mathrm{f}}[i]$ for $i = 0, 1, \cdots$.

S/P and P/S converter: The *serial-to-parallel* (S/P) converter of Figure 2.1(a) converts the serial symbol stream into N parallel symbols hosted in the i-th vector. By contrast, the *parallel-to-serial* (P/S) converter of Figure 2.1(a) converts the N parallel elements in the i-th symbol vector into a N-times higher-rate serial symbol stream, for $i = 0, 1, \cdots$. The S/P and P/S converters facilitate the processing of the serial symbols in parallel by DFT and IDFT.

DFT and IDFT: The N-point DFT matrix $\boldsymbol{\mathcal{F}}_N$ is given by [1]

$$\boldsymbol{\mathcal{F}}_N = \frac{1}{\sqrt{N}} \begin{bmatrix} 1 & 1 & \cdots & 1 \\ 1 & \exp\left(-j\frac{2\pi}{N}\right) & \cdots & \exp\left(-j\frac{2\pi(N-1)}{N}\right) \\ \vdots & \vdots & \ddots & \vdots \\ 1 & \exp\left(-j\frac{2\pi(N-1)}{N}\right) & \cdots & \exp\left(-j\frac{2\pi(N-1)(N-1)}{N}\right) \end{bmatrix}, \tag{2.2}$$

[1] Let $\{x(0), x(1), \cdots, x(N-1)\}$ be an N-length sequence, then the DFT and IDFT are defined as [102]

$$\text{DFT:} \quad X[n'] = \frac{1}{\sqrt{N}} \sum_{n=0}^{N-1} x[n] \exp\left(-j\frac{2\pi n' n}{N}\right), n' = 0, 1, \cdots, N-1; \tag{2.1a}$$

$$\text{IDFT:} \quad x[n] = \frac{1}{\sqrt{N}} \sum_{n'=0}^{N-1} X[n'] \exp\left(j\frac{2\pi n' n}{N}\right), n = 0, 1, \cdots, N-1. \tag{2.1b}$$

which is an orthonormal matrix, satisfying the property $\boldsymbol{\mathcal{F}}_N\boldsymbol{\mathcal{F}}_N^H = \boldsymbol{\mathcal{F}}_N^H\boldsymbol{\mathcal{F}}_N = \boldsymbol{I}_N$. Furthermore, we have

$$\boldsymbol{\mathcal{F}}_N^{-1} = \boldsymbol{\mathcal{F}}_N^H. \tag{2.3}$$

Multiplying the vector $\boldsymbol{x}^{\mathrm{f}}$ by $\boldsymbol{\mathcal{F}}_N^H$ implements the IDFT, as also seen in Figure 2.1(a).

Insert and remove CP: In the DFT/IDFT aided multi-carrier system of Figure 2.1 experiencing *linear time invariant* (LTI) multi-path fading channels, the linear convolution between the channel's input sequence, i.e. the transmitted signal containing $\boldsymbol{x}^{\mathrm{t}}[i]$ for $i = 0, 1, \cdots$ after P/S conversion, and the discrete-time *channel impulse response* (CIR) associated having a finite number of taps L, results in ISI between each consecutive serial data sequences $\boldsymbol{x}^{\mathrm{t}}[i]$ and $\boldsymbol{x}^{\mathrm{t}}[i+1]$ represented in the TD. One solution to this problem is to insert a CP, which copies the last $L_{\mathrm{CP}} \geq L$ samples, i.e. $\{x^{\mathrm{t}}_{N-L_{\mathrm{CP}}}[i], x^{\mathrm{t}}_{N-L_{\mathrm{CP}}+1}[i], \cdots, x^{\mathrm{t}}_{N-1}[i]\}$, from the end to the beginning of the serial sequence $\boldsymbol{x}^{\mathrm{t}}[i]$. This is required, because the inherent assumption facilitating DFT-based demodulation is that the received TD signal is periodic - at least for the duration of the channel's memory. A theoretically less well justified alternative method of mitigating the ISI is known as *zero-padding* (ZP) [100, 103].

Pulse shaping and matched filtering: In order to improve the spectral efficiency of the OFDM modulated signals, typically a pulse shaping technique using a raised-cosine filter is adopted at the transmitter. Let us assume that $\psi(t)$ represents a TD signalling waveform defined over the interval of $[0, T_\psi)$ satisfying the normalisation condition of $\int_0^{T_\psi} \psi^2(t)\mathrm{d}t = T_\psi$. Since each DFT block transmits N samples, the duration of each sample is given by $T_\psi = T/N$, where T denotes the OFDM block duration. Furthermore, the band-limited transmitted pulse $\psi(t)$ is convolved with the CIR $c(t)$ and the matched filter $\psi^*(-t)$ at the receiver, resulting in the effective received pulse given by the convolution of $\psi(t) * c(t) * \psi^*(-t)$ prior to sampling, as seen in Figure 2.1(b). Naturally, the *Nyquist criterion* [104] must be satisfied by the sampling of the effective received pulse for the sake of avoiding ISI between consecutive samples of the received signal.

Channel and equalisation: When the above-mentioned CP is employed and when it is sufficiently long, the self-interference of the OFDM symbol and the ISI between a pair of consecutive OFDM symbols is mitigated. Let the L-path CIR be expressed as

$$h(t) = \sum_{l=0}^{L-1} h_l^{\mathrm{t}} \delta(t - lT_c), \tag{2.4}$$

where h_l^{t} is the gain of the l-th resolvable path for $l = 0, 1, \cdots, L-1$. Then, after sampling, the channel matrix in the TD may be represented by a $(N \times N)$-element

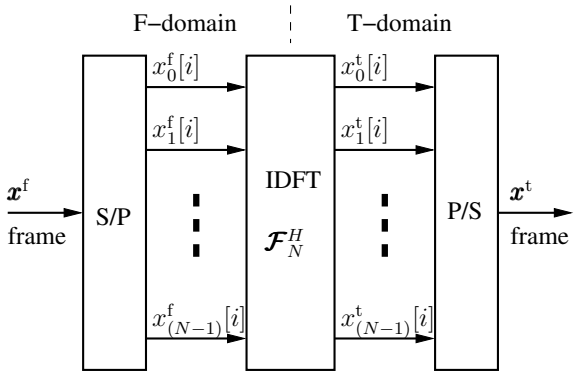

FIGURE 2.2: Transmitter schematic diagram of OFDM

circulant matrix given by [102]

$$\boldsymbol{H}^{\mathrm{t}} = \begin{bmatrix} h_0^{\mathrm{t}} & 0 & \cdots & 0 & h_{L-1}^{\mathrm{t}} & h_{L-2}^{\mathrm{t}} & \cdots & h_1^{\mathrm{t}} \\ h_1^{\mathrm{t}} & h_0^{\mathrm{t}} & \cdots & 0 & 0 & h_{L-1}^{\mathrm{t}} & \cdots & h_2^{\mathrm{t}} \\ \vdots & \vdots & \ddots & \vdots & \vdots & \vdots & \ddots & \vdots \\ h_{L-2}^{\mathrm{t}} & \cdots & h_1^{\mathrm{t}} & h_0^{\mathrm{t}} & 0 & \cdots & 0 & h_{L-1}^{\mathrm{t}} \\ h_{L-1}^{\mathrm{t}} & \cdots & h_2^{\mathrm{t}} & h_1^{\mathrm{t}} & h_0^{\mathrm{t}} & \cdots & 0 & 0 \\ \vdots & \vdots & \ddots & \vdots & \vdots & \vdots & \ddots & \vdots \\ 0 & 0 & \cdots & h_{L-1}^{\mathrm{t}} & h_{L-2}^{\mathrm{t}} & \cdots & h_1^{\mathrm{t}} & h_0^{\mathrm{t}} \end{bmatrix}, \tag{2.5}$$

which has the property that $\boldsymbol{H}^{\mathrm{t}} = \boldsymbol{\mathcal{F}}_N^H \boldsymbol{H}^{\mathrm{f}} \boldsymbol{\mathcal{F}}_N$, where $\boldsymbol{H}^{\mathrm{f}} = \mathrm{diag}\{h_0^{\mathrm{f}}, h_1^{\mathrm{f}}, \cdots, h_{N-1}^{\mathrm{f}}\}$. Therefore, after applying the DFT-based detection operation at the receiver and having in mind that IDFT-based modulation was applied at the transmitter, the equivalent FD channel transfer function (FDCHTF) can be represented as a $(N \times N)$-element diagonal matrix given by

$$\boldsymbol{H}^{\mathrm{f}} = \boldsymbol{\mathcal{F}}_N \boldsymbol{H}^{\mathrm{t}} \boldsymbol{\mathcal{F}}_N^H = \mathrm{diag}\{h_0^{\mathrm{f}}, h_1^{\mathrm{f}}, \cdots, h_{N-1}^{\mathrm{f}}\}. \tag{2.6}$$

Consequently, in OFDM systems, a low-complexity single-tap equaliser is required. As a benefit of the DFT/IDFT operation, the high complexity TD convolution-based equalisation may be replaced by the FD *subcarrier-by-subcarrier* based multiplication operation in a linear time-invariant system. Therefore, the computational complexity is significantly reduced.

2.1.2 Transmitted OFDM Signals

For mathematical convenience, complex baseband equivalent signals are considered [102]. Observe in Figure 2.2 that

$$\boldsymbol{x}^{\mathrm{f}} = [x_0^{\mathrm{f}}, x_1^{\mathrm{f}}, \cdots, x_{N-1}^{\mathrm{f}}]^T \tag{2.7}$$

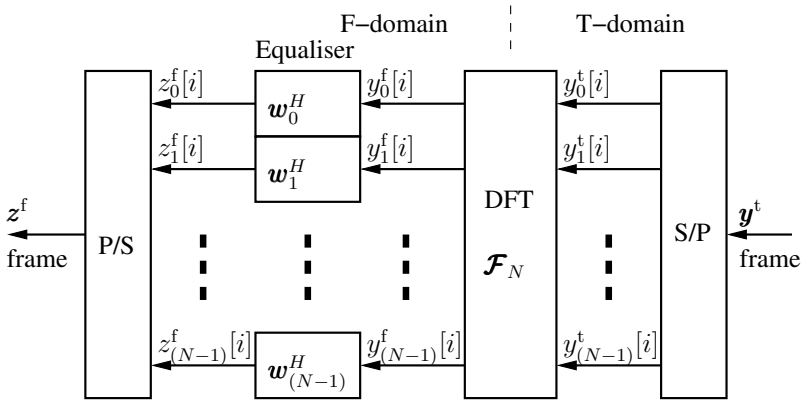

FIGURE 2.3: Receiver schematic diagram of OFDM

represents the FD data symbol vector, namely an *OFDM symbol*. Upon applying the N-point IDFT to $\boldsymbol{x}^{\mathrm{f}}$, the N-element transmitted TD OFDM symbol becomes

$$\boldsymbol{x}^{\mathrm{t}} = [x_0^{\mathrm{t}}, x_1^{\mathrm{t}}, \cdots, x_{N-1}^{\mathrm{t}}]^T = \boldsymbol{\mathcal{F}}_N \boldsymbol{x}^{\mathrm{f}}, \tag{2.8}$$

where $\boldsymbol{\mathcal{F}}_N$ is given by Eq. (2.2). After inserting the CP of length L_{CP}, we have

$$\breve{\boldsymbol{x}}^{\mathrm{t}} = [x_{N-L_{\mathrm{CP}}}^{\mathrm{t}}, x_{N-L_{\mathrm{CP}}+1}^{\mathrm{t}}, \cdots, x_0^{\mathrm{t}}, x_1^{\mathrm{t}}, \cdots, x_{N-1}^{\mathrm{t}}]^T, \tag{2.9}$$

which has a length of $(N + L_{\mathrm{CP}})$. Finally, $\breve{\boldsymbol{x}}^{\mathrm{t}}$ is transmitted on a *sample-by-sample* basis after pulse shaping.

2.1.3 Detection of OFDM Signals

The detailed principles of OFDM can be found in [55, 105]. When communicating over frequency-selective Rayleigh fading channels, the N-element complex baseband equivalent received observations $\boldsymbol{y}^{\mathrm{t}}$ seen in Figure 2.3 may be expressed as [102]

$$\boldsymbol{y}^{\mathrm{t}} = \boldsymbol{H}^{\mathrm{t}} \boldsymbol{\mathcal{F}}_N^H \boldsymbol{x}_k^{\mathrm{f}} + \boldsymbol{n}^{\mathrm{t}}, \tag{2.10}$$

after removing the CP and S/P conversion, where $\boldsymbol{H}^{\mathrm{t}}$ is given by Eq. (2.5). Furthermore, $\boldsymbol{n}^{\mathrm{t}}$ denotes a complex-valued *additive white Gaussian noise* (AWGN) vector, whose entries obey the complex Gaussian distribution with a zero mean and a variance of σ_{N}^2, which is denoted by $\mathcal{CN}(0, \sigma_{\mathrm{N}}^2)$. As shown in Figure 2.3, following the S/P conversion, $\boldsymbol{y}^{\mathrm{t}}$ is transformed to the FD by applying the N-point DFT operation, yielding

$$\boldsymbol{y}^{\mathrm{f}} = \boldsymbol{H}^{\mathrm{f}} \boldsymbol{x}^{\mathrm{f}} + \boldsymbol{\mathcal{F}}_N \boldsymbol{n}^{\mathrm{t}}, \tag{2.11}$$

where the diagonal matrix $\boldsymbol{H}^{\mathrm{f}}$ was given in Eq. (2.6).

Assuming that perfect channel estimation is available, then, decision variables representing the N transmitted symbols may be formed as

$$\boldsymbol{z}^{\mathrm{f}} = (\boldsymbol{H}^{\mathrm{f}})^{H}\boldsymbol{H}^{\mathrm{f}}\boldsymbol{x}^{\mathrm{f}} + \boldsymbol{n}^{\mathrm{f}}, \tag{2.12}$$

where $\boldsymbol{n}^{\mathrm{f}} = (\boldsymbol{H}^{\mathrm{f}})^{H}\boldsymbol{\mathcal{F}}_{N}\boldsymbol{n}^{\mathrm{t}}$, which has a zero mean and a covariance matrix $\sigma_{\mathrm{N}}^{2}\boldsymbol{H}^{\mathrm{f}}(\boldsymbol{H}^{\mathrm{f}})^{H}$. Explicitly, the decision variable for the n-th element of $\boldsymbol{x}^{\mathrm{f}}$ is given by

$$z_{n}^{\mathrm{f}} = |h_{n}^{\mathrm{f}}|^{2}x_{n}^{\mathrm{f}} + n_{n}^{\mathrm{f}}, \tag{2.13}$$

based on which the estimate of the transmitted symbol can be obtained.

2.1.4 Advantages and Disadvantages of OFDM

The OFDM signalling technique has the following advantages. Firstly, the ISI can be significantly mitigated with the aid of relatively low signal processing complexity at the receiver. Secondly, in OFDM signalling, using overlapping but orthogonal subcarriers leads to an increased spectral efficiency [100]. Thirdly, the FD channel fluctuations may be accommodated by invoking subband-based adaptive modulation in OFDM, where each subband of parallel subcarriers may be modulated using a FDCHTF-dependent number of bits, depending on the *signal-to-noise ratio* (SNR) of the individual subbands. As a result, the throughput of OFDM systems may be increased with the aid of adaptive modulation.

However, it is a disadvantage that in the absence of channel coding, the OFDM system is incapable of achieving diversity. When channel coding, such as BICM, is applied on an individual subcarrier basis, the system may achieve a certain time-diversity gain as a benefit of channel coding and interleaving, but no frequency-diversity may be attained, unless the same symbol is transmitted several times by mapping it to independently fading subcarriers, which have to reside outside the channel's coherent bandwidth. A better way of achieving frequency-diversity for OFDM is to exploit coding and interleaving applied right across all the subcarriers [106].

However, owning to transmitting multiple signals in parallel, OFDM signalling also has some disadvantages. Firstly, due to the superposition of a high number of modulated subcarrier signals, a high *peak-to-average power ratio* (PAPR) may be exhibited [55]. The PAPR problem imposes substantial challenges on the practical design of power amplifiers, which have a limited linear range. In case of non-linear amplification, the resultant high out-of-band harmonic distortion power may contaminate the adjacent channels, when the TD signal evolves from a low-power waveform to a high-power waveform [55]. Diverse techniques of PAPR reduction have been investigated widely in the literature [107–112]. A beneficial

low-complexity technique is based on employing a so-called block-coding technique [113], where some of the subcarriers do not convey useful data - instead, they are simply set to a value, which reduces the peak-power. Secondly, a further impediment of OFDM is that it is very sensitive to frequency offset and time offset [100].

2.2 Single-Carrier Frequency-Division Multiple-Access

Above, we have shown that multi-carrier modulation has some advantages over the conventional single-carrier modulation, but suffers from the above-mentioned PAPR problem. Naturally, single-carrier modulation having a significantly lower PAPR is more suitable for partial uplink transmissions compared to multi-carrier modulation, since the battery-size of the *mobile terminal* (MT) is limited, hence requiring power-efficient non-linear amplifiers. In order to take advantage of the benefits of both single-carrier and multi-carrier modulation, the single-carrier received signal may be transformed to and equalised in the FD with the aid of the IDFT and DFT operations. This arrangement is referred to as *single-carrier* modulation relying on *frequency-domain equalisation* (SC-FDE) [93, 94, 114]. Furthermore, by combining the SC-FDE and FDMA principles, SC-FDMA may rely either on TD or on FD signal generation [115]. The important development mile-stones of SC-FDMA are shown in Table 2.1. The FD signal generation approach, namely that of DFT-spread OFDMA, has been adopted by the *Third Generation Partnership Project's* (3GPP) - *Long Term Evolution* (LTE) initiative [2] as well as by its advanced version (LTE-Advanced) [35, 83, 116, 117] for the SC-FDMA based uplink transmissions within the *fourth generation* (4G) wide area cellular broadband wireless systems.

In this section, we review the principles of SC-FDE and SC-FDMA. Two types of SC-FDMA schemes are considered. In the first type, the signals in the transmitter are only processed in the TD, which is hence referred to as TD processing aided SC-FDMA, or TD SC-FDMA for short. By contrast, in the second type of SC-FDMA, the signals in transmitter are processed in both the TD and FD with the aid of the DFT/IDFT. Hence, this type is referred to as TFD SC-FDMA for the sake of distinction.

2.2.1 Transmitter of Time-Domain SC-FDMA

The schematic of the SC-FDE system [94, 134] is shown in Figure 2.4. At the transmitter of Figure 2.4(a), let the data symbols be divided into N-symbol block expressed as $\boldsymbol{x}_{\mathrm{t}}[i]$, $i = 0, 1, \cdots$. Then, each block $\boldsymbol{x}_{\mathrm{t}}[i]$ is transmitted in a conventional serial fashion in the TD within a duration of T_{v}. In order to suppress the ISI between symbol blocks at the transmitter, as shown in Figure 2.4(a), a CP is inserted between a pair of successive symbol

TABLE 2.1: Major contributions on SC-FDE and SC-FDMA techniques

Year	Authors	Contributions
1995	Sari *et al.* [93]	discussed the OFDM signalling limitations and inherent problems of OFDM emphasised the benefits of SC-FDE for digital TV broadcasting.
1998	Clark [118]	proposed adaptive frequency-domain equalisation and diversity combining.
	Sorger *et al.* [85, 95]	scheme proposed the original TD interleaved FDMA (IFDMA) signal generation scheme, while the receiver invokes equalisation in the TD.
2002	Galda *et al.* [96]	proposed the DFT-spreading aided OFDM scheme, which can be combined with FDMA as the TFD signal generation of IFDMA, while the receiver invokes linear equalisation (LE) and detection in the FD.
	Falconer *et al.* [94]	discussed the SC-FDE arrangement using FD LE or TD decision feedback equaliser (DFE)The comparison between SC-FDE and OFDM systems and their coexistence were addressed.
	Benvenuto *et al.* [119]	proposed the block-wise hybrid DFE structure for single-carrier system by using a FD feedforward filter and a TD feedback filter, and compared it to the OFDM system.
2003	Gusmão *et al.* [120]	investigated the CP-assisted SC-FDE as well as diversity combining and provided both numerical results and the analytical performance bound.
2004	Wang [121]	compared OFDM to SC-FDE systems using either ZP or CP over frequency-selective fading channels, and considered the PAPR, power amplifier back-off, carrier frequency offset impact, as well as the performance versus complexity for both uncoded and coded transmissions.
	Dinis *et al.* [122]	proposed a FD single-carrier signal generation scheme, which is equivalent to the OFDM-FDMA using the DFT-spreading of [96].
2005	Benvenuto *et al.* [123, 124]	proposed a block-wise DFE, where both the feedforward and the feedback filters were implemented in the FD relying on the MMSE criterion.
2006	Myung *et al.* [125, 126]	generalised the DFT-spread OFDM scheme of [96] by combining both the IFDMA and the localised FDMA (LFDMA) solutions, PAPR comparisons of IFDMA, LFDMA and of OFDMA signals were provided.
	Lim *et al.* [127, 128]	investigated the various types of multi-user scheduling schemes conceived for SC-FDMA systems.
2007	Frank *et al.* [129]	reviewed and discussed the IFDMA principle as a combination of OFDMA as well as CDMA and compared IFDMA, LFDMA, OFDMA as well as the single-carrier or the multi-carrier CDMA schemes.
2008	Myung *et al.* [91]	a book on the topic of SC-FDMA design for LTE uplink combined with beamforming, multi-user scheduling and PAPR evaluation.
	Berardinelli *et al.* [130–132]	investigated multi-user scheduling schemes designed for SC-FDMA in comparison to OFDMA in LTE-Advanced scenarios.
2009	Adachi *et al.* [133]	investigated the various combinations of SC-FDE with FDMA, CDMA, and a so-called block-spread CDMA. A hybrid single-carrier delay-time aided CDMA scheme was proposed.
	Adachi *et al.* [134]	overviewed the various SC-FDE schemes and introduced the over-lapped FDE and fractionally spaced FDE. An interference cancellation technique was invoked in order to mitigate the residual ISI. Further topics relying on MIMOs and channel estimation were also addressed.
	Yang [102]	investigated the subband allocation in SC-FDMA and discussed the trade-off between achieving a frequency diversity gain and mitigating the residual ISI.
2010	Choi *et al.* [135]	investigated multi-level BICM designed for SC-FDE.
	Yune *et al.* [136]	combined iterative multi-user detection (MUD) with FDE within the SC-FDMA framework and improved the power/spectral efficiency.
	Benvenuto *et al.* [114]	historically reviewed the various non-linear FDE schemes in the context of SC-FDE and SC-FDMA.
2011	Zhang *et al.* [137, 138]	proposed novel low-complexity FD DFE structures for SC-FDE systems and multi-user SC-FDMA systems.

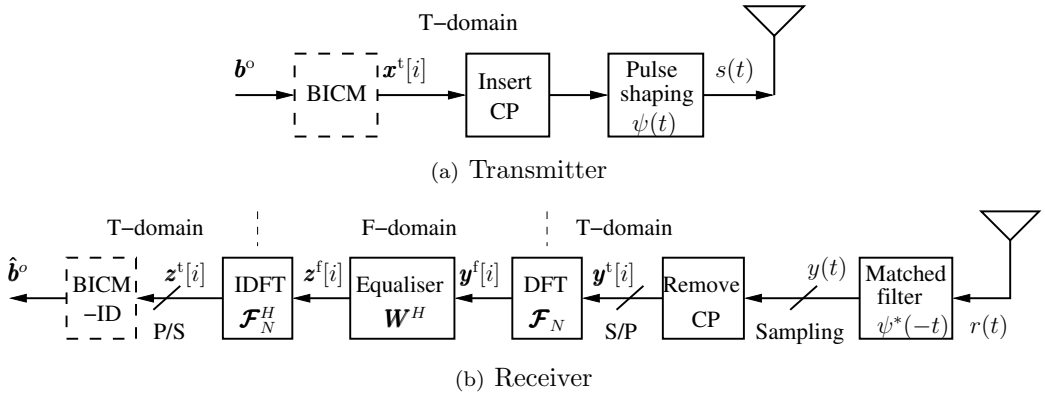

FIGURE 2.4: Block diagram of classic SC-FDE system

blocks. Hence, the duration T_{v} includes the duration of the CP. At the receiver side, as shown in Figure 2.4(b), the TD observations are firstly transformed to the FD with the aid of the DFT block, where the FDE is invoked. Then, the results are converted to the TD again using the IDFT of Figure 2.4(b), where the transmitted symbols are detected. When comparing the OFDM schematic of Figure 2.1 to Figure 2.4, we can see that in OFDM transceivers, the transmitter relies on the IDFT-based modulator, while the receiver invokes a DFT-based demodulator. By contrast, in the SC-FDE of Figure 2.4, both the IDFT and DFT are required at the receiver. More explicitly, given the low PAPR and the low-complexity single-tap FDE of SC-FDMA, we exploit the fact that the IDFT/DFT operations facilitate moderate-complexity transformations between the TD and FD.

According to Figure 2.4, after the CP was removed and following the N-point DFT operation, the FD received observation vector may be expressed as

$$\boldsymbol{y}^{\mathrm{f}} = \boldsymbol{\mathcal{F}}_N \boldsymbol{H}^{\mathrm{t}} \boldsymbol{x}^{\mathrm{t}} + \boldsymbol{\mathcal{F}}_N \boldsymbol{n}^{\mathrm{t}}. \tag{2.14}$$

Since the channel matrix obeys the circulant property of $\boldsymbol{H}^{\mathrm{t}} = \boldsymbol{\mathcal{F}}_N^H \boldsymbol{H}^{\mathrm{f}} \boldsymbol{\mathcal{F}}_N$, Eq. (2.14) may be rewritten as $\boldsymbol{y}^{\mathrm{f}} = \boldsymbol{H}^{\mathrm{f}} \boldsymbol{x}^{\mathrm{f}} + \boldsymbol{n}^{\mathrm{f}}$, where $\boldsymbol{H}^{\mathrm{f}}$ represents an $(N \times N)$-element diagonal FD channel matrix given by Eq. (2.6), while $\boldsymbol{x}^{\mathrm{f}} = \boldsymbol{\mathcal{F}}_N \boldsymbol{x}^{\mathrm{t}}$ and $\boldsymbol{n}^{\mathrm{f}} = \boldsymbol{\mathcal{F}}_N \boldsymbol{n}^{\mathrm{t}}$. Similar to OFDM, a single-tap FD equaliser may be employed in each subband. Finally, the resultant FD equalised symbol vector $\boldsymbol{z}^{\mathrm{f}}$ is transformed by the N-point IDFT to the estimated TD decision variable vector representing the N transmitted symbols, which may be expressed as

$$\boldsymbol{z}^{\mathrm{t}} = \boldsymbol{\mathcal{F}}^H \boldsymbol{W}^H \boldsymbol{H}^{\mathrm{f}} \boldsymbol{x}^{\mathrm{f}} + \boldsymbol{\mathcal{F}}^H \boldsymbol{W}^H \boldsymbol{n}^{\mathrm{f}}. \tag{2.15}$$

Finally, the BICM-ID decoder of Figure 2.4(b) is invoked for channel decoding. Note that in Eq. (2.15) the FDE weight-matrix $\boldsymbol{W}$ is a diagonal matrix, since $\boldsymbol{H}^{\mathrm{f}}$ is diagonal.

Again, we assume the perfect knowledge of FDCHTF H^{f} available at the BS's receiver. In

TABLE 2.2: Comparison of OFDM and SC-FDE systems

	OFDM	SC-FDE
Implementation	Similar, DFT/IDFT-aided, SC-FDE transmitter is simpler.	
ISI	Similar, non ISI by using CP	
Complexity	Similar, lower than that of the TD equaliser	
Modulation	Multi-carrier	Single-carrier
Transmission	Parallel	Serial
Symbol duration	N times per subcarrier	Unchanged
Bandwidth	$1/N$ per subcarrier	$1/N$ per subband at receiver
Frequency offset	Sensitive	Less sensitive
Against deep FD fading	Week	Robust
Bit/power loading	Frequency-selective adaptation	Not applicable

the SC-FDE, various FDE approaches may be employed based on diverse criteria. When the *matched-filtering* (MF), *zero-forcing* (ZF) or the *minimum mean-square-error* (MMSE) criterion is employed, the equaliser-weight matrix $\boldsymbol{W}$ may be expressed as [102, 133, 134].

$$\boldsymbol{W} = \begin{cases} \boldsymbol{H}^{\mathrm{f}}, & \text{MF-FDE} \\ (\boldsymbol{H}^{\mathrm{f}})^{-1}, & \text{ZF-FDE} \\ \left[\boldsymbol{H}^{\mathrm{f}}(\boldsymbol{H}^{\mathrm{f}})^{H} + \frac{1}{\bar{\gamma}}\boldsymbol{I}_N\right]^{-1}\boldsymbol{H}^{\mathrm{f}}, & \text{MMSE-FDE} \end{cases}, \tag{2.16}$$

where $\bar{\gamma} = P/\sigma_{\mathrm{N}}^2$ denotes the average SNR. It can be seen from Eq. (2.15) and Eq. (2.16) that the symbols within $\boldsymbol{x}^{\mathrm{t}}$ interfere with each other, when invoking the MF- and MMSE-based FDE (MF-FDE, MMSE-FDE) schemes, which results in a residual ISI. By contrast, the residual ISI is completely eliminated by the ZF based FDE (ZF-FDE), but as a price, the noise may be amplified by a factor of $1/h_n^{\mathrm{f}}$, when a deep FD fade is encountered in the n-th subband, for example. As a benefit, the MMSE-FDE strikes a trade-off between the *residual* ISI suppression and noise enhancement imposed on $\boldsymbol{z}^{\mathrm{t}}$ [102, 133].

The differences between the OFDM and SC-FDE transceiver structures lead to different features during signal transmissions. For example, the data detection of the SC-FDE receiver depends on the FDCHTF of all the subbands, hence any deep fade of a specific subband may be mitigated. By contrast, in OFDM, individually applying the data detection on a per subcarrier basis may result in decision errors for the subcarrier symbols suffering from deep FD fading. Furthermore, the SC-FDE signal cannot readily invoke adaptive bit- and power-loading depending on the subchannel qualities. By contrast, adaptive bit- and power-loading is feasible in OFDM, since the bit-to-symbol mapping may be carried out on a per-subcarrier basis after S/P conversion at the transmitter. In summary, we compare the features of OFDM and SC-FDE in Table 2.2 [91].

Above the SC-FDE scheme has only been considered in the context of single-user transmission. Let us now focus our attention on multi-user FDMA scenarios. In order to support

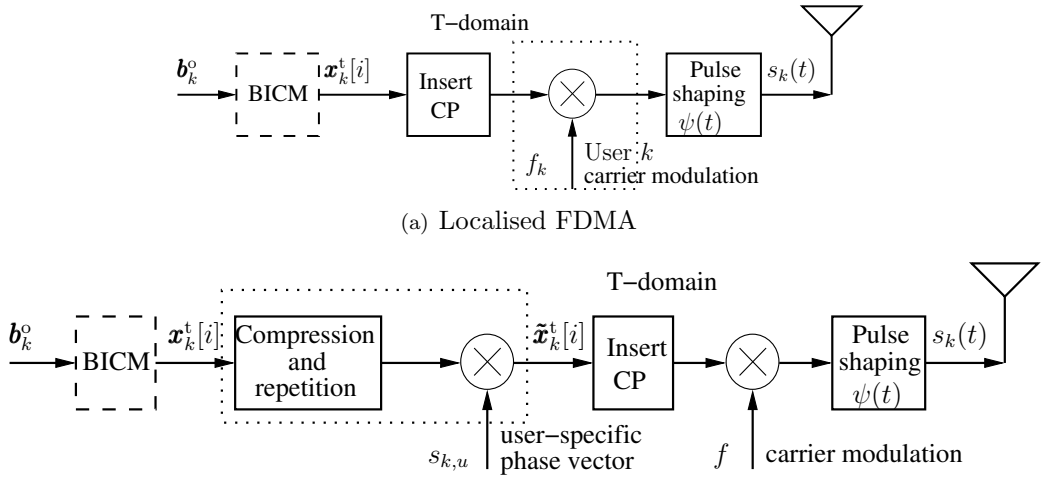

(a) Localised FDMA

(b) Interleaved FDMA

FIGURE 2.5: Transmitter schematic of the TD SC-FDMA signalling scheme. The corresponding waveforms are seen in Figure 2.6.

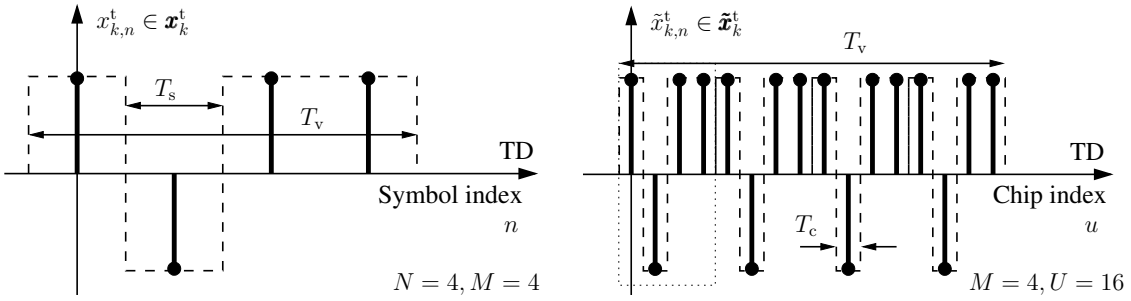

(a) Localised FDMA

(b) Interleaved FDMA

FIGURE 2.6: An example of transmitted signal waveforms of the TD SC-FDMA signalling systems using (a) LFDMA and (b) IFDMA, respectively. Both the systems have a block duration of T_{v}, with a symbol duration of T_{s} and the chip duration of IFDMA is $T_{\mathrm{c}} = T_{\mathrm{s}}/M = T_{\mathrm{s}}/4$. The system may support $K \leq M = 4$ users. The corresponding spectrum are seen in Figure 2.7.

K users in the uplink, two TD signalling schemes using SC-FDE have been considered by the 3GPP-LTE standardisation body [139,140], namely the *localised* FDMA (LFDMA) and the *interleaved* FDMA (IFDMA) schemes. Let us assume that the symbol duration is T_{s}. Then, the duration of a SC-FDE block is $T_{\mathrm{v}} = NT_{\mathrm{s}}$, when each SC-FDE block contains N symbols. As shown in Figure 2.7, we assume that the symbol rate is $B = 1/T_{\mathrm{s}}$. Hence, if the total system bandwidth is MB, the maximum number of users supported becomes $K = M$. Let us now detail the operational principles of the LFDMA and IFDMA schemes using SC-FDE.

TD localised FDMA [84, 139]: The transmitter schematic of the TD LFDMA is shown in Figure 2.5(a), which is the conventional FDMA-based SC-FDE. The transmitted TD signal waveform of LFDMA is shown in Figure 2.6(a). The signals of different

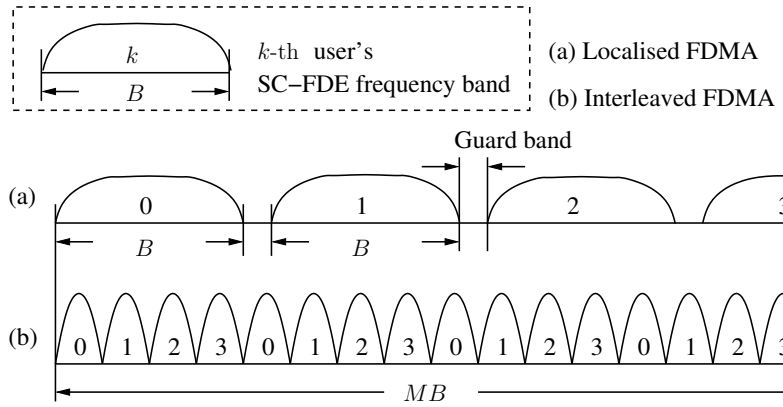

FIGURE 2.7: An example of band-conversion and bandwidth-expansion for the TD SC-FDMA systems using (a) LFDMA and (b) IFDMA, respectively. Both the systems have a total bandwidth of $MB = 4B$, with a symbol rate of B for supporting $K \leq M = 4$ users.

users are transmitted in different frequency bands associated with different carriers. Specifically, the k-th user's signal is conveyed by the k-th subband with a bandwidth of B Hz, as shown in Figure 2.5(a). As shown in Figure 2.7 (a), in order to guarantee the orthogonality between different users' signals, a guard band is inserted between two adjacent bands.

TD interleaved FDMA [85, 95]: The corresponding transmitter schematic is shown in Figure 2.5(b). In contrast to the above-mentioned TD LFDMA signalling, which allocates localised frequency bands to each of the users, the idea behind the TD IFDMA scheme is to disperse each user's signal equidistantly to N distributed subbands, each having a bandwidth of B/N Hz, which are equally distributed across the entire system bandwidth of MB Hz, as shown in Figure 2.7 (b). Therefore, each user still occupies B Hz and the system is capable of supporting a maximum of $K = M$ users. Observe in the TD IFDMA transmitter of Figure 2.5(b) that the original N symbols of user k having a symbol duration T_s are first compressed into N chips with a chip duration of T_s/M. Then, the k-th user's resultant N-chip segment is repeated M times, while being subjected to the user-specific phase rotation factor of k/T_v for $k = 0, 1, \cdots, K-1$. As shown in Figure 2.6(b), the resultant symbol vector having a duration of T_v is denoted as $\tilde{\boldsymbol{x}}_k^\mathrm{t}[i]$, which contains $U = MN$ chips, namely N chips from each of the K users. Finally, the u-th, $u = 0, 1, \cdots, U-1$, chip in $\tilde{\boldsymbol{x}}_k^\mathrm{t}[i]$ is expressed as

$$\tilde{x}_{k,u}^\mathrm{t}[i] = \begin{cases} \frac{1}{\sqrt{M}} \exp\left[j\frac{2\pi(mN+n)k}{U}\right] x_{k,n}^\mathrm{t}[i], & \text{if } u = mN+n, \\ 0, & \text{else,} \end{cases} \tag{2.17}$$

for $m = 0, 1, \cdots, M-1$ and $n = 0, 1, \cdots, N-1$, where $x_{k,n}^\mathrm{t}[i]$ represents the n-th symbol of the i-th symbol vector $\boldsymbol{x}_k^\mathrm{t}[i]$ of user k. Finally, the different users' signals can be transmitted orthogonally using the same carrier frequency. It can be shown that if

each of the K users transmits its signals in the form of Eq. (2.17), the received signal vector will be de-spread with the aid of the user-specific phase de-rotation vector [85]. Hence, applying the DFT to transform the TD signal to the FD, it may be expressed in the form of Eq. (2.14), which is beneficial, because it is capable of employing FDE.

Both the TD LFDMA and IFDMA schemes characterised in Figure 2.6 have their advantages and disadvantages. The main advantage of TD LFDMA which is explicitly shown in Figure 2.6(a) is that the different MTs map each user's signals to different carrier frequencies using different timing, hence synchronisation is not necessary, which facilitates asynchronous uplink communications. However, using guard bands reduce the spectral efficiency of the LFDMA. Additionally, the LFDMA system may not achieve frequency-diversity, if each user's signal is a narrow-band signal. By contrast, the TD IFDMA system characterised in Figure 2.6(b) transmits different users' signals at the same carrier frequency in conjunction with user-specific phase rotation. However, accurate timing should be guaranteed. Hence, it requires tight synchronisation in the uplink, which constitutes a challenge for MTs roaming at different distances and at a high speed. However, as a benefit, the IFDMA system does not require a guard band between the adjacent subbands. Therefore, the bandwidth efficiency of the IFDMA scheme may be higher than that of the LFDMA scheme. On the down-side again, when the MTs of the IFDMA system roam at a high velocity, the frequency offset due to the Doppler frequency shift may significantly degrade the performance of IFDMA systems.

2.2.2 Transmitter of Time-Frequency-Domain SC-FDMA

The transmitter schematic of TFD SC-FDMA is shown in Figure 2.8(a). In comparison to the OFDM scheme of Figure 2.1(a) and to the TD SC-FDMA arrangement of Figure 2.5, which has no DFT/IDFT at the transmitter, the transmitter of the TFD SC-FDMA has both the DFT and the IDFT. The DFT operation in the TFD SC-FDMA scheme is referred to as DFT-based spreading [96, 125], which transforms and spreads each TD symbol to the FD as a feature of DFT, yielding a modulated signal in the form of the OFDM modulated signal. Then, as shown in Figure 2.9, the subcarrier signals are mapped to different subbands according to the matrix $\boldsymbol{P}_k$ of Figure 2.8(a). Following mapping to the subbands, the results are transformed back to the TD by the IDFT, where the signals are transmitted following the principles of OFDM, after inserting the CP and pulse-shaping as seen in Figure 2.8(a). Let us now describe some of the components portrayed in Figure 2.8(a) in more detail.

Let us assume that the TFD SC-FDMA system employs $U = MN$ subbands to support $K \leq M$ uplink users, where each user occupies N subbands. According to [102], after S/P

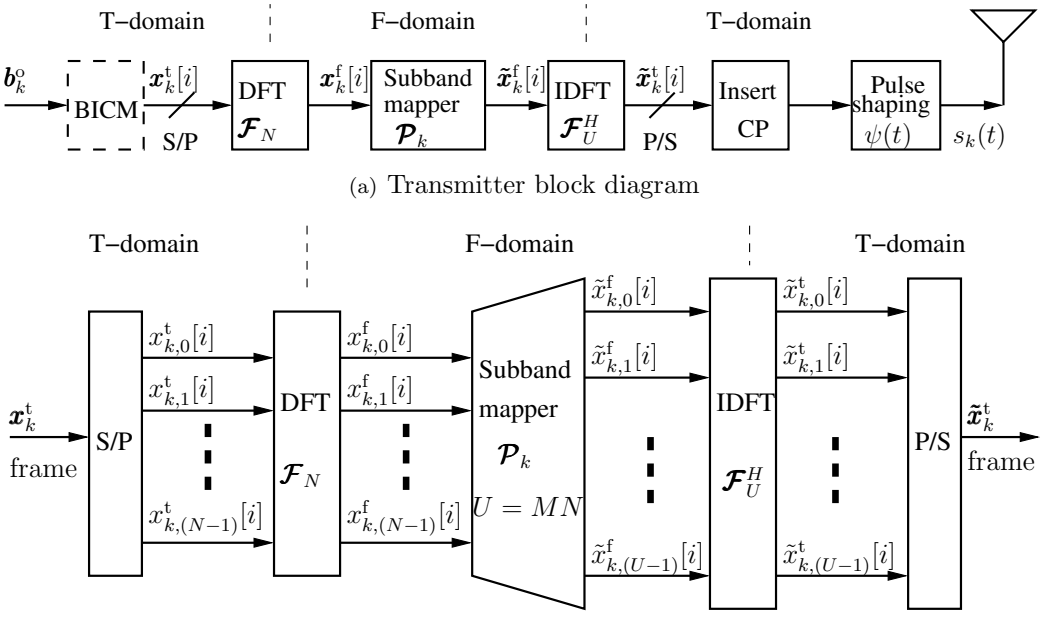

(a) Transmitter block diagram

(b) Baseband signal processing in the transmitter

FIGURE 2.8: Transmitter structure of the TFD SC-FDMA signalling adopting the principle of DFT-spread OFDMA. In contrast to the pure TD LFDMA/IFDMA schemes of Figure 2.5, in the TFD SC-FDMA we have the additional DFT - subband mapper - IDFT processing chain, which facilitates the flexible mapping of the symbols to subbands.

conversion, the k-th user's N symbols may be expressed in the TD as

$$\boldsymbol{x}_k^{\mathrm{t}} = [x_{k,0}^{\mathrm{t}}, x_{k,1}^{\mathrm{t}}, \cdots, x_{k,(N-1)}^{\mathrm{t}}]^T, \quad k = 0, 1, \cdots, K-1, \tag{2.18}$$

where the superscript t refers to the TD. Each element in $\boldsymbol{x}_k^{\mathrm{t}}$ is independent and identically-distributed (i.i.d.) with a normalised transmission power P. Following the N-point DFT-spreading using the DFT matrix $\boldsymbol{\mathcal{F}}_N$ of Figure 2.8(b), $\boldsymbol{x}_k^{\mathrm{t}}$ is transformed to the FD, yielding

$$\boldsymbol{x}_k^{\mathrm{f}} = [x_{k,0}^{\mathrm{f}}, x_{k,1}^{\mathrm{f}}, \cdots, x_{k,(N-1)}^{\mathrm{f}}]^T = \boldsymbol{\mathcal{F}}_N \boldsymbol{x}_k^{\mathrm{t}}, \tag{2.19}$$

where the superscript f refers to the FD. Note that a conventional OFDMA system may be formed, when $\boldsymbol{\mathcal{F}}_N$ is replaced by the identity matrix $\boldsymbol{I}_N$.

As shown in Figure 2.8(b), following the DFT operation, the k-th user's FD symbols in $\boldsymbol{x}_k^{\mathrm{f}}$ are mapped to the most appropriate N subbands, which are selected from the $U = (M \times N)$ subbands of the SC-FDMA system with the aid of the subband mapping matrix $\boldsymbol{\mathcal{P}}_k$ of user k. Following subband mapping, the U-length FD symbol vector may be expressed as

$$\tilde{\boldsymbol{x}}_k^{\mathrm{f}} = [\tilde{x}_{k0}^{\mathrm{f}}, \tilde{x}_{k1}^{\mathrm{f}}, \cdots, \tilde{x}_{k(U-1)}^{\mathrm{f}}]^T = \boldsymbol{\mathcal{P}}_k \boldsymbol{x}_k^{\mathrm{f}}. \tag{2.20}$$

Again, in the context of SC-FDMA typically two subband mapping schemes are used, namely

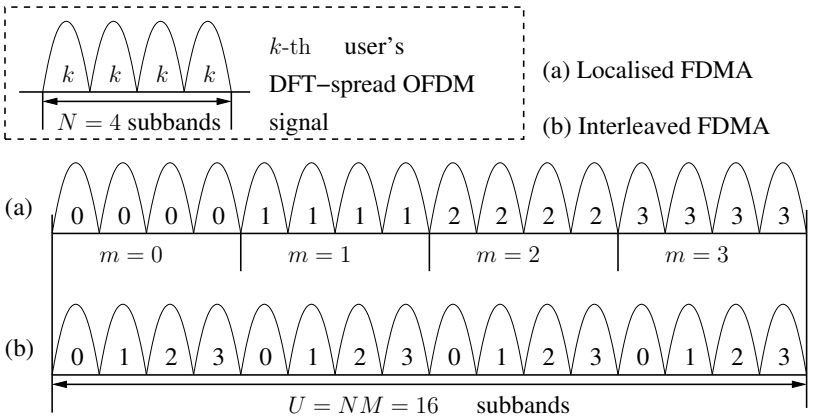

FIGURE 2.9: An example to illustrate the bandwidth expansion and subband mapping in the TFD SC-FDMA system of Figure 2.8 using a total of $U = 16$ subbands, and $N = 4$ subbands per user. The system can support $K \leq M = 4$ users.

the localised mapping and distributed mapping schemes shown in Figure 2.9.

Localised subband mapping: As shown in Figure 2.9 (a), the localised mapping allows each user's N symbols to be transmitted on N consecutive subbands of the U subbands. It can be shown that the entries of $\boldsymbol{\mathcal{P}}_k$ seen in Figure 2.8 are defined as

$$\mathcal{P}_{k,(u,n)} = \begin{cases} 1, & \text{if } u = kN + n \\ 0, & \text{otherwise} \end{cases} \tag{2.21}$$

for $n = 0, 1, \cdots, N-1$ and $u = 0, 1, \cdots, U-1$.

Distributed subband mapping: When the distributed mapping of Figure 2.9 (b) is employed, the N symbols of a user are spread across the entire bandwidth of U subbands. A typical distributed symbol-to-subband mapping scheme is the so-called *interleaved subband mapping* proposed in [96, 122], which allocates the N symbols of a user to equidistant subbands, where the entries of the mapping matrix $\boldsymbol{\mathcal{P}}_k$ are defined as

$$\mathcal{P}_{k,(u,n)} = \begin{cases} 1, & \text{for } u = nM + k \\ 0, & \text{otherwise} \end{cases} \tag{2.22}$$

for $n = 0, 1, \cdots, N-1$ and $u = 0, 1, \cdots, U-1$.

In the context of the TFD SC-FDMA scheme, the system invoking the localised subband mapping is referred to as the LFDMA, as shown in Figure 2.5(a), which has now been adopted by the 3GPP-LTE and the LTE-Advanced standards [2, 35]. By contrast, the TFD SC-FDMA system using the interleaved subband mapping is referred to as the TD IFDMA arrangement of Figure 2.5(b). In TFD SC-FDMA, the DFT-spread OFDMA structure allows the user signals to be transmitted with a high flexibility. For example, the length of the

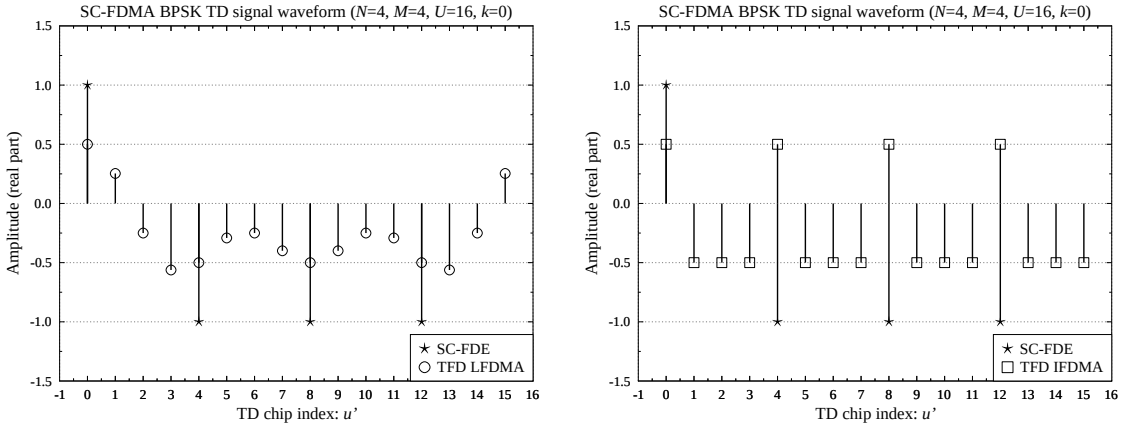

(a) Localised FDMA (b) Interleaved FDMA

FIGURE 2.10: An example of the $k = 0$-th user's transmitted signal waveforms of the TFD SC-FDMA signalling systems using (a) LFDMA and (b) IFDMA in comparison to SC-FDE, respectively. Both the systems have a block duration of T_{v}, with a symbol duration of T_{s} and the chip duration is $T_{\mathrm{c}} = T_{\mathrm{s}}/M = T_{\mathrm{s}}/4$. The system may support $K \leq M = 4$ users. The corresponding spectrum are seen in Figure 2.11.

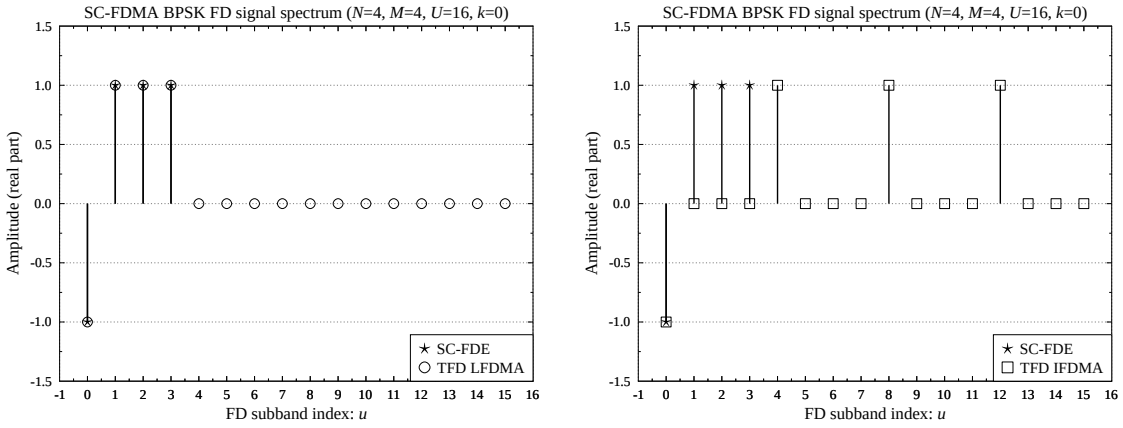

(a) Localised FDMA (b) Interleaved FDMA

FIGURE 2.11: An example of the $k = 0$-th user's transmitted signal spectrum of the TFD SC-FDMA signalling systems using (a) LFDMA and (b) IFDMA in comparison to SC-FDE, respectively. Both the systems have a system bandwidth of MB, with a subband bandwidth of B/N. The system may support $K \leq M = 4$ users. The corresponding subband mapping are seen in Figure 2.9.

transmitter's DFT/IDFT may be reconfigured adaptively for the sake of accommodating diverse time-varying channel environments in order to achieve frequency diversity. The length of the DFT/IDFT can also be adjusted, in order to support variable-rate services. When comparing the IDFMA scheme to LFDMA, it becomes plausible that the IFDMA system is capable of achieving the maximum attainable frequency diversity in dispersive multi-path fading channels, since each symbol of a user carried by N subcarriers is distributed evenly across the entire transmission band. By contrast, owing to experiencing correlated fading, the LFDMA system can only achieve frequency diversity, when using either *dynamic subband allocation* [141] or *multi-user scheduling* [91].

As seen in Figure 2.8(b), following the symbol-to-subband mapping, the U-point IDFT is invoked to transform the symbols of $\tilde{\boldsymbol{x}}_k^{\mathrm{f}}$ from the FD to the TD, yielding

$$\tilde{\boldsymbol{x}}_k^{\mathrm{t}} = [\tilde{x}_{k0}^{\mathrm{t}}, \tilde{x}_{k1}^{\mathrm{t}}, \cdots, \tilde{x}_{k(U-1)}^{\mathrm{t}}]^T = \boldsymbol{\mathcal{F}}_U^H \tilde{\boldsymbol{x}}_k^{\mathrm{f}} = \boldsymbol{\mathcal{F}}_U^H \boldsymbol{\mathcal{P}}_k \boldsymbol{\mathcal{F}}_N \boldsymbol{x}_k^{\mathrm{t}}. \tag{2.23}$$

Specifically, when considering TFD LFDMA and substituting Eq. (2.21) into Eq. (2.23), it can be shown in Figure 2.11(a) that the u-th element of $\tilde{\boldsymbol{x}}_k^{\mathrm{f}}$ becomes zero, provided that we have $u \neq kN + n$, while the u'-th, $u' = 0, 1, \cdots, U-1$, element of $\tilde{\boldsymbol{x}}_k^{\mathrm{t}}$ can be expressed as [102]

$$\tilde{x}_{k,u'}^{\mathrm{t}} = \frac{1}{\sqrt{M}} \exp\left(j\frac{2\pi u' k}{M}\right) x_{k,n}^{\mathrm{t}}, \tag{2.24a}$$

if $u' = nM$, and

$$\begin{aligned} \tilde{x}_{k,u'}^{\mathrm{t}} = & \frac{1}{\sqrt{M}} \exp\left(j\frac{2\pi u' k}{M}\right) \\ & \times \left[1 - \exp\left(j\frac{2\pi u'}{M}\right)\right] \frac{1}{N} \sum_{n'=0}^{N-1} \frac{x_{k,n}^{\mathrm{t}}}{1 - \exp(j2\pi u'/U)\exp(-j2\pi n'/N)}, \end{aligned} \tag{2.24b}$$

otherwise. Observe in Eq. (2.24a), Eq. (2.24b) as well as Figure 2.10(a), we can see that the N symbols of $x_{k,0}^{\mathrm{t}}, x_{k,1}^{\mathrm{t}}, \cdots, x_{k,(N-1)}^{\mathrm{t}}$ are transmitted as the chips $\tilde{x}_{k,u'}^{\mathrm{t}}$ of Figure 2.10(a) within the chip durations of $u' = 0, M, \cdots, (N-1)M$, respectively, within the same subcarrier frequency kN/T_{v}, which corresponds to ku'/M in Eq. (2.24a) and Figure 2.10(a), when we have $u' = nM$. Otherwise, when $u' \neq nM$, the original symbols in $\boldsymbol{x}_k^{\mathrm{t}}$ are transmitted by three subcarriers with the frequencies kN/T_{v}, N/T_{v} and $1/T_{\mathrm{v}}$, corresponding to ku'/M, u'/M and u'/U, as seen in Eq. (2.24b) and Figure 2.10(a). Therefore, the spectrum of the TFD LFDMA signal is similar to that of the conventional TD LFDMA signal, as shown in Figure 2.5(a). However, in the TFD LFDMA the guard band between the adjacent multi-user channels that used in the conventional TD LFDMA is not necessary. Hence, the bandwidth efficiency of TFD LFDMA may be enhanced. Since the TFD LFDMA scheme only transmits three subcarriers regardless of the value of N and U, TFD LFDMA is capable of attaining a much lower PAPR, in comparison with OFDMA.

By contrast, in the context of the TFD IFDMA, when substituting Eq. (2.22) into Eq. (2.23), we find that the u-th element of $\tilde{\boldsymbol{x}}_k^{\mathrm{f}}$ is zero for any $u \neq nM + k$ as shown in Figure 2.10(b), while we have [102]

$$\tilde{x}_{k,u'}^{\mathrm{t}} = \frac{1}{\sqrt{M}} \exp\left[j\frac{2\pi(mN+n)k}{U}\right] x_{k,n}^{\mathrm{t}}, \tag{2.25}$$

when $u' = mN + n$, for $m = 0, 1, \cdots, M-1$ and $n = 0, 1, \cdots, N-1$. Observe from Eq. (2.25), for the k-th user only a single subcarrier located at the frequency of k/T_{v} is activated to convey each of N symbols in $\boldsymbol{x}_k^{\mathrm{t}}$ which is transmitted repeatedly M times with a within

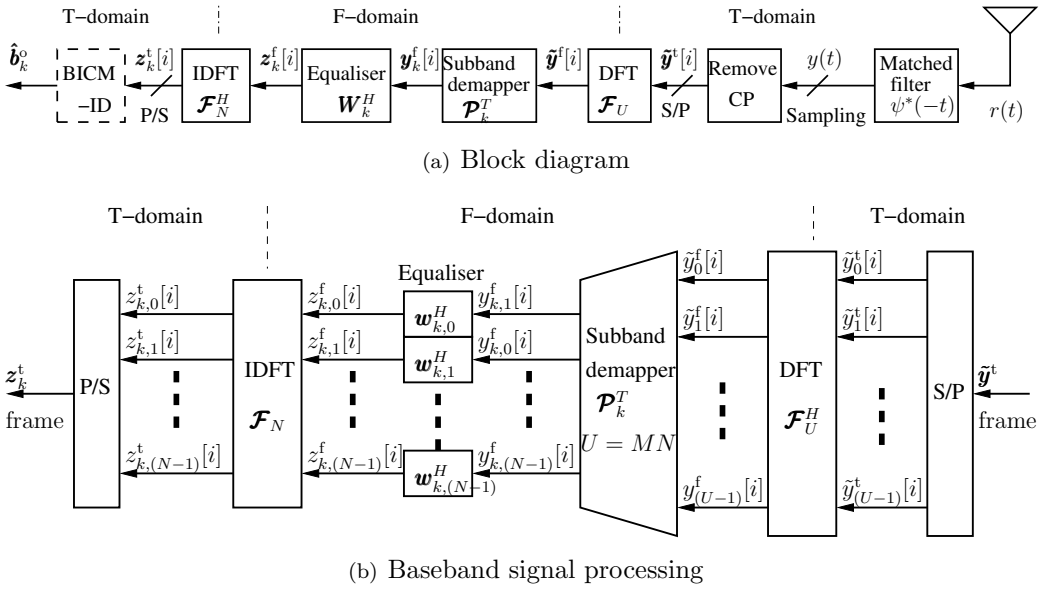

(a) Block diagram

(b) Baseband signal processing

FIGURE 2.12: Receiver structure of the TFD SC-FDMA scheme. The corresponding transmitter was shown in Figure 2.8, while the associated waveforms in Figure 2.10.

a segment duration of T_{v}. Hence, it can be shown that the transmitted signal's spectrum in TFD IFDMA of Figure 2.11(b) is equivalent to that of the TD IFDMA signal, as seen in Figure 2.7(b). Since TFD IFDMA only transmits a single carrier at any time, it does not impose any severe PAPR problems as OFDM.

Finally, as seen in Figure 2.8(b), the TFD SC-FDMA (LFDMA, IFDMA) signals are transmitted after P/S conversion, CP concatenation and chip waveform filtering. Let us now consider the receiver.

2.2.3 Receiver of Time-Frequency-Domain SC-FDMA

The receiver schematic of TFD SC-FDMA is shown in Figure 2.12(a). More details are illustrated in Figure 2.12(b). Explicitly, the receiver typically carries out the inverse operations of the transmitter. Since the symbols are transmitted in blocks in TFD SC-FDMA systems, they are also detected on a block-by-block basis. Considering a specific block, after the matched-filtering, the CP is removed. Then, U-point DFT is carried out to transform the TD observations to the FD, where subband demapping and FDE are invoked. Finally, following the N-point IDFT, which transforms the equalised FD signals to the TD, the decision variables can be formed for the N transmitted symbols of a user.

To elaborate a little further, after matched-filtering and CP removal, as well as S/P conver-

sion, the TD observations may be expressed as [102]

$$\tilde{\boldsymbol{y}}^{\mathrm{t}} = \sum_{k=0}^{K-1} \tilde{\boldsymbol{H}}_k^{\mathrm{t}} \tilde{\boldsymbol{x}}_k^{\mathrm{t}} + \tilde{\boldsymbol{n}}^{\mathrm{t}}, \tag{2.26}$$

where $\tilde{\boldsymbol{H}}_k^{\mathrm{t}}$ represents a $(U\times U)$-element TD equivalent CIR matrix for user k', which is a circulant matrix in the form of Eq. (2.5). Furthermore,

$$\tilde{\boldsymbol{n}}^{\mathrm{t}} = [\tilde{n}_0^{\mathrm{t}}, \tilde{n}_1^{\mathrm{t}}, \cdots, \tilde{n}_{U-1}^{\mathrm{t}}]^T \tag{2.27}$$

represents the complex-valued Gaussian distributed noise vector associated with a zero mean and a covariance matrix $\sigma_N^2 \boldsymbol{I}_U$, where $\boldsymbol{I}_U$ is a $(U\times U)$-element identity matrix.

Upon applying the U-point DFT of Figure 2.12(b), $\tilde{\boldsymbol{y}}^{\mathrm{t}}$ is transformed from the TD to the FD, giving $\tilde{\boldsymbol{y}}^{\mathrm{f}} = \boldsymbol{\mathcal{F}}_U \tilde{\boldsymbol{y}}^{\mathrm{t}}$. Then, the subband-to-symbol demapping is carried out. Specifically for user k', $k' = 0, 1, \cdots, K-1$, we exploit the property of [102]

$$\boldsymbol{\mathcal{P}}_{k'}^T \boldsymbol{\mathcal{P}}_k = \begin{cases} \boldsymbol{I}_N, & \text{for } k = k', \\ \boldsymbol{0}_N, & \text{for } k \neq k', \end{cases} \tag{2.28}$$

which allows us to express the result as [102]

$$\begin{aligned} \boldsymbol{y}_{k'}^{\mathrm{f}} &= \boldsymbol{\mathcal{P}}_{k'}^T \sum_{k=0}^{K-1} \boldsymbol{\mathcal{F}}_U \tilde{\boldsymbol{H}}_k^{\mathrm{t}} \boldsymbol{\mathcal{F}}_U^H \tilde{\boldsymbol{x}}_k^{\mathrm{f}} + \boldsymbol{\mathcal{P}}_{k'}^T \boldsymbol{\mathcal{F}}_U \tilde{\boldsymbol{n}}^{\mathrm{t}} \\ &= \boldsymbol{\mathcal{P}}_{k'}^T \tilde{\boldsymbol{H}}_{k'}^{\mathrm{f}} \boldsymbol{\mathcal{P}}_{k'} \boldsymbol{x}_{k'}^{\mathrm{f}} + \sum_{k'\neq k, k=0}^{K-1} \boldsymbol{\mathcal{P}}_{k'}^T \tilde{\boldsymbol{H}}_k^{\mathrm{f}} \boldsymbol{\mathcal{P}}_k \boldsymbol{x}_k^{\mathrm{f}} + \boldsymbol{n}_{k'}^{\mathrm{f}} \\ &= \boldsymbol{H}_{k'}^{\mathrm{f}} \boldsymbol{x}_{k'}^{\mathrm{f}} + \boldsymbol{n}_{k'}^{\mathrm{f}}, \end{aligned} \tag{2.29}$$

where $\boldsymbol{H}_{k'}^{\mathrm{f}}$ represents the k'-th user's FDCHTF matrix, which is a $(N\times N)$-element diagonal matrix, given by

$$\boldsymbol{H}_{k'}^{\mathrm{f}} = \boldsymbol{\mathcal{P}}_{k'}^T \boldsymbol{\mathcal{F}}_U \tilde{\boldsymbol{H}}_k^{\mathrm{t}} \boldsymbol{\mathcal{F}}_U^H \boldsymbol{\mathcal{P}}_k = \mathrm{diag}\{h_{k,0}^{\mathrm{f}}, h_{k,1}^{\mathrm{f}}, \cdots, h_{k,(N-1)}^{\mathrm{f}}\}. \tag{2.30}$$

Additionally, it can be shown that in Eq. (2.29), we have $\boldsymbol{n}_{k'}^{\mathrm{f}} = \boldsymbol{\mathcal{P}}_{k'}^T \boldsymbol{\mathcal{F}}_U \tilde{\boldsymbol{n}}^{\mathrm{t}}$, which obeys $\mathcal{CN}(0, \sigma_{\mathrm{N}}^2 \boldsymbol{I}_N)$.

Let us assume that the BS exploits our knowledge about the *channel state information* (CSI) associated with all K users. Then, as discussed in Section 2.2.1, the k'-th user's signal can be equalised by a single-tap FDE using a $(N\times N)$-element diagonal weight matrix, expressed as $\boldsymbol{W}_{k'} = \mathrm{diag}\{w_{k',0}, w_{k',1}, \cdots, w_{k',(N-1)}\}$ for user k'. The design of the weight-matrix may be based on diverse criteria, yielding $\boldsymbol{z}_{k'}^{\mathrm{f}} = \boldsymbol{W}_{k'}^H \boldsymbol{y}_{k'}^{\mathrm{f}}$. For example, when the MMSE based FDE

is employed, the (n', n')-th entry of $\boldsymbol{W}_{k'}$ for $n' = 0, 1, \cdots, N-1$ and $k' = 0, 1, \cdots, K-1$ is given by [102]

$$w_{k',n'} = \frac{h^{\mathrm{f}}_{k',n'}}{|h^{\mathrm{f}}_{k',n'}|^2 + 1/\bar{\gamma}}, \tag{2.31}$$

where $\bar{\gamma} = P/\sigma^2_{\mathrm{N}}$ denotes the average SNR.

Finally, upon carrying out the N-point IDFT seen in Figure 2.12(b), the decision variables for the k'-th user's transmitted symbols may be expressed as

$$\boldsymbol{z}^{\mathrm{t}}_{k'} = \boldsymbol{\mathcal{F}}^H_N \boldsymbol{z}^{\mathrm{f}}_{k'} = \boldsymbol{\mathcal{F}}^H_N \boldsymbol{W}^H_{k'} \boldsymbol{H}^{\mathrm{f}}_{k'} \boldsymbol{\mathcal{F}}_N \boldsymbol{x}^{\mathrm{t}}_{k'} + \boldsymbol{n}^{\mathrm{t}}_{k'}, \tag{2.32}$$

where we have $\boldsymbol{n}^{\mathrm{t}}_{k'} = \boldsymbol{\mathcal{F}}^H_N \boldsymbol{W}^H_{k'} \boldsymbol{\mathcal{P}}^T_{k'} \boldsymbol{\mathcal{F}}_U \tilde{\boldsymbol{n}}^{\mathrm{t}}$. Therefore, the symbols of the k'-th user can be detected from Eq. (2.32) and channel decoding using BICM-ID may be carried out.

2.2.4 Expression of the Signal-to-Interference-plus-Noise Ratio

Since knowledge of the *signal-to-interference-plus-noise ratio* (SINR) is beneficial for the receiver, below we derive the SINR expression of SC-FDMA using the MMSE-FDE. In Eq. (2.32), we let [142]

$$\boldsymbol{A}^{\mathrm{t}}_{k'} = \boldsymbol{\mathcal{F}}^H_N \boldsymbol{W}^H_{k'} \boldsymbol{H}^{\mathrm{f}}_{k'} \boldsymbol{\mathcal{F}}_N. \tag{2.33}$$

Then, it may be readily shown that the relationship between $\boldsymbol{x}^{\mathrm{t}}_{k'}$ and its estimate $\boldsymbol{z}^{\mathrm{t}}_{k'}$ is given by the diagonal elements of the matrix $\boldsymbol{A}^{\mathrm{t}}_{k'}$, formulated as

$$A_{k'} = a^{\mathrm{t}}_{k',(n,n)} = \frac{1}{N} \sum_{n'=0}^{N-1} w^*_{k',n'} h^{\mathrm{f}}_{k',n'}, \tag{2.34}$$

which are independent of the index n, hence, we have the same value for $n = 0, 1, \cdots, N-1$. In this case, from Eq. (2.32) we arrive at

$$\boldsymbol{z}^{\mathrm{t}}_{k'} = A_{k'} \boldsymbol{x}^{\mathrm{t}}_{k'} + \left(\boldsymbol{A}^{\mathrm{t}}_{k'} - A_{k'} \boldsymbol{I}_N \right) \boldsymbol{x}^{\mathrm{t}}_{k'} + \boldsymbol{n}^{\mathrm{t}}_{k'}, \tag{2.35}$$

where the first term is the desired one, while the second term represents the *residual* ISI. Hence, the SINR $\gamma_{k'}$, which determines the detection reliability of user k' can be expressed as [143, 144]

$$\gamma_{k'} = \left[\left(\frac{1}{N} \sum_{n'=0}^{N-1} \frac{|h^{\mathrm{f}}_{k',n'}|^2}{|h^{\mathrm{f}}_{k',n'}|^2 + \sigma^2_{\mathrm{N}}/P} \right)^{-1} - 1 \right]^{-1} = \left(\frac{1}{N} \sum_{n'=0}^{N-1} \frac{1}{\gamma_{k',n'} + 1} \right)^{-1} - 1, \tag{2.36}$$

where $\gamma_{k',n'} = P|h^{\mathrm{f}}_{k'n'}|^2/\sigma^2_N$ denotes the SNR in the n'-th subband of the k'-th user.

Moreover, the normalised estimation error vector $\boldsymbol{e}_{k'}^{\mathrm{t}}$ between the transmitted signal $\boldsymbol{x}_{k'}^{\mathrm{t}}$ and the estimated signal $\boldsymbol{z}_{k'}^{\mathrm{t}}$ may be expressed as

$$\begin{aligned}\boldsymbol{e}_{k'}^{\mathrm{t}} &= \frac{1}{\sqrt{P}}(\boldsymbol{x}_{k'}^{\mathrm{t}} - \boldsymbol{z}_{k'}^{\mathrm{t}}) = \frac{1}{\sqrt{P}}(\boldsymbol{x}_{k'}^{\mathrm{t}} - \boldsymbol{A}_{k'}^{\mathrm{t}}\boldsymbol{x}_{k'}^{\mathrm{t}} - \boldsymbol{n}_{k'}^{\mathrm{t}}) \\ &= \frac{1 - A_{k'}}{\sqrt{P}}\boldsymbol{x}_{k'}^{\mathrm{t}} - \frac{1}{\sqrt{P}}(\boldsymbol{A}_{k'}^{\mathrm{t}} - A_{k'}\boldsymbol{I}_N)\boldsymbol{x}_{k'}^{\mathrm{t}} - \frac{1}{\sqrt{P}}\boldsymbol{n}_{k'}^{\mathrm{t}}.\end{aligned} \tag{2.37}$$

The covariance matrix of $\boldsymbol{e}_{k'}^{\mathrm{t}}$ is given by

$$\boldsymbol{R}_{e_{k'}^{\mathrm{t}}} = \mathrm{E}[\boldsymbol{e}_{k'}^{\mathrm{t}}(\boldsymbol{e}_{k'}^{\mathrm{t}})^H] = \left[\boldsymbol{I}_N - 2\Re\{\boldsymbol{A}_{k'}^{\mathrm{t}}\} + \boldsymbol{A}_{k'}^{\mathrm{t}}(\boldsymbol{A}_{k'}^{\mathrm{t}})^H\right] + \frac{\sigma_{\mathrm{N}}^2}{P}\boldsymbol{I}_N, \tag{2.38}$$

with $\Re\{\boldsymbol{A}_{k'}^{\mathrm{t}}\}$ denoting the real part of $\boldsymbol{A}_{k'}^{\mathrm{t}}$. It can be shown that, $\boldsymbol{R}_{e_{k'}^{\mathrm{t}}}$ is also a $(N\times N)$-element circulant matrix having identical diagonal elements. This implies that due to the averaging effect of the N-point IDFT operation, all the k-th users' resultant TD symbols within the vector have the same MMSE value $e_{k'}$. This MMSE value can be calculated as the average of the FD MMSE values over N subbands, yielding

$$e_{k'} = \frac{1}{N}\sum_{n'=0}^{N-1} e_{k',n'} = \frac{1}{N}\sum_{n'=0}^{N-1}\frac{1}{\gamma_{k',n'}+1}, \tag{2.39}$$

where $e_{k',n'}$ is the MMSE of the n'-th subband of user k'.

Finally, upon comparing Eq. (2.36) to Eq. (2.39), we can see that the overall SINR in Eq. (2.36) and the MMSE in Eq. (2.39) satisfy the relationship of

$$\gamma_{k'} = e_{k'}^{-1} - 1, \tag{2.40}$$

which is a general result for the optimum MMSE solution [102, 145].

2.2.5 Comparison of OFDMA and TFD SC-FDMA Schemes

In Table 2.3, the major differences among OFDMA and the TFD SC-FDMA schemes are summarised, where both the LFDMA and IFDMA are considered. Let us explain the table in detail [91, 102, 129, 132].

1. Both the OFDMA and SC-FDMA adopt the IDFT/DFT for multi-carrier modulation/demodulation at the transmitter/receiver, respectively. However, in SC-FDMA, the DFT-based spreading operation seen in the transmitter of Figure 2.8 results in single-carrier transmission for SC-FDMA. By contrast, the OFDMA scheme transmits all the subcarriers in parallel simultaneously.

TABLE 2.3: Comparison of OFDMA, TFD SC-FDMA (LFDMA and IFDMA) schemes

	OFDMA	LFDMA	IFDMA
Transmitter	IDFT	DFT, IDFT	
Receiver	DFT	DFT, IDFT	
Complexity	Similar		
MUI	Non		
ISI	Non-ISI between two OFDMA/SC-FDMA symbols by using CP		
Residual ISI	Absence	Presence, unless using ZF-FDE	
Transmission	Parallel	Serial	
Carrier modulation	Multi-carrier	Single-carrier	
Involved subcarriers	U subcarriers	1 or 3 subcarriers	1 subcarrier
PAPR	Highest	Very low	Lowest
Symbol duration	$NT_s = T_v$	T_s (M chip duration)	T_s/M (1 chip duration)
Symbol bandwidth	B/N (compressed)	B (localised)	MB (distributed)
Frequency diversity gain	Non, unless FEC	Limited	Significant
Multiuser scheduling gain	Significant	Sufficient	Limited
Mobility scenario (speed)	Depends (scheduling)	Low (scheduling)	High
Channel estimation	Depends (subc. mapp.)	Low overhead	High overhead

2. Both the OFDMA and SC-FDMA schemes are free from *multi-user interference* (MUI), owing to the orthogonal subcarrier/subband mapping scheme of the users supported.

3. The CP-based technique is employed by both OFDMA and SC-FDMA transmissions in order to suppress the effects of ISI.

4. Symbols within one data block do not interfere with each other in the OFDMA system. However, due to the IDFT operation used at the receiver of Figure 2.12, the symbols in one block may interfere with each other in the SC-FDMA systems, when the channel's fading becomes frequency selective.

5. Both the LFDMA and IFDMA schemes may achieve a certain diversity gain in the presence of frequency-selective fading. Nevertheless, this frequency-diversity gain is only achievable, when the residual ISI is efficiently mitigated, for example with the aid of the MMSE based FDE schemes of Figure 2.12. By contrast, frequency-diversity is not inherent in the OFDM(A) systems of Figure 2.1, unless the same symbols are mapped to several independently fading subcarriers, which reduces the throughput. Similar to the OFDM, a frequency diversity gain may be also achieved, when OFDMA is combined with other techniques, such as channel coding/interleaving [55] or multi-user scheduling [58].

6. In the IFDMA scheme, each user's symbols are evenly distributed over the entire frequency band of the system, while in LFDMA, the symbols of a user are conveyed by a set of consecutive subbands. Therefore, the achievable frequency-diversity gain of the IFDMA system is typically higher than that of the LFDMA system. By contrast, multi-user scheduling can be efficiently carried out in the context of the LFDMA

system, since the co-located subbands may be allocated to the most appropriate frequency bands associated with a high channel gain. Additionally, similar to OFDMA, multi-user scheduling may be invoked by the LFDMA scheme in order to attain a higher *multi-user diversity* gain than that of the IFDMA system.

7. Multi-user scheduling may be carried out, when communicating over slowly fading correlated channels corresponding to a relatively low Doppler frequency. Otherwise, the overhead imposed by the reference symbols or pilots, which is required for channel estimation will be increased in order to obtain an accurate CSI estimate. As a result, the spectral efficiency of the LFDMA or OFDMA system may degrade, when the MTs travel at a higher speed.

8. In order to carry out the FDE operation of Figure 2.12, channel estimation is required. It can be shown that in a given mobility scenario associated with a specific multi-path power delay profile, the LFDMA system may require a lower channel estimation overhead than IFDMA, since the co-located subbands of LFDMA experience correlated fading, while the distributed subbands of IFDMA may experience independent fading.

9. In the OFDMA system all the subcarriers are transmitted simultaneously, leading to a high PAPR. In comparison to OFDMA, the PAPR of LFDMA is substantially decreased, since either one or three subcarriers are transmitted as seen in Figure 2.10(a) in terms of Eq. (2.24a) and Eq. (2.24a). Among the three schemes, IFDMA guarantees the lowest PAPR, since only one subcarrier is transmitted at any time as shown in Figure 2.10(b) according to Eq. (2.25). The PAPR of the OFDMA, IFDMA and the LFDMA schemes were quantified in [91].

10. As a benefit of its diversity gain, SC-FDMA - especially the IFDMA scheme - outperforms the OFDMA scheme in terms of its achievable *bit-error rate* (BER) performance [102], when no other BER enhancement techniques are invoked. The IFDMA arrangement outperforms LFDMA in terms of both its BER and the *block-error rate* (BLER) performance, when operating without the assistance of other techniques [146].

Let us now consider the basic principles of the BICM.

2.3 Bit-Interleaved Coded Modulation Using Iterative Decoding

Coded modulation schemes may be classified into two main categories in terms of their symbol generation techniques [92]. The first category uses the symbol-based interleaving,

which is referred to as *trellis-coded modulation* (TCM). The TCM concept was originally proposed by Ungerboeck in [147] for Gaussian channels and then it was further developed for fading channels in [148–150]. The TCM schemes have also been introduced as component codes into the generalised parallel-concatenated turbo code structure, forming the class of *turbo trellis-coded modulation* (TTCM) [151]. In both TCM and TTCM, the so-called *set-partitioning* (SP) based signal labelling [150] is adopted to map the encoded bits to the modulated symbols by ensuring that the constellation points that are unprotected are far apart, while the points in each other's close proximity are error correction coded. Again, the SP-based labelling guarantees maximising the minimum Euclidean distance among the unprotected constellation points, hence providing a low error probability even without error correction coding.

With the aim of increasing the diversity order of TCM schemes, the second family of coded modulation schemes was conceived by invoking bit-based interleaving, which is known as *bit-interleaved coded modulation* (BICM) and was proposed by Zehavi in [152]. In the BICM scheme Gray labelling is employed. In [153–155], a comprehensive investigation of BICM has been provided in the context of a general information-theoretic framework, along with a range of design guidelines. When the BICM philosophy is combined with *iterative decoding* (ID), the BICM-ID scheme is conceived, which was originally proposed by Li [97, 98]. The BICM-ID scheme also adopts SP-based labelling, which has an increased Euclidean distance in comparison to Gray labelling . BICM has been widely studied in the literature, for example in [156–162]. Focusing our attention on multi-carrier systems, in [106] a TFD BICM scheme has been proposed for OFDM in order to achieve both time- and frequency-diversity for transmission over broadband time-varying channels. Detailed performance comparison of BICM-aided SC-FDE and BICM-aided OFDM have been provided in [163], when communicating over interference-infested channels. Additionally, multi-level BICM schemes conceived for SC-FDE systems have been studied in [135, 164].

In Ungerboeck's original TCM schemes [147] the *forward error correction* (FEC) codes were *recursive systematic convolutional* (RSC) codes. They were replaced by non-systematic convolutional (NSC) codes in the original BICM arrangement of [152]. In this thesis, the BICM-ID used will invoke either RSC component codes as in TCM for the sake of improving the achievable power-efficiency.

2.3.1 BICM Encoding

The BICM encoder is shown in Figure 2.13. Specifically, at the k-th MT, ($k = 0, 1, \cdots, K-1$), the N_{b}-length binary source data stream $\boldsymbol{b}_k^{\mathrm{o}}$ is initially encoded by an outer FEC code having a coding rate of R_{c}, generating N_{c} coded bits. Then, the outer encoded bit frame

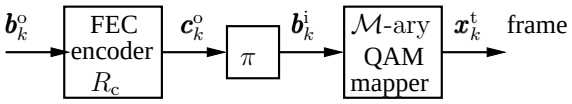

FIGURE 2.13: Block diagram of the BICM encoder.

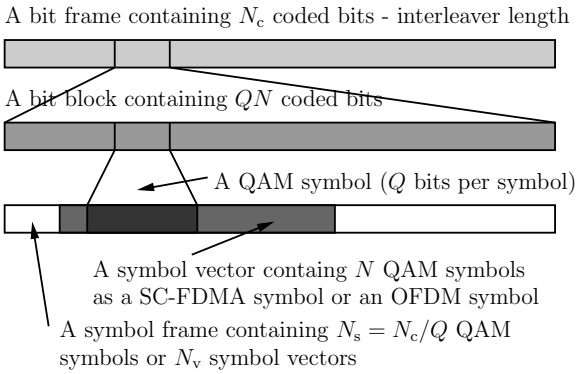

FIGURE 2.14: Transmission frame structure in terms of bits and symbols.

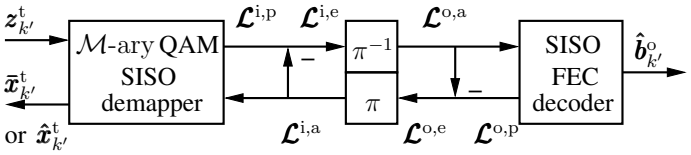

FIGURE 2.15: Schematic diagram of BICM decoder using iterative decoding. The encoder was shown in Figure 2.13, and the transmission frame structure is portrayed in Figure 2.14.

$\boldsymbol{c}_k^{\mathrm{o}}$ is interleaved by a N_{c}-length random bit-based interleaver π and its output bit frame $\boldsymbol{b}_k^{\mathrm{i}} = [(\boldsymbol{b}_{k,0}^{\mathrm{i}})^T, (\boldsymbol{b}_{k,1}^{\mathrm{i}})^T, \cdots, (\boldsymbol{b}_{k,(N_{\mathrm{s}}-1)}^{\mathrm{i}})^T]^T$ is fed into the $\mathcal{M}$-ary QAM mapper for transmitting Q bits per symbol, where we have $N_{\mathrm{s}} = N_{\mathrm{c}}/Q$ and $\mathcal{M} = 2^Q$. Hence, the N_{c}-length bit sequence $\boldsymbol{b}_k^{\mathrm{i}}$ of Figure 2.13 is partitioned into N_{s} segments $\boldsymbol{b}_{k,n_{\mathrm{s}}}^{\mathrm{i}}$, $n_{\mathrm{s}} = 0, 1, \cdots, N_{\mathrm{s}} - 1$, each having Q bits. Moreover, the N_{s} modulated symbols are converted to N_{v} symbol vectors expressed as $\boldsymbol{x}_k^{\mathrm{t}}[n_{\mathrm{v}}]$, (or $\boldsymbol{x}_k^{\mathrm{f}}[n_{\mathrm{v}}]$, $\boldsymbol{x}^{\mathrm{t}}[n_{\mathrm{v}}]$), $n_{\mathrm{v}} = 0, 1, \cdots, N_{\mathrm{v}} - 1$, each of which contains N symbols $x_{k,n}^{\mathrm{t}}[n_{\mathrm{v}}]$ (or $x_{k,n}^{\mathrm{f}}[n_{\mathrm{v}}]$, $x_n^{\mathrm{t}}[n_{\mathrm{v}}]$), $(n = 0, 1, \cdots, N - 1)$, that are transmitted by a single SC-FDMA (or OFDM, SC-FDE) symbol. Note that, the index n_{v} mentioned above corresponds to the index i used in Figures 2.2, 2.3, 2.8(b) and 2.12(b).

2.3.2 Iterative Decoding of BICM

The BICM-ID decoder considered is similar to that detailed in [92], which employs an $\mathcal{M}$-ary symbol-to-bits *soft-input soft-output* (SISO) demapper, a bit-wise random interleaver and deinterleaver, as well as a SISO FEC decoder, as shown in Figure 2.15. When non-iterative detection is invoked, the BICM-ID decoder automatically becomes a BICM decoder, operating without a feedback loop. Below we detail the BICM-ID scheme. In Section 2.3.2.1, the

Gaussian approximation of the received constellation symbols' *probability density function* (PDF) is introduced for characterising the distribution of the decision variables. Then, the soft-information conversion from symbol-to-bit-probabilities as well as the iterative detection mechanism, are addressed in Section 2.3.2.2 and Section 2.3.2.3, respectively. Finally, in Section 2.3.2.4, we detail the soft-estimation of the transmitted symbols. For detailed discussions on turbo detection in general, and BICM-ID in particular, please refer to [92].

2.3.2.1 Distribution of the BICM Decision Variables

As discussed in Section 2.2.3, after equalisation was carried out in the FD, the final decision variable vector is given by $\boldsymbol{z}^{\mathrm{t}}_{k'}$ for user k'. As shown in Figure 2.15, the vector $\boldsymbol{z}^{\mathrm{t}}_{k'}$ is input to the $\mathcal{M}$-QAM SISO demapper. According to [145, 165], the element $z^{\mathrm{t}}_{k',n}$ of $\boldsymbol{z}^{\mathrm{t}}_{k'}$ can be approximated by a complex-valued Gaussian random variable $\mathcal{CN} \sim (\mu_{k',n}, \sigma^2_{k',n})$, which has the PDF expressed as

$$f(z^{\mathrm{t}}_{k',n}|x^{\mathrm{t}}_{k',n} = \mathsf{s}_i) = \frac{1}{\sqrt{\pi}\sigma_{k',n}} \exp \frac{-|z^{\mathrm{t}}_{k'} - \mu_{k',n}|^2}{\sigma^2_{k',n}}, \tag{2.41}$$

where the mean and variance of $z^{\mathrm{t}}_{k',n}$ are given by

$$\mu_{k',n} = \mathrm{E}[z_{k',n}|x_{k',n} = \mathsf{s}_i] \quad \sigma^2_{k',n} = \mathrm{Var}[z_{k',n}|x_{k',n} = \mathsf{s}_i], \tag{2.42}$$

and $i = 0, 1, \cdots, \mathcal{M} - 1$ denotes the symbol index of constellation points.

2.3.2.2 Iterative Joint Demapping and Decoding Mechanism

Given the mean and variance of $\mu_{k',n}$ and $\sigma^2_{k',n}$ for each of the $\mathcal{M}$-QAM symbols, the demapper of Figure 2.15 is capable of converting the *symbol probabilities* to the *bit probabilities*, yielding the *a-posteriori probabilities* in form of their *logarithmic-likelihood ratio* (LLR) representations $\boldsymbol{\mathcal{L}}^{\mathrm{i,p}}$ for the FEC-coded bits in frame $\boldsymbol{b}^{\mathrm{i}}_{k'}$. As shown in Figure 2.15, the notation $\boldsymbol{\mathcal{L}}^{(.)}(.)$ represents the LLRs of the bit frame of Figure 2.14, where the superscript $^{\mathrm{i}}$ relates to the *inner* BICM demapper, while $^{\mathrm{o}}$ corresponds to the *outer* FEC decoder. Additionally, the superscripts $^{\mathrm{a}}$, $^{\mathrm{p}}$ and $^{\mathrm{e}}$ denote the nature of the LLRs, with a, p and e indicating *a-priori*, *a-posteriori* and *extrinsic* LLRs, respectively. As shown in Figure 2.15, the *a-priori* information $\boldsymbol{\mathcal{L}}^{\mathrm{i,a}}(\boldsymbol{b}^{\mathrm{i}}_{k'})$ provided by the BICM demapper is subtracted from the *a-posteriori* information $\boldsymbol{\mathcal{L}}^{\mathrm{i,p}}(\boldsymbol{b}^{\mathrm{i}}_{k'})$, in order to generate the *extrinsic* information $\boldsymbol{\mathcal{L}}^{\mathrm{i,e}}(\boldsymbol{b}^{\mathrm{i}}_{k'})$. Then, this *extrinsic* information is de-interleaved by the random soft-bit de-interleaver π^{-1} of Figure 2.15, yielding $\boldsymbol{\mathcal{L}}^{\mathrm{o,a}}(\boldsymbol{c}^{\mathrm{o}}_{k'})$, which is passed to the outer FEC decoder as the *a-priori* information for the coded bits $\boldsymbol{c}^{\mathrm{o}}_{k'}$. Based on $\boldsymbol{\mathcal{L}}^{\mathrm{o,a}}(\boldsymbol{c}^{\mathrm{o}}_{k'})$, the outer FEC decoder of Fig-

ure 2.15 computes the corresponding *a-posteriori* LLR values $\boldsymbol{\mathcal{L}}^{\mathrm{o,p}}(\boldsymbol{c}^{\mathrm{o}}_{k'})$ with the aid of the *Bahl-Cocke-Jelinek-Raviv* (BCJR) algorithm [166] or the *logarithmic maximum a-posteriori probability* (Log-MAP) algorithm [92, 167], etc.

During the soft decision feedback phase of Figure 2.15, the *extrinsic* LLRs $\boldsymbol{\mathcal{L}}^{\mathrm{o,e}}(\boldsymbol{c}^{\mathrm{o}}_{k'})$ are generated by subtracting the *a-priori* LLRs $\boldsymbol{\mathcal{L}}^{\mathrm{o,a}}(\boldsymbol{c}^{\mathrm{o}}_{k'})$ from the *a-posteriori* LLRs $\boldsymbol{\mathcal{L}}^{\mathrm{o,p}}(\boldsymbol{c}^{\mathrm{o}}_{k'})$. Then, the LLRs $\boldsymbol{\mathcal{L}}^{\mathrm{o,p}}(\boldsymbol{c}^{\mathrm{o}}_{k'})$ are fed back to the inner demapper as the *a-priori* LLRs $\boldsymbol{\mathcal{L}}^{\mathrm{i,a}}(\boldsymbol{b}^{\mathrm{i}}_{k'})$ after appropriately reordering them using the soft-bit interleaver π, as portrayed in Figure 2.15. Using the information provided by $\boldsymbol{\mathcal{L}}^{\mathrm{i,a}}(\boldsymbol{b}^{\mathrm{i}}_{k'})$, the SISO demapper can re-calculate the *a-posteriori* LLRs $\boldsymbol{\mathcal{L}}^{\mathrm{i,p}}(\boldsymbol{b}^{\mathrm{i}}_{k'})$ for the next iteration. Additionally, based on the *a-priori* LLRs $\boldsymbol{\mathcal{L}}^{\mathrm{i,a}}(\boldsymbol{b}^{\mathrm{i}}_{k'})$, the BICM demapper may also compute the soft estimates $\bar{\boldsymbol{x}}^{\mathrm{t}}_{k'}$ of the transmitted symbols for further processing by *frequency-domain turbo equalisation* [90], which will be adopted for SC-FDMA in Chapter 5.

2.3.2.3 Logarithmic-Likelihood-Ratio of SISO Demapper

In order to calculate the LLRs with respect to the n_{v}-th symbol vector $\boldsymbol{z}^{\mathrm{t}}_{k'}[n_{\mathrm{v}}]$, observe with reference to the frame structure of Figure 2.14 that the ι-th element of $\boldsymbol{\mathcal{L}}^{\mathrm{i,a}}(\boldsymbol{b}^{\mathrm{i}}_{k'})$, $\boldsymbol{\mathcal{L}}^{\mathrm{i,p}}(\boldsymbol{b}^{\mathrm{i}}_{k'})$ and $\boldsymbol{\mathcal{L}}^{\mathrm{i,e}}(\boldsymbol{b}^{\mathrm{i}}_{k'})$ may be represented by the $(nQ+q)$-th elements of the n_{v}-th segment in $\boldsymbol{\mathcal{L}}^{\mathrm{i,a}}(\boldsymbol{b}^{\mathrm{i}}_{k'})$, $\boldsymbol{\mathcal{L}}^{\mathrm{i,p}}(\boldsymbol{b}^{\mathrm{i}}_{k'})$ and $\boldsymbol{\mathcal{L}}^{\mathrm{i,e}}(\boldsymbol{b}^{\mathrm{i}}_{k'})$, where $\iota = (n_{\mathrm{v}}N+n)Q+q$. Hence, we have $\mathcal{L}^{\mathrm{i},(\cdot)}_{k',\iota} = \mathcal{L}^{\mathrm{i},(\cdot)}_{k',(nQ+q)}[n_{\mathrm{v}}]$, where again, the notation $(\cdot)$ represents 'a', 'p' or 'e' for the *a-priori*, *a-posteriori*, or *extrinsic* information, respectively. Furthermore, the LLRs $\mathcal{L}^{\mathrm{i,a}}_{k',\iota}$, $\mathcal{L}^{\mathrm{i,p}}_{k',\iota}$ and $\mathcal{L}^{\mathrm{i,e}}_{k',\iota}$ correspond to the q-th *a-priori*, *a-posteriori* and *extrinsic* LLRs of the bit vector $\boldsymbol{b}^{\mathrm{i}}_{k',n_{\mathrm{s}}}$, where we have $n_{\mathrm{s}} = n_{\mathrm{v}}N+n$ for $n_{\mathrm{s}} = 0, 1, \cdots, N_{\mathrm{s}}-1$, $n = 0, 1, \cdots, N-1$ and $q = 0, 1, \cdots, Q-1$. Specifically, the *a-priori* LLR value can be expressed as [92]

$$\mathcal{L}^{\mathrm{i,a}}_{k',\iota} = \ln\left[\frac{P(b^{\mathrm{i}}_{k',n_{\mathrm{s}},q}=0)}{P(b^{\mathrm{i}}_{k',n_{\mathrm{s}},q}=1)}\right], \quad n_{\mathrm{s}} = 0, 1, \cdots, N_{\mathrm{s}}-1, \tag{2.43}$$

and the *a-posteriori* LLR values may be formulated as [90, 92]

$$\mathcal{L}^{\mathrm{i,p}}_{k',\iota} = \ln\left[\frac{P(b^{\mathrm{i}}_{k',n_{\mathrm{s}},q}=0|z^{\mathrm{t}}_{k',n}[n_{\mathrm{v}}])}{P(b^{\mathrm{i}}_{k',n_{\mathrm{s}},q}=1|z^{\mathrm{t}}_{k',n}[n_{\mathrm{v}}])}\right] = \ln\left[\frac{\sum_{\forall \boldsymbol{b}^{\mathrm{i}}_{k',n_{\mathrm{s}}}:b^{\mathrm{i}}_{n_{\mathrm{s}},q}=0} f(z^{\mathrm{t}}_{k',n}[n_{\mathrm{v}}]|\boldsymbol{b}^{\mathrm{i}}_{k',n_{\mathrm{s}}})P(\boldsymbol{b}^{\mathrm{i}}_{k',n_{\mathrm{s}}})}{\sum_{\forall \boldsymbol{b}^{\mathrm{i}}_{k',n_{\mathrm{s}}}:b^{\mathrm{i}}_{n_{\mathrm{s}},q}=1} f(z^{\mathrm{t}}_{k',n}[n_{\mathrm{v}}]|\boldsymbol{b}^{\mathrm{i}}_{k',n_{\mathrm{s}}})P(\boldsymbol{b}^{\mathrm{i}}_{k',n_{\mathrm{s}}})}\right], \tag{2.44}$$

for $n_{\mathrm{s}} = 0, 1, \cdots, N_{\mathrm{s}}-1$.

Based on (2.43) and (2.44), the corresponding *extrinsic* LLRs are given by [90, 92]

$$\mathcal{L}^{\mathrm{i,e}}_{k',\iota} = \mathcal{L}^{\mathrm{i,p}}_{k',\iota} - \mathcal{L}^{\mathrm{i,a}}_{k',\iota} = \ln\left[\frac{\sum_{\forall \mathbf{b}_i:\mathrm{b}_{i,q}=0} \exp\left(-\varrho_{n_{\mathrm{s}},i} + \frac{1}{2}\mathring{\mathbf{b}}^T_{i,\lceil q\rceil}\boldsymbol{\mathcal{L}}^{\mathrm{i,a}}_{k,n_{\mathrm{s}},\lceil q\rceil}\right)}{\sum_{\forall \mathbf{b}_i:\mathrm{b}_{i,q}=1} \exp\left(-\varrho_{n_{\mathrm{s}},i} + \frac{1}{2}\mathring{\mathbf{b}}^T_{i,\lceil q\rceil}\boldsymbol{\mathcal{L}}^{\mathrm{i,a}}_{k,n_{\mathrm{s}},\lceil q\rceil}\right)}\right], \tag{2.45}$$

for $n_s = 0, 1, \cdots, N_s - 1$, where the Q-element vector $\mathbf{b}_i$ contains the bits of the i-th symbol in the $\mathcal{M}$-QAM constellation $\mathcal{S}$ and the q-th element of $\mathbf{b}_i$ is given by

$$\mathring{\mathsf{b}}_{i,q} = \begin{cases} +1, & \mathsf{b}_{i,q} = 0, \\ -1, & \mathsf{b}_{i,q} = 1. \end{cases} \tag{2.46}$$

Moreover, in Eq. (2.45), $\mathring{\mathbf{b}}_{i,\lceil q \rceil}$ denotes the subvector obtained from $\mathring{\mathbf{b}}_i$ by omitting its q-th element $\mathring{\mathsf{b}}_{i,q}$, while $\boldsymbol{\mathcal{L}}^{\mathrm{i,a}}_{k,n_s,\lceil q \rceil}$ denotes the corresponding vector holding all the *a-priori* LLR values $\boldsymbol{\mathcal{L}}^{\mathrm{api}}_{k,n_s}$, except for the q-th element $\mathcal{L}^{\mathrm{i,a}}_{k,(n_s Q+q)}$. Additionally, in Eq. (2.45), $\varrho_{n_s,i}$ is given by

$$\varrho_{n_s,i} = \frac{|z^{\mathrm{t}}_{k',n} - \mu_{n,i}|^2}{\sigma^2_{n,i}}, \tag{2.47}$$

where $\mu_{n,i}$ and $\sigma^2_{n,i}$ were defined in Eq. (2.42).

2.3.2.4 Soft-Estimation of the Transmitted Symbol

In order to generate the soft-estimates of the modulated symbols, the corresponding bit probabilities given by the *a-priori* LLR values are first converted to the symbol probabilities. Let $P(x^{\mathrm{t}}_{k',n} = \mathsf{s}_i)$ represent the probability that we have $x^{\mathrm{t}}_{k',n} = \mathsf{s}_i$ for the i-th $\mathcal{M}$-QAM symbol, which may be obtained from the bit probabilities $P(b_{n_s,q} = \mathsf{b}_{i,q})$ for $q = 0, 1, \cdots, Q-1$, as their product, provided that the bit-interleavers are sufficiently long for ensuring the independence of the bits, yielding [92]

$$P(x^{\mathrm{t}}_{k',n} = \mathsf{s}_i) = \prod_{q=0}^{Q-1} P(b_{n_s,q} = \mathsf{b}_{i,q}) = \prod_{q=0}^{Q-1} \frac{1}{2} \left(1 + \mathring{\mathsf{b}}_{i,q} \tanh \frac{\mathcal{L}^{\mathrm{i,a}}_{k',(n_s Q+q)}}{2} \right), \tag{2.48}$$

where $n_s = n_v N + n$, $n_s = 0, 1, \cdots, N_s - 1$ and $n = 0, 1, \cdots, N-1$. Then, the soft-estimated $\bar{x}^{\mathrm{t}}_{k'}$ of the transmitted symbol $x^{\mathrm{t}}_{k'}$ can be expressed as

$$\bar{x}^{\mathrm{t}}_{k',n} = \mathrm{E}[x^{\mathrm{t}}_{k',n}] = \sum_{\mathsf{s}_i \in \mathcal{S}} \mathsf{s}_i \cdot P(x^{\mathrm{t}}_{k',n} = \mathsf{s}_i), \quad n = 0, 1, \cdots, N-1. \tag{2.49}$$

2.4 Summary

In Sections 2.1, 2.2 and 2.3 we have reviewed the basic principles of the OFDM, SC-FDMA and BICM-ID techniques, respectively. Comparisons of these schemes have also been carried out in Section 2.2.5.

We have shown that OFDM is capable of reducing the effects of ISI with the aid of the CP. However, as argued in Section 2.1.4, it transmits all the subcarriers simultaneously,

hence yielding a high PAPR. Furthermore, the OFDM scheme is in general unable to attain frequency-diversity and time-diversity, in the absence of FEC coding and inter-subcarrier interleaving or subcarrier-repetition, which reduces the throughput.

In the SC-FDE scheme of Figure 2.4, single-carrier TD signals are transmitted, hence, the OFDM-specific PAPR problem is eliminated. At the receiver of the SC-FDE, invoking DFT and IDFT allows low-complexity single-tap equalisation to be carried out in the FD. Therefore, both the joint complexity of the equaliser, DFT and IDFT may be reduced in comparison to the conventional TD equaliser having a high number of taps. However, residual ISI may exist, when non-ZF types of FD equalisers are employed.

The SC-FDMA is also capable of maintaining a low PAPR compared to multi-carrier modulation schemes, hence they are suitable for high-rate uplink transmissions. As argued in Section 2.2.1, the implementation complexity of the TD SC-FDMA transmitter of Figure 2.5 is lower than that of the TFD SC-FDMA transmitter, which invokes the DFT-spread OFDMA structure of Figure 2.8(a). The receiver complexity of both the TD SC-FDMA and TFD SC-FDMA is the same. However, the TFD SC-FDMA transmitter benefits from a more flexible reconfigurable transceiver architecture, which is capable of combining the advantages of both the LFDMA signalling of Figure 2.5(a) and of the IFDMA scheme of Figure 2.5(b). Both the LFDMA and IFDMA versions of the TFD SC-FDMA systems discussed in Section 2.2.2 may achieve some diversity gain, in the presence of frequency-selective fading. Indeed, IFDMA is capable of achieving the maximum attainable frequency-diversity in dispersive multi-path fading channels. By contrast, the LFDMA has degraded frequency diversity in comparison to the IFDMA. However, the LFDMA scheme has to invoke intelligent symbol-to-subband allocation schemes or multi-user scheduling in order to achieve the multi-user diversity. Nevertheless, as argued in Section 2.2.5, for both the LFDMA and IFDMA, the frequency-diversity gain is only achievable, when the residual ISI was efficiently mitigated.

The introduction of BICM to the OFDM, SC-FDMA, etc, systems enjoys various benefits. Firstly, FEC coding gain may be attained. Secondly, BICM was designed for increasing the time-diversity gain of coded modulation in order to mitigate the effects of fading. It was shown in [92] that given a total complexity of 64 trellis states, BICM-ID outperforms BICM in both AWGN and uncorrelated fading channels. It was also shown in [92] that as expected, the performance of BICM is dependent on the interleaver length in correlated fading channels, but not in uncorrelated fading, which models an infinite-interleaver scenario. By contrast, the error performance of BICM-ID is highly dependent on the interleaver length in both AWGN and correlated fading channels.

In the following chapters, we will simply refer to the TFD SC-FDMA as SC-FDMA. In the

next chapter, we will investigate the the single-relay assisted amplify-and-forward cooperative SC-FDMA for multi-user uplink transmissions.

Chapter 3

Single-Relay Assisted Amplify-and-Forward Cooperative SC-FDMA Uplink

3.1 Introduction

As alluded to in Chapter 1, cooperative communications and relaying have attracted substantial research attention over the past decade as a benefit of their *spatial diversity gain* attained in a virtual *multiple-input multiple-output* (MIMO) scenario created by the distributed single-antenna terminals by sharing resources with their cooperative partners. This cooperation allows the system to mitigate the radio channel's fading by jointly exploiting the benefits of *frequency-*, *time-* and *spatial-diversity*. Furthermore, the cooperative strategy may also be used to increase the attainable system capacity [37, 39, 40, 46]. Recently, the diversity-multiplexing trade-off encountered in *multiple-access amplify-and-forward* relaying was considered for transmission over block fading channels in [168]. Moreover, both the single-user and multi-user performance of relay-assisted *direct-sequence code-division multiple-access* (DS-CDMA) was discussed in [63, 169, 170]. The relay-based *single-carrier modulated frequency-domain equalisation* (SC-FDE) [94, 171] aided *space-frequency block coding* assisted interleave-division multiple-access uplink was investigated in [136, 172, 173]. Prior studies considered relay-aided cooperation both in a single-user and in a multi-user context, but their employment was typically restricted to transmission over frequency-flat fading channels. Naturally, at high bit rates the channel becomes frequency-selective and hence its deleterious effects have to be mitigated. Furthermore, both the *multi-user interference* (MUI) and *inter-symbol interference* (ISI) should be cancelled. The associated

processing imposes a high complexity, especially when the number of users is high.

Against this background, in this chapter we investigate the cooperative diversity benefits achievable in the single-relay assisted *single-carrier frequency-division multiple-access* (SC-FDMA) uplink for transmission over frequency-selective fading channels. As we argued in Section 2.2.2, the SC-FDMA technique advocated adopts SC-FDE combined with orthogonal subcarrier mapping in order to support multiple users without contamination by MUI. Furthermore, our single-relay assisted SC-FDMA system allows user cooperation to achieve a diversity gain without imposing MUI by the cooperating sources and relays upon the uplink-receiver at the base station (BS). It is worth noting that SC-FDMA is capable of exploiting the benefits of multi-path diversity for transmission over broadband channels, while in *orthogonal frequency-division multiplexing* (OFDM) [55] introduced in Section 2.1, each subcarrier experiences flat-fading, hence no *frequency-selection diversity gain* is achieved. It has been indicated in Section 2.2.5 of Chapter 2 that SC-FDMA attains a similar overall performance as *orthogonal frequency division multiple access* (OFDMA), but it is more suitable for uplink transmission due to its lower *peak-to-average power ratio* (PAPR), which is typically high in multi-carrier systems [55, 91, 102]. Additionally, the combination of multi-carrier modulation with the *discrete Fourier transform* (DFT) and *inverse discrete Fourier transform* (IDFT) aided SC-FDMA can be adaptively reconfigured in order to mitigate the effects of time-variant channels. The system also benefits from cooperative communications. *Hence, our novel contribution in this chapter is that we design a sophisticated SC-FDMA scheme, for* ***amplify-and-forward*** *(AF) based single-relay assisted user cooperation aided uplink transmissions. Our simulation results show that cooperative diversity may be achieved for both the* ***single-dedicated-relaying*** *(SDR) and* ***single-shared-relaying*** *(SSR) strategies in both single-path and multi-path scenarios. As a result, the proposed subband-based AF scheme is combined with subband remapping at the relay. By contrast, the system invokes a minimum mean-square error (MMSE) assisted FD equaliser for each of the cooperative branches at the BS, where a simple* ***equal-gain combiner*** *(EGC) [100] is adopted in the TD. The resultant system is capable of achieving a multi-user performance, which is better than that of the conventional single-user AF protocol operating in a multi-path environment.*

This chapter is organised as follows. The system model of AF single-relay assisted SC-FDMA uplink is detailed in Section 3.2, including both direct transmission and relay channels. In Section 3.3, we propose subband-based AF aided cooperative relaying with subcarrier-remapping, which will be compared to conventional AF techniques in the context of both SDR and SSR schemes. Moreover, the MMSE assisted FDE schemes applied in both the direct and relaying branches are investigated for our proposed systems in Section 3.4. Additionally, we discuss our simulation results in Section 3.5 and finally conclude in Section 3.6.

3.2 System Models for Relay Assisted Cooperation

In the SC-FDMA system we investigated, K mobile terminals (MT) are active as information sources, while the inactive nodes act as relays. The AF-based relay simply amplifies the signal of each source without changing their carrier frequency. For the sake of separating multiple users in the *frequency-domain* (FD) and hence to avoid MUI, each source only selects a single relay node, which can be dedicated to a single user or may be shared by multiple users, based on the specific relaying topology shown in Figure 3.1 according to the SDR or SSR philosophy of Figure 3.1. Furthermore, we assume *time division duplexing* (TDD) in the perfectly synchronised system considered. Observe in Figure 3.1 that during the 1-st time slot (TS_1), all the K sources transmit their messages $\boldsymbol{s}_k^{\mathrm{S,t}}, (k = 0, 1, \cdots, K-1)$, which are simultaneously received by the relay(s) and by the BS via the *source-to-relay* (S-R) and the *source-to-destination* (S-D) link, respectively. Then, during the 2-nd time slot (TS_2), the relay forwards its received signal to the BS via the *relay-to-destination* (R-D) link according to the specific cooperative strategies to be described in Section 3.3. We note that the effects of path-loss and shadowing have not been taken into account in this contribution, which implies the assumption of perfect power control for all links. The effects of realistic *power control errors* (PCE) will be considered in Chapter 4. Furthermore, the total signal power of each user received via both the direct and relay branches was set to unity according to

$$P_{\mathrm{S}} + P_{\mathrm{R}} = 1. \tag{3.1}$$

3.2.1 Transmitted Source Signal

The SC-FDMA technique used in our work adopts the interleaved subband mapping aided DFT-spread OFDM arrangement of Section 2.2.2 at the transmitter portrayed in Figure 3.2, i.e. we opted for an *interleaved* FDMA (IFDMA) system. Specifically, the N-point DFT is used to transform the k-th user's N consecutive time-domain (TD) symbols hosted by the vector $\boldsymbol{x}_k^{\mathrm{t}} = [x_{k,0}, x_{k,1}, \cdots, x_{k,N-1}]^T$ of duration T_v into the FD, yielding $\boldsymbol{x}_k^{\mathrm{f}} = \boldsymbol{\mathcal{F}}_N \boldsymbol{x}_k^{\mathrm{t}}$, which is constituted by N orthogonal narrow subbands, where $\boldsymbol{\mathcal{F}}_N$ denotes the normalised N-point DFT matrix given in Eq. 2.2. Then, the resultant N FD symbols are mapped to orthogonal FD subbands as shown in Figure 2.9 (b), which obey the bandwidth expansion factor M, yielding a total bandwidth of $U = N \times M$. For further details on the SC-FDMA technique please refer to Section 2.2. Suffice to say that the baseband equivalent discrete-time expression of the transmitted signal before inserting the cyclic-prefix (CP) is given by

$$\boldsymbol{s}_k^{\mathrm{S,t}} = \sqrt{P_{\mathrm{S}}} \boldsymbol{\mathcal{F}}_U^H \boldsymbol{\mathcal{P}}_k \boldsymbol{\mathcal{F}}_N \boldsymbol{x}_k^{\mathrm{t}}, \tag{3.2}$$

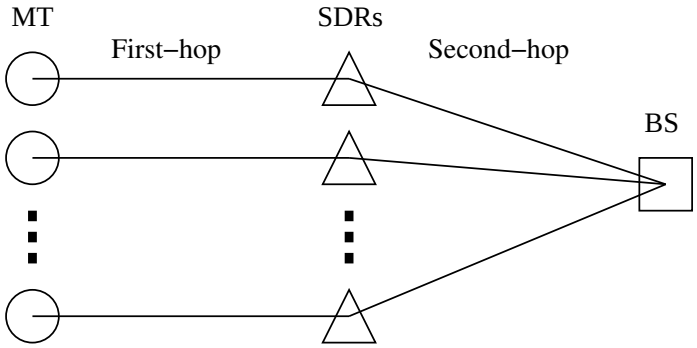

(a) Single-dedicated-relaying (SDR)

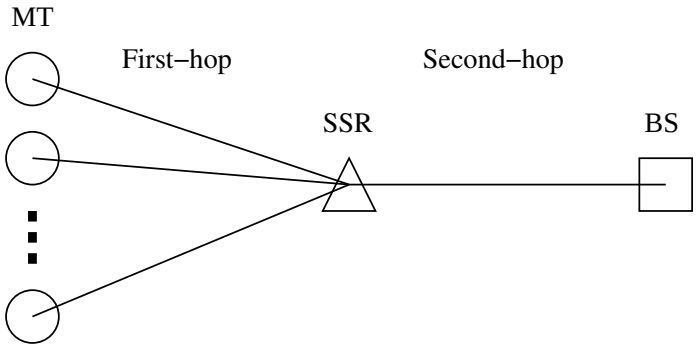

(b) Single-shared-relaying (SSR)

FIGURE 3.1: Relaying topologies for SC-FDMA uplink transmissions. The corresponding transceiver schematics of the source MTs, relays and the BS are portrayed in Figures 3.2, 3.3 and 3.4.

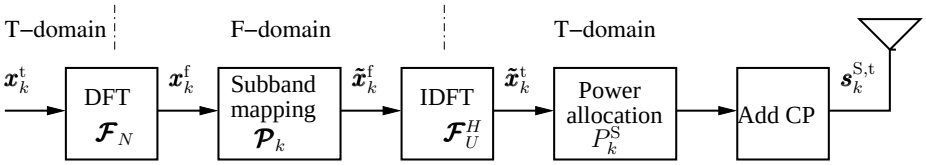

FIGURE 3.2: Transmitter schematic of the SC-FDMA source MT. The DFT-spread OFDMA-style transmitter is invoked as we introduced in Section 2.2.2. The corresponding TD and FD signals using IFDMA scheme were seen in Figure 2.10(b) and Figure 2.11(b), respectively. In the transmitter of a source MT, power allocation is introduced associated with transmit power of P_k^{S}, where we have the total transmit power constraint of the source and relay given in Eq. (3.1). By contrast, in the SC-FDMA transmitter of Figure 2.8 for direct transmission (DT), the transmitter power is normalised to $P = 1$, hence the power allocation is not necessary.

where the superscripts $^{\mathrm{S}}$ denotes the signal at the source MT and $^{\mathrm{t}}$ refers to the signal represented in the TD. Furthermore, $\boldsymbol{\mathcal{F}}_U$ denotes the normalised U-point DFT matrix in the form of Eq. (2.2), while $\boldsymbol{\mathcal{P}}_k$ is the *symbol-to-subband mapping* matrix of the k-th user having a normalised transmit power of P_{S}. To elaborate a little further, the FD subband mapping scheme of Figure 2.9, which is also known as subcarrier mapping in multi-carrier systems, has to be designed to achieve the maximum attainable frequency diversity in dispersive

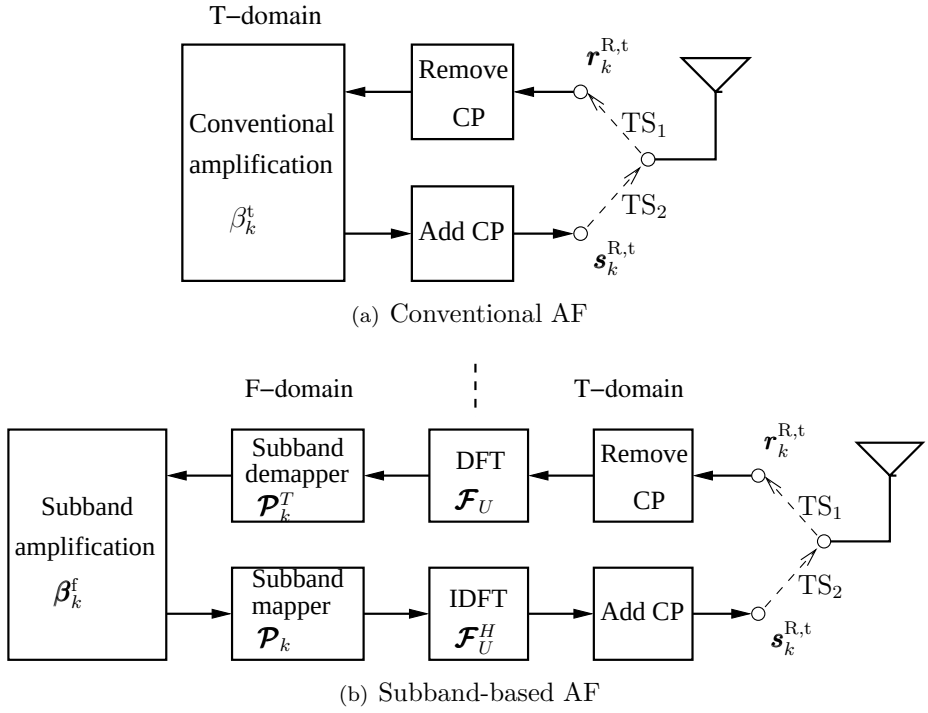

(a) Conventional AF

(b) Subband-based AF

FIGURE 3.3: Transceiver schematic of the relay using (1) conventional AF; (2) subband-based AF. The matching source transmitter was shown in Figure 3.2 and the destination receiver in Figure 3.4. The conventional AF relaying is carried out in the TD only discussed in Section 3.3.1, while the subband-based AF employs DFT/IDFT operation in order to process the amplification in the FD and invokes subband demapping/mapping for noise suppression which will be detailed in Section 3.3.2.

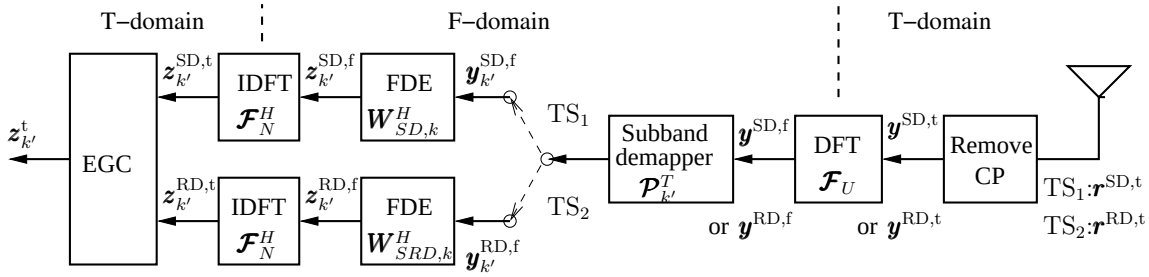

FIGURE 3.4: Receiver schematic of the SC-FDMA using TD-EGC at the BS. The source and relay transmitter schematics were shown in Figure 3.2 and Figure 3.3, respectively. During TS_0, the BS's receiver function is similar to the DT receiver of Figure 2.12, in which the FDE is invoked for S-D channel; while during TS_1, the FDE mitigate the fading effects of both S-R and R-D links jointly. Finally, a low-complexity TD-EGC combines the two branches signals in order to achieve the cooperative diversity gain.

multi-path fading channels according to Section 2.2.2

$$\mathcal{P}_{k,(u,n)} = \begin{cases} 1, & \text{for } u = nM + k, \\ 0, & \text{otherwise}, \end{cases} \tag{3.3}$$

where $\mathcal{P}_{k,(u,n)}$ is the (u,n)-th entry of $\boldsymbol{\mathcal{P}}_k$ and we have $u = 0, 1, \cdots, U-1,\ n = 0, 1, \cdots, N-1$.

3.2.2 The BS's Received Signal via Direct Branch

We assume that the BS perfectly estimated the *channel state information* (CSI) of the S-D link. Then, during TS_1 the BS directly receives all the K users' source signal via the S-D link subject to multi-path fading. After removing the CP, the received signal may be formulated as:

$$\boldsymbol{r}_{\mathrm{SD}}^{\mathrm{t}} = \sum_{k=0}^{K-1} \tilde{\boldsymbol{H}}_{\mathrm{SD},k}^{\mathrm{t}} \boldsymbol{s}_{k}^{\mathrm{S,t}} + \tilde{\boldsymbol{n}}_{1}^{\mathrm{D,t}}, \tag{3.4}$$

where the TD *channel impulse response* (CIR) $\tilde{\boldsymbol{H}}_{\mathrm{SD},k}^{\mathrm{t}}$ is a $(U \times U)$-element circulant matrix in the form of Eq. (2.5) for the S-D link of the k-th source user, while the U-length vector $\tilde{\boldsymbol{n}}_{0}^{\mathrm{D,t}}$ is the complex-valued *additive white Gaussian noise* (AWGN) component with a zero mean and a variance of σ_{N}^2, i.e. we have $\mathcal{CN}(0, \sigma_{\mathrm{N}}^2)$ at the BS.

In order to detect each user's signal in the FD at a low complexity, the *subband demapping* technique of Figure 3.4 and Section 2.2.3 is implemented, followed by a U-point DFT, where we have $\boldsymbol{\mathcal{P}}_{k'}^{T}\boldsymbol{\mathcal{P}}_{k} = \boldsymbol{I}$ if $k' = k$, otherwise $\boldsymbol{\mathcal{P}}_{k'}^{T}\boldsymbol{\mathcal{P}}_{k} = \boldsymbol{0}$ if $k' \neq k$, and the user index at the BS's receiver is $k' = 0, 1, \cdots, K-1$. The subband demapping matrix is capable of removing the MUI imposed by all other users, leading to a single-user vector $\boldsymbol{y}_{k'}^{\mathrm{SD,f}}$ of N symbols during TS_1 via the S-D link, yielding

$$\boldsymbol{y}_{k'}^{\mathrm{SD,f}} = \sqrt{P_{\mathrm{S}}}\boldsymbol{H}_{k'}^{\mathrm{SD,f}}\boldsymbol{x}_{k'}^{\mathrm{f}} + \boldsymbol{n}_{0}^{\mathrm{D,f}}, \tag{3.5}$$

where the superscript $^{\mathrm{f}}$ denotes the FD signal. In Eq. (3.5), the equivalent FD *channel transfer function* (FDCHTF) of the k'-th user signal in the S-D link is a $(N \times N)$-size diagonal matrix, given by

$$\boldsymbol{H}_{k'}^{\mathrm{SD,f}} = \boldsymbol{\mathcal{P}}_{k'}^{T}\boldsymbol{\mathcal{F}}_{U}\tilde{\boldsymbol{H}}_{k'}^{\mathrm{SD,t}}\boldsymbol{\mathcal{F}}_{U}^{H}\boldsymbol{\mathcal{P}}_{k'} = \mathrm{diag}\{h_{k',0}^{\mathrm{SD,f}}, h_{k',1}^{\mathrm{SD,f}}, \cdots, h_{k',(N-1)}^{\mathrm{SD,f}}\}, \tag{3.6}$$

and $\boldsymbol{n}_{0}^{\mathrm{D,f}}$ represents the N-length AWGN vector associated with $\mathcal{CN}(0, \sigma_{\mathrm{N}}^2)$ and imposed at the BS during TS_1:

$$\boldsymbol{n}_{0}^{\mathrm{D,f}} = \boldsymbol{\mathcal{P}}_{k'}^{T}\boldsymbol{\mathcal{F}}_{U}\tilde{\boldsymbol{n}}_{0}^{\mathrm{D,t}}. \tag{3.7}$$

3.2.3 Single-Dedicated-Relaying

In the *single-dedicated-relaying* (SDR) aided topology shown in Figure 3.1(a), we assume that there are many inactive mobile terminals available which can play the role of relays during the cooperation phase in a cell. Each of these inactive mobile terminals forwards the strongest signal received from a nearby source user, provided that it has a sufficiently high channel quality between them. Hence, there are a total of K sources and K relays in

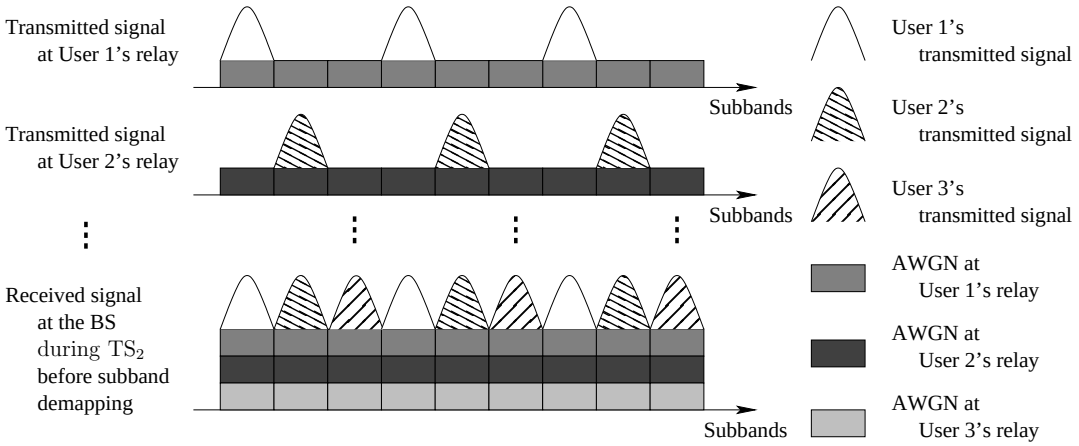

FIGURE 3.5: An example of spectrum for the conventional AF relay using the transceiver schematics of Figure 3.3(a). The IFDMA system has a total $U = 9$ subbands to support $K = M = 3$ users, while each user's signal is allocated in $N = 3$ distributed subbands. Each relay imposes an AWGN across the all 9 subbands. Besides of the noise imposed in the user's 3 subbands forwarded by the dedicated-relay, there are $(K-1)$ noise imposed in the remaining $(U-N) = 6$ subbands at the other $(K-1) = 2$ relays forwarded to the BS. Observe in this figure, for the relaying link, $K = 3$ AWGN components are imposed on each user's signal and forwarded to the BS. Clearly, these cumulated noise components erodes all $K = 3$ users' signals at the BS, not only the noise components forwarded by their dedicated relays.

the system. The signal received by the k-th relay as well as by the BS during TS_1 and TS_2 respectively, are expressed as follows,

$$\boldsymbol{r}_k^{\mathrm{SR,t}} = \tilde{\boldsymbol{H}}_k^{\mathrm{SR,t}} \boldsymbol{s}_k^{\mathrm{S,t}} + \tilde{\boldsymbol{n}}_k^{\mathrm{R,t}}, \tag{3.8a}$$

$$\boldsymbol{r}^{\mathrm{RD,t}} = \sum_{k=0}^{K-1} \tilde{\boldsymbol{H}}_k^{\mathrm{RD,t}} \boldsymbol{s}_k^{\mathrm{R,t}} + \tilde{\boldsymbol{n}}_1^{\mathrm{D,t}}, \tag{3.8b}$$

where $(U \times U)$-size circulant matrices $\tilde{\boldsymbol{H}}_k^{\mathrm{SR,t}}$ and $\tilde{\boldsymbol{H}}_k^{\mathrm{RD,t}}$ host the TD CIR for the k-th source user's signal of the S-R link and R-D link, respectively. In Eq. (3.8), $\tilde{\boldsymbol{n}}_k^{\mathrm{R,t}}$ and $\tilde{\boldsymbol{n}}_1^{\mathrm{D,t}}$ represent the U-length AWGN vectors associated with $\mathcal{CN}(0, \sigma_{\mathrm{N}}^2)$ imposed at the k-th relay and at the BS, respectively.

Moreover, for each user, both the source and the relay transmit their signal at the same normalised power, i.e. we have $P_{\mathrm{S}} = P_R$. Hence, the uplink system contains K S-R, S-D as well as the R-D links respectively, and the signals received via both the S-R link and the R-D link experience L independently fading multi-path components. Naturally, every source also has its direct link to the BS, which is also subject to independent frequency-selective fading.

It is important to note that the AWGN imposed by the relay should also be taken into account. Observe in Figure 3.5 that the noise component $\tilde{\boldsymbol{n}}_k^{\mathrm{R,t}}$ imposed by the k-th user's relay spreads across all U subbands in the FD, where only N subbands carry the k-th user's

signal effectively. When considering all the K relays, there are K noise sources forwarded from relays to the BS imposed in each user's subbands, as seen in Figure 3.5. However, the subband demapping at the BS of Figure 3.4 is incapable of removing these extra AWGN contributions in each user's subbands. As a result, these noise components may degrade the BS's receiver performance during TS_2, especially when K is high. Additionally, when taking into account the BS receiver's noise contribution during TS_1 and TS_2, a total of $(K+2)$ noise sources having an overall average power at σ_N^2 exist in the system. Thus, the total noise power imposed by all the K relays may become the dominant source of performance degradation. Of course, the noise effects may be eliminated by more complex *decode-and-forward* (DF) relaying.

3.2.4 Single-Shared-Relaying

In contrast to the SDR of Figure 3.1(a), when the number of inactive mobile stations becomes insufficient, to find a shared relay for all active user, the so-called *single-shared-relaying* (SSR) scheme of Figure 3.1(b) may be invoked. As shown in Figure 3.1(b), we assume that the relay is capable of receiving and forwarding signals from a cluster of K source users, so that these sources can share the relay, which simultaneously forwards their signals to the BS. Therefore, the representation of the signals received at the relay and BS is given by

$$\boldsymbol{r}^{\mathrm{SR,t}} = \sum_{k=0}^{K-1} \tilde{\boldsymbol{H}}_k^{\mathrm{SR,t}} \boldsymbol{s}_k^{\mathrm{S,t}} + \tilde{\boldsymbol{n}}^{\mathrm{R,t}}, \tag{3.9a}$$

$$\boldsymbol{r}^{\mathrm{RD,t}} = \tilde{\boldsymbol{H}}^{\mathrm{RD,t}} \boldsymbol{s}^{\mathrm{R,t}} + \tilde{\boldsymbol{n}}_1^{\mathrm{D,t}}, \tag{3.9b}$$

where $(U \times U)$-element circulant matrix $\tilde{\boldsymbol{H}}^{\mathrm{RD,t}}$ denotes TD CIR for the R-D link. Specifically, in Eq. (3.9) each of the K source signals embedded in the forwarded messages is still transmitted on the same subcarriers as the one they used for transmission from their respective source transmitters. Thus, the uplink system contains K pairs of S-R and S-D links, but only a single R-D link. This implies that the transmissions containing the composite K-user signal forwarded from the relay to the BS is affected by the same multi-path channel and contaminated by a single noise source at the relay. In other words, the performance degradation imposed by the relay is not related to the number of users K, which is in contrast to the SDR scheme of Section 3.2.3.

However, it is unrealistic to provide sufficient relay power for the simultaneous transmission of all the K users' signals. A simple realistic solution is to limit the total power of all the K users to unity, formulated as

$$P_\Sigma^{\mathrm{R}} = K P_{\mathrm{R}} = 1. \tag{3.10a}$$

Then subjected to Eq. (3.1), the average transmit power of each user's message at the source

node has to be set to

$$P_{\mathrm{S}} = 1 - 1/K. \tag{3.10b}$$

3.3 Cooperative Strategies at the Relay

Let us now discuss the relay-aided AF SC-FDMA approach in this section. The conventional AF technique will be presented first in Section 3.3.1. Then in Section 3.3.2 we propose an improved AF processing scheme operating at a subband-level, which includes both subband remapping and FDE for employment in both SDR and SSR systems.

3.3.1 Conventional AF Relaying

The classic AF scheme of Figure 3.3(a) is based on analogue amplification of the received signal at the relay by a factor depending on received signal powers at relay under the maximum power constraint of Eq. (3.1) [46]. In the SC-FDMA system, we assume that the BS perfectly estimated both the S-D and R-D links. The multi-user source signals are processed at the BS as follows.

3.3.1.1 Conventional AF and SDR Aided BS Reception

For the SDR topology, we have the transmitted signal $\boldsymbol{s}_k^{\mathrm{R,t}}$ of the k-th relay expressed as

$$\boldsymbol{s}_k^{\mathrm{R,t}} = \beta_k^{\mathrm{t}} \boldsymbol{r}_k^{\mathrm{SR,t}} = \beta_k^{\mathrm{t}} \sqrt{P_{\mathrm{S}}} \tilde{\boldsymbol{H}}_k^{\mathrm{SR,t}} \boldsymbol{\mathcal{F}}_U^H \boldsymbol{\mathcal{P}}_k \boldsymbol{\mathcal{F}}_N \boldsymbol{x}_k^{\mathrm{t}} + \beta_k^{\mathrm{t}} \tilde{\boldsymbol{n}}_k^{\mathrm{R,t}}, \tag{3.11}$$

where the TD amplification factor of the k-th relay is expressed as [46]

$$\beta_k^{\mathrm{t}} = \sqrt{\frac{P_{\mathrm{R}}}{P_{\mathrm{S}} |\bar{h}_k^{\mathrm{SR,t}}|^2 + \sigma_{\mathrm{N}}^2}}, \tag{3.12}$$

and the term $|\bar{h}_k^{\mathrm{SR,t}}|^2$ in the denominator of Eq. (3.12) is given by

$$|\bar{h}_k^{\mathrm{SR,t}}|^2 = \mathrm{Tr}[\tilde{\boldsymbol{H}}_k^{\mathrm{SR,t}} (\tilde{\boldsymbol{H}}_k^{\mathrm{SR,t}})^H]/U. \tag{3.13}$$

After U-point IDFT and subband demapping as seen in the schematic of Figure 3.4, the BS receives the messages forwarded from all the K relays, where the resultant FD received signal is given by

$$\boldsymbol{y}_{k'}^{\mathrm{RD,f}} = \beta_{k'}^{\mathrm{t}} \sqrt{P_{\mathrm{S}}} \boldsymbol{H}_{k'}^{\mathrm{SRD,f}} \boldsymbol{x}_{k'}^{\mathrm{f}} + \bar{\boldsymbol{n}}_1^{\mathrm{D,f}}, \tag{3.14}$$

with a $(N \times N)$-size diagonal matrix $\boldsymbol{H}_{k'}^{\mathrm{SRD,f}}$ formulated as

$$\boldsymbol{H}_{k'}^{\mathrm{SRD,f}} = \boldsymbol{\mathcal{P}}_{k'}^{T} \boldsymbol{\mathcal{F}}_{U} \tilde{\boldsymbol{H}}_{k'}^{\mathrm{RD,t}} \tilde{\boldsymbol{H}}_{k'}^{\mathrm{SR,t}} \boldsymbol{\mathcal{F}}_{U}^{H} \boldsymbol{\mathcal{P}}_{k'} = \mathrm{diag}\{h_{k',0}^{\mathrm{SRD,f}}, h_{k',1}^{\mathrm{SRD,f}}, \cdots, h_{k',(N-1)}^{\mathrm{SRD,f}}\}, \tag{3.15}$$

which represents the k'-th user's equivalent FDCHTF for the S-R-D link. By contrast, for the R-D link, we have

$$\boldsymbol{H}_{k'}^{\mathrm{RD,f}} = \boldsymbol{\mathcal{P}}_{k'}^{T} \boldsymbol{\mathcal{F}}_{U} \tilde{\boldsymbol{H}}_{k'}^{\mathrm{RD,t}} \boldsymbol{\mathcal{F}}_{U}^{H} \boldsymbol{\mathcal{P}}_{k'} = \mathrm{diag}\{h_{k',0}^{\mathrm{RD,f}}, h_{k',1}^{\mathrm{RD,f}}, \cdots, h_{k',(N-1)}^{\mathrm{RD,f}}\}. \tag{3.16}$$

The total noise encountered by the BS in the FD includes the equivalent relaying noise imposed by the K AF relays and the noise directly contributed by the BS's receiver during TS_2, which is formulated as:

$$\bar{\boldsymbol{n}}_{1}^{\mathrm{D,f}} = \boldsymbol{\mathcal{P}}_{k'}^{T} \boldsymbol{\mathcal{F}}_{U} \left(\sum_{k=0}^{K-1} \beta_{k}^{\mathrm{t}} \tilde{\boldsymbol{H}}_{k}^{\mathrm{RD,t}} \tilde{\boldsymbol{n}}_{k}^{\mathrm{R,t}} + \tilde{\boldsymbol{n}}_{1}^{\mathrm{D,t}} \right). \tag{3.17}$$

3.3.1.2 Conventional AF and SSR Aided BS Reception

However, in contrast to the SDR technique characterised in Eq. (3.11), for the SSR method, we have

$$\boldsymbol{s}^{\mathrm{R,t}} = \beta^{\mathrm{t}} \boldsymbol{r}^{\mathrm{SR,t}} = \beta^{\mathrm{t}} \sum_{k=0}^{K-1} \sqrt{P_{\mathrm{S}}} \tilde{\boldsymbol{H}}_{k}^{\mathrm{SR,t}} \boldsymbol{\mathcal{F}}_{U}^{H} \boldsymbol{\mathcal{P}}_{k} \boldsymbol{\mathcal{F}}_{N} \boldsymbol{x}_{k}^{\mathrm{t}} + \beta^{\mathrm{t}} \tilde{\boldsymbol{n}}^{\mathrm{R,t}}, \tag{3.18}$$

where the amplification factor of the SSR normalises the sum of all the K source signals according to

$$\beta^{\mathrm{t}} = \sqrt{\frac{P_{\Sigma}^{\mathrm{R}}}{\sum_{k=0}^{K-1} P_{\mathrm{S}} |\bar{h}_{k}^{\mathrm{SR,t}}|^2 + \sigma_{\mathrm{N}}^2}}. \tag{3.19}$$

Similar to the SDR-AF regime of Section 3.3.1.1, during TS_2, the k-th user's FD received signal representation after U-point IDFT and subband demapping using the schematic of Figure 3.4 and spectral plots of Figure 2.9(b) is given by

$$\boldsymbol{y}_{k'}^{\mathrm{RD,f}} = \beta^{\mathrm{t}} \sqrt{P_{\mathrm{S}}} \boldsymbol{H}_{k'}^{\mathrm{SRD,f}} \boldsymbol{x}_{k'}^{\mathrm{f}} + \bar{\boldsymbol{n}}_{1}^{\mathrm{D,f}}, \tag{3.20}$$

where we have:

$$\boldsymbol{H}_{k'}^{\mathrm{SRD,f}} = \boldsymbol{\mathcal{P}}_{k'}^{T} \boldsymbol{\mathcal{F}}_{U} \tilde{\boldsymbol{H}}^{\mathrm{RD,t}} \tilde{\boldsymbol{H}}_{k'}^{\mathrm{SR,t}} \boldsymbol{\mathcal{F}}_{U}^{H} \boldsymbol{\mathcal{P}}_{k'}, \quad \boldsymbol{H}_{k'}^{\mathrm{RD,f}} = \boldsymbol{\mathcal{P}}_{k'}^{T} \boldsymbol{\mathcal{F}}_{U} \tilde{\boldsymbol{H}}^{\mathrm{RD,t}} \boldsymbol{\mathcal{F}}_{U}^{H} \boldsymbol{\mathcal{P}}_{k'}. \tag{3.21}$$

However, the total received noise component of k'-th user at the BS contains only a single relay's noise contribution, plus that of the BS, yielding the FD expression of

$$\bar{\boldsymbol{n}}_{1}^{\mathrm{D,f}} = \boldsymbol{\mathcal{P}}_{k'}^{T} \boldsymbol{\mathcal{F}}_{U} \left(\beta^{\mathrm{t}} \tilde{\boldsymbol{H}}^{\mathrm{RD,t}} \tilde{\boldsymbol{n}}^{\mathrm{R,t}} + \tilde{\boldsymbol{n}}_{1}^{\mathrm{D,t}} \right). \tag{3.22}$$

3.3.2 Subband-Based AF Relaying Combined with Subband Remapping

As we mentioned in Section 3.2.3, the total equivalent noise of the SDR topology of Figure 3.1(a), which contaminates the BS's input signal is a function of the number of relays in the conventional AF system. Moreover, since the SSR topology of Figure 3.1(b) forwards the received signals of all the K users jointly from the relay to the BS, this kind of AF scheme is unable to amplify the signal for each user differently, unless dedicated subband-amplifiers are used. Additionally, we note for both the SDR and SSR architectures of Figure 3.1 that the conventional AF scheme's signals transmitted in each of the subbands are amplified by the same factor for each user. However, provided that the S-R link was perfectly estimated, the relay may process the received signal for each user individually in the FD. Compared to the conventional AF scheme of Figure 3.3(a), the proposed subband-based AF scheme of Figure 3.3(b) invokes both the DFT operation and subband demapping at the relay's receiver, while the subband mapping and IDFT are employed at the relay's transmitter. This arrangement allows the signal amplification to be carried in the FD on a subband-by-subband basis. Specifically, the relay's signal corresponding to the k-th user is mapped to the subbands assigned to the k-th source MT. We refer to the joint subband mapping and demapping procedure as the *subband remapping* operation. By invoking the *subband remapping* and amplification of each subband, the BS is capable of equalising the two-hop relay link in the FD by a simple single-tap FD equaliser. Therefore, the proposed subband-based AF scheme of Figure 3.3(b) aims for reducing the ISI and the noise of each user.

In this subsection, we investigate the relay carrying out subband remapping relying on the schematic of Figure 3.3(b) and spectral plots of Figure 3.6, for the sake of removing noise at other user's subbands for each user and for amplifying each FD signal of the user-specific subbands individually. The SDR and SSR topologies are considered in Sections 3.3.2.1 and 3.3.2.2 respectively.

3.3.2.1 Subband Remapping for AF SDRs

To elaborate a little further, here we propose subband-based AF relying on the subband remapping schematic of Figure 3.3(b) and on the spectral plots of Figure 3.6 for an SDR system. The transmitted signal of the k-th relay during TS_2 is expressed as

$$\boldsymbol{s}_k^{\mathrm{R,t}} = \sqrt{P_{\mathrm{S}}}\boldsymbol{\mathcal{F}}_U^H \boldsymbol{\mathcal{P}}_k \boldsymbol{\beta}_k^{\mathrm{f}} \boldsymbol{H}_k^{\mathrm{SR,f}} \boldsymbol{x}_k^{\mathrm{f}} + \bar{\boldsymbol{n}}_k^{\mathrm{R,t}}, \tag{3.23}$$

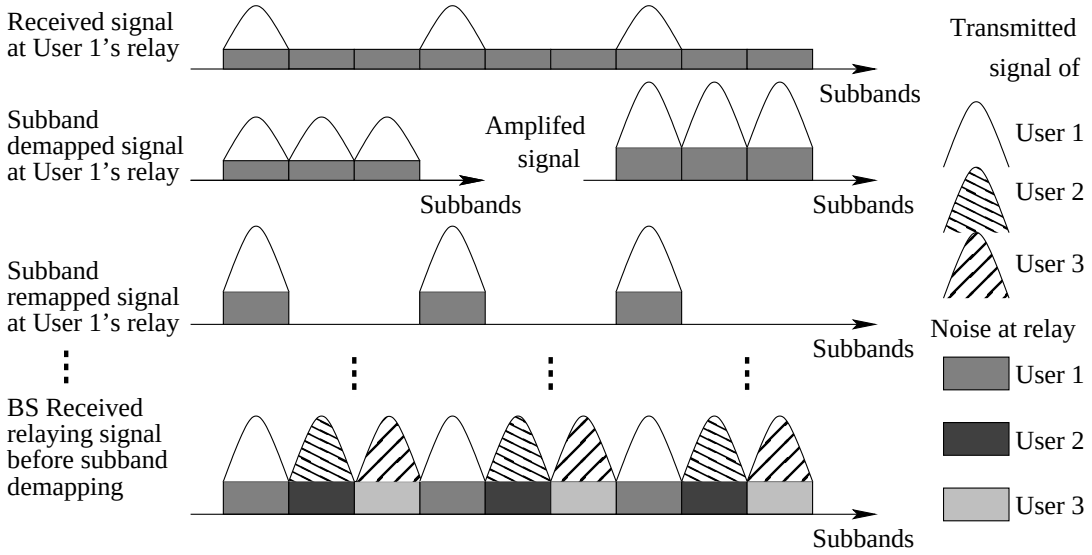

FIGURE 3.6: An example of spectrum for the subband-based AF relay transceiver of Figure 3.3(b), which may be contrasted to the conventional AF relaying spectrum of Figure 3.5. The subband remapping and subband-based amplification techniques are invoked at the relay, in order to removing noise in other user's subbands for each user and for amplifying each FD signal of the user-specific subbands individually.

where $\boldsymbol{\beta}_k^{\mathrm{f}}$ and $\boldsymbol{H}_k^{\mathrm{SR,f}}$ are the k-th user's FD amplification factor and the equivalent FDCHTF, respectively, both of which are $(N\times N)$-element diagonal matrices, which are formulated as

$$\boldsymbol{\beta}_k^{\mathrm{f}} = \mathrm{diag}\{\beta_{k,0}^{\mathrm{f}}, \beta_{k,1}^{\mathrm{f}}, \cdots, \beta_{k,(N-1)}^{\mathrm{f}}\}, \tag{3.24}$$

$$\boldsymbol{H}_k^{\mathrm{SR,f}} = \boldsymbol{\mathcal{P}}_k^T \boldsymbol{\mathcal{F}}_U \tilde{\boldsymbol{H}}_k^{\mathrm{SR,t}} \boldsymbol{\mathcal{F}}_U^H \boldsymbol{\mathcal{P}}_k = \mathrm{diag}\{h_{k,0}^{\mathrm{SR,f}}, h_{k,1}^{\mathrm{SR,f}}, \cdots, h_{k,(N-1)}^{\mathrm{SR,f}}\}. \tag{3.25}$$

The n-th entry of $\boldsymbol{\beta}_k^{\mathrm{f}}$ in Eq. (3.24) is given by

$$\beta_{k,n}^{\mathrm{f}} = \sqrt{\frac{P_{\mathrm{R}}}{P_{\mathrm{S}}|h_{k,n}^{\mathrm{SR,f}}|^2 + \sigma_{\mathrm{N}}^2}}, \tag{3.26}$$

which affects the n-th subband signal in the FD. It is important to note that the noise contribution of the k-th user's signal is affected at the relay as follows:

$$\bar{\boldsymbol{n}}_k^{\mathrm{R,t}} = \boldsymbol{\mathcal{F}}_U^H \boldsymbol{\mathcal{P}}_k \boldsymbol{\beta}_k^{\mathrm{f}} \boldsymbol{\mathcal{P}}_k^T \boldsymbol{\mathcal{F}}_U \tilde{\boldsymbol{n}}_k^{\mathrm{R,t}} \tag{3.27}$$

where the noise imposed at all other users' subbands are removed, as visualised in the spectral plots of Figure 3.6.

Hence, the received signal of the k'-th user after U-point IDFT and subband demapping at the BS during TS_2 and using the schematic of Figure 3.4 can be described as:

$$\boldsymbol{y}_{k'}^{\mathrm{RD,f}} = \sqrt{P_{\mathrm{S}}} \boldsymbol{H}_{k'}^{\mathrm{RD,f}} \boldsymbol{\beta}_{k'}^{\mathrm{f}} \boldsymbol{H}_{k'}^{\mathrm{SR,f}} \boldsymbol{x}_{k'}^{\mathrm{f}} + \bar{\boldsymbol{n}}_1^{\mathrm{D,f}}, \tag{3.28}$$

where the total received noise component of the k'-th user at the BS's receiver of Figure 3.4 includes the noise contribution imposed by the k'-th relay after subband remapping plus that of the BS, which is hence expressed as

$$\bar{\boldsymbol{n}}_1^{\mathrm{D,f}} = \boldsymbol{\mathcal{P}}_{k'}^T \boldsymbol{\mathcal{F}}_U (\tilde{\boldsymbol{H}}_{k'}^{\mathrm{RD,t}} \bar{\boldsymbol{n}}_{k'}^{\mathrm{R,t}} + \tilde{\boldsymbol{n}}_1^{\mathrm{D,t}}). \tag{3.29}$$

3.3.2.2 Subband Remapping for AF SSRs

Considering the SSR, when the subband-based AF approach relying on the schematic of Figure 3.3(b) and on the spectral of Figure 3.6 is implemented in conjunction with subband remapping, the relay's composite transmitted signal containing all the K users' signals is formulated as

$$\boldsymbol{s}^{\mathrm{R,t}} = \sum_{k=0}^{K-1} \left(\sqrt{P_{\mathrm{S}}} \boldsymbol{\mathcal{F}}_U^H \boldsymbol{\mathcal{P}}_k \boldsymbol{\beta}_k^{\mathrm{f}} \boldsymbol{H}_k^{\mathrm{SR,f}} \boldsymbol{x}_k^{\mathrm{f}} + \bar{\boldsymbol{n}}_k^{\mathrm{R,t}} \right), \tag{3.30}$$

where the n-th entry of $\boldsymbol{\beta}_k^{\mathrm{f}}$, $\boldsymbol{H}_k^{\mathrm{SR,f}}$ and $\bar{\boldsymbol{n}}_k^{\mathrm{R,t}}$ is the same as those in Eq. (3.24), Eq. (3.25) and Eq. (3.27) for the SDR approach. Note that each user's signal forwarded by this common relay shares the total transmission power by obeying the power-constraint of Eq. (3.10a). The FD processing of the SSR regime obeying Eq. (3.28) and carried out at the BS's receiver portrayed in Figure 3.4 during TS_2 is the same as for the SDR scenario.

3.4 Frequency-Domain Equalisation for Cooperative Branches at BS Receiver

In Section 3.3, we have investigated two different cooperative strategies conceived for both the SDR and SSR topologies of Figure 3.1. According to [100], the main benefit of diversity is that of coherently combining the independently fading paths, hence leading to the mitigation of the fading effects. For the sake of achieving cooperative diversity, the amplified and forwarded signal received by BS relying on the schematic of Figure 3.4 during TS_2 via the S-R and R-D links should be combined with the signal that arrives at the BS during TS_1 via the S-D link. The MMSE FDE solution of Figure 2.12(b) in Section 2.2.3 can be invoked on each of the S-D and S-R-D links individually. Then the pair of estimated signals are combined by equal-gain combiner (EGC) [100] in the TD, denoted as TD-EGC. In this Section, we analysis the FDE aided TD-EGC schemes of Figure 3.4 in the SDR and SSR user-cooperation scenarios of Figure 3.1.

3.4.1 MMSE FDE of the Source-Destination Direct Branch

According to Section 2.2.3, the FD single-user N-symbol vector $\boldsymbol{y}_{k'}^{\mathrm{SD,f}}$ of Eq. (3.5) can be equalised by the single-tap MMSE FDE of Section 2.2.3. The MMSE equalisation criterion strikes an attractive trade-off between mitigating the effects of noise and ISI. Based on the schematic of Figure 3.4, the FDE's output vector $\boldsymbol{z}_{SD,k'}^{(f)}$ can hence be expressed for the k'-th user as

$$\boldsymbol{z}_{k'}^{\mathrm{SD,f}} = \sqrt{P_{\mathrm{S}}}(\boldsymbol{W}_{k'}^{\mathrm{SD}})^H \boldsymbol{H}_{k'}^{\mathrm{SD,f}} \boldsymbol{x}_{k'}^{\mathrm{f}} + \hat{\boldsymbol{n}}_0^{\mathrm{D,f}}, \tag{3.31}$$

where the MMSE equaliser weights are hosted by an $(N \times N)$-element diagonal matrix expressed as

$$\boldsymbol{W}_{k'}^{\mathrm{SD}} = \boldsymbol{H}_{k'}^{\mathrm{SD,f}}[P_{\mathrm{S}}(\boldsymbol{H}_{k'}^{\mathrm{SD,f}})^H \boldsymbol{H}_{k'}^{\mathrm{SD,f}} + (\sigma_{\mathrm{N}}^2/P_{\mathrm{S}})\boldsymbol{I}_N]^{-1} = \mathrm{diag}\{w_{k',0}^{\mathrm{SD}}, w_{k',1}^{\mathrm{SD}}, \cdots, w_{k',(N-1)}^{\mathrm{SD}}\}, \tag{3.32}$$

and its n-th element is given by

$$w_{k',n}^{\mathrm{SD}} = \frac{h_{k',n}^{\mathrm{SD,f}}}{|h_{k',n}^{\mathrm{SD,f}}|^2 + \sigma_{\mathrm{N}}^2/P_{\mathrm{S}}}. \tag{3.33}$$

In Eq. (3.31), the noise component $\hat{\boldsymbol{n}}_0^{\mathrm{D,f}}$ is a $(N \times N)$-element diagonal matrix given by

$$\hat{\boldsymbol{n}}_0^{\mathrm{D,f}} = (\boldsymbol{W}_{k'}^{\mathrm{SD}})^H \boldsymbol{n}_0^{\mathrm{D,f}}, \tag{3.34}$$

while the power of its n-th entry is expressed as

$$\hat{\mathcal{N}}_{0,n}^{\mathrm{D}} = \sigma_{\mathrm{N}}^2 |w_{k',n}^{\mathrm{SD}}|^2. \tag{3.35}$$

It was shown in Section 2.2.4 that the normalised MMSE and *signal-to-interference-plus-noise ratio* (SINR) of the k'-th user's signal transmitted via the S-D link may be expressed as

$$e_{k'}^{\mathrm{SD}} = \frac{1}{N} \sum_{n=0}^{N-1} \frac{1}{\gamma_{k',n}^{\mathrm{SD}} + 1}, \tag{3.36}$$

$$\gamma_{k'}^{\mathrm{SD}} = \left(\frac{1}{N} \sum_{n=0}^{N-1} \frac{1}{\gamma_{k',n}^{\mathrm{SD}} + 1} \right)^{-1} - 1, \tag{3.37}$$

respectively, where the *signal-to-noise ratio* (SNR) of the n-th subband is given by

$$\gamma_{k',n}^{\mathrm{SD}} = \frac{P_{\mathrm{S}} |h_{k',n}^{\mathrm{SD,f}}|^2}{\sigma_{\mathrm{N}}^2}. \tag{3.38}$$

3.4.2 MMSE FDE of the Conventional AF Relaying Branch

Let us now consider the conventional AF aided MMSE FDE scheme of Figure 3.4 for both the SDR and SSR systems of Figure 3.1. Based on Section 3.3.1, when applying the MMSE FDE to the S-R-D branch's received signal vector $\boldsymbol{y}_{k'}^{\mathrm{RD,f}}$, the decision variables of the k'-th transmitted symbols may be expressed as

$$\boldsymbol{z}_{k'}^{\mathrm{RD,f}} = (\boldsymbol{W}_{k'}^{\mathrm{SRD}})^H \boldsymbol{y}_{k'}^{\mathrm{RD,f}} = \sqrt{P_{\mathrm{S}}}\beta_{k'}^{\mathrm{t}} (\boldsymbol{W}_{k'}^{\mathrm{SRD}})^H \boldsymbol{H}_{k'}^{\mathrm{SRD,f}} \boldsymbol{x}_{k'}^{\mathrm{f}} + \hat{\boldsymbol{n}}_1^{\mathrm{D,f}}, \tag{3.39}$$

where the MMSE equaliser weights are hosted by an $(N \times N)$-element diagonal weight matrix expressed as

$$\begin{aligned} \boldsymbol{W}_{k'}^{\mathrm{SRD}} &= \beta_{k'}^{\mathrm{t}} \boldsymbol{H}_{k'}^{\mathrm{SRD,f}} \left[P_{\mathrm{S}} (\beta_{k'}^{\mathrm{t}})^2 (\boldsymbol{H}_{k'}^{\mathrm{SRD,f}})^H \boldsymbol{H}_{k'}^{\mathrm{SRD,f}} + (1/P_{\mathrm{S}}) (\bar{\boldsymbol{n}}_1^{\mathrm{D,f}})^H \bar{\boldsymbol{n}}_1^{\mathrm{D,f}} \right]^{-1} \\ &= \mathrm{diag}\{ w_{k',0}^{\mathrm{SRD}}, w_{k',1}^{\mathrm{SRD}}, \cdots, w_{k',(N-1)}^{\mathrm{SRD}} \}, \end{aligned} \tag{3.40}$$

where the (n,n)-th entry is given by

$$w_{k',n}^{\mathrm{SRD}} = \frac{\beta_{k'}^{\mathrm{t}} h_{k',n}^{\mathrm{SRD,f}}}{(\beta_{k'}^{\mathrm{t}})^2 |h_{k',n}^{\mathrm{SRD,f}}|^2 + \mathcal{N}_{1,n}^{\mathrm{D}} / P_{\mathrm{S}}}. \tag{3.41}$$

Additionally, the noise term of Eq. (3.39) is given by $\hat{\boldsymbol{n}}_1^{\mathrm{D,f}} = (\boldsymbol{W}_{k'}^{\mathrm{SRD}})^H \bar{\boldsymbol{n}}_1^{\mathrm{D,f}}$. Note that for the SDR system of Figure 3.1(a), the amplification factor $\beta_{k'}^{\mathrm{t}}$ is given by Eq. (3.12), while for SSR system of Figure 3.1(b) it should be replaced by β^{t} of Eq. (3.19). Hence, the power of the n-th entry on the diagonal of $\bar{\boldsymbol{n}}_1^{\mathrm{D,f}}$, namely $\mathcal{N}_{1,n}^{\mathrm{D}}$, represents the normalised total power of the equivalent noise jointly imposed by the K AF relays plus the noise directly contributed by the BS receiver of Figure 3.4 during TS_2. Referring to Eq. (3.17) deduced for the SDR system, we have

$$\mathcal{N}_{1,n}^{\mathrm{D}} = \mathrm{E}\left\{ \mathrm{Tr}[\bar{\boldsymbol{n}}_1^{\mathrm{D,f}} (\bar{\boldsymbol{n}}_1^{\mathrm{D,f}})^H] \right\} = \sigma_{\mathrm{N}}^2 \sum_{k=0}^{K-1} (\beta_k^{\mathrm{t}})^2 |h_{k,n}^{\mathrm{RD,f}}|^2 + \sigma_{\mathrm{N}}^2. \tag{3.42}$$

Additionally, referring to Eq. (3.22) of the SSR system, $\mathcal{N}_{1,n}^{\mathrm{D}}$ is expressed as

$$\mathcal{N}_{1,n}^{\mathrm{D}} = \sigma_{\mathrm{N}}^2 (\beta^{\mathrm{t}})^2 |h_{k',n}^{\mathrm{RD,f}}|^2 + \sigma_{\mathrm{N}}^2. \tag{3.43}$$

According to Section 2.2.4, the normalised MMSE $e_{k'}^{\mathrm{SRD}}$ of conventional AF encountered in the relaying branch may be formulated as

$$e_{k'}^{\mathrm{SRD}} = \frac{1}{N} \sum_{n=0}^{N-1} \frac{\mathcal{N}_{1,n}^{\mathrm{D}}}{(\beta_{k'}^{\mathrm{t}})^2 |h_{k',n}^{\mathrm{SRD,f}}|^2 + \mathcal{N}_{1,n}^{\mathrm{D}} / P_{\mathrm{S}}} = \frac{1}{N} \sum_{n=0}^{N-1} \frac{1}{\gamma_{k',n}^{\mathrm{SRD}} + 1}, \tag{3.44}$$

and the corresponding SINR $\gamma_{k'}^{\mathrm{SRD}}$ may be expressed as

$$\gamma_{k'}^{\mathrm{SRD}} = \left(\frac{1}{N} \sum_{n=0}^{N-1} \frac{1}{\gamma_{k',n}^{\mathrm{SRD}} + 1} \right)^{-1} - 1, \tag{3.45}$$

where the SNR of the n-th subband of the relaying branch is given by

$$\gamma_{k',n}^{\mathrm{SRD}} = \frac{P_{\mathrm{S}} (\beta_{k'}^{\mathrm{t}})^2 |h_{k',n}^{\mathrm{SRD,f}}|^2}{\mathcal{N}_{1,n}^{\mathrm{D}}}. \tag{3.46}$$

By substituting $\beta_{k'}^{\mathrm{t}}$ of Eq. (3.12) into Eq. (3.46), we arrive at

$$\gamma_{k',n}^{\mathrm{SRD}} = \frac{P_{\mathrm{R}} P_{\mathrm{S}} |h_{k',n}^{\mathrm{SRD,f}}|^2}{\sigma_{\mathrm{N}}^2 \beta_{\mathrm{N},k',n}}, \tag{3.47}$$

where we introduced the noise enhancement factor denoted by $\beta_{\mathrm{N},k',n}$ within the n-th subband of the k-th user. Specifically, we have:

$$\beta_{\mathrm{N},k',n} = \begin{cases} P_{\mathrm{R}} \sum_{k=0}^{K-1} |h_{k,n}^{\mathrm{RD,f}}|^2 + P_{\mathrm{S}} |\bar{h}_{k'}^{\mathrm{SR,t}}|^2 + \sigma_{\mathrm{N}}^2, & \text{for the SDR system;} \\ P_{\Sigma}^{\mathrm{R}} |h_{k',n}^{\mathrm{RD,f}}|^2 + \sum_{k=0}^{K-1} |\bar{h}_{k}^{\mathrm{SR,t}}|^2 + \sigma_{\mathrm{N}}^2, & \text{for the SSR system,} \end{cases} \tag{3.48}$$

where $\bar{h}_{k}^{\mathrm{SR,t}}$ was defined in Eq. (3.13).

3.4.3 MMSE FDE of the Subband-Based AF Relaying Branch

Similar to the conventional AF scheme of Section 3.4.2, the MMSE FDE of subband-based AF relaying relying on subcarrier remapping procedure of Figure 3.3(b) can be carried out as follows. By applying the MMSE FDE scheme of Section 2.2.3 to the k'-th user's FD received signal $\boldsymbol{y}_{k'}^{\mathrm{RD,f}}$ in Eq. (3.28), we have

$$\boldsymbol{z}_{k'}^{\mathrm{RD,f}} = \sqrt{P_{\mathrm{S}}} (\boldsymbol{W}_{k'}^{\mathrm{SRD}})^H \boldsymbol{H}_{k'}^{\mathrm{RD,f}} \boldsymbol{\beta}_{k'}^{\mathrm{f}} \boldsymbol{H}_{k'}^{\mathrm{SR,f}} \boldsymbol{x}_{k'}^{\mathrm{f}} + \hat{\boldsymbol{n}}_{1}^{\mathrm{D,f}}, \tag{3.49}$$

where $\boldsymbol{\beta}_{k'}^{\mathrm{f}}$ is given in Eq. (3.24) and we have $\hat{\boldsymbol{n}}_{1}^{\mathrm{D,f}} = (\boldsymbol{W}_{k'}^{\mathrm{SRD}})^H \bar{\boldsymbol{n}}_{1}^{\mathrm{D,f}}$. The MMSE equaliser weights $\boldsymbol{W}_{k'}^{\mathrm{SRD}}$ are hosted by an $(N \times N)$-element diagonal matrix given by

$$\begin{aligned} \boldsymbol{W}_{k'}^{\mathrm{SRD}} &= \left\{ \begin{array}{l} \boldsymbol{H}_{k'}^{\mathrm{RD,f}} \boldsymbol{\beta}_{k'}^{\mathrm{f}} \boldsymbol{H}_{k'}^{\mathrm{SR,f}} \\ \times \Big[\; (\boldsymbol{H}_{k'}^{\mathrm{RD,f}})^H \boldsymbol{H}_{k'}^{\mathrm{RD,f}} (\boldsymbol{\beta}_{k'}^{\mathrm{f}})^H \boldsymbol{\beta}_{k'}^{\mathrm{f}} (\boldsymbol{H}_{k'}^{\mathrm{SR,f}})^H \boldsymbol{H}_{k'}^{\mathrm{SR,f}} + (1/P_{\mathrm{S}}) (\bar{\boldsymbol{n}}_{1}^{\mathrm{D,f}})^H \bar{\boldsymbol{n}}_{1}^{\mathrm{D,f}} \; \Big]^{-1} \end{array} \right\}, \\ &= \mathrm{diag}\{ w_{k',0}^{\mathrm{SRD}}, w_{k',1}^{\mathrm{SRD}}, \cdots, w_{k',(N-1)}^{\mathrm{SRD}} \}, \end{aligned} \tag{3.50}$$

while the n-th element of $\boldsymbol{W}_{k'}^{\mathrm{SRD}}$ may be expressed as

$$w_{k',n}^{\mathrm{SRD}} = \frac{\beta_{k',n}^{\mathrm{f}} h_{k',n}^{\mathrm{RD,f}} h_{k',n}^{\mathrm{SR,f}}}{(\beta_{k',n}^{\mathrm{f}})^2 |h_{k',n}^{\mathrm{RD,f}}|^2 |h_{k',n}^{\mathrm{SR,f}}|^2 + \mathcal{N}_{1,n}^{\mathrm{D}}/P_{\mathrm{S}}}, \tag{3.51}$$

where $\beta_{k',n}^{\mathrm{f}}$ is given by (3.26) and the noise power of the n-th entry in the diagonal of $\bar{\boldsymbol{n}}_1^{\mathrm{D,f}}$ in Eq. (3.27) and (3.29) is given by

$$\mathcal{N}_{1,n}^{\mathrm{D}} = \sigma_{\mathrm{N}}^2 (\beta_{k',n}^{\mathrm{f}})^2 |h_{k',n}^{\mathrm{RD,f}}|^2 + \sigma_{\mathrm{N}}^2. \tag{3.52}$$

Therefore, we are now ready to derive the normalised MMSE for subband-based AF on the S-R-D branch, which is given by

$$e_{k'}^{\mathrm{SRD}} = \frac{1}{N} \sum_{n=0}^{N-1} \frac{\mathcal{N}_{1,n}^{\mathrm{D}}}{P_{\mathrm{S}} (\beta_{k',n}^{\mathrm{f}})^2 |h_{k',n}^{\mathrm{RD,f}}|^2 |h_{k',n}^{\mathrm{SR,f}}|^2 + \mathcal{N}_{1,n}^{\mathrm{D}}} = \frac{1}{N} \sum_{n=0}^{N-1} \frac{1}{\gamma_{k',n}^{\mathrm{SRD}} + 1}. \tag{3.53}$$

Additionally, the SNR on the n-th subband in the relaying branch is given by

$$\gamma_{k',n}^{\mathrm{SRD}} = \frac{P_{\mathrm{S}} (\beta_{k',n}^{\mathrm{f}})^2 |h_{k',n}^{\mathrm{RD,f}}|^2 |h_{k',n}^{\mathrm{SR,f}}|^2}{\mathcal{N}_{1,n}^{\mathrm{D}}} = \left(\frac{1}{\gamma_{k',n}^{\mathrm{SR}}} + \frac{1}{\gamma_{k',n}^{\mathrm{RD}}} \right)^{-1}, \tag{3.54}$$

where the k'-th user's SNR on the n-th subband of the S-R and R-D links may be expressed as

$$\gamma_{k',n}^{\mathrm{SR}} = \frac{P_{\mathrm{S}} |h_{k',n}^{\mathrm{SR,f}}|^2}{\sigma_{\mathrm{N}}^2}, \tag{3.55a}$$

$$\gamma_{k',n}^{\mathrm{RD}} = \frac{(\beta_{k',n}^{\mathrm{f}})^2 |h_{k',n}^{\mathrm{RD,f}}|^2}{\sigma_{\mathrm{N}}^2 / (P_{\mathrm{S}} |h_{k',n}^{\mathrm{SR,f}}|^2)} = \frac{P_{\mathrm{S}} P_{\mathrm{R}} |h_{k',n}^{\mathrm{SR,f}}|^2 |h_{k',n}^{\mathrm{RD,f}}|^2}{\sigma_{\mathrm{N}}^2 (P_{\mathrm{S}} |h_{k',n}^{\mathrm{SR,f}}|^2 + \sigma_{\mathrm{N}}^2)}, \tag{3.55b}$$

respectively.

Consequently, by substituting Eq. (3.54) into Eq. (3.45), the k'-th user's SINR across the whole spectral band of the relaying branch can be expressed as

$$\gamma_{k'}^{\mathrm{SRD}} = \left(\frac{1}{N} \sum_{n=0}^{N-1} \frac{1}{\gamma_{k',n}^{\mathrm{SRD}} + 1} \right)^{-1} - 1 = \left\{ \frac{1}{N} \sum_{n=0}^{N-1} \left[\left(\frac{1}{\gamma_{k',n}^{\mathrm{SR}}} + \frac{1}{\gamma_{k',n}^{\mathrm{RD}}} \right)^{-1} + 1 \right]^{-1} \right\}^{-1} - 1. \tag{3.56}$$

3.4.4 Time-Domain Equal-Gain Combining

According to [100], the time-varying output SNR at a receiver equipped with multiple receive antennas may be different to that of the individual receiver branches. However, the

low-complexity *equal-gain combining* (EGC) constitutes a simple linear diversity combining technique, which is capable of combining all the signals gleaned from $N_{\rm r}$ branches without the knowledge of the time-varying SNR of each branch. This implies that the $n_{\rm r}$-th branch's weight can be expressed as $w_{n_{\rm r}} = e^{-j\theta_{n_{\rm r}}}$, where $\theta_{n_{\rm r}}$ is the phase of the signal received by the $n_{\rm r}$-th branch. Let $y_{n_{\rm r}}$ and $\mathcal{N}_{n_{\rm r}}$ denote the signal and the equivalent noise power component of the $n_{\rm r}$-th branch at input of the combiner, which leads to the total received SNR expressed by [100]

$$\gamma_{\Sigma} = \frac{\left|\sum_{n_{\rm r}=0}^{N_{\rm r}-1} w_{n_{\rm r}} y_{n_{\rm r}}\right|^2}{\sum_{n_{\rm r}=0}^{N_{\rm r}-1} w_{n_{\rm r}}^2 \mathcal{N}_{n_{\rm r}}} = \frac{\left|\sum_{n_{\rm r}=0}^{N_{\rm r}-1} y_{n_{\rm r}}\right|^2}{\sum_{n_{\rm r}=0}^{N_{\rm r}-1} \mathcal{N}_{n_{\rm r}}}. \tag{3.57}$$

However, since the MMSE FDE may not entirely remove the residual ISI, the resultant estimated signals of both the direct and relaying branches remain contaminated both by ISI component as well as by the noise. Furthermore, since the N-point IDFT transforms the signals estimated by the FDE to the TD before combining the two branch signals, due to the nature of the IDFT operation, the power of each TD symbol in the N-length signal vector can be quantified by the average power of all N elements of FD signal vector. Thus, it is the SINR at the EGC's output that should be evaluated instead of the SNR, where the power of the TD signals including the desired symbol, the ISI and the noise components of each branch can be calculated respectively.

Specifically, we have the TD signal vector after the N-point IDFT of Figure 3.4 on the direct and relaying branches given by

$$\boldsymbol{z}_{k'}^{\rm SD,t} = \boldsymbol{\mathcal{F}}_N^H \boldsymbol{z}_{k'}^{\rm SD,f} = \boldsymbol{A}_{k'}^{\rm SD,t} \boldsymbol{x}_{k'}^{\rm t} + \hat{\boldsymbol{n}}_0^{\rm D,t}, \tag{3.58}$$

$$\boldsymbol{z}_{k'}^{\rm RD,t} = \boldsymbol{\mathcal{F}}_N^H \boldsymbol{z}_{k'}^{\rm RD,f} = \boldsymbol{A}_{k'}^{\rm RD,t} \boldsymbol{x}_{k'}^{\rm t} + \hat{\boldsymbol{n}}_1^{\rm D,t}, \tag{3.59}$$

where $\boldsymbol{z}_{k'}^{\rm SD,f}$ is the FDE output signal of the S-D link given by Eq. (3.31), and $\boldsymbol{z}_{k'}^{\rm RD,f}$ is that of the S-R-D relaying link given by Eq. (3.39) for the conventional AF scheme of Figure 3.3(a) or by Eq. (3.49) for the subband-based AF scenario of Figure 3.3(b). Since we have $\boldsymbol{A}_{k'}^{\rm SD,t} = \boldsymbol{\mathcal{F}}_N^H \boldsymbol{A}_{k'}^{\rm SD,f} \boldsymbol{\mathcal{F}}_N$ and $\boldsymbol{A}_{k'}^{\rm RD,t} = \boldsymbol{\mathcal{F}}_N^H \boldsymbol{A}_{k'}^{\rm RD,f} \boldsymbol{\mathcal{F}}_N$, where $\boldsymbol{A}_{k'}^{\rm SD,t}, \boldsymbol{A}_{k'}^{\rm RD,t}$ are both $(N \times N)$-element circulant interference matrices of the desired signal, where the gains between the desired signal $\boldsymbol{x}_{k'}^{\rm t}$ and the estimated signals $\boldsymbol{z}_{k'}^{\rm SD,t}$ and $\boldsymbol{z}_{k'}^{\rm RD,t}$ are given by the diagonal elements $a_{k',(n,n)}^{\rm SD,t}$ and $a_{k',(n,n)}^{\rm RD,t}$ of $\boldsymbol{A}_{k'}^{\rm SD,t}$ and $\boldsymbol{A}_{k'}^{\rm RD,t}$, respectively.

As we studied in Section 2.2.4, it is worth noting that the gains in the TD are identical within each signal vector, where the n-th entry of the diagonal matrix $\boldsymbol{A}_{k'}^{\rm SD,f}$ of the direct branch is given by

$$a_{k',(n,n)}^{\rm SD,f} = \frac{P_{\rm S}|h_{k',n}^{\rm SD,f}|^2}{P_{\rm S}|h_{k',n}^{\rm SD,f}|^2 + \sigma_{\rm N}^2}. \tag{3.60}$$

By contrast, the n-th entry of the diagonal matrix $\boldsymbol{A}_{k'}^{\mathrm{RD,f}}$ of the relaying branch may be calculated for the conventional AF aided SDR system as

$$a_{k',(n,n)}^{\mathrm{RD,f}} = \frac{P_{\mathrm{S}}(\beta_{k'}^{\mathrm{t}})^2 |h_{k',n}^{\mathrm{SRD,f}}|^2}{P_{\mathrm{S}}(\beta_{k'}^{\mathrm{t}})^2 |h_{k',n}^{\mathrm{SRD,f}}|^2 + \mathcal{N}_{1,n}^{\mathrm{D}}}, \tag{3.61}$$

where $\beta_{k'}^{\mathrm{t}}$ is given by Eq. (3.12), $\boldsymbol{W}_{k'}^{\mathrm{SRD}}$ is given by Eq. (3.40) and $N_{1,n}^{\mathrm{D}}$ is given by Eq. (3.42). Furthermore, when considering the conventional AF aided SSR system, $\beta_{k'}^{\mathrm{t}}$ is replaced by β^{t} of Eq. (3.19) and $N_{1,n}^{\mathrm{D}}$ is given by Eq. (3.43). When we consider the subband-based AF method of Figure 3.3(b) in Section 3.4.3, we have

$$a_{k',(n,n)}^{\mathrm{RD,f}} = \frac{P_{\mathrm{S}}(\beta_{k',n}^{\mathrm{f}})^2 |h_{k',n}^{\mathrm{RD,f}}|^2 |h_{k',n}^{\mathrm{SR,f}}|^2}{P_{\mathrm{S}}(\beta_{k',n}^{\mathrm{f}})^2 |h_{k',n}^{\mathrm{RD,f}}|^2 |h_{k',n}^{\mathrm{SR,f}}|^2 + \mathcal{N}_{1,n}^{\mathrm{D}}}, \tag{3.62}$$

where $\boldsymbol{W}_{k'}^{\mathrm{SRD}}$, $\beta_{k',n}^{\mathrm{f}}$ and $\mathcal{N}_{1,n}^{\mathrm{D}}$ are given by Eq. (3.50), Eq. (3.26) and Eq. (3.52) respectively. Hence, the gain of the direct branch may be expressed as

$$a_{k',(n,n)}^{\mathrm{SD,t}} = \frac{1}{N}\mathrm{Tr}\left[\boldsymbol{A}_{k'}^{\mathrm{SD,t}}\right] = \frac{1}{N}\sum_{n=0}^{N-1} a_{k',(n,n)}^{\mathrm{SD,f}}, \tag{3.63}$$

and that of the relaying branch is given by

$$a_{k',(n,n)}^{\mathrm{RD,t}} = \frac{1}{N}\mathrm{Tr}\left[\boldsymbol{A}_{k'}^{\mathrm{RD,t}}\right] = \frac{1}{N}\sum_{n=0}^{N-1} a_{k',(n,n)}^{\mathrm{RD,f}}. \tag{3.64}$$

Moreover, the output signal of the EGC can be expressed as

$$\boldsymbol{z}_{k'}^{\mathrm{t}} = \boldsymbol{z}_{k'}^{\mathrm{SD,t}} + \boldsymbol{z}_{k'}^{\mathrm{RD,t}} = \boldsymbol{A}_{k'}^{\mathrm{t}}\boldsymbol{x}_{k'}^{\mathrm{t}} + \hat{\boldsymbol{n}}_{\mathrm{D}}^{\mathrm{t}}, \tag{3.65}$$

where $\boldsymbol{A}_{k'}^{\mathrm{t}} = \boldsymbol{A}_{k'}^{\mathrm{SD,t}} + \boldsymbol{A}_{k'}^{\mathrm{RD,t}}$ and $\hat{\boldsymbol{n}}_{\mathrm{D}}^{\mathrm{t}} = \hat{\boldsymbol{n}}_{0}^{\mathrm{D,t}} + \hat{\boldsymbol{n}}_{1}^{\mathrm{D,t}}$. Specifically, $\boldsymbol{A}_{k'}^{\mathrm{t}}$ is a $(N\times N)$-element circulant matrix of the desired signal, where the gain between the desired signal and the combined estimated signals of the two branches is given by the diagonal elements of $\boldsymbol{A}_{k'}^{\mathrm{t}}$, which are identical in the TD. Thus, the power of the desired signal at any instant is given by

$$P_{\mathrm{des}} = P_{\mathrm{S}}\left\{\frac{1}{N}\mathrm{Tr}\left[\boldsymbol{A}_{k'}^{\mathrm{t}}\right]\right\}^2 = P_{\mathrm{S}}\left[\frac{1}{N}\sum_{n=0}^{N-1}(a_{k',(n,n)}^{\mathrm{SD,f}} + a_{k',(n,n)}^{\mathrm{RD,f}})\right]^2. \tag{3.66}$$

Additionally, the power P_{est} of the combined estimated signal, which is equal to the power P_{des} of the desired signal plus the power P_{ISI} of the ISI component, is given by the diagonal

elements of the covariance matrix of the combined estimated signal $\boldsymbol{A}_{k'}^{\mathrm{t}}\boldsymbol{x}_{k'}^{\mathrm{t}}$, yielding

$$P_{\mathrm{est}} = \frac{1}{N}\mathrm{Tr}\left\{\mathrm{E}\left[\boldsymbol{A}_{k'}^{\mathrm{t}}\boldsymbol{x}_{k'}^{\mathrm{t}}(\boldsymbol{x}_{k'}^{\mathrm{t}})^H(\boldsymbol{A}_{k'}^{\mathrm{t}})^H\right]\right\} = \frac{P_{\mathrm{S}}}{N}\sum_{n=0}^{N-1}(a_{k',(n,n)}^{\mathrm{SD,f}} + a_{k',(n,n)}^{\mathrm{RD,f}})^2. \tag{3.67}$$

Since we have $\hat{\boldsymbol{n}}_0^{\mathrm{D,t}} = \boldsymbol{\mathcal{F}}_N^H\hat{\boldsymbol{n}}_0^{\mathrm{D,f}}$ and $\hat{\boldsymbol{n}}_1^{\mathrm{D,t}} = \boldsymbol{\mathcal{F}}_N^H\hat{\boldsymbol{n}}_1^{\mathrm{D,f}}$, the power of the noise that contaminates the desired signal at both the direct and relaying branch is given by the diagonal elements of the covariance matrix $\hat{\boldsymbol{n}}_{\mathrm{D}}^{\mathrm{t}}$ in Eq. (3.65), yielding

$$\hat{\mathcal{N}}_{\mathrm{D}} = \frac{1}{N}\mathrm{Tr}\left\{\mathrm{E}[\hat{\boldsymbol{n}}_{\mathrm{D}}^{\mathrm{t}}(\hat{\boldsymbol{n}}_{\mathrm{D}}^{\mathrm{t}})^H]\right\} = \frac{1}{N}\sum_{n=0}^{N-1}\left\{\hat{\mathcal{N}}_{0,n}^{\mathrm{D}} + \hat{\mathcal{N}}_{1,n}^{\mathrm{D}}\right\} \tag{3.68}$$

where $\hat{\mathcal{N}}_{0,n}^{\mathrm{D}}$ is shown in Eq.(3.35) while $\hat{\mathcal{N}}_{1,n}^{\mathrm{D}} = \mathcal{N}_{1,n}^{\mathrm{D}}|w_{k',n}^{\mathrm{SRD}}|^2$ denotes the power of the n-th entry of the diagonal matrix, and $w_{k',n}^{\mathrm{SRD}}$ and $\mathcal{N}_{1,n}^{\mathrm{D}}$ are given by Eq. (3.42) and Eq. (3.41) in the Section 3.4.2.

Finally, we arrive at the k'-th user's total equivalent SINR for the proposed systems expressed as

$$\gamma_{\Sigma,k'} = \frac{P_{\mathrm{des}}}{P_{\mathrm{est}} - P_{\mathrm{des}} + \hat{\mathcal{N}}_{\mathrm{D}}}. \tag{3.69}$$

3.5 Simulation Results and Discussions

In this section, we provide a range of simulation results for characterising the achievable *bit-error rate* (BER) performance of the single-relay assisted SC-FDMA system based on the different cooperative approaches investigated. We assume that the transmitted signals are *binary phase-shift keying* (BPSK) modulated without channel coding, when communicating over frequency-selective Rayleigh fading channels in the absence of large-scale fading.

3.5.1 Performance of Single-Relay-Assisted Cooperative SC-FDMA

In this section, we provide performance comparisons between the conventional AF scheme of Section 3.3.1 and the subband-based AF scheme of Section 3.3.2, when the BS's receiver invokes the TD-EGC scheme of Figure 3.4 relying on the MMSE FDE. The performance of the non-cooperative direct transmission (DT) based SC-FDMA system is our benchmark. Our parameters are summarised in Table 3.1 and Table 3.2.

Figures 3.7 and 3.8 characterise the BER versus E_b/N_0 performance of both the conventional AF (on the left) and of the subband-based AF (on the right) aided SDR assisted SC-FDMA

TABLE 3.1: Channel modelling of single-relay aided cooperation

Topology	SDR or SSR
S-D, S-R, R-D channels	Frequency-selective Rayleigh fading
Power delay spread	Uniform
Shadowing	Absent
Path-loss	Absent
Channel correlation	Uncorrelated
Power control	Perfect
Number of CIR taps (paths)	$L = 1, 4, 8$

TABLE 3.2: Resource allocation for single-relay aided AF cooperative SC-FDMA

Subband mapping	Interleaved
Subband allocation	Static
Number of subbands per user	$N = 4, 8$
Bandwidth expansion factor	$M = 16, 8$
Total number of subbands	$U = 64$
Number of users (source MTs)	$K = 1, 2, 4, 8, 16$
Number of BS receiver antennas	$N_r = 1$
Total transmit power per user	$P_k = 1$
Source transmit power per user	SDR: $P_S = 0.5$ SSR for $K = 1$: $P_S = 0.5$ SSR for $K > 1$: $P_S = 1 - 1/K$
Relay transmit power per user	SDR: $P_R = 0.5$ SSR for $K = 1$: $P_R = 0.5$ SSR for $K > 1$: $P_R = 1/K$

system, when using the MMSE FDE based TD-EGC for different number of users K and for L CIR taps. Furthermore, we have $N = 4, M = 16, L = 1, 4$ and $N = 8, M = 8, L = 1, 8$.

Observe in Figures 3.7(a) and 3.8(a) that a cooperative diversity gain is achieved by the conventional AF aided SDR scheme for a single-user system communicating over single-path fading channels. By contrast, observe in Figure 3.7(c) and 3.8(c), that for the multi-path scenario of $L = 4$ and $L = 8$, cooperative diversity gains are only achieved at high SNRs for a single-user scenario. Moreover, as a consequence of the excessive noise imposed by the relays of the K users across all subbands, the cooperative diversity gains of the SDR scheme are eroded in a multi-user scenario, when K is increased. Additionally, compared to the single-path scenario, the multi-path diversity gain provided by frequency-selective fading is retained, regardless of the number of users. The maximum diversity gain was achieved for $L = 4$, when we had $N = 4$, as shown in Fig. 3.7(c), and for $L = 8$ when we had $N = 8$, as quantified by Fig. 3.8(c).

In the subband-based AF aided SDR scenario we only had single relay that contaminated the signal by the AWGN, as stated in Subsection 3.3.2. Thus, the multi-user performance of the subband-based AF aided SDR approach is the same as that of the single-user case

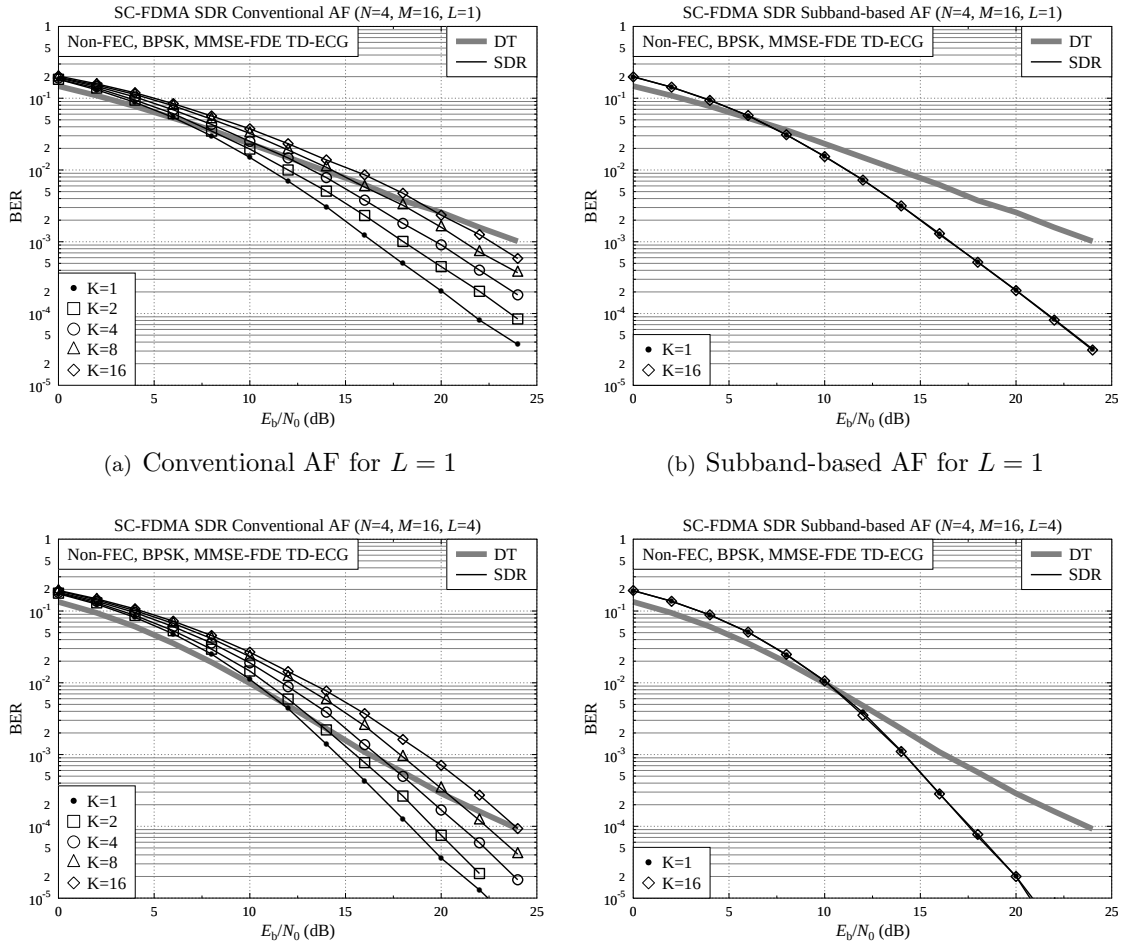

(a) Conventional AF for $L = 1$

(b) Subband-based AF for $L = 1$

(c) Conventional AF for $L = 4$

(d) Subband-based AF for $L = 4$

FIGURE 3.7: BER versus E_b/N_0 performance of the conventional AF and subband-based AF aided SDR systems of Figure 3.1(a), respectively, when the BS's receiver invokes MMSE FDE assisted TD-EGC of Figure 3.4 upon varying the number of users K for $N = 4, M = 16$, respectively. The system parameters were summarised in Table 3.1 and Table 3.2.

supported by a single relay, where we have $L = 1, 4$ and 8, as shown in Figures 3.7(b), 3.7(d), 3.8(b) and 3.8(d). On the other hand, a cooperative diversity gain is attained also in a multi-user scenario when communicating over a single-path fading channel for $L = 1$, which can be preserved for transmission over multi-path channels, provided that the SNR is sufficiently high, as shown in Figures 3.7(b) and 3.7(d). Since the subband-based AF scheme has a similar effect as a FDE invoked at the relay, plus the MMSE FDE employed at the BS for the entire relay branch, both the noise imposed by the relay as well as the ISI imposed by the multi-path components have been suppressed at the BS. Hence, as demonstrated by Figures 3.7 and 3.8 the achievable performance becomes better than that of the corresponding single-user performance of the conventional AF aided SDR scheme, where the same amplification factor was applied to all the subbands.

Let us now discuss the performance of both the conventional AF as well as of the subband-

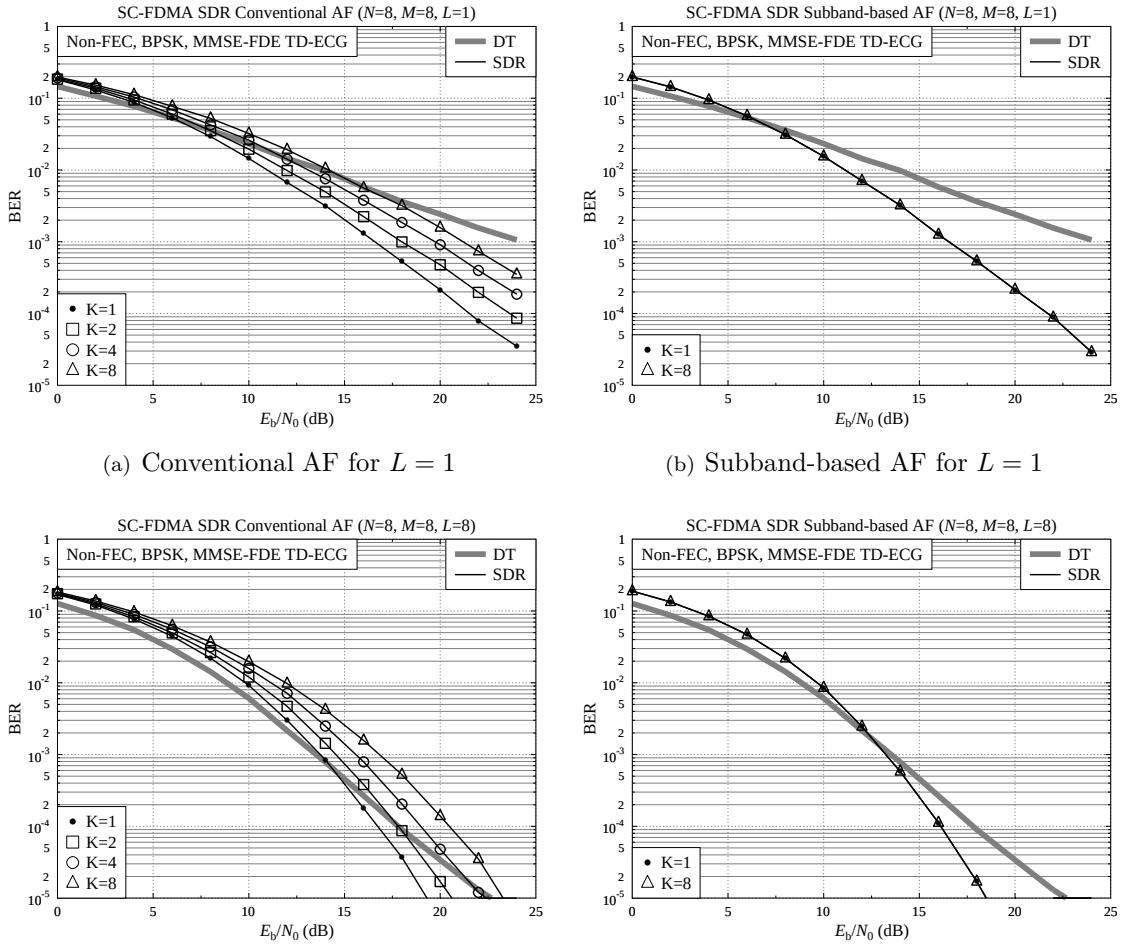

(a) Conventional AF for $L = 1$

(b) Subband-based AF for $L = 1$

(c) Conventional AF for $L = 8$

(d) Subband-based AF for $L = 8$

FIGURE 3.8: BER versus E_b/N_0 performance of the conventional AF and subband-based AF aided SDR systems of Figure 3.1(a), respectively, when the BS's receiver invokes MMSE FDE assisted TD-EGC of Figure 3.4 upon varying the number of users K for $N = M = 8$. The system parameters were summarised in Tables 3.1 and 3.2.

based AF aided SSR systems upon varying the number of users K, which is illustrated in Figure 3.9 and Figure 3.10, for $N = 4, M = 16, L = 1, 4$ and $N = 8, M = 8, L = 1, 8$, respectively.

Observe in Figures 3.9(a), 3.9(c), 3.10(a) and 3.10(c) that a cooperative diversity gain of $5-8$dB or $6-8$dB is achieved by the conventional AF aided SSR system for transmission over a single-path channel for $N = 4$, $M = 16$, $L = 1$ or $N = 8$, $M = 8$, $L = 1$ at a BER of 10^{-3}. However, since the multi-path diversity gain is high, when we have $N = 4, M = 16, L = 4$ or $N = 8, M = 8, L = 8$, the cooperative diversity aided performance is eroded by the interference inflicted by the dispersive channel.

By contrast, the performance recorded upon varying the number of users supported by the subband-based AF aided SSR approach is characterised in Figures 3.9(b) and 3.9(d) as

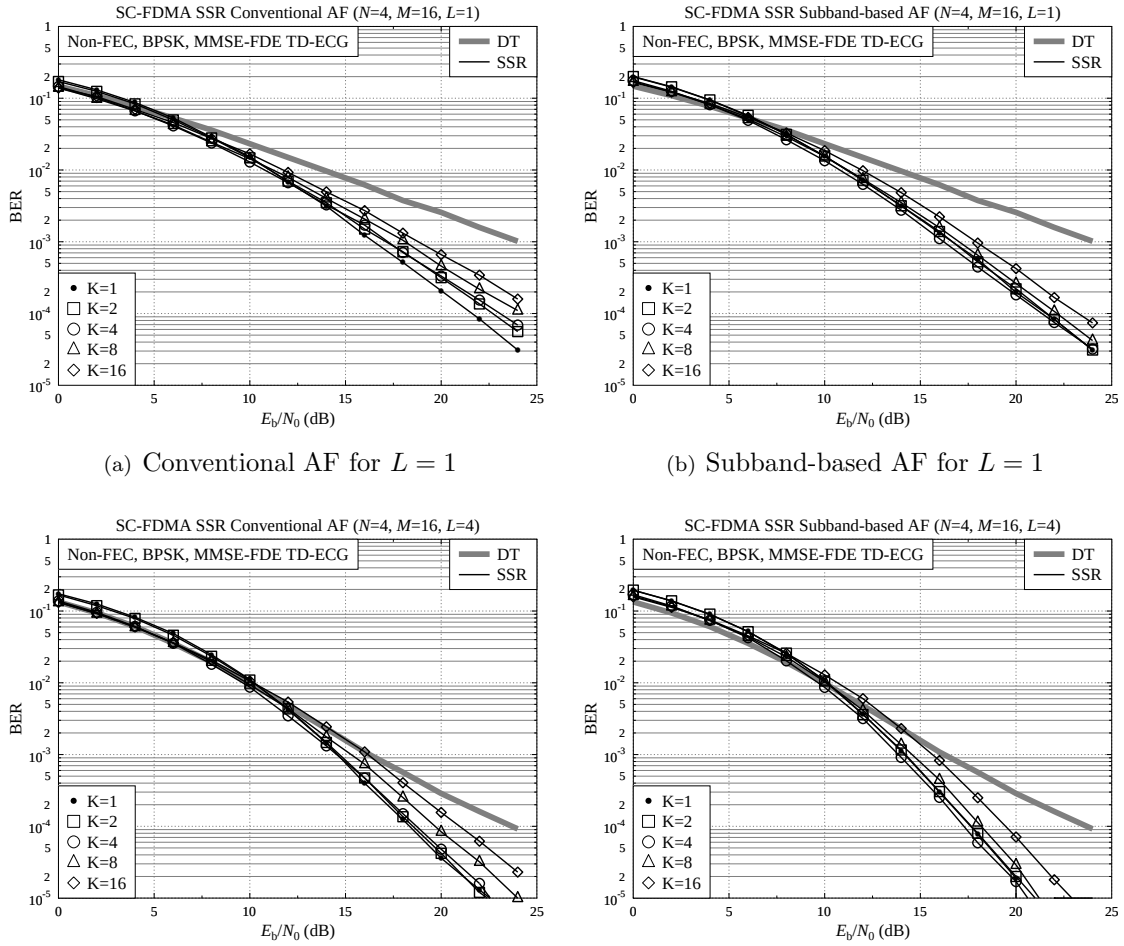

(a) Conventional AF for $L = 1$

(b) Subband-based AF for $L = 1$

(c) Conventional AF for $L = 4$

(d) Subband-based AF for $L = 4$

FIGURE 3.9: BER versus E_b/N_0 performance of the conventional AF and subband-based AF aided SSR systems of Figure 3.1(b), respectively, when the BS's receiver invokes MMSE FDE assisted TD-EGC of Figure 3.4 upon varying the number of users K for $N = 4, M = 16$. The system parameters were summarised in Tables 3.1 and 3.2.

well as in Figures 3.10(b) and 3.10(d) for both $N = 4$, $M = 16$, $L = 1, 4$ as well as for $N = 8$, $M = 8$, $L = 1, 8$, respectively. Compared to the corresponding conventional AF aided SSR scheme of Figures 3.9(a), 3.9(c), 3.10(a) and 3.10(c), the cooperative diversity gain was increased by both the single-user and multi-user system in Figures 3.9(b), 3.9(d), 3.10(b) and 3.10(d), when employing the subband-based AF aided SSR scheme, particularly in a multi-path environment. This is expected, because in addition to the beneficial fading mitigation effect of multi-path diversity, the ISI imposed by the dispersive channel was also suppressed by including the subband-based AF scheme of Figure 3.3(b) at relay and MMSE FDE of Figure 3.4 at the BS. The achievable cooperative diversity gain ranges from $5-8$dB for $N = 4, M = 16, L = 4$ at a BER of 10^{-4}, as shown in Figure 3.9(d). By contrast, for the case of $N = 8, M = 8, L = 8$, observe in Figure 3.10(d) that the achievable cooperative diversity gain remains as low as $1-2$dB at a BER of 10^{-4} in the multi-user environment.

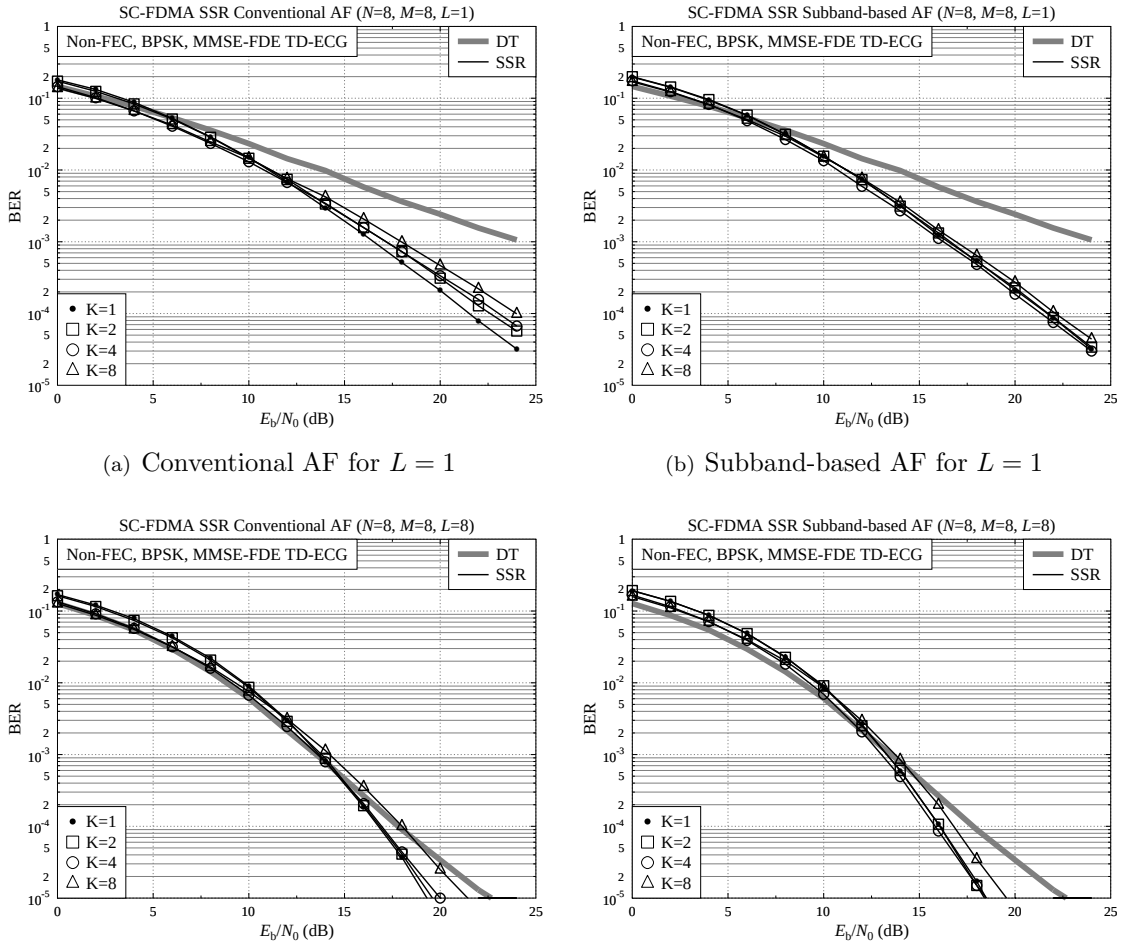

(a) Conventional AF for $L = 1$

(b) Subband-based AF for $L = 1$

(c) Conventional AF for $L = 8$

(d) Subband-based AF for $L = 8$

FIGURE 3.10: BER versus E_b/N_0 performance of the conventional AF and subband-based AF aided SSR systems of Figure 3.1(b), respectively, when the BS's receiver invokes MMSE FDE assisted TD-EGC of Figure 3.4 upon varying the number of users K for $N = M = 8$. The system parameters were summarised in Tables 3.1 and 3.2.

Additionally, since no path-loss is considered, the DT may be the best in comparison to the AF relaying, when the E_b/N_0 is up to 15 as shown in Figure 3.8(c) and Figure 3.10(c) for example.

3.6 Summary

In this chapter, we investigated the AF aided fixed-relay assisted cooperative SC-FDMA scheme using IFDMA signalling. Both the SDR and SSR topologies of Figure 3.1 were considered, when the multi-user systems have either K relays, so that each of them is dedicated to a single user, or the systems have insufficient relays, when the relays have to be shared by multiple users. In this chapter, two types of AF relaying schemes were studied for both the SDR and SSR topologies, namely the conventional AF scheme of Figure 3.3(a)

TABLE 3.3: Power reduction in terms of SNR gain per bit $\gamma_{\mathrm{b}}^{\Delta}$ of the various single-relay assisted AF schemes for the cooperative SC-FDMA uplink compared to the DT benchmark, when communicating over frequency-selective fading channels. The schemes are listed in descending order of complexity.

$\gamma_{\Delta}^{\mathrm{b}}$ (dB)	$N = L = 4$, $K = 16$		$N = L = K = 8$	
	SDR	SSR	SDR	SSR
Subband-based AF	8	5	2	1
Conventional AF	0	3	−3	0

and the proposed subband-based AF scheme of Figure 3.3(b). Specifically, the proposed subband-based AF relaying scheme of Section 3.3.2 was designed for the sake of imposed noise suppression at the relays. Furthermore, the MMSE based FDE of Figure 3.4 was employed separately for both the direct- and relaying-channels. Then the decision variables generated were combined by the simple TD-EGC of Figure 3.4.

The performance results of Figures 3.7 to 3.10 demonstrated that the proposed single-relay assisted cooperative SC-FDMA schemes are free from MUI at the relays, when communicating over frequency-selective fading channels. The IFDMA signalling scheme of Figure 2.9(b) is capable of providing a significant frequency diversity gain for the cooperative systems, where cooperative diversity may be achieved for both topologies in both single-path and multi-path fading channels. As a result, the subband-based AF scheme of Figure 3.3(b) is capable of achieving a multi-user performance, which is better than that of the conventional single-user AF protocol of Figure 3.3(a) operated in a multi-path environment, which is an explicit benefit of the subband-based AF scheme as well as that of noise suppression capability of the relay. It can be shown that the achievable power reduction may be up to 8 dB at a BER of 10^{-4}, when compared to the DT benchmark. Finally, Table 3.3 summarises the power reduction in terms of the SNR gain per bit $\gamma_{\Delta}^{\mathrm{b}}$ recorded at the BER of 10^{-4} for the various single-relay assisted AF schemes of the cooperative SC-FDMA uplink compared to the DT benchmark, when experiencing frequency-selective fading. The schemes are listed in descending order of complexity.

In the next chapter, we will consider dynamic relaying scenarios, where both relay selection schemes and power allocation schemes will be conceived for the cooperative SC-FDMA systems in the presence of path-loss and shadowing.

Chapter 4

The Opportunistic Amplify-and-Forward Cooperative SC-FDMA Uplink

4.1 Introduction

Cooperative communication [31] systems have attracted the attention of both academia and industry in recent years, since they are capable of achieving a diversity gain in large-scale fading environments by sharing the resources of the cooperating user terminals. This allows us to jointly exploit the benefits of both *time*- and *frequency-diversity* for the sake of mitigating the deleterious effects of wireless propagation and/or for increasing the attainable system throughput and *energy-efficiency* [39, 40, 43, 46]. Recently, the family of *cooperative diversity* oriented *multiple-access* and virtual *multiple-input multiple-output* (MIMO) aided *multiplexing* techniques has been invoked in order to design the uplink of advanced cooperative cellular networks [63,64,174]. Furthermore, the cooperative concepts have been extended to broadband systems by designing techniques for mitigating the effects of frequency-selective fading with the aid of multi-carrier techniques associated with appropriate *source/relay power allocation* [80, 175].

From a multi-user networking perspective, the cooperative link spanning from the source *mobile terminals* (MT) to the *base station* (BS) can be determined by choosing either a single or multiple relays [33] from a cluster of idle MTs. Generally, *static relay selection* (SRS) assigns the relays for the entire duration of a session, hence the achievable gains depend on the velocity of the cooperating nodes. Furthermore, the *random relay selection* (RRS) philosophy allows the BS to appoint a relay randomly without any channel knowledge, but in

this scenario the simultaneous relay-aided path-loss reduction and selection diversity gains remain limited. By contrast, the so-called *distance-dependent relay selection* [64] policy is based on the distance from the relay to the source MT or BS, hence the relays which benefit from a high path-loss reduction may experience deep shadowing and fast fading. However, the *channel-dependent relay selection* regime benefits from a certain *degree-of-freedom* owing to selecting inactive MTs as relays by monitoring the instantaneous channel conditions in a distributed scenario, including the associated path-loss, shadowing and multi-path fading effects. Therefore, it is also known as *opportunistic relaying* [65], which is capable of exploiting the selection diversity that we refer to as *multi-user diversity* arising from appropriate relay selection [16, 66, 67, 81]. However, the low-quality direct link between the source MT and the BS may be ignored in the context of opportunistic relaying. Nonetheless, if the knowledge of direct link's quality is available, the signals received from both the direct link and from the opportunistic relaying links may be beneficially combined at the BS for the sake of achieving a cooperative diversity gain. We refer to this regime as *opportunistic cooperation* (OC)[1] [176–181].

The *single-carrier frequency-domain multiple-access* (SC-FDMA) technique [125] was adopted for the uplink of the *Third Generation Partnership Project*'s (3GPP) *Long Term Evolution* (LTE) standard [35]. Falconer *et al.* [94, 114] combined single-carrier modulation with both linear and non-linear *frequency-domain equalisation* (FDE) [171] techniques for high-rate broadband receiver solutions. Furthermore, the SC-FDMA uplink scheme of Section 2.2 and the *discrete Fourier transform* (DFT)-spread *orthogonal frequency-division multiple-access* (OFDMA) transmitter structures using either the *interleaved* or *localised subband mapping* schemes of Section 2.2.2 were studied in [91, 102]. SC-FDMA was shown to be capable of avoiding the *multi-user interference* (MUI) imposed by the cooperative sources and relays upon the uplink receiver of the BS, while maintaining a low *peak-to-average power ratio* (PAPR).

In Chapter 3 [182], the *amplify-and-forward* (AF) single-relay assisted SC-FDMA uplink scheme was proposed for both the *single-dedicated-relaying* (SDR) and *single-shared-relaying* (SSR) scheme of Figure 3.1. The AF relay estimates the received power of each subband and equalises the power-differences of the subbands, which corresponds to the subband-based equalisation regime of Figure 3.3(b). By inheriting the features of the SC-FDMA system invoking DFT-spread OFDMA-style transmitter of Figure 3.2, this relaying scheme invokes *subband remapping* of Figure 3.6 at the relay in order to remove the effects of both noise and interference inflicted by other relays. This is achieved without changing the frequency band of the signals transmitted from the source MT as detailed in Section 3.3.2.

[1] In this chapter, we assume that the direct link is available, hence we use the terminology of 'opportunistic cooperation'. In Chapter 5, we will assume that the direct link is unavailable, therefore we will use the terminology of 'opportunistic relaying'.

An *orthogonal frequency-division multiplexing* (OFDM) [55] scheme of Figure 2.1 relying on time-division multiplexing based cooperative relaying and using the *minimum mean-square error* (MMSE) assisted *frequency-domain linear equalisers* (FD-LE) of Figure 3.4 in Section 3.4 was proposed in [183]. However, in [182] and [183], the MMSE FD-LE operated in isolation for the direct and relaying branches, which were then combined with the aid of the *time-domain equal-gain combiner* (TD-EGC) of Figure 3.4 in Section 3.4. In [118, 120, 184–186], adaptive linear FDEs relying on *diversity combining* schemes were invoked for either multiple-antenna aided single-carrier or for OFDM-based block transmissions. Furthermore, in [187–189] a range of receive diversity combining techniques designed for SC-FDMA and relying on cooperative relays were considered by stipulating the idealised simplifying assumption that the relays demodulate/detect the source signals perfectly, before forwarding them to the destination.

- Although the authors of the above-mentioned articles proposed various FDEs amalgamated with diversity combining schemes designed for MIMOs, for OFDM or for relaying systems, owing to the potentially non-white noise contribution of AF cooperative relaying, the equivalent noise encountered at the BS's receiver also becomes non-white. Furthermore, we typically encounter a different noise power at each cooperative branch, hence the conventional *maximum ratio combiner* (MRC) [100] becomes sub-optimal, unless *noise whitening* is adopted. To the best of our knowledge, no article investigated the joint design of the linear single-tap MMSE FD-LE amalgamated with the diversity combiner of the direct- and relay-link using noise-whitening for the AF relaying assisted SC-FDMA uplink.

- Since finite-delay *power control* schemes using a discrete step-size cannot perform perfectly in realistic wireless uplink transmissions, the source/relay power allocation employed imposes a time-varying level of *power control error* (PCE) [190]. In [63,80,81, 175], various relay selection and source/relay power allocation schemes were proposed and studied, but no such schemes were designed for the cooperative SC-FDMA uplink under imperfect power control with the goal of improving the energy-efficiency.

- The authors of [191–193] studied various relay selection schemes designed for both OFDM and *code-division multiple-access* (CDMA) systems subjected to both path-loss and multi-path fading. However, cooperative relaying allows the collaborating mobiles to avoid the typical diversity gain erosion imposed by shadowing effects, as a benefit of their geographically separated locations. Hence we embarked on investigating the benefits of relay selection for our system in the presence of shadow fading, whose impact on the energy-efficiency of cooperative SC-FDMA systems has not been documented in the open literature.

In this chapter, we propose and investigate ***energy-efficient*** *OC schemes designed for SC-FDMA arrangements. The* ***joint frequency-domain equalisation and diversity combining*** *(JFDEC) aided receiver is designed for detecting the cooperative SC-FDMA uplink signals. Both* ***single-user relay selection*** *(SU-RS) and* ***multi-user relay selection*** *(MU-RS) as well as* ***multiple-access relay selection*** *(MA-RS) are considered in diverse OC scenarios. By contrast, in [194] only the SU-RS and MU-RS schemes based on the JFDEC receiver were studied in the context of the SDR topology.*

- *Furthermore, in contrast to the open literature, our focus is mainly on the analysis of the energy-efficiency of the cooperative SC-FDMA system, where the energy-efficiency is quantified in terms of* ***energy consumption gain*** *(ECG)*[2]*.*

- *The MMSE criterion aided JFDEC scheme considered in [194] is further detailed, which amalgamates the design of the linear single-tap MMSE FD-LE and that of the diversity combiner of the direct- and relay-link with noise whitening applied at the BS.*

- *Furthermore, we investigate the MA-RS scheme created by generalising both the SU-RS and MU-RS philosophies developed from the SDR to SSR topologies of Figure 3.1, where the relative merits of the SU-RS, MU-RS and MA-RS schemes are discussed in the light of their complexity. The effects of* ***imperfect power control***[3] *are also quantified.*

- *Additionally, we demonstrate that upon encountering a realistic propagation* ***path-loss*** *and* ***shadowing****, a significant* ***relaying-assisted path-loss reduction*** *and* ***selection diversity gain*** *are attainable by the proposed* ***optimal power allocation*** *(OPA)*[4] *aided SU-RS, MU-RS and MA-RS schemes, which allows us to reduce the required* ***signal-to-interference-plus-noise ratio*** *(SINR) for the sake of improving the performance of ECG. Finally, the practicability and feasibility of various power allocation schemes are discussed in terms of their computational complexity.*

This chapter is organised as follows. In Section 4.2, the system model of the cooperative SC-FDMA uplink is presented. In Sections 4.3 and 4.5, we outline the improved signal detection and investigate the relay selection schemes, respectively. The attainable performance of our proposed schemes is quantified by the simulation results of Section 4.6. Finally, we conclude in Section 4.7.

[2]As the metric of comparing two different systems, the ECG is simply defined in [1] as the ratio of *energy consumption per bit* by a reference system divided by that of a proposed system under test, where the absolute measure of *energy consumption per bit* is defined as the peak power divided by the maximum throughput.

[3]PCEs are imposed on the MT's transmit power due to the feedback delay and estimation errors at the BS.

[4]Optimised transmit power allocation of cooperative MTs is assigned by the BS via feedback channel by ignoring PCE.

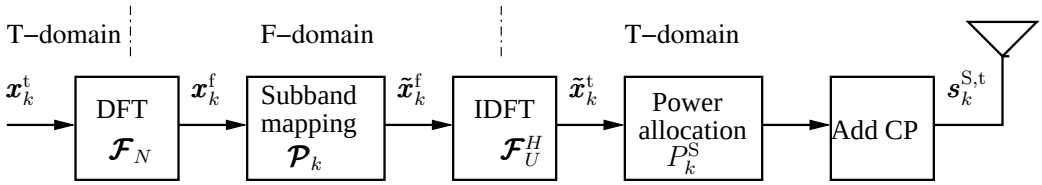

FIGURE 4.1: Transmitter schematic of the SC-FDMA source MT. This figure was repeated from Figure 3.2 for convenience. The corresponding TD and FD signals using IFDMA scheme were seen in Figure 2.10(b) and Figure 2.11(b), respectively. The transceiver schematic of the relay is portrayed in Figure 4.3 while the corresponding receivers at the BS is shown in Figure 4.4.

4.2 Relay Assisted SC-FDMA System Model

4.2.1 Transmitted Signal of Source MT

The relay-assisted SC-FDMA system considered supports K uplink users referred to as the source MTs in a cell. There are also idle terminals, which can be activated as the relays. The transmitter's block diagram is seen in the Figure 4.1. The U-symbol baseband equivalent discrete-time signal transmitted by the k-th source MT before inserting the *cyclic-prefix* (CP) was given in Eq. (3.2) and expressed as

$$\boldsymbol{s}_k^{\mathrm{S,t}} = \sqrt{P_k^{\mathrm{S}}}\boldsymbol{\mathcal{F}}_U^H \boldsymbol{\mathcal{P}}_k \boldsymbol{\mathcal{F}}_N \boldsymbol{x}_k^{\mathrm{t}}, \tag{4.1}$$

where the superscript $^{\mathrm{t}}$ refers to the time-domain (TD) signal, while $\boldsymbol{\mathcal{F}}_U$ and $\boldsymbol{\mathcal{F}}_N$ denote the normalised U-point and N-point DFT matrices in the form of Eq. (2.2), respectively. Furthermore, $\boldsymbol{\mathcal{P}}_k$ represents the mapping of the k-th user's symbols to the most appropriate N subbands selected from the entire set of $U = M \times N$ subbands, where M is the bandwidth expansion factor as seen in the FD plots of Figure 2.9. We refer to this operation as subband mapping, which relied on the schematic of Figure 2.8(b). In the FDMA context considered this subband mapping regime guarantees that the maximum number of orthogonal FD users supported is equal to the bandwidth expansion factor, i.e. we have $K \leqslant M$, and the multi-user system operates at its full-load, when we have $K = M$. Moreover, according to Section 2.2.2, the interleaved subband mapping mode of Figure 2.9(b) used in our system is defined as $\mathcal{P}_{k,(u,i)} = 1$ if $u = iM + k$, otherwise $\mathcal{P}_{k,(u,i)} = 0, (0 < u < U-1, 0 < i < N-1)$, where $\mathcal{P}_{k,(u,n)}$ is the (u,n)-th entry of $\boldsymbol{\mathcal{P}}_k$ and we have $u = 0, 1, \cdots, U-1,\ n = 0, 1, \cdots, N-1$. Additionally, $\boldsymbol{x}_k^{\mathrm{t}}$ denotes the original N-symbol information packet of the k-th user. Finally, P_k^{S} is the source MT's transmitted power determined by the power allocation, which is always subject to a certain PCE in practice as it will be discussed in Section 4.2.2.

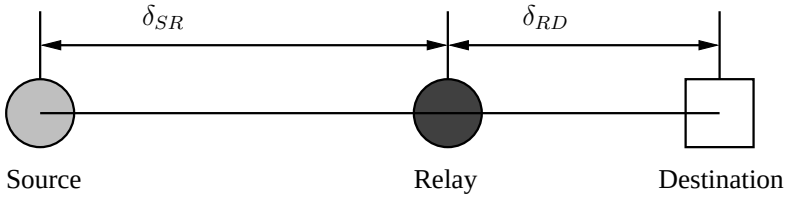

FIGURE 4.2: Schematic of two-dimensional (2D) relaying map. The source-relay (S-R) distance δ_k^{SR} and relay-destination (R-D) distance δ_k^{RD} are normalised by the S-D distance.

4.2.2 Channel Modelling and Assumptions

For the sake of simplicity, we assume that all the source MTs, the relays as well as the BS are aligned within a line, and the relays are geographically distributed and roaming between the *source* and *destination* along this line as shown in Figure 4.2. Let us assume that the length of the *source-destination* (S-D) link is the reference distance in the propagation model having a *path-loss exponent* of η [100]. Then, the *instantaneous* path-loss values of the relay channels for the user k, which are denoted by G_k^{SR} for the *source-relay* (S-R) and G_k^{RD} for the *relay-destination* (R-D), respectively, become the corresponding relaying-assisted path-loss reductions, referred as *relaying gain*, incorporating the effects of the *average* path-loss combined with shadowing. Specifically, the average path-losses of the S-R and R-D links are denoted by $(\delta_k^{\mathrm{SR}})^{-\eta}$ and $(\delta_k^{\mathrm{RD}})^{-\eta}$, respectively, where $\delta_k^{\mathrm{SR}} + \delta_k^{\mathrm{RD}} = 1$, and δ_k^{SR} and δ_k^{RD} represent the S-R and R-D distances normalised by the S-D distance. The shadowing component is characterised by the *log-normal* distribution associated with a *zero mean* and a *standard deviation* of σ_ξ, i.e. we have $\xi(dB) \sim \mathcal{N}(0, \sigma_\xi^2)$. Therefore, we can write $G_k^{\mathrm{SR}} = \xi_{\mathrm{SR}}(\delta_k^{\mathrm{SR}})^{-\eta}$, $G_k^{\mathrm{RD}} = \xi_{\mathrm{RD}}(\delta_k^{\mathrm{RD}})^{-\eta}$, while the shadowing effect at the S-D link is denoted by ξ_{SD} [195].

We consider a small-scale fading scenario, where the system experiences frequency-selective fading associated with L paths. However, each subcarrier is assumed to experience flat fading. We assume that perfect *channel state information* (CSI) is available for both the relays and the BS, including the path-loss, shadowing and small-scale fading.

Furthermore, in order to guarantee a fair comparison between the cooperative and *direct transmission* (DT) systems, the total signal power P of each user is normalised to *unity*. Specifically, the source and relay MTs' transmit power assigned to the k-th user are quantified as $P_k^{\mathrm{S}} = \epsilon_k^{\mathrm{S}} \alpha_k^{\mathrm{S}} P$ and $P_k^{\mathrm{R}} = \epsilon_k^{\mathrm{R}} \alpha_k^{\mathrm{R}} P$, respectively. The *imperfect* power control effects imposed on the transmitted power of the MTs can be evaluated by modelling it using the classic log-normally distributed PCE having a standard deviation of σ_ϵ in dB, i.e. we have $\epsilon(dB) \sim \mathcal{N}(0, \sigma_\epsilon^2)$ [190]. Additionally, based on Eq. (3.1), we quantify the power constraints of the source and relay as

$$\alpha_k^{\mathrm{S}} + \alpha_k^{\mathrm{R}} = 1, \tag{4.2}$$

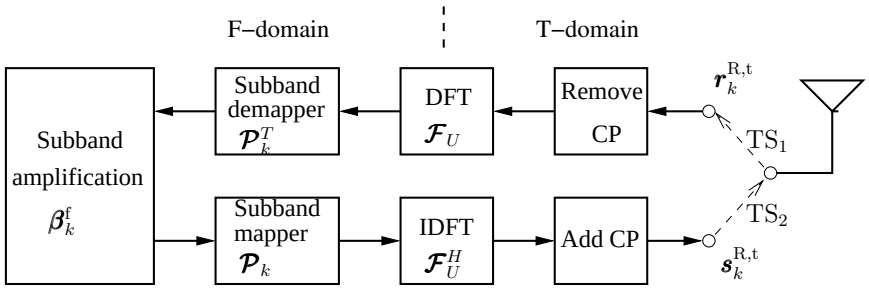

FIGURE 4.3: Transceiver schematic of the subband-based AF relay designed for matching the source transmitter of Figure 4.1 and destination receiver of Figure 4.4. The corresponding TD/FD plots are seen Figure 2.10(b) and Figure 2.11(b). This figure is repeated from Figure 3.3(b) for convenience.

where α_k^{S} and α_k^{R} represent the power allocation between the source and relay. Note that in the SSR topology of Figure 3.1(b), the single-relay simultaneously transmits all the K users' signals, while obeying the power constraint given in Eq. (3.10). Hence we arrive at

$$\alpha_{\Sigma}^{\mathrm{R}} = \sum_{k=0}^{K-1} \alpha_k^{\mathrm{R}} = 1. \tag{4.3}$$

4.2.3 Relaying Models

In order to separate multiple users in the *frequency-domain* (FD) and hence to avoid the MUI, each source MT is assigned a single relay by the BS according to the *opportunistic cooperation* (OC) mechanism to be detailed in our forthcoming discourse in Section 4.5. The block diagram of the subband-based AF relay model of Section 3.3.2 is shown in Figure 4.3. We assume that the cooperation is *half-duplex time-division* based. Hence during the first *time-slot* (TS$_1$) all the K source MTs *broadcast* their messages represented by $\boldsymbol{s}_k^{\mathrm{S,t}}, (k = 0, 1, \cdots, K-1)$, which are received by both the relays and the BS via the S-R and S-D links, respectively. During the second time-slot (TS$_2$), which is the *cooperation-phase*, we consider both the SDR and SSR scenarios.

In the SDR system of Figure 3.1(a) we investigated in Section 3.2.3, the relays only forward the signals from the dedicated source MT to the BS via the R-D links, implying that a total of K relays are required for K source MTs. Based on Eq. 3.8 and taking the relaying gain into account, the signal received by the k'-th relay ($k' = 0, 1, \cdots, K-1$) as well as by the BS during TS$_1$ and TS$_2$, respectively, are expressed by the U-length vectors of

$$\boldsymbol{r}_{k'}^{\mathrm{R,t}} = \sqrt{G_k^{\mathrm{SR}}} \sum_{k=0}^{K-1} \tilde{\boldsymbol{H}}_k^{\mathrm{SR,t}} \boldsymbol{s}_k^{\mathrm{S,t}} + \tilde{\boldsymbol{n}}_k^{\mathrm{R,t}}, \tag{4.4a}$$

$$\boldsymbol{r}_1^{\mathrm{D,t}} = \sqrt{G_k^{\mathrm{RD}}} \sum_{k'=0}^{K-1} \tilde{\boldsymbol{H}}_{k'}^{\mathrm{RD,t}} \boldsymbol{s}_{k'}^{\mathrm{R,t}} + \tilde{\boldsymbol{n}}_1^{\mathrm{D,t}}, \tag{4.4b}$$

where the $(U\times U)$-element circulant matrices $\tilde{\boldsymbol{H}}_k^{\mathrm{SR,t}}$ and $\tilde{\boldsymbol{H}}_{k'}^{\mathrm{RD,t}}$ in the form of Eq. (2.5) host the TD *channel impulse response* (CIR) of the S-R and R-D links for the k-th and k'-th source MT's signals, respectively. In Eq. (4.4), $\tilde{\boldsymbol{n}}_k^{\mathrm{R,t}}$ and $\tilde{\boldsymbol{n}}_1^{\mathrm{D,t}}$ represent the U-length complex-valued *additive white Gaussian noise* (AWGN) vectors having a zero mean and a variance of σ_{N}^2 at each element, i.e. we have $\mathcal{CN}(0,\sigma_{\mathrm{N}}^2)$ at both the k-th relay and the BS, respectively.

Alternatively, as we discussed in Section 3.2.4, a single relay may be shared by K source MTs to form a SSR uplink of Figure 3.1(b). Therefore, based on Eq. (3.9), the representation of the signals received at the relay and BS benefited from the relaying gain is given by

$$\boldsymbol{r}^{\mathrm{R,t}} = \sqrt{G_k^{\mathrm{SR}}}\sum_{k=0}^{K-1}\tilde{\boldsymbol{H}}_k^{\mathrm{SR,t}}\boldsymbol{s}_k^{\mathrm{S,t}} + \tilde{\boldsymbol{n}}_{\mathrm{R,t}}, \tag{4.5a}$$

$$\boldsymbol{r}_1^{\mathrm{D,t}} = \sqrt{G_k^{\mathrm{RD}}}\tilde{\boldsymbol{H}}^{\mathrm{RD,t}}\boldsymbol{s}^{\mathrm{R,t}} + \tilde{\boldsymbol{n}}_1^{\mathrm{D,t}}, \tag{4.5b}$$

where all the K source signals are embedded in the forwarded messages, which is denoted by $\boldsymbol{s}^{\mathrm{R,t}}$.

By invoking the subband-based AF scheme of Figure 4.3, the relay's received TD signals are firstly transformed to the FD by the U-point DFT operation and then demapped to the appropriate N subbands by $\boldsymbol{\mathcal{P}}_k^T$, which we refer to as *subband demapping* characterised by the FD plots of Figure 3.6. According to Section 3.3.2, each user's resultant signal is multiplied by the $(N\times N)$-element diagonal matrix given by

$$\boldsymbol{\beta}_k^{\mathrm{f}} = \mathrm{diag}\{\beta_{k,0}^{\mathrm{f}}, \beta_{k,1}^{\mathrm{f}}, \cdots, \beta_{k,(N-1)}^{\mathrm{f}}\}, \tag{4.6}$$

which is repeated from Eq. (3.24) for convenience. In Eq. (4.6), the n-th element is the specific *gain factor* of the n-th subband given in Eq. (3.26). When considering on the relaying gain, we arrive at

$$\beta_{k,n}^{\mathrm{f}} = \sqrt{P_k^{\mathrm{R}}/[P_k^{\mathrm{S}}G_k^{\mathrm{SR}}|h_{k,n}^{\mathrm{SR,f}}|^2 + \sigma_{\mathrm{N}}^2]}. \tag{4.7}$$

Then the relay's signal corresponding to the k-th user is mapped to the subbands assigned to the k-th source MT. We refer to the joint subband mapping and demapping procedure as the *subband remapping* operation, which is characterised by the FD plots of Figure 3.6. Therefore, the relay's transmission is free from interference, since neither the source MT nor the relay inflict interference during relaying. Still referring to the schematic of Figure 4.3, the U-point *inverse discrete Fourier transform* (IDFT) operation is invoked to transform the signal to the TD, before it is transmitted to the BS. Finally, similar to Eq. (3.23), the

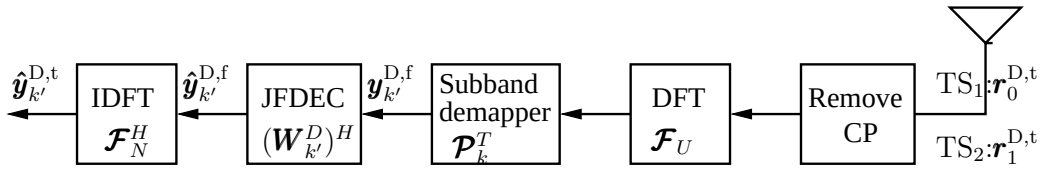

FIGURE 4.4: Receiver schematic of the BS invoking JFDEC for SC-FDMA. The corresponding source and relay transmitters were shown in Figures 4.1 and 4.3, respectively, while the relevant TD and FD signals in Figures 2.10(b) and 2.11(b).

relaying gain aided transmitted signal of the k-th relay during TS_2 is expressed as

$$\boldsymbol{s}_k^{\mathrm{R,t}} = \sqrt{P_k^{\mathrm{S}} G_k^{\mathrm{SR}}} \boldsymbol{\mathcal{F}}_U^H \boldsymbol{\mathcal{P}}_k \boldsymbol{\beta}_k^{\mathrm{f}} \boldsymbol{H}_k^{\mathrm{SR,f}} \boldsymbol{x}_k^{\mathrm{f}} + \bar{\boldsymbol{n}}_k^{\mathrm{R,t}}, \tag{4.8}$$

where $\boldsymbol{H}_k^{\mathrm{SR,f}}$ represents the k-th user's equivalent FD *channel transfer function* (FDCHTF) characterising the S-R link hosted by a $(N\times N)$-element diagonal matrix, i.e. we have

$$\boldsymbol{H}_k^{\mathrm{SR,f}} = \boldsymbol{\mathcal{P}}_k^T \boldsymbol{\mathcal{F}}_U \tilde{\boldsymbol{H}}_k^{\mathrm{SR,t}} \boldsymbol{\mathcal{F}}_U^H \boldsymbol{\mathcal{P}}_k = \mathrm{diag}\{h_{k,0}^{\mathrm{SR,f}}, h_{k,1}^{\mathrm{SR,f}}, \cdots, h_{k,(N-1)}^{\mathrm{SR,f}}\}. \tag{4.9}$$

Note that the noise imposed on the k-th user's signal is affected at the relay according to Eq. (3.27)

$$\bar{\boldsymbol{n}}_k^{\mathrm{R,t}} = \boldsymbol{\mathcal{F}}_U^H \boldsymbol{\mathcal{P}}_k \boldsymbol{\beta}_k^{\mathrm{f}} \boldsymbol{\mathcal{P}}_k^T \boldsymbol{\mathcal{F}}_U \tilde{\boldsymbol{n}}_k^{\mathrm{R,t}}, \tag{4.10}$$

where the noise inflicted upon the other users' subbands is removed, which is a substantial additional benefit.

4.3 Signal Detection

4.3.1 Representation of Received Signal at the BS

The BS receiver structure is portrayed in Figure 4.4. The corresponding source and relay transmitters were shown in Figures 4.1 and 4.3, respectively, while the relevant TD and FD signals in Figures 2.10(b) and 2.11(b). After removing the CP, the U-point DFT transforms the TD signal to the FD, followed by subband demapping at the BS receiver. Then the FD signals of the k-th user received via the direct branch during TS_1 and those arriving via the relaying branch during TS_2 can be expressed by the N-symbol vectors of

$$\boldsymbol{y}_{0,k'}^{\mathrm{D,f}} = \sqrt{P_{k'}^{\mathrm{S}} \xi_{\mathrm{SD}}} \boldsymbol{H}_{k'}^{\mathrm{SD,f}} \boldsymbol{x}_{k'}^{\mathrm{f}} + \boldsymbol{n}_0^{\mathrm{D,f}}, \tag{4.11a}$$

$$\boldsymbol{y}_{1,k'}^{\mathrm{D,f}} = \sqrt{P_{k'}^{\mathrm{S}} G_k^{\mathrm{RD}} G_k^{\mathrm{SR}}} \boldsymbol{H}_{k'}^{\mathrm{RD,f}} \boldsymbol{\beta}_{k'}^{\mathrm{f}} \boldsymbol{H}_{k'}^{\mathrm{SR,f}} \boldsymbol{x}_{k'}^{\mathrm{f}} + \bar{\boldsymbol{n}}_1^{\mathrm{D,f}}, \tag{4.11b}$$

where $\boldsymbol{H}_{k'}^{\mathrm{SD,f}}$ and $\boldsymbol{H}_{k'}^{\mathrm{RD,f}}$ are the $(N\times N)$-element equivalent FDCHTF diagonal matrices of the S-D and R-D links, respectively. Furthermore, $\boldsymbol{n}_0^{\mathrm{D,f}}$ and $\bar{\boldsymbol{n}}_1^{\mathrm{D,f}}$ represent the AWGN vectors

having a length of N and represented by $\mathcal{CN}(0, \sigma_{\mathrm{N}}^2)$, which are imposed at the BS during the two time-slots, respectively. We amalgamate the above two equations into a $2N$-length joint observation vector as

$$\boldsymbol{y}_{k'}^{\mathrm{D,f}} = \sqrt{P_{k'}^{\mathrm{S}}}\boldsymbol{H}_{k'}^{\mathrm{D,f}}\boldsymbol{x}_{k'}^{\mathrm{f}} + \boldsymbol{n}^{\mathrm{D,f}}, \tag{4.12}$$

where the $(2N \times N)$-element joint equivalent FD channel matrix is given by

$$\boldsymbol{H}_{k'}^{\mathrm{D,f}} = \begin{bmatrix} \boldsymbol{H}_{0,k'}^{\mathrm{D,f}} \\ \boldsymbol{H}_{1,k'}^{\mathrm{D,f}} \end{bmatrix} = \begin{bmatrix} \sqrt{\xi_{\mathrm{SD}}}\boldsymbol{H}_{k'}^{\mathrm{SD,f}} \\ \sqrt{G_k^{\mathrm{RD}}G_k^{\mathrm{SR}}}\boldsymbol{H}_{k'}^{\mathrm{RD,f}}\boldsymbol{\beta}_{k'}^{\mathrm{f}}\boldsymbol{H}_{k'}^{\mathrm{SR,f}} \end{bmatrix}. \tag{4.13}$$

Additionally, we formulate the n-th element of the diagonal matrices $\boldsymbol{H}_{0,k'}^{\mathrm{D,f}}$ and $\boldsymbol{H}_{1,k'}^{\mathrm{D,f}}$ as

$$h_{0,k',n}^{\mathrm{D,f}} = \sqrt{\xi_{\mathrm{SD}}}h_{SD,k'n}^{\mathrm{f}}, \tag{4.14a}$$

$$h_{1,k',n}^{\mathrm{D,f}} = \beta_{k',n}^{\mathrm{f}}\sqrt{G_k^{\mathrm{RD}}G_k^{\mathrm{SR}}}h_{k',n}^{\mathrm{RD,f}}h_{k',n}^{\mathrm{SR,f}}. \tag{4.14b}$$

Similarly, the total received noise of the k'-th user at the BS includes the noise contribution imposed by the k'-th relay after the above-mentioned subband remapping operation shown in the FD plots of Figure 3.6 plus that added at the BS during the two time slots, which is expressed by a $2N$-length vector as

$$\boldsymbol{n}^{\mathrm{D,f}} = \begin{bmatrix} \boldsymbol{n}_0^{\mathrm{D,f}} \\ \bar{\boldsymbol{n}}_1^{\mathrm{D,f}} \end{bmatrix} = \begin{bmatrix} \boldsymbol{\mathcal{P}}_{k'}^T\boldsymbol{\mathcal{F}}_U\tilde{\boldsymbol{n}}_0^{\mathrm{D,t}} \\ \boldsymbol{\mathcal{P}}_{k'}^T\boldsymbol{\mathcal{F}}_U(\sqrt{G_k^{\mathrm{RD}}}\tilde{\boldsymbol{H}}_{k'}^{\mathrm{RD,t}}\bar{\boldsymbol{n}}_{k'}^{\mathrm{R,t}} + \tilde{\boldsymbol{n}}_1^{\mathrm{D,t}}) \end{bmatrix}. \tag{4.15}$$

4.3.2 MMSE assisted Joint Frequency-Domain Equalisation and Diversity Combining

According to Section 2.2.3, it can be readily shown that the *optimum* MMSE FDE solution is given by

$$\boldsymbol{W}_{k'}^{\mathrm{D}} = (\boldsymbol{R}_{k'}^{\mathrm{yD}})^{-1}\boldsymbol{R}_{k'}^{\mathrm{yxD}}, \tag{4.16}$$

which is based on Eq. (4.12), where the *auto-correlation* matrix of $\boldsymbol{y}_{k'}^{\mathrm{D,f}}$ is expressed as

$$\boldsymbol{R}_{k'}^{\mathrm{yD}} = P_{k'}^{\mathrm{S}}\boldsymbol{H}_{k'}^{\mathrm{D,f}}(\boldsymbol{H}_{k'}^{\mathrm{D,f}})^H + \boldsymbol{R}_{\mathrm{nD}}, \tag{4.17}$$

with $\boldsymbol{R}_{\mathrm{nD}} = \mathrm{E}[\boldsymbol{n}^{\mathrm{D,f}}(\boldsymbol{n}^{\mathrm{D,f}})^H] = \mathrm{diag}\{\boldsymbol{R}_0^{\mathrm{nD}}, \boldsymbol{R}_1^{\mathrm{nD}}\}$ denoting the *covariance* matrix of $\boldsymbol{n}^{\mathrm{D,f}}$, where we have

$$\boldsymbol{R}_0^{\mathrm{nD}} = \mathrm{E}[\boldsymbol{n}_0^{\mathrm{D,f}}(\boldsymbol{n}_0^{\mathrm{D,f}})^H] = \sigma_{\mathrm{N}}^2\boldsymbol{I}_N, \tag{4.18a}$$

$$\boldsymbol{R}_1^{\mathrm{nD}} = \mathrm{E}[\bar{\boldsymbol{n}}_1^{\mathrm{D,f}}(\bar{\boldsymbol{n}}_1^{\mathrm{D,f}})^H] = \sigma_{\mathrm{N}}^2\left[G_k^{\mathrm{RD}}\boldsymbol{H}_{k'}^{\mathrm{RD,f}}\boldsymbol{\beta}_{k'}^{\mathrm{f}}(\boldsymbol{\beta}_{k'}^{\mathrm{f}})^H(\boldsymbol{H}_{k'}^{\mathrm{RD,f}})^H + \boldsymbol{I}_N\right]. \tag{4.18b}$$

Thus, the corresponding power of the noise components $\boldsymbol{n}_0^{\mathrm{D,f}}$ and $\bar{\boldsymbol{n}}_1^{\mathrm{D,f}}$ in the n-th subband during TS_1 and TS_2 can be expressed as

$$\mathcal{N}_{0,n}^{\mathrm{D}} = \sigma_{\mathrm{N}}^2 \tag{4.19a}$$

$$\mathcal{N}_{1,n}^{\mathrm{D}} = \sigma_{\mathrm{N}}^2(\beta_{k',n}^{\mathrm{f}})^2 G_k^{\mathrm{RD}} |h_{k',n}^{\mathrm{RD,f}}|^2 + \sigma_{\mathrm{N}}^2, \tag{4.19b}$$

respectively. In Eq. (4.16), $\boldsymbol{R}_{k'}^{\mathrm{yxD}}$ is the *cross-correlation* matrix between $\boldsymbol{y}_{k'}^{\mathrm{D,f}}$ and $\boldsymbol{x}_{S,k'}^{\mathrm{f}}$, which may be formulated as

$$\boldsymbol{R}_{k'}^{\mathrm{yxD}} = P_{k'}^{\mathrm{S}} \boldsymbol{H}_{k'}^{\mathrm{D,f}}. \tag{4.20}$$

Therefore, when substituting Eq. (4.17) and Eq. (4.20) into Eq. (4.16), the $(2N\times N)$-element *optimum weight* matrix of the MMSE aided JFDEC is formulated as

$$\boldsymbol{W}_{k'}^{\mathrm{D}} = P_{k'}^{\mathrm{S}} [P_{k'}^{\mathrm{S}} \boldsymbol{H}_{k'}^{\mathrm{D,f}} (\boldsymbol{H}_{k'}^{\mathrm{D,f}})^H + \boldsymbol{R}_{\mathrm{nD}}]^{-1} \boldsymbol{H}_{k'}^{\mathrm{D,f}}, \tag{4.21a}$$

where the matrix inversion operation can be applied to the $(N\times N)$-element diagonal matrices $\boldsymbol{R}_0^{\mathrm{nD}}$ in Eq. (4.18a) and $\boldsymbol{R}_1^{\mathrm{nD}}$ in Eq. (4.18b), respectively. It is worth noting that $\boldsymbol{R}_{k'}^{\mathrm{yD}}$ is an $(2N\times 2N)$-element non-diagonal matrix. Hence, the complexity of inverting $\boldsymbol{R}_{k'}^{\mathrm{yD}}$ might be high. In order to implement the low complexity single-tap MMSE FD-LE of Figure 2.12(b) and diversity combining jointly, the *matrix inversion lemma*[5] of [102] can be invoked. Then Eq. (4.21a) is reformulated as

$$\boldsymbol{W}_{k'}^{\mathrm{D}} = P_{k'}^{\mathrm{S}} \boldsymbol{R}_{\mathrm{nD}}^{-1} \boldsymbol{H}_{k'}^{\mathrm{D,f}} [P_{k'}^{\mathrm{S}} (\boldsymbol{H}_{k'}^{\mathrm{D,f}})^H \boldsymbol{R}_{\mathrm{nD}}^{-1} \boldsymbol{H}_{k'}^{\mathrm{D,f}} + \boldsymbol{I}_N]^{-1}. \tag{4.21b}$$

Consequently, by substituting $\boldsymbol{H}_{k'}^{\mathrm{D,f}}$ and $\boldsymbol{R}_{\mathrm{nD}}$ into the above equation, we obtain $\boldsymbol{W}_{k'}^{\mathrm{D}}$, which is constituted by two $(N\times N)$-element diagonal matrices, yielding

$$\boldsymbol{W}_{k'}^{\mathrm{D}} = \begin{bmatrix} (\boldsymbol{R}_0^{\mathrm{nD}})^{-1} \boldsymbol{H}_{0,k'}^{\mathrm{D,f}} \\ (\boldsymbol{R}_1^{\mathrm{nD}})^{-1} \boldsymbol{H}_{1,k'}^{\mathrm{D,f}} \end{bmatrix} \left[(\boldsymbol{H}_{0,k'}^{\mathrm{D,f}})^H (\boldsymbol{R}_0^{\mathrm{nD}})^{-1} \boldsymbol{H}_{0,k'}^{\mathrm{D,f}} + (\boldsymbol{H}_{1,k'}^{\mathrm{D,f}})^H (\boldsymbol{R}_1^{\mathrm{nD}})^{-1} \boldsymbol{H}_{1,k'}^{\mathrm{D,f}} + \frac{1}{P_{k'}^{\mathrm{R}}} \boldsymbol{I}_N \right]^{-1}. \tag{4.21c}$$

Hence the n-th and $(n+N)$-th element of the FDE weight matrix $\boldsymbol{W}_{k'}^{\mathrm{D}}$ can be expressed as

$$w_{k',n}^{\mathrm{D}} = h_{0,k',n}^{\mathrm{D,f}} e_{k'n} / \sigma_{\mathrm{N}}^2, \quad w_{k',(n+N)}^{\mathrm{D}} = h_{1,k',n}^{\mathrm{D,f}} e_{k'n} / \mathcal{N}_{1,n}^{\mathrm{D}}, \tag{4.22}$$

where $e_{k'n}$ is given by

$$e_{k'n} = \left(|h_{0,k',n}^{\mathrm{D,f}}|^2 / \sigma_{\mathrm{N}}^2 + |h_{1,k',n}^{\mathrm{D,f}}|^2 / \mathcal{N}_{1,n}^{\mathrm{D}} + 1/P_{k'}^{\mathrm{R}} \right)^{-1}. \tag{4.23}$$

[5]Assuming that the matrices $\boldsymbol{A}$ and $\boldsymbol{B}$ have $(N\times N)$ and $(N\times M)$ elements, respectively, and that $\boldsymbol{I}_M$ is an $(M\times M)$-element identity matrix, we have $(\boldsymbol{A}+\boldsymbol{B}\boldsymbol{B}^H)^{-1}\boldsymbol{B} = \boldsymbol{A}^{-1}\boldsymbol{B}(\boldsymbol{B}^H\boldsymbol{A}^{-1}\boldsymbol{B}+\boldsymbol{I}_M)^{-1}$.

Actually, $e_{k'n}$ is the FD MMSE value at the output of the FDE in the n-th subband of the k'-th user's signal, which will be discussed in more detail in Section 4.3.3. Specifically, it will be shown that the weight matrix $\boldsymbol{W}_{k'}^{\mathrm{D}}$ is capable of carrying out both single-tap MMSE FD-LE and diversity combining of the direct and relay branches jointly. Specifically, the coefficients $h_{0,k',n}^{\mathrm{D,f}} e_{k'n}$ and $h_{1,k',n}^{\mathrm{D,f}} e_{k'n}$ in Eq. (4.22) are used for the single-tap MMSE FD-LE in conjunction with diversity combining, while obeying the MMSE criterion, where noise whitening is carried out within both branches by normalising it according to the noise power σ_{N}^2 and $\mathcal{N}_{1,n}^{\mathrm{D}}$, respectively.

4.3.3 Relationships of the MMSE, SNR and SINR at the Output of the JFDEC

Correspondingly, upon applying the FDE weight matrix $(\boldsymbol{W}_{k'}^{\mathrm{D}})^H$ to $\boldsymbol{y}_{k'}^{\mathrm{D,f}}$, the signals arriving from both the direct and relaying branches are combined into an N-length observation vector in the FD, which are then transformed into the TD decision variable vector $\boldsymbol{z}_{k'}^{\mathrm{D,t}}$ for $\boldsymbol{x}_{k'}^{\mathrm{t}}$ by the N-point IDFT using the schematic of Figure 4.4, yielding

$$\boldsymbol{z}_{k'}^{\mathrm{D,t}} = \boldsymbol{\mathcal{F}}_N^H (\boldsymbol{W}_{k'}^{\mathrm{D}})^H \boldsymbol{y}_{k'}^{\mathrm{D,f}} = \sqrt{P_{k'}^{\mathrm{S}}} \boldsymbol{A}_{k'}^{\mathrm{t}} \boldsymbol{x}_{k'}^{\mathrm{t}} + \boldsymbol{n}_D^{\mathrm{t}}, \tag{4.24}$$

where $\boldsymbol{A}_{k'}^{\mathrm{t}}$ is the $(N\times N)$-element TD circulant interference matrix of the desired signals introduced in Sections 2.2.4 and 3.4.4, while $\boldsymbol{n}_D^{\mathrm{t}}$ is the N-length TD noise vector after equalisation. The gain factor between $\boldsymbol{x}_{k'}^{\mathrm{t}}$ and its estimate of $\boldsymbol{z}_{k'}^{\mathrm{D,t}}$ is given by the diagonal elements of the matrix $\boldsymbol{A}_{k'}^{\mathrm{t}}$ [142].

Furthermore, the TD normalised estimation error vector $\boldsymbol{e}_{k'}^{\mathrm{t}}$ between the transmitted signal $\boldsymbol{x}_{k'}^{\mathrm{t}}$ and the estimated signal $\boldsymbol{z}_{k'}^{\mathrm{D,t}}$ can be expressed as

$$\boldsymbol{e}_{k'}^{\mathrm{t}} = \frac{1}{\sqrt{P}} (\boldsymbol{x}_{k'}^{\mathrm{t}} - \boldsymbol{z}_{k'}^{\mathrm{D,t}}) = \frac{1}{\sqrt{P_{k'}^{\mathrm{S}}}} \boldsymbol{x}_{k'}^{\mathrm{t}} - \frac{1}{\sqrt{P_{k'}^{\mathrm{S}}}} \boldsymbol{A}_{k'}^{\mathrm{t}} \boldsymbol{x}_{k'}^{\mathrm{t}} - \frac{1}{\sqrt{P_{k'}^{\mathrm{S}}}} \boldsymbol{n}_D^{\mathrm{t}}, \tag{4.25}$$

where the covariance matrix of $\boldsymbol{e}_{k'}^{\mathrm{t}}$ is given by

$$\boldsymbol{R}_{e_{k'}^{\mathrm{t}}} = \mathrm{E}[\boldsymbol{e}_{k'}^{\mathrm{t}} (\boldsymbol{e}_{k'}^{\mathrm{t}})^H] = \left[\boldsymbol{I}_N - 2\Re\{A_{k'}^{\mathrm{t}}\} + \boldsymbol{A}_{k'}^{\mathrm{t}} (\boldsymbol{A}_{k'}^{\mathrm{t}})^H\right] + \frac{\sigma_{\mathrm{N}}^2}{P_{k'}^{\mathrm{S}}} \boldsymbol{I}_N, \tag{4.26}$$

with $\Re\{\boldsymbol{A}_{k'}^{\mathrm{t}}\}$ denoting the real part of $\boldsymbol{A}_{k'}^{\mathrm{t}}$. As we discussed in Section 2.2.4, $\boldsymbol{R}_{e_{k'}^{\mathrm{t}}}$ is also an $(N\times N)$-element circulant matrix, having identical diagonal elements, which implies that due to the averaging effects of the N-point IDFT operation seen in the schematic of Figure 4.4, all the k-th users' resultant TD symbols within the vector have the same MMSE value $e_{k'}$. This MMSE value can be calculated as the average of the FD MMSE values over N

subbands, yielding the MMSE of the joint solution as

$$e_{k'} = \frac{1}{N}\sum_{n=0}^{N-1} e_{k',n} = \frac{1}{N}\mathrm{Tr}\left[\boldsymbol{R}_{e^{\mathrm{f}}_{k'}}\right]. \tag{4.27}$$

Hence, Eq. (4.23) can also be derived by

$$\begin{aligned} e_{k',n} &= \left[\boldsymbol{R}_{e^{\mathrm{f}}_{k'}}\right]_n = [\boldsymbol{I}_N - \frac{1}{P^{\mathrm{S}}_{k'}}(\boldsymbol{R}^{\mathrm{yxD}}_{k'})^H \boldsymbol{W}^{\mathrm{D}}_{k'}]_n \\ &= (\gamma^{\mathrm{D0}}_{k',n} + \gamma^{\mathrm{D1}}_{k',n} + 1)^{-1}, \end{aligned} \tag{4.28}$$

where the instantaneous received SNRs of the direct and relaying branches in the n-th subband are expressed as

$$\gamma^{\mathrm{D0}}_{k',n} = \gamma^{\mathrm{SD}}_{k',n} = P^{\mathrm{S}}_{k'}\xi_{\mathrm{SD}}|h^{\mathrm{f}}_{SD,k'n}|^2/\sigma^2_{\mathrm{N}}, \tag{4.29a}$$

$$\gamma^{\mathrm{D1}}_{k',n} = \left(1/\gamma^{\mathrm{SR}}_{k',n} + 1/\gamma^{\mathrm{RD}}_{k',n}\right)^{-1}, \tag{4.29b}$$

$$\gamma^{\mathrm{SR}}_{k',n} = P^{\mathrm{S}}_{k'}G^{\mathrm{SR}}_{k}|h^{\mathrm{SR,f}}_{k',n}|^2/\sigma^2_{\mathrm{N}}, \tag{4.29c}$$

$$\gamma^{\mathrm{RD}}_{k',n} = \frac{P^{\mathrm{R}}_{k'}G^{\mathrm{RD}}_{k}G^{\mathrm{SR}}_{k}|h^{\mathrm{RD,f}}_{k',n}|^2|h^{\mathrm{SR,f}}_{k',n}|^2}{\sigma^2_{\mathrm{N}}(G^{\mathrm{SR}}_{k}|h^{\mathrm{SR,f}}_{k',n}|^2 + \sigma^2_{\mathrm{N}}/P^{\mathrm{S}}_{k'})}. \tag{4.29d}$$

We note that $e_{k',n}$ has already appeared in Eq. (4.23) and it is also equivalent to the general result for the optimum MMSE solution of the non-cooperative scenario of Figure 2.12 discussed in Section 2.2.4.

Consequently, according to the relationship between the SINR and MMSE as a general feature of the MMSE criterion [102], we obtain the k'-th user's instantaneous overall received SINR at the output of our proposed scheme in the form of

$$\gamma_{k'} = e^{-1}_{k'} - 1 = \left\{ \frac{1}{N}\sum_{n=0}^{N-1} \left[\begin{array}{c} 1 + \gamma^{\mathrm{SD}}_{k',n} + \\ \left(1/\gamma^{\mathrm{SR}}_{k',n} + 1/\gamma^{\mathrm{RD}}_{k',n}\right)^{-1} \end{array} \right]^{-1} \right\}^{-1} - 1, \tag{4.30}$$

which is derived in the Appendix in the form of Eq. (4.47).

4.4 Energy Consumption Metrics

In order to evaluate the multi-user system's performance in terms of the achievable power reduction, we introduce two energy consumption metrics, namely the *energy consumption per bit* expressed in units of Joule per bit and the *energy consumption gain* (ECG), which is defined as the ratio of the energy consumption per bit of the reference system over that of the system advocated [1]. Therefore, the energy consumption per bit of single-hop DT

operating without cooperation may be defined as

$$\varepsilon_{\mathrm{DT}} = \frac{\sum_{k=0}^{K-1} P_k T}{\sum_{k=0}^{K-1} R_k^{\mathrm{DT}} T} = \frac{\sum_{k=0}^{K-1} P_k}{\sum_{k=0}^{K-1} R_k^{\mathrm{DT}}} = \frac{KP}{R_\Sigma^{\mathrm{DT}}} \quad (J/bit), \tag{4.31}$$

where T denotes the time-slot duration, i.e. time duration per hop, while $R_k^{(\cdot)}$ $R_\Sigma^{(\cdot)}$ denote the achievable ergodic single-user rate and multi-user sum-rates of the $(\cdot)$-type transmission, i.e. either of direct or of AF-cooperative transmissions.

Similarly, the energy consumption per bit of two-hop AF-cooperative transmissions may be expressed as

$$\varepsilon_{\mathrm{AF}} = \frac{\sum_{k=0}^{K-1} (P_k^{\mathrm{S}} T + P_k^{\mathrm{R}} T)}{\sum_{k=0}^{K-1} R_k^{\mathrm{AF}} 2T} = \frac{\sum_{k=0}^{K-1} (P_k^{\mathrm{S}} + P_k^{\mathrm{R}})}{\sum_{k=0}^{K-1} 2R_k^{\mathrm{AF}}} \quad (J/bit). \tag{4.32}$$

Since we assume $\sum_{k=0}^{K-1} (P_k^{\mathrm{S}} + P_k^{\mathrm{R}}) = KP$, by using the DT as a reference, the ECG of cooperative transmissions is given by

$$ECG = \frac{ECR_{\mathrm{DT}}}{ECR_{\mathrm{AF}}} = \frac{2R_\Sigma^{\mathrm{AF}}}{R_\Sigma^{\mathrm{DT}}}. \tag{4.33}$$

We assume that the system bandwidth was normalised to unity in our baseband processing, hence the sum-rate $R_\Sigma^{(\cdot)}$ expressed in terms of bits/sec/Hz is given by

$$R_\Sigma^{(\cdot)} = \mathrm{E}\left[\sum_{k=0}^{K-1} \frac{1}{N_{\mathrm{TS}}} \log_2 \left(1 + \gamma_k^{(\cdot)} \right) \right], \tag{4.34}$$

where the factor $1/N_{\mathrm{TS}}$ indicates the effect of the N_{TS} time-slots required for direct or cooperative transmission.

Therefore, the corresponding instantaneous SINR of the k-th user may be expressed as

$$\gamma_k^{(\cdot)} = \left[\frac{1}{N} \sum_{n=0}^{N-1} \left(1 + \gamma_{k,n}^{(\cdot)} \right)^{-1} \right]^{-1} - 1. \tag{4.35}$$

Specifically, for DT, we have an equivalent instantaneous SNR in the n-th subband of the k-th user given by

$$\gamma_{k,n}^{\mathrm{DT}} = P_k \xi_{\mathrm{DT}} |h_{k,n}^{\mathrm{dir,f}}|^2 / \sigma_{\mathrm{N}}^2. \tag{4.36}$$

By contrast, for AF-cooperation, the k-th user's received equivalent instantaneous SNR in the n-th subband may be expressed according to Eq. (4.30) as,

$$\gamma_{k,n}^{\mathrm{AF}} = \gamma_{k,n}^{\mathrm{SD}} + \left[\left(\gamma_{k,n}^{\mathrm{SR}} \right)^{-1} + \left(\gamma_{k,n}^{\mathrm{RD}} \right)^{-1} \right]^{-1}. \tag{4.37}$$

4.5 Opportunistic Cooperation Invoking Power Allocation

The *opportunistic cooperation* (OC) philosophy allows a single relay to be selected from a set of $J(J > 0)$ relays which are inactive MTs, depending on which MT provides the best *end-to-end* link between the source and destination [65]. In this section, the source/relay power allocation and relay selection are investigated for the sake of power-efficient OC. We assume that the multiple relays are geographically distributed in three typical scenarios, namely when we have a sufficiently high number of relays, a moderate number of relays and an insufficient number of relays. The corresponding relay selection schemes, namely the *single-user relay selection* (SU-RS), *multi-user relay selection* (MU-RS) and *multiple-access relay selection* (MA-RS) regimes are shown in Figure 4.5. The BS is assumed to be capable of acquiring the *channel state information at the receiver* (CSIR) and the SNR of all the cooperative links based on pilot-assisted channel estimation, which were formulated in Eq. (4.29a), Eq. (4.29c) and Eq. (4.29d). The power allocation and relay selection are carried out with the objective of maximising the average received instantaneous SINR of each user at the BS for both the direct and relaying branches. Additionally, we assume that the transmissions of the S-D, S-R and R-D links are orthogonal and hence they do not impose an increased MUI. [6]

4.5.1 Source/Relay Power Allocation

The proposed systems invoke the various source/relay power allocation modes detailed below. The family of linear power allocation includes *equal power allocation* (EPA) and *default power allocation* (DPA) for the SDR and SSR systems, respectively. Specifically, the EPA mode adjusts the transmitted powers of the k-th source and j-th relay to be equal, while the DPA mode shares the transmitted power between the source MT and relay according to the number of active source users K within system. Hence we have

$$\text{EPA for SDR}: \qquad \alpha^{\mathrm{S}}_{k,j} = \alpha^{\mathrm{R}}_{k,j} = 0.5, \tag{4.38a}$$

$$\text{DPA for SSR}: \qquad \alpha^{\mathrm{S}}_{k,j} = 1 - 1/K, \alpha^{\mathrm{R}}_{k,j} = 1/K. \tag{4.38b}$$

Alternatively, the OPA mode may be invoked for both the SDR and SSR systems of Figure 4.5, which maximises the average SINR expression of Eq. (4.30) for the k-th user with the

[6] Let us define the notations as follows. The notations $\mathcal{K}$, $\mathcal{J}$ Γ, denote the set of users $k = 0, 1, 2, \cdots, K-1$, $(\forall k \in \mathcal{K})$, the set of the relays $j = 0, 1, 2, \cdots, J-1$, $(\forall j \in \mathcal{J})$ and the set of the SINRs of Eq. (4.30), respectively. Given the elements in the set $\mathcal{A}$, $(\forall a \in \mathcal{A})$, the notation $\check{a}$ represents the selected element of a and is collected in the set $\check{\mathcal{A}}$; the notation $\mathring{a}_i$ denotes the element a with ordering index i in the ordered version $\mathring{\mathcal{A}}$ of the original set $\mathcal{A}$. The notation $\varnothing$ represents the 'clear' operation. The notation $\cup$, $\setminus$ indicates that the element in $\{a\}$ is incorporated or excluded from the set $\mathcal{A}$, respectively.

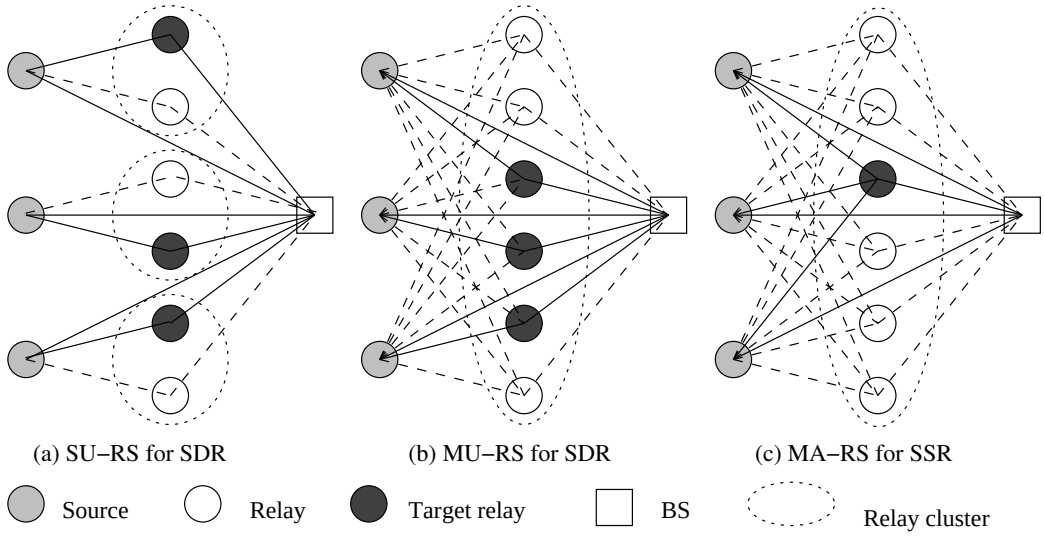

FIGURE 4.5: The snapshot of topologies for various OC schemes in the SC-FDMA uplink. We assume that the multiple relays are geographically distributed in three typical scenarios. Firstly, when the number of relays is sufficiently high in the system, the *single-user relay selection* (SU-RS) scheme is designed using the SDR topology of subfigure (a). Secondly, when the system has a moderate number of relays, the *multi-user relay selection*(MU-RS) scheme is designed using the SDR topology shown in subfigure (b). Thirdly, if the number of relays is insufficient, particularly lower than the number of source MTs, the *multiple-access relay selection* (MA-RS) scheme is designed using the SSR topology seen in subfigure (c). However, we consider a fair comparison using $K = 3$ users and a total of $J = 6$ relays for all the relay selection schemes in subfigures (a), (b) and (c). When the specific relays are selected depending on the instantaneous SINR in Eq. (4.30), the solid lines in (a), (b) and (c) characterise the corresponding SDR and SSR topologies portrayed in Figure 3.1, while the dashed lines indicate the other opportunistic cooperation via SDR/SSR links.

aid of the j-th relay by exploiting the knowledge of CSIR, yielding

$$\begin{aligned} \max_{\alpha^{\mathrm{S}}_{k,j},\alpha^{\mathrm{R}}_{k,j}} \quad & \gamma^{\mathrm{AF}}_{k,j}(\alpha^{\mathrm{S}}_{k,j},\alpha^{\mathrm{R}}_{k,j}) \\ \text{subject to} \quad & \alpha^{\mathrm{S}}_{k,j}+\alpha^{\mathrm{R}}_{k,j}=1, \quad \alpha^{\mathrm{S}}_{k,j}>0, \quad \alpha^{\mathrm{R}}_{k,j}>0, \\ & \text{for SSR}: \sum_{k=0}^{K-1}\alpha^{\mathrm{R}}_{k,j}=1. \end{aligned} \tag{4.39}$$

4.5.2 Single-User Relay Selection

Initially, we examine the relay selection schemes designed for the SDR topology. If the total number of idle MTs accessing the single-cell BS considered is high, more candidates may be considered for activation as the target relays. In our proposed SU-RS scheme, each source MT set $\mathcal{K}$ is capable of seeking a target relay from a cluster of J/K relays within the set $\mathcal{J}_k$ for $J \geq K$, which are independent from the other source MT's relays, i.e. we have $\mathcal{J}_k \neq \mathcal{J}_{k'}$ for $k, k' \in \mathcal{K}$. Hence, a total of J inactive MTs employed as relays in the set $\mathcal{J}$ are required in order to support K source MTs. In other words, for all $k \in \mathcal{K}$, $\mathcal{J}_k$ is a subset of $\mathcal{J}$.

TABLE 4.1: Channel-dependent *single-user relay selection* (SU-RS) algorithm

1. Initialisation:	If $J \geq K$, let $\check{\mathcal{J}} = \varnothing$;
2. Searching:	For the source $k = 0, 1, \cdots, K-1$, $(k \in \mathcal{K})$, (a) Consider the relay cluster $\mathcal{J}_k$, (b) Find the relay $\check{j}_k = \arg\max_{j \in \mathcal{J}_k} \{\gamma_{j,k}^{\mathrm{AF}}\}$, (c) Update $\check{\mathcal{J}} = \{\check{j}_k\} \cup \check{\mathcal{J}}$; (d) Assign the relay $\check{j}_k$ to the k-th source MT. (e) Terminate if $k = K-1$, otherwise let $k = k+1$ and return to step (1).

Specifically, we have $\mathcal{J}_k \subseteq \mathcal{J}$ if $K = 1$ and $\mathcal{J}_k \subset \mathcal{J}$ if $K > 1$.

To elaborate it a little further, we describe the procedure as follows. Initially, we define the set of desired relays to be empty, i.e. we have $\check{\mathcal{J}} = \varnothing$. For the k-th user in the set $\mathcal{K}$, the BS calculates its overall SINR $\gamma_{j,k}^{\mathrm{AF}}$, while tentatively relying on any of the J/K relays in the set $\mathcal{J}_k$ and then selects the one having the maximum SINR for $j \in \mathcal{J}_k$, which is associated with the index of $\check{j}_k$, as formulated in

$$\check{j}_k = \arg\max_{j \in \mathcal{J}_k} \{\gamma_{j,k}^{\mathrm{AF}}\}, \quad (J \geq K). \tag{4.40}$$

Thus, we may update the set $\check{\mathcal{J}} = \{\check{j}_k\} \cup \check{\mathcal{J}}$ and assign the relay $\check{j}_k$ to the k-th user.

Consequently, the associated algorithm may be summarised in Table 4.1.

4.5.3 Multi-User Relay Selection

However, when the total number of inactive MTs roaming within a cell is low, the number of available relays may become moderate, since a total of K independent clusters of relays would be required for K sources in the regime SU-RS of Figure 4.5(a). In order to circumvent this limitation of the SDR regime of Figure 3.1(a), we propose the MU-RS scheme of Figure 4.5(b), which allows the multiple source users to access one or more relays, where each source's data is forwarded by selecting a single desired relay for cooperative transmission. Specifically, a cluster of K source MTs of set $\mathcal{K}$ is collectively associated with a cluster of $J(J \geq K)$ relays of the set $\mathcal{J}$, but the system only requires a total of K target relays defined by the set $\mathring{\mathcal{J}}$. Since we have a total of K source MTs in the SDR system, the dynamic relays must not be assigned to different users simultaneously. Therefore, an *optimal partner ordering* algorithm is introduced, which arranges the source-relay pairs by monitoring the SINR of each of the $(K \times J)$ S-R-D and K S-D links in a descending order. The scenario of $K = 1$ is similar to the *relay ordering* scheme of [67], where all the dynamic relays serve only a single user. Specifically, our regime calculates the overall SINR of all the K source MTs' signal by tentatively assuming cooperation with all the J relays, and chooses the specific

TABLE 4.2: Channel-dependent *multi-user relay selection* (MU-RS) algorithm

1. Initialisation:	If $J \geq K$, let $\mathring{\mathcal{K}} = \varnothing$, $\mathring{\mathcal{J}} = \varnothing$ and $\mathring{\Gamma} = \varnothing$;
2. Searching:	Consider the sources in $\mathcal{K}$ and the relay cluster $\mathcal{J}$, Obtain the SINR set $\Gamma = \bigcup_{k\in\mathcal{K}, j\in\mathcal{J}} \gamma_{k,j}^{\mathrm{AF}}$, For $i = 0, 1, \cdots$, (a) Obtain the source-relay pair $(\mathring{k}_i, \mathring{j}_i) = \arg\max_{k\in\mathcal{K}, j\in\mathcal{J}} \{\gamma_{k,j}^{\mathrm{AF}}\}$, (b) Update $\mathring{\Gamma} = \mathring{\Gamma} \bigcup \{\gamma_{\mathring{k}_i,\mathring{j}_i}^{\mathrm{AF}}\}$, $\mathcal{K} = \mathcal{K} \setminus \{\mathring{k}_i\}$ and $\mathcal{J} = \mathcal{J} \setminus \{\mathring{j}_i\}$, (c) Assign the relay $\mathring{j}_i$ to the source $\mathring{k}_i$. (d) Terminate if $i = K - 1$, otherwise let $i = i + 1$, return to step 2-(a).

source relay pairs having the highest K received SINR values at the BS, which are provided by the relays corresponding to the particular source MTs.

We describe the procedure as follows in detail. Firstly, the ordered sets of users and desired relays are initialised to be empty, i.e. we have $\mathring{\mathcal{K}} = \varnothing$ and $\mathring{\mathcal{J}} = \varnothing$, respectively. Secondly, at the i-th iteration, the desired relay's index $\mathring{j}_i$ selected for assisting the ordered user $\mathring{k}_i$ is assumed to be the pairing index i, which are compiled in descending order, yielding

$$(\mathring{k}_i, \mathring{j}_i) = \arg\max_{k\in\mathcal{K}, j\in\mathcal{J}} \{\gamma_{k,j}^{\mathrm{AF}}\}, \quad (J \geq K). \tag{4.41}$$

Thirdly, upon removing the user $\mathring{k}_i$ and the relay $\mathring{j}_i$ from the selection pools, which is mathematically denoted by $\mathcal{K} = \mathcal{K} \setminus \{\mathring{k}_i\}$ and $\mathcal{J} = \mathcal{J} \setminus \{\mathring{j}_i\}$, the target relay of the next user $\mathring{k}_{(i+1)}$ may be allocated during the next iteration using Eq. (4.41).

Therefore, the associated algorithm is summarised in Table 4.2.

4.5.4 Multiple-Access Relay Selection

In contrast to the SDR based relay selection schemes seen in Figures 4.5(a) and (b), when the number of relays is insufficient, particularly lower than the number of source MTs, the SSR based relay selection may be considered as a beneficial design alternative. Hence, we propose the MA-RS scheme shown in Figure 4.5(c), which takes into account the overall performance of all the links from all source MTs aiming to share a relay. This is necessary, because the multiple source MTs in the set $\mathcal{K}$ have to gain access to a common target relay by evaluating the benefits of an entire cluster of J relays in set $\mathcal{J}$, where the minimum number of relays is independent of the number of sources, i.e. we have $J > 0$. Hence, this regime looks for a single relay indexed by $\check{j}$, which offers the maximum sum of SINRs for all the K source MTs, which is formulated as:

$$\check{j} = \arg\max_{j\in\mathcal{J}} \{\sum_{k\in\mathcal{K}} \gamma_{k,j}^{\mathrm{AF}}\}, \quad (J > 0). \tag{4.42}$$

TABLE 4.3: Channel-dependent *multi-user relay selection* (MU-RS) algorithm

1. Initialisation:	If $J > 0$;
2. Searching:	Consider the source cluster $\mathcal{K}$ and the relay cluster $\mathcal{J}$, Obtain the SINR set $\Gamma = \bigcup_{k\in\mathcal{K}, j\in\mathcal{J}} \gamma_{k,j}^{\mathrm{AF}}$, (a) For the relay $j = 0, 1, \cdots, J-1$, obtain $\gamma_{\Sigma,j} = \sum_{k\in\mathcal{K}} \gamma_{k,j}^{\mathrm{AF}}$, (b) Find $\check{j} = \arg\max_{j\in\mathcal{J}}\{\gamma_{\Sigma,j}\}$, (c) Assign the relay $\check{j}$ to all the sources in $\mathcal{K}$. (d) Terminate.

TABLE 4.4: Examples of *single-user relay selection* (SU-RS), *multi-user relay selection* (MU-RS) and *multiple-access relay selection* (MA-RS) schemes for the OC aided SC-FDMA when we have $K = 3$ users and $J = 6$ total relays. Specifically, the relays indicated by the numbers printed in boldface denote the highest SINR $\gamma_{j,k}^{\mathrm{AF}}$ in each column for a specific user index k, where we have the corresponding relay index j in the rows. The assigned relays of each user are marked by underlining them. Moreover, the specific assignment of relay j to each user k is given by $\check{j}$.

(a) SU-RS for SDR

$\gamma_{k,j}^{\mathrm{AF}}$	$k=0$	$k=1$	$k=2$
$j=0$	0.05	–	–
$j=1$	**0.16**	–	–
$j=2$	–	**1.44**	–
$j=3$	–	0.33	–
$j=4$	–	–	0.81
$j=5$	–	–	**1.90**
$\check{j}$	1	2	5

(b) MU-RS for SDR

$\gamma_{k,j}^{\mathrm{AF}}$	$k=0$	$k=1$	$k=2$
$j=0$	0.05	0.53	**2.26**
$j=1$	0.16	0.20	0.57
$j=2$	**1.42**	1.44	0.70
$j=3$	0.18	0.33	0.21
$j=4$	0.90	**3.07**	0.81
$j=5$	0.04	0.09	1.90
$\check{j}$	2	4	0

(c) MA-RS for SSR

$\gamma_{k,j}^{\mathrm{AF}}$	$k=0$	$k=1$	$k=2$
$j=0$	0.05	0.53	**2.26**
$j=1$	0.16	0.20	0.57
$j=2$	**1.42**	1.44	0.70
$j=3$	0.18	0.33	0.21
$j=4$	0.90	**3.07**	0.81
$j=5$	0.04	0.09	1.90
$\check{j}$	4	4	4

Therefore, the associated algorithm is summarised in Table 4.3.

4.5.5 Relay Selection Examples

Table 4.4 illustrates diverse examples of the above-mentioned SU-RS, MU-RS and MA-RS schemes for the OC aided SC-FDMA uplink in the scenario of $K = 3$ users and a total of $J = 6$ relays. According to Table 4.4(a) the SU-RS scheme of Figure 4.5(a) benefits from a diversity order of $J = 2$ as a benefit of having $J/K = 2$ relays per user available for selection, resulting in an assignment, where relay $\check{j} = 1, 2$ and 5 assist the users of $k = 0, 1$ and 2,

respectively. By contrast, according to Table 4.4(b), the MU-RS method of Figure 4.5(b) is capable of achieving a diversity order of up to $J = 6$. Therefore the relay $\check{j} = 4$ may be assigned to the user $k = 1$ associated with the maximum SINR of $\gamma_{0,4}^{\mathrm{AF}} = 3.07$ among all the channels spanning across multiple users to be assigned to specific relays and the available relays. By employing the MU-RS regime, the users $k = 0$ and $k = 2$ in Table 4.4(b) may have the chance to benefit from a higher receiver SINR of $\gamma_{0,2}^{\mathrm{AF}} = 1.42$ via the relay $\check{j} = 2$ and from an SINR of $\gamma_{2,0}^{\mathrm{AF}} = 2.26$ provided by the relay $\check{j} = 0$ compared to those obtained by the SU-RS approach in Table 4.4(a). Additionally, given a diversity order of $J = 6$, again, upon invoking the MA-RS algorithm of Figure 4.5(c) detailed in Section 4.5.4, the shared relay $\check{j} = 4$ of Table 4.4(c) is assigned to multiple users associated with a maximum sum of the SINRs given by $\gamma_{0,4}^{\mathrm{AF}} + \gamma_{1,4}^{\mathrm{AF}} + \gamma_{2,4}^{\mathrm{AF}} = 4.78$.

4.5.6 Power Allocation and Relay Selection Complexity

The computational complexity of the different power allocation schemes of Section 4.5.1and of the relay selection procedures of Sections 4.5.2, 4.5.3 and 4.5.4 should be quantified in order to find the most suitable algorithm. The EPA of Eq. (4.38a) benefits from the lowest complexity, regardless of the number of users and relays involved, while the DPA of Eq. (4.38b) requires both the sources and the relays to have the knowledge of K, but beneficially - it dispenses with any iterations. The OPA of Eq. (4.39) exhibits the highest complexity, which depends on both the specific optimisation algorithm employed as well as on the step-size of the power control strategy adopted. From a multi-user point of view, the SU-RS regime of Figure 4.5(a) requires J iterations for assigning relays to all the K users, while the MU-RS and MA-RS regimes of Figure 4.5(b) and 4.5(c) require $(K \times J)$ iterations. However, from a SU point of view, the SU-RS only needs an average of J/K iterations per user, while the MU-RS still requires $(K \times J)$ iterations for calculating the index of the desired relay for each source MT. Additionally, the RRS does not require any iterations among the relays. We assume that in practical cellular systems the number of cooperative users and the number of relays within each clusters may be insufficiently high, say less than 10 in total, but lower-complexity search algorithms may be considered for this selection stage in order to reduce the signal processing complexity and time delay imposed.

4.6 Simulation Results and Discussions

In our simulations, we investigate the uncoded *binary phase shift keying* (BPSK) modulated *bit-error rate* (BER) performance of the proposed schemes using no *forward error correction* (FEC), but invoking IFDMA scheme of Figure 2.9(b) subject to shadowing under imperfect

TABLE 4.5: General simulation parameters for both the static selected single-relay aided cooperation of Figure 3.1 and the OC scheme of Figure 4.5 in SC-FDMA systems.

Modulation and coding	BPSK, non-FEC
Subband mapping	Interleaved
Relaying topology	SDR or SSR
Relaying strategy	Subband-based AF
Number of subbands per user	$N = 4, 8$
Bandwidth expansion factor	$M = 16, 8$
Total number of subbands	$U = 64$
Number of source users	$K = 8, 16$

TABLE 4.6: Specific simulation parameters used in Section 4.6.1 for the fixed AF single-relay aided cooperation.

S-D, S-R, R-D channels	Frequency-selective Rayleigh fading
Number of CIR taps	$L = 1, 4, 8$
Power delay spread	Uniform
Shadowing	Absent
Path-loss	Absent
Power control	Perfect, i.e. PCE variance $\sigma_\epsilon^2 = 0$ dB
8-source mode	$N = K = M = 8$
16-source mode	$N = 4, K = M = 16$
Source transmit power per user	SDR: $\alpha_k^{\mathrm{S}} = 0.5$ SSR for $K = 1$: $\alpha_k^{\mathrm{S}} = 0.5$ SSR for $K > 1$: $\alpha_k^{\mathrm{S}} = 1 - 1/K$
Relay transmit power per user	SDR: $\alpha_k^{\mathrm{R}} = 0.5$ SSR for $K = 1$: $\alpha_k^{\mathrm{R}} = 0.5$ SSR for $K > 1$: $\alpha_k^{\mathrm{R}} = 1/K$
BS receiver	MMSE FD-LE invoking TD-EGC or JFDEC

power control. The effects of both propagation path-loss and of frequency-selective fading are also considered. Our parameters are summarised in Table 4.5 and the source MT's transmitter schematics of Figure 4.1 and relay's transceiver schematic of Figure 4.3 are used.

4.6.1 BER Performance of Fixed AF Single-Relay Aided Cooperation in the Absence of Large-Scale Fading

Initially, we consider a simple fixed AF relay aided system for both the SDR and SSR topologies of Figure 3.1 experiencing small-scale fading only, while the effects of shadowing, path-loss, relay location and power control are all ignored. Our parameters are summarized in Table 4.6 and the system invokes the BS's receiver schematic of either Figure 3.4 or Figure 4.4 for performance comparison.

Figures 4.6 and 4.7 illustrate the BER versus E_{b}/N_0 performance of the subband-based

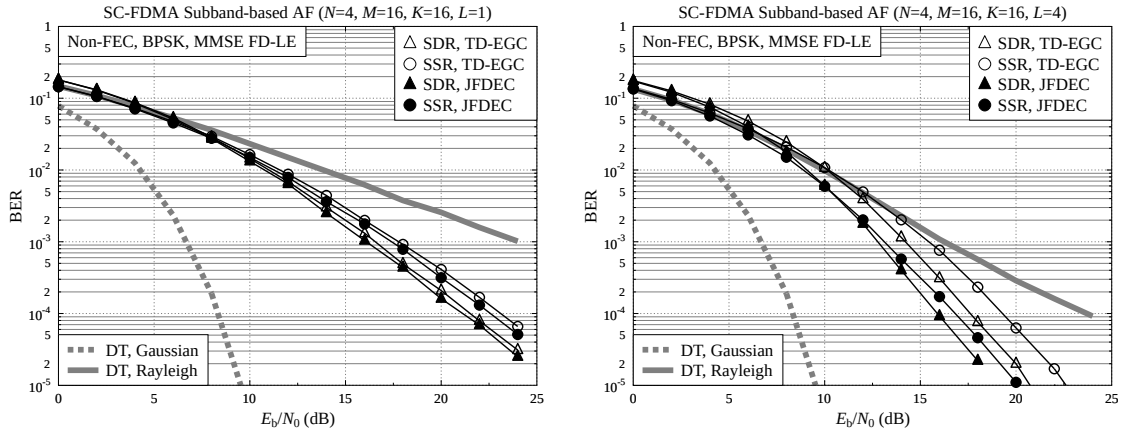

(a) The number of CIR taps is $L = 1$

(b) The number of CIR taps is $L = 4$

FIGURE 4.6: BER versus E_b/N_0 performance of the subband-based AF in the context of both the SDR and SSR aided IFDMA systems invoking either the MMSE FD-LE TD-EGC receiver of Figure 3.4 or the MMSE JFDEC receiver of Figure 4.4, when communicating over frequency-selective Rayleigh fading channels upon varying the number of CIR taps L in the absence of path-loss and shadowing for $N = 4, K = M = 16$. The source and relay schematics were shown in Figures 4.1 and 4.3, while the system parameters were summarised in Tables 4.5 and 4.6.

AF relaying system of Figure 4.3 relying on different receiver solutions for *full-load* uplink transmissions experiencing frequency-selective Rayleigh fading, upon varying the number of paths for $L = 1, 4$ or 8, while supporting $K = 16$ or 8 users for $U = 64$, respectively. Compared to the TD-EGC schematic of Figure 3.4, the proposed JFDEC scheme of Figure 4.4 carries out the MMSE FD-LE and diversity combining jointly with the aid of the optimised weights of Eq. (4.22) over each subband for both the direct and relaying branches. Although the JFDEC scheme exhibits only a modest improvement, when communicating over a single-path fading channel associated with $L = 1$ observe in Figures 4.6(a) and 4.7(a) that it achieves slightly more significant improvements for $L = 4$ and 8. Quantitatively, at a BER of 10^{-4}, our proposed scheme of Figure 4.4 is capable of achieving upto 8 dB power reduction for $N = L = 4, K = M = 16$, as shown in Figure 4.6(b) and an approximately 4 dB power reduction for $N = L = K = M = 8$, as shown in Figure 4.7(b). These gains are the explicit benefits of the cooperative diversity gain, while the TD-EGC scheme only saves 6 and 2 dB power, respectively in the same scenarios.

4.6.2 BER Performance of Power Allocation and Relay Location in the Presence of Large-Scale Fading

Furthermore, in order to characterise the effects of varying the ratio of the source/relay power and the locations of the static selected relays in the presence of path-loss and shadowing, we evaluate the BER versus $(\alpha_k^S, \delta_k^{RD})$ performance of our proposed schemes. Our parameters

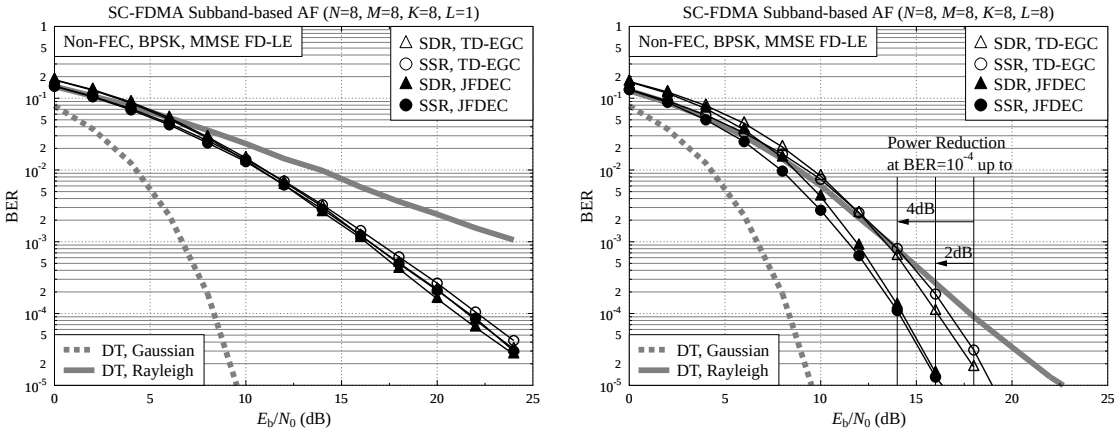

(a) The number of CIR taps is $L = 1$

(b) The number of CIR taps is $L = 8$

FIGURE 4.7: BER versus E_b/N_0 performance of the subband-based AF in the context of both the SDR and SSR aided IFDMA systems invoking either the MMSE FD-LE aided TD-EGC receiver of Figure 3.4 or the MMSE JFDEC receiver of Figure 4.4, when communicating over frequency-selective Rayleigh fading channels upon varying the number of CIR taps L in the absence of path-loss and shadowing for $N = M = K = 8$. The source and relay schematics were shown in Figures 4.1 and 4.3, while the system parameters were summarised in Tables 4.5 and 4.6.

TABLE 4.7: Specific simulation parameters used in Sections 4.6.2 and 4.6.3 for the *static relay selection* (SRS) aided single AF relay at various location using power allocation schemes in Section 4.5.1.

S-D, S-R channels	Frequency-selective Rayleigh fading
R-D channel	Frequency-selective Rayleigh/Rician fading
R-D Rician factor	$\kappa_{\mathrm{RD}} = 2$ dB
Number of CIR taps	$L = 8$
Path-loss exponent	$\eta = 3, 4$
Shadowing variance	$\sigma_\xi^2 = 0, 4, 8, 12$ dB
PCE variance	$\sigma_\epsilon^2 = 0$ dB or varying
SNR per bit	$E_b/N_0 = 8$ dB
8-source mode	$K = M = N = 8$
Relay mobility	Roaming
Relay selection	Static
BS receiver	MMSE FD-LE invoking JFDEC

are summarized in Table 4.7 and the system invokes the BS's receiver schematic of Figure 4.4.

Figures 4.8 and 4.9 depict the BER versus $(\alpha_k^{\mathrm{S}}, \delta_k^{\mathrm{RD}})$ performance of both the SDR and SSR topologies of Figure 3.1 experiencing frequency-selective fading in either Rayleigh distribution or Rician distribution associated with $\kappa_{\mathrm{RD}} = 2$ dB, for path-loss exponents of $\eta = 3$ or 4 subject to a shadowing variance of $\sigma_\xi^2 = 0$ dB or 4 dB at $E_b/N_0 = 8$ dB, where perfect power control is assumed for both the source and relay. Specifically, observe in Figure 4.8(a) that since the path-loss of the S-R and R-D links is lower than that of the S-D link, high relaying gains are attainable at the BS via the relaying branch, which is confirmed by the

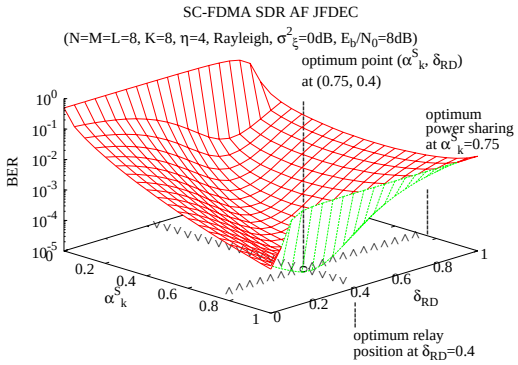

(a) SDR for $K = 8$

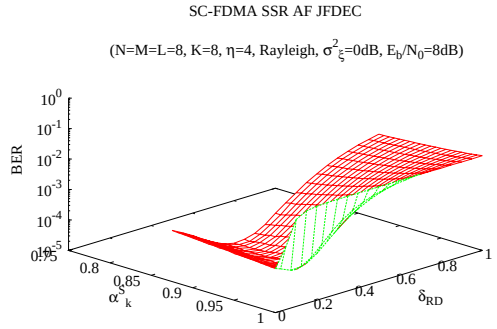

(b) SSR for $K = 8$

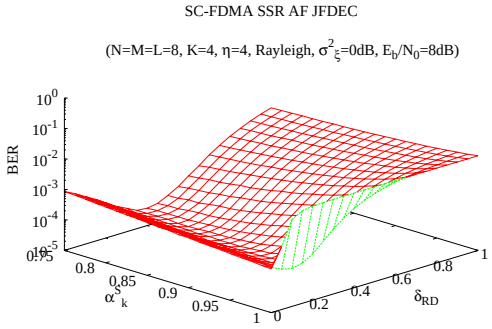

(c) SSR for $K = 4$

FIGURE 4.8: BER versus $(\alpha_k^{\mathrm{S}}, \delta_k^{\mathrm{RD}})$ performance of the subband-based AF in the context of both the SDR and SSR aided IFDMA systems for $N = M = 8$, $K = 4$ or 8, when the BS invokes MMSE JFDEC receiver of Figure 4.4. The systems experience frequency-selective Rayleigh fading associated with the number of CIR paths $L = 8$, for the path-loss exponent $\eta = 4$ in the absence of shadowing, when $E_{\mathrm{b}}/N_0 = 8$ dB. The source and relay schematics were shown in Figures 4.1 and 4.3, while the system parameters were summarised in Tables 4.5 and 4.7.

curve denoted by the $\vee$ marker in Figure 4.8(a). Since we assume that the total transmitted power of the system is constant, the source MT can transmit its own signal at a higher α_k^{S}, as indicated by the curve marked by $\wedge$ for $\alpha_k^{\mathrm{S}} = 0.75$, which is then attenuated by the long-distance S-D and S-R link during TS_1. By contrast, the relay transmits the signal forwarded to the destination at a lower α_k^{R} during TS_2, when the relay is roaming within the desired relaying area near to the BS, as indicated by the curve marked by the legend $\vee$ for $\delta_k^{\mathrm{RD}} = 0.4$, which is expected to have a high relaying gain. Therefore, observing the relay located at this optimum position, the BER performance of the EPA mode recorded for $\alpha_k^{\mathrm{S}} = 0.5$ only slightly decreases compared to the OPA mode for $\alpha_k^{\mathrm{S}} = 0.75$, but requires a lower complexity. Additionally, due to the power constraint of the SSR uplink, the default transmit power of the source MT is a function of K, as shown in Figures 4.8(b) and 4.8(c). Hence, the optimum value of α_k^{S} may be the α_k^{S} of DPA for the SSR topology, which is larger than the optimum value of α_k^{S} designed for the SDR topology, as shown in Figure

TABLE 4.8: Optimum Ranges of α_k^{S} and δ_k^{RD} in Figures 4.8 and 4.9.

Figure	Topology	Fading	σ_ξ^2	η	α_k^{S}	δ_k^{RD}	BER
Fig. 4.8(a)	SDR	Rayleigh	0 dB	4	0.75	0.4	$3.8e-5$
Fig. 4.8(b)	SSR	Rayleigh	0 dB	4	0.875	0.3	$4.4e-5$
Fig. 4.8(c)	SSR	Rayleigh	0 dB	4	0.75	0.4	$3.7e-5$
Fig. 4.9(a)	SDR	Rician	0 dB	3	0.85	0.25	$2.02e-4$
Fig. 4.9(b)	SSR	Rician	0 dB	3	0.875	0.2	$2.03e-4$
Fig. 4.9(c)	SDR	Rician	0 dB	4	0.775	0.4	$3.8e-5$
Fig. 4.9(d)	SSR	Rician	0 dB	4	0.875	0.325	$4.5e-5$
Fig. 4.9(e)	SDR	Rician	4 dB	4	0.75	0.4	$4.04e-4$
Fig. 4.9(f)	SSR	Rician	4 dB	4	0.875	0.35	$4.62e-4$

4.8(b). In summary, both the EPA of Eq. (4.38a) and the DPA of Eq. (4.38b) are more practical schemes when subjected to imperfect power control, which is an explicit benefit of their low complexity, when invoked in the context of the SDR and SSR topologies of Figure 3.1, respectively. By contrast, the OPA of Eq. (4.39) improves the achievable performance at an increased complexity.

We may now infer the optimum ranges of α_k^{S} and δ_k^{RD} from the simulation results of Figures 4.8 and 4.9 which are summarised in Table 4.8.

Figure 4.10 characterises the BER versus E_{b}/N_0 performance of the EPA, DPA or OPA modes under perfect power control upon varying the shadowing effects at a path-loss exponent of $\eta = 4$, when the SRS aided relay's location is assumed to be at the mid-point in the 2D map of Figure 4.2 or at the optimal point in the Table 4.8. As expected, the BER increases, when the shadowing variance increases from $\sigma_\xi^2 = 0$ to 8 dB. Naturally, the best performance is achieved in the absence of shadowing, exhibiting a BER of 10^{-4} at $E_{\mathrm{b}}/N_0 = 7$ dB, which is a benefit of having the highest relaying gain when the relay is at the optimal position, in comparison to the non path-loss scenario as seen in Figure 3.8(d) and Figure 3.10(b). Furthermore, we note that at least 1.5 dB power saving can be achieved, when the SDR system invokes OPA and the relaying distance is optimum, when compared to the EPA benchmark using a relay in the middle of the S-D link. However, owing to the power constraint of the SSR system, the performance of the DPA is close to that of the OPA. Hence, from a computational complexity point of view, using the OPA is not necessary in the SSR system. Additionally, compared to non-cooperative transmission, the BER of the cooperative scenario remains better at low E_{b}/N_0 values, when the system is subjected to high-variance shadowing associated with $\sigma_\xi^2 = 8$ dB.

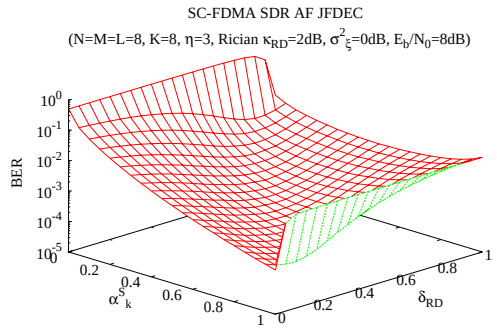

(a) SDR for $\eta = 3$ and $\sigma_\xi^2 = 0$ dB

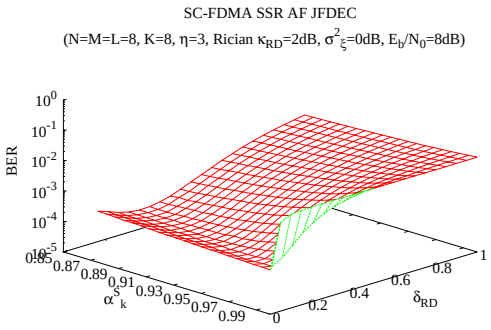

(b) SSR for $\eta = 3$ and $\sigma_\xi^2 = 0$ dB

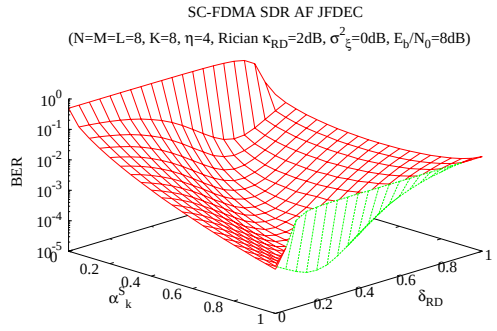

(c) SDR for $\eta = 4$ and $\sigma_\xi^2 = 0$ dB

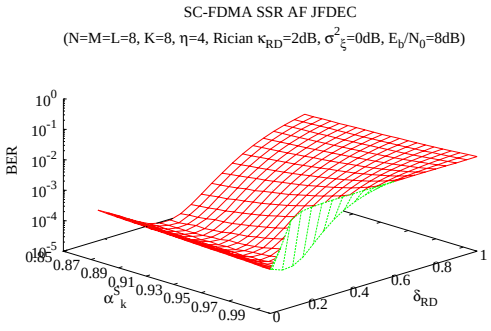

(d) SSR for $\eta = 4$ and $\sigma_\xi^2 = 0$ dB

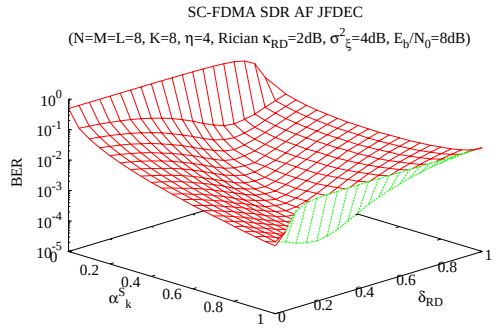

(e) SDR for $\eta = 4$ and $\sigma_\xi^2 = 4$ dB

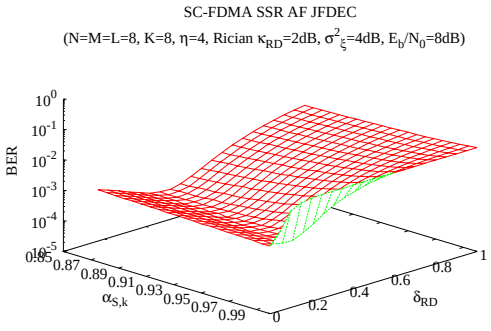

(f) SSR for $\eta = 4$ and $\sigma_\xi^2 = 4$ dB

FIGURE 4.9: BER versus $(\alpha_k^{\mathrm{S}}, \delta_k^{\mathrm{RD}})$ performance of the subband-based AF in the context of both the SDR and SSR aided IFDMA systems for $N = M = 8$, $K = 8$, when the BS invokes MMSE JFDEC receiver of Figure 4.4. The systems experience frequency-selective Rician fading associated with $\kappa_{\mathrm{RD}} = 2$ dB and the number of CIR paths $L = 8$ upon varying path-loss exponent η in the absence and presence of shadowing, when $E_{\mathrm{b}}/N_0 = 8$ dB. The source and relay schematics were shown in Figures 4.1 and 4.3, while the system parameters were summarised in Tables 4.5 and 4.7.

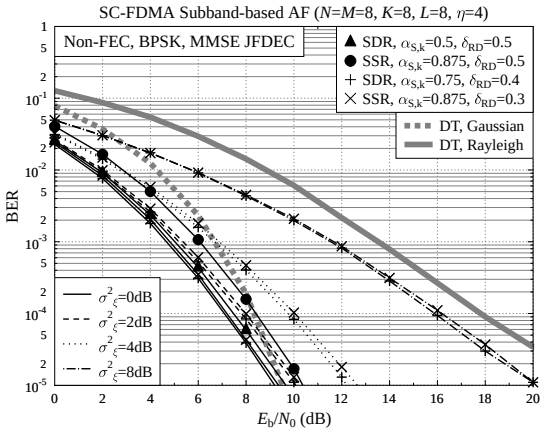

FIGURE 4.10: BER versus E_b/N_0 performance of the SRS aided subband-based AF based relay associated with the specific power allocations and relaying positions, in the context of both the SDR and the SSR aided IFDMA system for $N = M = 8$, $K = 8$, when the BS invokes MMSE JFDEC receiver of Figure 4.4. The systems communicate over frequency-selective Rayleigh fading channels associated with the number of CIR taps $L = 8$ for the path-loss exponent $\eta = 4$, upon varying shadow variance σ_ξ^2 by assuming the perfect power control. The source and relay schematics were shown in Figures 4.1 and 4.3, while the system parameters were summarised in Tables 4.5 and 4.7.

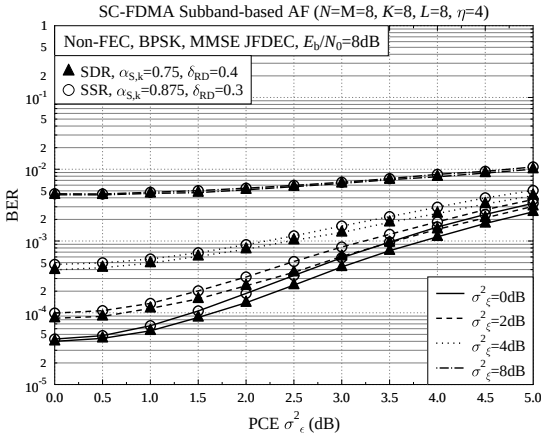

FIGURE 4.11: BER versus PCE variance σ_ϵ^2 of the SRS aided subband-based AF based relay invoking OPA at the best relaying position, in the context of both SDR and SSR aided IFDMA systems for $N = M = 8$ and $K = 8$, when the BS invokes MMSE JFDEC receiver of Figure 4.4. The systems communicate over frequency-selective Rayleigh fading channels associated with the number of CIR taps $L = 8$ for the path-loss exponent $\eta = 4$, upon varying shadow variance σ_ξ^2 under imperfect power control when $E_b/N_0 = 8$ dB. The source and relay schematics were shown in Figures 4.1 and 4.3, while the system parameters were summarised in Tables 4.5 and 4.7.

4.6.3 BER Performance of Imperfect Power Control in the Presence of Large-Scale Fading

When considering imperfect power control, Figure 4.11 illustrates the BER versus the PCE variance σ_ϵ^2 of the SRS aided relay using OPA of Eq. (4.39) at the best relaying position upon varying the shadowing variance for $K = 8$ users employing the SDR and SSR systems

TABLE 4.9: Specific simulation parameters used in Sections 4.6.4 to 4.6.6 for the OC systems invoking various relay selection schemes in Sections 4.5.2 to 4.5.4.

S-D, S-R, R-D channels	Frequency-selective Rayleigh fading
Power delay spread	Uniform
Number of CIR taps	$L = 8$
Path-loss exponent	$\eta = 4$
Shadowing variance	$\sigma_\xi^2 = 0, 2, 4, 8$ dB
PCE variance	$\sigma_\epsilon^2 = 0, 2$ dB
Relay mobility	Roaming
Relay selection	Dynamic
Number of source users	$K = 4, 8$
Number of relays (candidates)	$J = 16$ or varying
Number of subbands per user	$N = 8$
Bandwidth expansion factor	$M = 8$
Total number of subbands	$U = 64$
BS receiver	MMSE FD-LE invoking JFDEC

of Figure 3.1 at E_b/N_0 of 8 dB. It is shown in Figure 4.11 that the effect of imperfect power control on the BER performance is not severe, when σ_ϵ^2 is less than 1 dB. Moreover, the BER may increase logarithmically upon increasing σ_ϵ^2, provided that we have weak shadowing. By contrast, the PCE effects become less dominant, when the cooperative transmission regime is subjected to deep shadow fading of $\sigma_\xi^2 = 8$ dB in Figure 4.11, in which case, the performance of cooperative relaying depends more substantially on the shadowing.

4.6.4 BER Performance of Relay Selection Combined with Power Allocation

For the sake of fair comparisons, we assume that we have $K = 4$ source MTs, assisted by $J = 16$ relays for both the SU-RS and the MU-RS of Figure 4.5(a) and 4.5(b). Our parameters are summarised in Table 4.9, while the systems schematic is shown in Figures 4.1, 4.3 and 4.4. Upon varying the effects of shadowing under imperfect power control of all the links for transmission over Rayleigh fading channels in the presence of a path-loss exponent of $\eta = 4$, Figure 4.12 characterises the overall average BER versus E_b/N_0 performance of different relay selection aided AF-SDR systems invoking the EPA and OPA schemes of Section 4.5.1, respectively. Observe in Figures 4.12(b) and 4.12(d) that the achievable gain of the OPA recorded for $\alpha_k^S = 0.75$ is limited to about 1 dB at a BER of 10^{-4} compared to the EPA curves recorded for $\alpha_k^S = 0.5$ in Figures 4.12(a) and 4.12(c), which indicates the robustness of the proposed cooperative regime. We know additionally that according to Figure 4.8(a), the activation of a relay roaming in the vicinity of the optimal location is capable of achieving a similar performance to OPA. Compared to the RRS characterised in both Figure 4.12(a) and 4.12(b), the static selected relay associated with the optimal relay position of $\delta_k^{RD} = 0.4$ offers a 3 dB relaying gain at a BER of 10^{-4}, while both the SU-RS

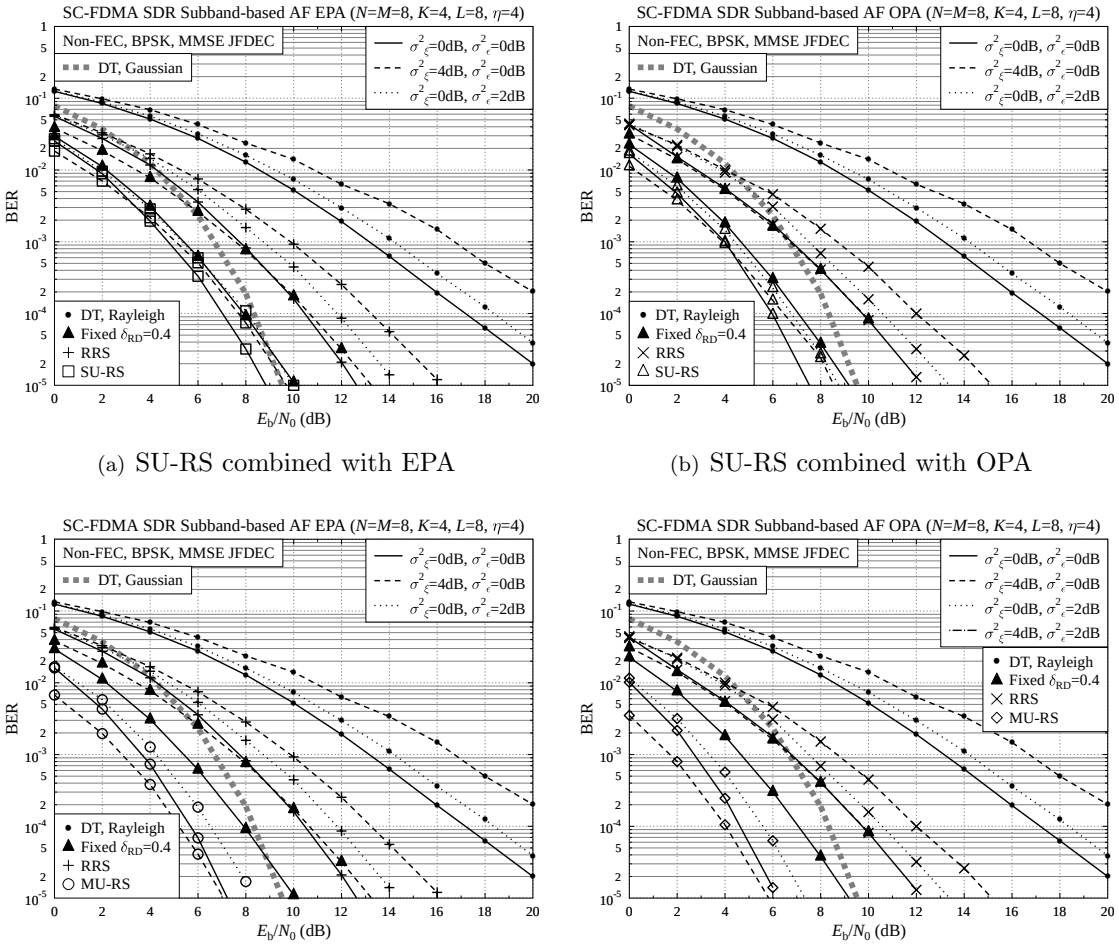

(a) SU-RS combined with EPA

(b) SU-RS combined with OPA

(c) MU-RS combined with EPA

(d) MU-RS combined with OPA

FIGURE 4.12: BER versus E_b/N_0 performance of various relay selection schemes combined with power allocation for OC using the subband-based AF aided SDR in the context of IFDMA system for $N = M = 8$, $K = 4$ and $J = 16$, when the BS invokes MMSE JFDEC receiver of Figure 4.4. The systems communicate over frequency-selective Rayleigh fading channels associated with $L = 8$ with path-loss exponent $\eta = 4$, upon varying the shadowing variance σ_ξ^2 under imperfect power control by varying PCE variance σ_ϵ^2. The source and relay schematics were shown in Figures 4.1 and 4.3, while the system parameters were summarised in Tables 4.5 and 4.9.

and MU-RS regimes of Figure 4.5(a) and 4.5(b) provide a substantial multi-user diversity gain, which is about 4 dB at a BER of 10^{-4}. Furthermore, the proposed MU-RS has the edge over the SU-RS, providing an additional multi-user diversity gain in excess of 2 dB, which is a benefit of the relay selection procedure that avoids the effects of deep shadow fading[7]. As a result, the transmitted power can be reduced by about $(E_b/N_0)_\Delta = 4$ dB at a BER of 10^{-4}, when we have $\sigma_\xi^2 = 4$ dB, $\sigma_\epsilon^2 = 0$ dB.

By contrast, the benefits of relay selection on the attainable BER performance of the SSR

[7]By comparing the various relay selection schemes for the same J as a fairness, the additional selection diversity gain may be observed in Figures 4.12 and 4.13. By contrast, alternative ways of benchmarking may be relying on different J for the specific relay selection schemes in terms of their applied scenarios.

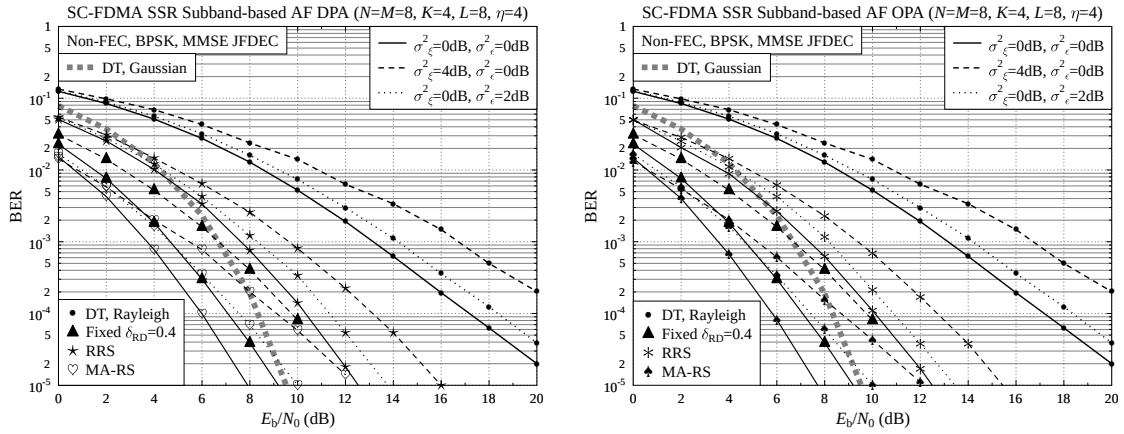

(a) MA-RS combined with DPA

(b) MA-RS combined with OPA

FIGURE 4.13: BER versus E_b/N_0 performance of various relay selection schemes combined with power allocation for the OC using the subband-based AF aided SSR in the context of IFDMA system for $N = M = 8$, $K = 4$ and $J = 16$, when the BS invokes MMSE JFDEC receiver of Figure 4.4. The systems communicate over frequency-selective Rayleigh fading channels associated with $L = 8$, path-loss exponent $\eta = 4$, upon varying the shadowing variance σ_ξ^2 under imperfect power control by varying PCE variance σ_ϵ^2. The source and relay schematics were shown in Figures 4.1 and 4.3, while the system parameters were summarised in Tables 4.5 and 4.9.

system upon varying the shadow fading variance under imperfect power control are characterised in Figure 4.13 for $J = 16$. The static selected relay is capable of achieving a 3 dB relaying gain, which is similar to that of the SDR system. Although only a single R-D link exists in the system, this target relay can be selected by considering the position trade-off among multiple source MTs and multiple relays, in an effort to reduce the path-loss. Meanwhile, a useful diversity gain is still attainable by relay selection for transmission over Rayleigh fading channels. However, the MA-RS considers the single-relay based support of all the K source users, whose signal occupies all the $(K \times N)$ subbands, while considering all the $(K \times J)$ possible S-R links. Thus, the selection diversity gain achieved in the presence of deep shadow fading does not improve the link-level reliability quantified in terms of the BER performance. Therefore, the DPA aided MA-RS allows the system to achieve a BER of 10^{-4} at $E_b/N_0 = 6$ dB, when we have $\sigma_\xi^2 = \sigma_\epsilon^2 = 0$ dB. Additionally, since the power control determines the transmit power of all source MTs and relays, the corresponding performance differences between $\sigma_\epsilon^2 = 0$ dB and $\sigma_\epsilon^2 = 2$ dB are quantified in Figures 4.12 and 4.13 for the EPA, DPA and OPA schemes of Section 4.5.1 in the presence of both perfect and imperfect power control.

4.6.5 Capacity of Opportunistic Cooperation Invoking Power Allocation

In addition to the above BER performance analysis of Figures 4.12 and 4.13, we quantify the sum-rate of all users' data transmissions in order to represent the attainable multi-user

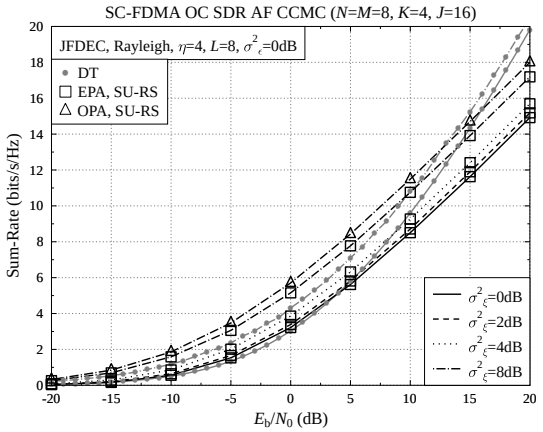

(a) SU-RS in SDR

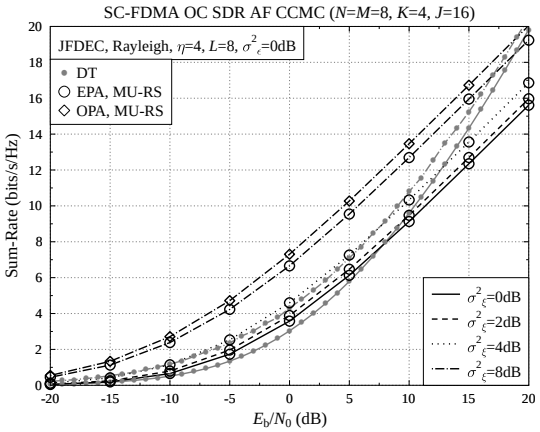

(b) MU-RS in SDR

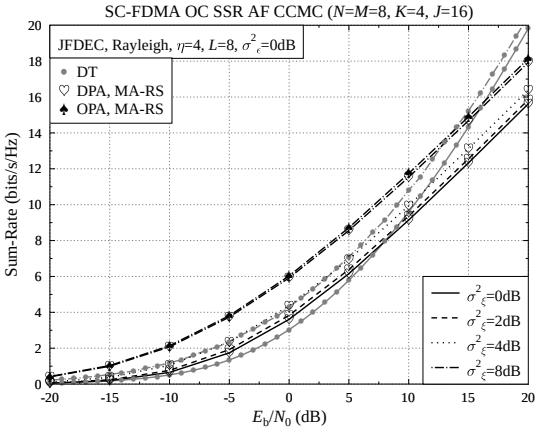

(c) MA-RS in SSR

FIGURE 4.14: Sum-rate versus E_b/N_0 performance of various relay selection schemes combined with power allocation for the OC using the subband-based AF in the context of IFDMA systems for $N = M = 8$, $K = 4$ and $J = 16$, when the BS invokes MMSE JFDEC receiver of Figure 4.4. The systems communicate over frequency-selective Rayleigh fading channels associated with $L = 8$, path-loss exponent $\eta = 4$, upon varying the shadowing variance σ_ξ^2 under perfect power control. The source and relay schematics were shown in Figures 4.1 and 4.3, while the system parameters were summarised in Tables 4.5 and 4.9.

system throughput in terms of Shannon's *continuous-input continuous-output memoryless channel* (CCMC) capacity [196].

Figure 4.14 depicts the sum-rate versus E_b/N_0 performance of various relay selection schemes invoking power allocation for $J = 16$ relays. It may be observed in Figure 4.14(b) that if the E_b/N_0 value is relatively low, the proposed MU-RS aided cooperative system exhibits up to 4bits/s/Hz higher sum-rate than its DT based counterpart, when experiencing a shadow fading variance of 8 dB. However, as the overall E_b/N_0 increases to a relatively high value, the benefits of invoking a MU-RS aided cooperative system for achieving either a high sum-rate or high ECG erode. Indeed, this is not unexpected, because sharing the total transmit power between the source and relay as well as the provision of two time-slots

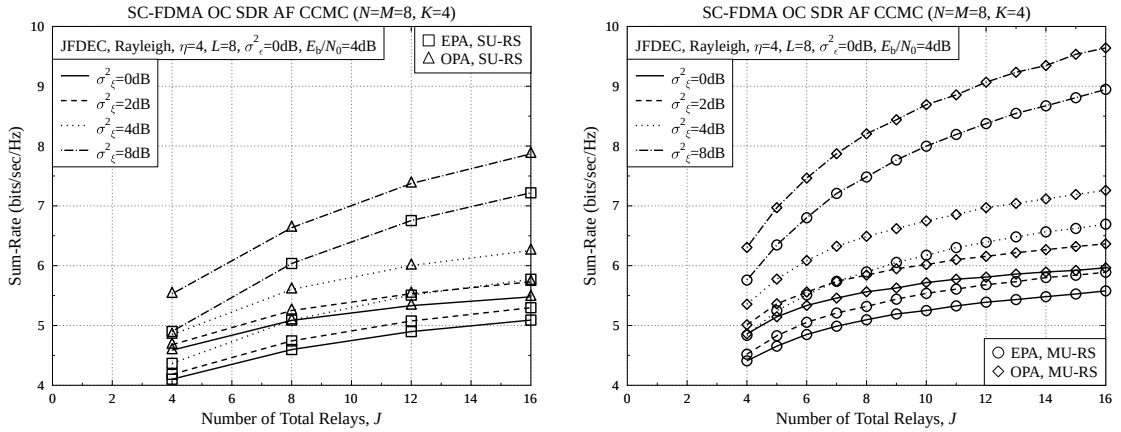

(a) SU-RS in SDR

(b) MU-RS in SDR

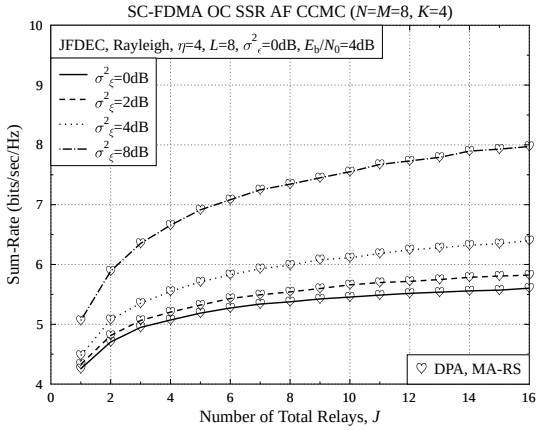

(c) MA-RS in SSR

FIGURE 4.15: Sum-rate versus the number of relays J performance of various relay selection schemes combined with power allocation for OC using the subband-based AF in the context of IFDMA systems for $N = M = 8$ and $K = 4$, when the BS invokes MMSE JFDEC receiver of Figure 4.4. The systems communicate over frequency-selective Rayleigh fading channels associated with $L = 8$, path-loss exponent $\eta = 4$, upon varying the shadowing variance σ_ξ^2 under perfect power control at $E_b/N_0 = 4$ dB. The source and relay schematics were shown in Figures 4.1 and 4.3, while the system parameters were summarised in Tables 4.5 and 4.9.

results in a throughput loss, which is not fully compensated by the relaying-gain attained. In addition, Figure 4.14(b) indicated up to 9 dB gains, when the shadow-fading variance was 8 dB and the sum-rate was 1bits/s/Hz. At higher sum-rates the system still maintain an approximately 6 dB power gain.

From a resource management point of view, Figure 4.15 depicts the attainable system throughput as a function of the total number of relays, when the number of source MTs was fixed to $K = 4$ and we had $E_b/N_0 = 4$ dB. Observe in Figure 4.15 that the sum-rate improves upon increasing the number of relays. Specifically, the MU-RS scheme in Figure 4.15(b) is capable of substantially improving the throughput compared to the SU-RS approach in 4.15(a), particularly when communicating over channels subject to shadow fading.

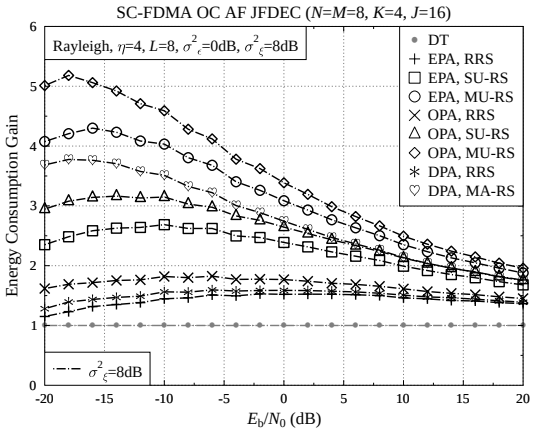

FIGURE 4.16: ECG versus E_b/N_0 performance of various relay selection schemes combined with power allocation for the OC using the subband-based AF in the context of IFDMA systems for $N = M = 8$, $K = 4$ and $J = 16$, when the BS invokes MMSE JFDEC receiver of Figure 4.4. The systems communicate over frequency-selective Rayleigh fading channels associated with $L = 8$, path-loss exponent $\eta = 4$ and shadowing variance $\sigma_\xi^2 = 8$ dB under perfect power control. The source and relay schematics were shown in Figures 4.1 and 4.3, while the system parameters were summarised in Tables 4.5 and 4.9.

Moreover, the sum-rate of the MA-RS in Figure 4.15(c) is not unduly affected by varying the number of relays, when compared to both the SU-RS and MU-RS schemes. Additionally, we note that the MA-RS is capable of supporting OC, even when the number of relays is $J < K$.

4.6.6 Energy-Efficiency of Opportunistic Cooperation Subject to Shadowing

For the sake of quantifying the attainable energy-efficiency, Figure 4.16 illustrates the ECG versus the E_b/N_0 performance of both the SDR and SSR in the context of OC systems invoking different power allocation and relay selection schemes for a shadowing variance of 8 dB under perfect power control for the SU-RS in conjunction with $J = 4$ and for the MU-RS using $J = 16$. Clearly, when aiming for a fixed target E_b/N_0 of say -10 dB in the presence of shadowing compared to a non-cooperative DT scenario, the multi-user diversity gain that accrued from avoiding small-scale fading allows the MU-RS scheme to achieve a significant ECG of 4 for EPA and 4.5 for OPA, while the SU-RS attains gains of 2.6 and 3.1 for EPA and OPA, respectively. The MA-RS obtains a similar ECG as the OPA aided SU-RS, but imposes a significantly lower complexity. Finally, the RRS has the lowest gain of about 1.5, regardless of the specific power allocation employed.

Furthermore, since we adopt the direct transmission regime in the absence of shadowing as a reference, the shadowing effects imposed on ECG are illustrated in Figures 4.17(a) and 4.17(b) for the SU-RS and MU-RS invoking EPA, while in Figure 4.17(c) for DPA

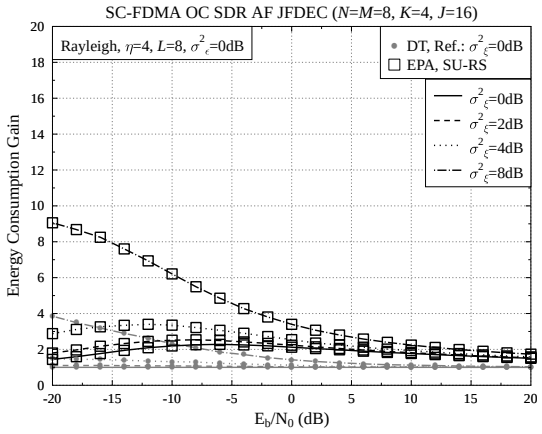

(a) SU-RS combined with EPA in SDR

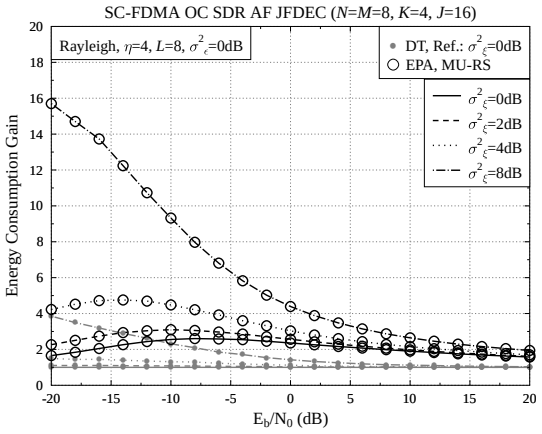

(b) MU-RS combined with EPA in SDR

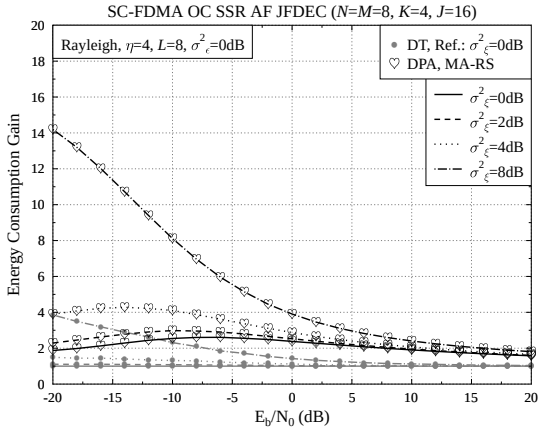

(c) MA-RS combined with DPA in SSR

FIGURE 4.17: ECG versus E_b/N_0 performance of various relay selection schemes combined with power allocation for the OC using the subband-based AF in the context of IFDMA system for $N = M = 8$, $K = 4$ and $J = 16$, when the BS invokes MMSE JFDEC receiver of Figure 4.4. The systems communicate over frequency-selective Rayleigh fading channels associated with $L = 8$, path-loss exponent $\eta = 4$ upon varying the shadowing variance σ_ξ^2 under perfect power control. The source and relay schematics were shown in Figures 4.1 and 4.3, while the system parameters were summarised in Tables 4.5 and 4.9.

aided MA-RS associated with $J = 16$ under perfect power control. The ECG difference between the scenarios associated with different shadowing variances implies that opportunistic scheduling constitutes a power-efficient design, when communicating over realistic shadow fading channels associated with $\sigma_\xi^2 = 0, 2, 4, 8$ dB, compared to the DT benchmark. Specifically, when reducing the transmit power and hence E_b/N_0, the ECGs of both MU-RS and MA-RS are increased more substantially for $\sigma_\xi^2 = 8$ dB compared to the lower fading variances considered. For instance, the MU-RS and MA-RS may achieve an ECG of 9 and 8 at $E_b/N_0 = -10$ dB, respectively.

4.7 Summary

In this chapter, we assumed that the relays were roamed in a geographically distributed scenario. The performance benefits of the energy-efficient opportunistic cooperation conceived for the multi-user SC-FDMA uplink were evaluated, when communicating over frequency-selective fading channels in large-scale fading environments. In order to maintain MUI free conditions at the relays, each relay was assumed to employ the subband-based AF scheme of Figure 3.3(b). Furthermore, since the noise imposed at BS's receiver both by the direct- and relaying links has a coloured spectral density, the MMSE FD-LE based JFDEC solution of Figure 4.4 was proposed, which jointly optimised the equalisation and receiver diversity combining at the BS's receiver, in order to maximise the cooperative diversity gain. Moreover, a number of energy consumption metrics were adopted for evaluating the energy-efficiency of the proposed schemes. In this chapter, we proposed three different types of channel-dependent relay selection schemes designed for opportunistic cooperation, which relied on specifically designed source/relay power allocation in the presence of both pass-loss and shadowing, while subjected to imperfect power control. Firstly, the SU-RS scheme of Figure 4.5(a) was designed, when assuming that the number of available relays is sufficient for each cluster of relays serving a single source MT. Secondly, assuming that the number of available relays is insufficient, the proposed MU-RS scheme of Figure 4.5(b) allows multiple users to share the same cluster of relays. Finally, the MA-RS scheme dynamically assigns a single relay to serve all the source MTs, when the number of relays is lower than the number of source MTs.

Our performance results demonstrated that at a BER of 10^{-4}, the proposed JFDEC aided BS's receiver of Figure 4.4 is capable of saving 2 dB power by achieving a higher cooperative diversity gain than the conventional receiver of Figure 3.4. Furthermore, as shown in Figure 4.8(a), the optimal location of the AF relay is close to the BS and the AF relay requires a lower transmit power than the source MT. When the relays are dynamically distributed, the proposed SU-RS, MU-RS and MA-RS schemes of Figure 4.5 benefit from substantial selection diversity gains in diverse shadowing scenarios. For instance, when the channel exhibits as high shadowing variance as 8 dB at $E_b/N_0 = -10$ dB, an ECG of $2.5 - 4.5$ is attainable by invoking the proposed SU-RS, MU-RS and MA-RS schemes in comparison to the conventional DT scenario. Most importantly, the ECG gleaned from our MU-RS and MA-RS schemes may increase to $4 - 8$, when the shadowing variance is increased from 4 to 8 dB, compared to the DT in the absence of shadowing at $E_b/N_0 = -10$ dB. Finally, Table 4.10 summarises the power reduction in terms of the SNR gain per bit γ_b^{Δ} recorded at the BER of 10^{-4} for the various relay selection schemes using OPA for the AF based OC SC-FDMA uplink compared to the DT benchmark using $N = L = M = 8$, when communicating over frequency-selective fading channels. The schemes are listed in

TABLE 4.10: Power reduction in terms of the SNR gain per bit $\gamma_{\mathrm{b}}^{\Delta}$ (dB) for the various relay selection schemes using OPA for the AF based OC assisted SC-FDMA uplink compared to the DT benchmark using $N = L = M = 8$, when communicating over frequency-selective fading channels. The schemes are listed in descending order of complexity.

Scheme	Figure	$\gamma_{\mathrm{b}}^{\Delta}$ (dB)
MU-RS	4.12(d)	18
MA-RS	4.13(b)	16
SU-RS	4.12(b)	16
SRS	4.12(b), 4.13(b)	11
RRS	4.12(b), 4.13(b)	7

descending order of complexity.

In the next chapter, we will consider dynamic resource allocation aided opportunistic relaying conceived for the SC-FDMA uplink, where we assume that the relays are geographically localised in each other's vicinity.

Appendix

It follows from Eq. (4.24) in Section 4.3.2 that all the diagonal elements of $\boldsymbol{A}_{k'}^{\mathrm{t}}$ are equal, which are given by

$$a_{k'nn}^{\mathrm{t}} = \frac{1}{N}\mathrm{Tr}\left[\boldsymbol{A}_{k'}^{\mathrm{t}}\right] = \frac{1}{N}\sum_{n=0}^{N-1}\left((w_{k',n}^{\mathrm{D}})^{*}h_{0,k',n}^{\mathrm{D,f}} + (w_{k',(n+N)}^{\mathrm{D}})^{*}h_{1,k',n}^{\mathrm{D,f}}\right). \tag{4.43}$$

The power of the desired signal at any instant is expressed as

$$P_{\mathrm{des}} = P_k^{\mathrm{S}}(a_{k'nn}^{\mathrm{t}})^2 = P_k^{\mathrm{S}}\left[\frac{1}{N}\sum_{n=0}^{N-1}\left(\frac{|h_{0,k',n}^{\mathrm{D,f}}|^2}{\sigma_{\mathrm{N}}^2} + \frac{|h_{1,k',n}^{\mathrm{D,f}}|^2}{\mathcal{N}_{1,n}^{\mathrm{D}}}\right)e_{k'n}\right]^2. \tag{4.44}$$

In parallel, the power of the estimated signal, which is defined as the power of the desired signal plus the power of the ISI, is given by the circulant covariance matrix of the estimated signal $\boldsymbol{z}_{k'}^{\mathrm{D,t}}$ as follows:

$$\begin{aligned} P_{\mathrm{est}} = P_{\mathrm{des}} + P_{\mathrm{ISI}} &= \frac{1}{N}\mathrm{Tr}\left\{\mathrm{E}\left[\boldsymbol{A}_{k'}^{\mathrm{t}}\boldsymbol{x}_{k'}^{\mathrm{t}}(\boldsymbol{x}_{k'}^{\mathrm{t}})^{H}(\boldsymbol{A}_{k'}^{\mathrm{t}})^{H}\right]\right\} \\ &= \frac{P_k^{\mathrm{S}}}{N}\sum_{n=0}^{N-1}\left[\left(\frac{|h_{0,k',n}^{\mathrm{D,f}}|^2}{\sigma_{\mathrm{N}}^2} + \frac{|h_{1,k',n}^{\mathrm{D,f}}|^2}{\mathcal{N}_{1,n}^{\mathrm{D}}}\right)e_{k'n}\right]^2. \end{aligned} \tag{4.45}$$

Additionally, the desired signal is also corrupted by the noise, whose power is given by the diagonal elements of the covariance matrix of the equivalent noise at the receiver, yielding

$$\hat{\mathcal{N}} = \frac{1}{N}\mathrm{Tr}\left\{\mathrm{E}\left[\boldsymbol{n}_D^{\mathrm{t}}(\boldsymbol{n}_D^{\mathrm{t}})^H\right]\right\} = \frac{1}{N}\sum_{n=0}^{N-1}\left(\frac{|h_{0,k',n}^{\mathrm{D,f}}|^2}{\sigma_{\mathrm{N}}^2} + \frac{|h_{1,k',n}^{\mathrm{D,f}}|^2}{\mathcal{N}_{1,n}^{\mathrm{D}}}\right)e_{k'n}^2. \tag{4.46}$$

Hence, we may express the overall signal-to-interference-and-noise ratio (SINR) $\gamma_{k'}$ per bit as below

$$\begin{aligned}\gamma_{k'} = \frac{P_{\mathrm{des}}}{P_{\mathrm{ISI}} + \hat{\mathcal{N}}} &= \left[\left(\frac{1}{N}\sum_{n=0}^{N-1}\frac{\gamma_{k',n}^{\mathrm{D0}} + \gamma_{k',n}^{\mathrm{D1}}}{\gamma_{k',n}^{\mathrm{D0}} + \gamma_{k',n}^{\mathrm{D1}} + 1}\right)^{-1} - 1\right]^{-1} \\ &= \left(\frac{1}{N}\sum_{n=0}^{N-1}\frac{1}{\gamma_{k',n}^{\mathrm{D0}} + \gamma_{k',n}^{\mathrm{D1}} + 1}\right)^{-1} - 1 = e_{k'}^{-1} - 1.\end{aligned} \tag{4.47}$$

Chapter 5

First-Hop Quality-Aware Dynamic Resource Allocation for the Opportunistically Relayed SC-FDMA Uplink

5.1 Introduction

Relay-assisted radio frequency communications [197] have been explored in the context of diverse ad-hoc and cellular networks for the sake of improving the attainable spectral-efficiency or energy-efficiency of classic *direct transmissions* (DT) [42, 51, 198]. Single or multiple [43, 44], serial or parallel [45], static or dynamic [65] relaying have been investigated, providing diversity gains in the *time*-, *frequency*- and *spatial*-domains. Naturally, the availability of inactive mobiles as candidate relays has the potential of mitigating the effects of fading. The activation of multiple relays results in cooperative diversity and when dynamically reassigning the relays based on their location and/or channel quality, we arrive at the concept of *opportunistic relaying* (OR)[1] [16, 66, 67, 81, 199], where the direct link is unavailable.

As we argued in Chapter 1, *orthogonal frequency-division multiplexing* (OFDM) style broadband *single-carrier frequency-division multiple-access* (SC-FDMA) systems, such as the *Third Generation Partnership Project*'s (3GPP) *Long Term Evolution* (LTE) system's up-

[1]In this chapter, we assume that the direct link is unavailable, hence we use the terminology of '*opportunistic relaying*' (OR). In Chapter 4, we assumed that the direct link was available, therefore we used the terminology of '*opportunistic cooperation*' (OC) .

link scheme [91,102] and its downlink *orthogonal* FDMA (OFDMA) scheme [200,201], conveniently facilitate near-instantaneous adaptive subband/subcarrier allocation and multi-user scheduling. These techniques rely on the *channel state information* (CSI) of the subbands/-subcarriers [56–58, 60, 70–72, 202–205], when communicating over frequency-selective fading channels. Compared to classic single-hop transmissions, optimising resource allocation for relay-assisted dual-hop transmissions is more challenging. As a benefit, the system enjoys an improved performance at the cost of an increased complexity. However, directly adopting the conventional OR concept of [65, 199] to OFDM based systems at the OFDM-symbol level fails to exploit the different channel conditions of the different subcarriers or of the different relays. More advanced techniques such as adaptive subcarrier allocation are required [74, 175, 191]. However, since relay-assisted OFDM transmissions are subjected to two-hop fading channels, dynamically rearranging the subcarriers at multiple relays may offer some additional diversity gains by appropriately pairing the subcarriers of the two hops. This subcarrier pairing philosophy was employed in [73, 75–78] for relay-assisted *amplify-and-forward* (AF) as well as *decode-and-forward* (DF) *single-user* OFDM systems. This approach may also be applied in multi-user scenarios, such as in OFDMA, where the subcarriers of the two hops may be paired on a per-user basis [79], hence also minimising the *multi-user interference* (MUI). The corresponding resource allocation and multi-user scheduling may be carried out on a subband-group basis per user in the *frequency-domain*(FD). As a further advance, multiple relay selection schemes were investigated in [41, 206–209] in a single-user scenario. Selecting multiple relays may be capable of increasing the achievable cooperative/spatial diversity gain, but as a result, the potential selection diversity gain will be decreased, when the total number of opportunistic relays is the same. Furthermore, the interference among the multiple activated relays should be mitigated, which imposes further complexity on the transceivers. Therefore, carefully assigning the subbands/subcarriers in the context of OR is capable of improving the diversity gain by avoiding the extra multi-relay interference, while retaining the MUI-free nature of SC-FDMA and OFDMA systems.

In Chapter 4, we proposed relay selection schemes for the energy-efficient *opportunistic cooperative* (OC) SC-FDMA uplink, but no CSI-controlled subband allocation was considered. Although both *dynamic relay selection* (DRS) [67, 199] and *dynamic subband/subcarrier allocation* (DSA) techniques [71, 204, 205] are capable of providing a power gain, conventional DSA aided OR may be incapable of exploiting both. The main reason for this limitation is that the two hops of the relay channel limit the capacity to that of the lower-capacity link of the two hops. In the context of OR assisted SC-FDMA systems, both the AF relay and the DF relay limit the attainable multi-user performance, depending on the quality of the first-hop. The consideration of the received signal at multiple relays is capable of further improving the performance of *dynamic resource allocation* (DRA) [58] aided OR systems. As a further advantage of channel coded OR, the length of the interleavers combined with

forward error correction (FEC), such as *bit-interleaved coded modulation* (BICM) [92] introduced in Section 2.3, may be shortened, since the effects of fading are further randomised by OR. As a benefit, the delay of the entire FEC-coded DF-relaying aided system is reduced. To the best of our knowledge, these issues were not considered in the open literature.

In Section 5.3, we propose two DRA strategies designed for the OR SC-FDMA uplink, where the ORs may invoke either the AF or the soft-decision aid DF protocols [49, 210]. We assume that the multiple relays are capable of exchanging the pilot-based *channel quality information* (CQI) of all the users, facilitating cooperation at the relays in order to carry out joint DRA (JDRA). The original multi-user information exchange scheme operating with the aid of a single relay was referred to as *multi-way relaying* (MWR) [2] in [211]. We assume that multiple relays participate in the MWR procedure for the sake

- *In contrast to the solutions mentioned above, our focus is mainly on the energy-efficiency of the DRA aided OR assisted SC-FDMA system, where the energy-efficiency is quantified in terms of the* ***energy consumption gain*** *(ECG)*[3] *as introduced in Chapter 4. Additionally, we evaluated the impact of the channel estimation overhead and that of the MWR-aided CQI exchange overhead on the energy-efficiency.*

- *Furthermore, we dedicate special attention to two main aspects, namely to the '****first-hop quality awareness****'(FHQA) of our DRA schemes and to the '****buffering delay awareness****' of our interleaver-aided channel coded systems.*

    1. *Specifically, we exploit any potential extra selection diversity for the sake of reducing the transmit power required and/or for improving the attainable system performance. To this end, we combine DRS and DSA based on the associated first-hop transmission qualities. Furthermore, two different types of FHQA based JDRA algorithms are investigated, depending on whether the S-R or the R-D channel quality dominates the attainable performance, when the system invokes either single or multiple antennas at the BS receiver.*
    2. *Moreover, we quantify the benefits of OR combined with DSA in the context of interleaver-aided DF relaying for transmission over correlated fading channels, in terms of reducing the interleaving delay and/or the total transmit power with the aid of joint OR and DSA.*

[2] This terminology is reminiscent of the process used in [211] for describing the data-exchange that takes place amongst multiple data-source and destinations, but again, we only assume the employment of MWR for CQI exchange.

[3] As the metric of comparing two different systems, the ECG is simply defined in [1] as the ratio of **energy consumption per bit** by a reference system divided by that of a proposed system under test, where the absolute measure of **energy consumption per bit** is defined as the peak power divided by the maximum throughput.

- *Our investigations involve two advanced frequency-domain equalisation (FDE) schemes, namely one designed for uncoded and one for channel coded SC-FDMA systems. More explicitly:*

  1. *One of them is the* ***minimum mean-square error*** *(MMSE) criterion based* ***frequency-domain decision-feedback equaliser*** *(FD-DFE) relying on the principles of* ***successive interference cancellation*** *(SIC) [86, 87].*
  2. *The other one is the MMSE based turbo* ***frequency-domain linear equaliser*** *(FD-LE) in the principle of turbo equalisation proposed in [88–90] combined with BICM using* ***iterative decoding****(ID) [92, 152] introduced in Section 2.3.2. Additionally, the performance benefits of both single- and multi-antenna aided BS receivers have been considered.*

This chapter is organised as follows. In Section 5.2, we will first outline the system model of the OR assisted SC-FDMA uplink. In Sections 5.3 and 5.2.4, we investigate the resource allocation schemes invoked and outline the signal detection procedures employed at the multi-antenna aided BS receiver, respectively. The attainable performance of our proposed schemes is quantified by the simulation results of Section 5.4. Finally, we conclude in Section 5.5.

5.2 Opportunistic Relaying for SC-FDMA System Model

5.2.1 Scope and Assumptions

Figure 5.1 illustrates the topology of the *opportunistic relaying* (OR) for SC-FDMA system considered, which supports the K uplink users of the set $\mathcal{K}$ referred to as the source MTs of a traffic cell. The idle terminals located in each other's vicinity are members of the set $\mathcal{J}$, which may act as a cluster of relays. We assume that these relays of a cluster are located midway between the source MT and the destination BS, hence they are assumed to experience an identical path-loss of $G_{\rm SR} = G_{\rm RD} = 0.5^{-4}$. On one hand, each source MT, such as the k-th user's, is dynamically assigned to an appropriately selected single relay, say $\check{j}_k$, i.e. we have

$$\bigcap_{k\in\mathcal{K}} \check{\mathcal{J}}_k = \varnothing, \quad \forall \check{j}_k \in \check{\mathcal{J}}_k, \tag{5.1}$$

where $\check{\mathcal{J}}_k$ represents the best relay set of user k. On the other hand, each relay is capable of forwarding up to K users' signals at a time, so that the j-th relay may serve the specific users hosted by the paired set $\mathcal{K}_j$. We note that no relays are involved in the data transmission process, when the set of eligible relays is empty, i.e. we have $\mathcal{K}_j = \varnothing$. Therefore, we define

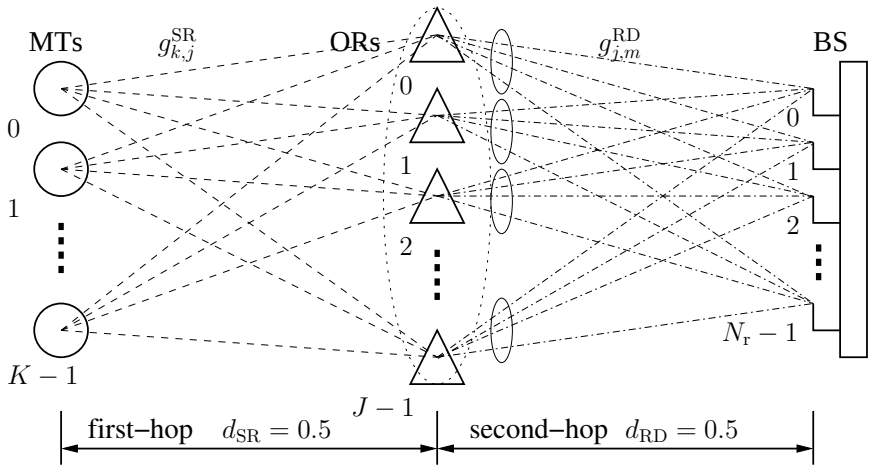

FIGURE 5.1: The topology of opportunistic relayed multi-user SC-FDMA uplink. This is a generalised case of the relay selection schemes of Figure 4.5. Compared to Figure 4.5, the basic differences rely on that (1) the direct link is unavailable; (2) cooperating relays geographically localised in a cluster are capable of exchanging CSI; (3) the BS's receiver employs multiple antennas. The corresponding transceiver schematics are portrayed in Figures 5.2 for source MT's transmitter, Figure 3.3(b) for AF relay, Figure 5.4 for DF relay and BS, as well as Figure 5.5(a) for BS receiver in uncoded system.

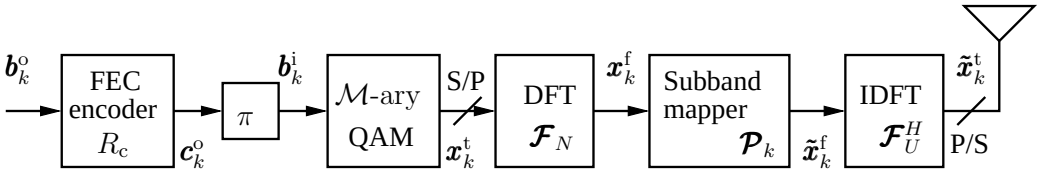

FIGURE 5.2: Transmitter schematic of the source MT relying on a BICM aided SC-FDMA. The corresponding frame structure of BICM aided SC-FDMA transmission was portrayed in Figure 2.14. The principle of uncoded SC-FDMA was introduced in Section 2.2.2 and the BICM principle was detailed in Section 2.3. The corresponding TD/FD signal plots are seen Figure 2.10(a) and Figure 2.11(a). The corresponding transceiver schematic of the subband-based AF relay was portrayed in Figure 3.3(b), while the receiver schematic of the DF relay and the BS of BICM aided SC-FDMA will be characterised in Figure 5.4.

all the selected relays in the set $\check{\mathcal{J}}$, $(\forall \check{j} \in \check{\mathcal{J}})$, according to

$$\begin{aligned} \check{\mathcal{J}} &= \bigcup_{k\in\mathcal{K}} \check{\mathcal{J}}_k, \quad \check{\mathcal{J}} \subseteq \mathcal{J}, \\ \text{s.t.} &: \mathcal{K}_j \neq \varnothing. \end{aligned} \tag{5.2}$$

5.2.2 Source MT's Transmitter Model

5.2.2.1 Transmitted Signals of Source MT

The channel coded SC-FDMA transmitter adopted the *bit-interleaved coded modulation* (BICM) [92, 152] structure of Figure 5.2 introduced in Section 2.3.1. Specifically, at the k-th source MT, the N_{b}-length binary source data stream $\boldsymbol{b}_k^{\mathrm{o}}$ is initially encoded by an

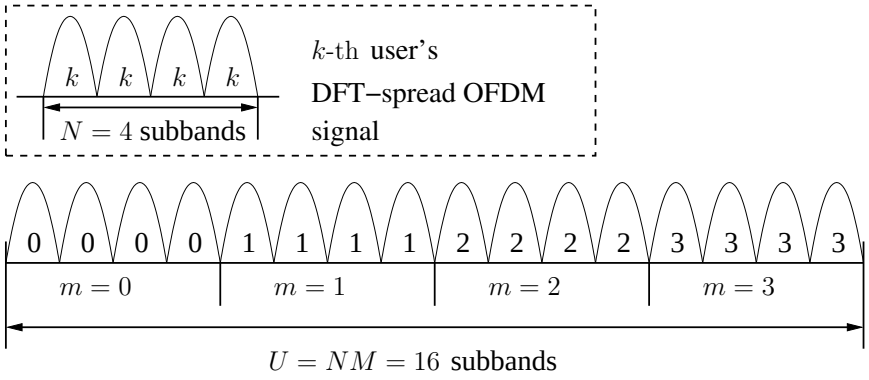

FIGURE 5.3: An example to illustrate bandwidth expansion and localised subband mapping schemes in the SC-FDMA system using total $U = 16$ subbands for $N = 4$ subbands per user. The system can support $K \leq M = 4$ users. We originally introduced this figure in Section 2.2.2.

outer channel code, such as a *recursive systematic convolutional* (RSC) code or a turbo code, having a coding rate of $R_{\rm c}$. Then the outer encoded bit stream $\boldsymbol{c}_k^{\rm o}$ of Figure 5.2 is interleaved by a $N_{\rm c}$-length random bit-wise interleaver $\pi_{\rm S}$ and its output bit stream $\boldsymbol{b}_k^{\rm i} = [(\boldsymbol{b}_{k,0}^{\rm i})^T, (\boldsymbol{b}_{k,1}^{\rm i})^T, \cdots, (\boldsymbol{b}_{k,(N_{\rm s}-1)}^{\rm i})^T]^T$ is fed into the $\mathcal{M}$-ary *quadrature amplitude modulation* (QAM) mapper transmitting Q bits per symbol, where we have $N_{\rm s} = N_{\rm c}/Q$ and $\mathcal{M} = 2^Q$. Hence we partition the $N_{\rm c}$-length bit sequence $\boldsymbol{b}_k^{\rm i}$ of Figure 5.2 into $N_{\rm s}$ segments $\boldsymbol{b}_{k,n_{\rm s}}^{\rm i}$, each having a length of Q for $n_{\rm s} = 0, 1, \cdots, N_{\rm s} - 1$. Moreover, the $N_{\rm s}$-length modulated symbol sequence of Figure 5.2 is then converted to $N_{\rm v}$ *symbol vectors* $\boldsymbol{x}_k^{\rm S,t}[n_{\rm v}]$, $(\forall n_{\rm v} = 0, 1, \cdots, N_{\rm v} - 1)$, in which each vector $\boldsymbol{x}_k^{\rm S,t}$ is constituted by a SC-FDMA symbol, which contains N consecutive modulated symbol elements $x_{k,n}^{\rm S,t}$ in the *time-domain*(TD), $(n = 0, 1, \cdots, N - 1)$.

Furthermore, in the so-called *discrete Fourier transform* (DFT)-spread OFDMA transmitter of Figure 5.2, the symbol vector is transformed by an N-point DFT from the TD to the FD, yielding $\boldsymbol{x}_k^{\rm S,f} = \boldsymbol{\mathcal{F}}_N \boldsymbol{x}_k^{\rm S,t}$, where the normalised N-point DFT matrix $\boldsymbol{\mathcal{F}}_N$ acts similarly to a Walsh-Hadamad spreading matrix often employed in *code-division multiple-access* (CDMA) systems [102,212]. As shown in Figure 5.3, the k-th user's resultant symbols are then mapped to the most appropriate N subbands selected from the entire set of $U = (M \times N)$ subbands with the aid of the matrix $\boldsymbol{\mathcal{P}}_k^{\rm S}$ at the source MT. We referred to this operation as subband mapping in Section 2.2.2, which will be further detailed in Section 5.2.2.2. Hence, the SC-FDMA symbol originally hosted by N subbands is expanded by a factor of M, hence we refer to M as the bandwidth expansion factor. Additionally, the resultant U-element FD symbol vector is transformed to the TD by the U-point *inverse discrete Fourier transform* (IDFT) operation, which is similar to the action of the OFDM transmitter of Figure 2.1(a) discussed in Section 2.1.1. The corresponding TD/FD signal plots are seen Figure 2.10(a) and Figure 2.11(a). Hence, the U-symbol baseband-equivalent discrete-time signal $\boldsymbol{s}_k^{\rm S,t}$ transmitted by

the k-th source MT before inserting the *cyclic-prefix* (CP) may be expressed as Eq. (4.1)

$$\boldsymbol{s}_k^{\mathrm{S,t}} = \sqrt{P_k^{\mathrm{S}}}\boldsymbol{\mathcal{F}}_U^H \boldsymbol{\mathcal{P}}_k^{\mathrm{S}} \boldsymbol{\mathcal{F}}_N \boldsymbol{x}_k^{\mathrm{S,t}}, \tag{5.3}$$

where the superscript $^{\mathrm{t}}$ refers to the TD signal. We assume that the source and relay share the normalised transmit power of unity equally, i.e. we have $P_k^{\mathrm{S}} = P_{k_j^{\sim}}^{\mathrm{R}} = 0.5$, while $\boldsymbol{\mathcal{F}}_U^H$ denotes the normalised U-point IDFT matrix defined in Section 2.1.1.

5.2.2.2 Localised Subband Mapping Invoking Subband Allocation

In the context of the SC-FDMA system of Figure 5.1, the subband mapping regime guarantees that the maximum number of orthogonal users that may be supported for transmissions in a single time slot is equal to the bandwidth expansion factor, i.e. we have $K \leqslant M$. For instance, the multi-user system operates at its full-load, when we have $K = M$. Furthermore, the so-called *localised subband mapping* mode, which was detailed in Section 2.2.2, allows each user's SC-FDMA symbols to be mapped to N consecutive subbands in the entire set of U subbands, as detailed below. When the CSI of each user's signal is available at the transmitter (CSIT), the DSA allows the localised group of subbands portrayed in Figure 5.3 to be allocated dynamically on a group-by-group basis, depending on the CQI of different users.

To elaborate a little further, the subband allocation philosophy of our system is based on the localised subband mapping portrayed in Figure 5.3 and defined as

$$\begin{aligned} \mathcal{P}_{u,n}^{(k,m)} &= \begin{cases} 1, & \text{if } u = mN + n \\ 0, & \text{otherwise} \end{cases} \\ m &= 0, 1, \cdots, M-1, \\ n &= 0, 1, \cdots, N-1, \\ u &= 0, 1, \cdots, U-1, \end{aligned} \tag{5.4}$$

where $\mathcal{P}_{u,n}^{(k,m)}$ is the (u,n)-th entry of $\boldsymbol{\mathcal{P}}_k^{\mathrm{S}}$ and $m \in \mathcal{M}$ refers to the index of the individual spectral blocks seen in Figure 5.3. Each block consists of N consecutive subbands in the so-called subband group defined for resource allocation. Additionally, we define the *static subband allocation* (SSA) regime as having $m = k$ in Eq. (5.4), which results in the localised FDMA (LFDMA) signalling seen in Figure 5.3 adopted in both our source MT's transmitter and in the relay's receiver. Furthermore, $m \neq k$ refers to the DSA supported by our relay's transmitter and the BS's receiver. We will detail the DSA in Section 5.3.

5.2.3 Relay Models

5.2.3.1 Signal Reception at the Relay

Again, there are J candidates for potential opportunistic participation in relaying and all of them are capable of listening to all the K source MTs. After the conventional CP removal, the TD signal received at the j-th relay may be expressed as

$$\boldsymbol{r}_j^{\mathrm{R,t}} = \sqrt{G_{\mathrm{SR}}} \sum_{k \in \mathcal{K}} \tilde{\boldsymbol{H}}_{k,j}^{\mathrm{SR,t}} \boldsymbol{s}_k^{\mathrm{S,t}} + \tilde{\boldsymbol{n}}_j^{\mathrm{R,t}}, \tag{5.5}$$

where $\tilde{\boldsymbol{H}}_{k,j}^{\mathrm{SR,t}}$ hosts the $(U \times U)$-element TD channel coefficient matrix of the S-R links from the k-th source MT to the j-th relay, while $\tilde{\boldsymbol{n}}_j^{\mathrm{R,t}}$ represents the U-element complex-valued *additive white Gaussian noise* (AWGN) vectors having a zero mean and a variance of σ_N^2 as regards to each element, i.e. we have $\mathcal{CN}(0, \sigma_N^2)$ at the j-th relay.

The k-th user's signals $\boldsymbol{r}_j^{\mathrm{R,t}}$ received by the j-th relay are firstly transformed to the FD by the U-point DFT operation and then demapped to the appropriate N subbands with the aid of the matrix $(\boldsymbol{\mathcal{P}}_k^{\mathrm{S}})^T$ defined in Eq. (5.4), yielding its equivalent FD representation in the form of

$$\boldsymbol{y}_{k_j}^{\mathrm{R,f}} = (\boldsymbol{\mathcal{P}}_k^{\mathrm{S}})^T \boldsymbol{\mathcal{F}}_U \boldsymbol{r}_j^{\mathrm{R,t}} = \sqrt{G_{\mathrm{SR}}} \boldsymbol{H}_{k,j}^{\mathrm{SR,f}} \boldsymbol{x}_{k,j}^{\mathrm{S,f}} + (\boldsymbol{\mathcal{P}}_k^{\mathrm{S}})^T \boldsymbol{\mathcal{F}}_U \tilde{\boldsymbol{n}}_j^{\mathrm{R,t}}, \tag{5.6}$$

where $\boldsymbol{H}_{k,j}^{\mathrm{SR,f}}$ is the $(N \times N)$-element equivalent FD channel coefficient matrix after subband demapping, which is given by

$$\boldsymbol{H}_{k,j}^{\mathrm{SR,f}} = (\boldsymbol{\mathcal{P}}_k^{\mathrm{S}})^T \boldsymbol{\mathcal{F}}_U \tilde{\boldsymbol{H}}_{k,j}^{\mathrm{SR,t}} \boldsymbol{\mathcal{F}}_U^H \boldsymbol{\mathcal{P}}_k^{\mathrm{S}} = \mathrm{diag}[h_{k,j,0}^{\mathrm{SR,f}}, h_{k,j,1}^{\mathrm{SR,f}}, \cdots, h_{k,j,(N-1)}^{\mathrm{SR,f}}]. \tag{5.7}$$

5.2.3.2 Transmitted Signal of the Relays

Let us now consider the transmitted signals of the relays. We assume that the transmitter of the SC-FDMA relay is identical to that of the source MT. Before inserting the CP at the j-th relay of the set $\mathcal{J}$, the U-element TD transmitted signal $\boldsymbol{s}_j^{\mathrm{R,t}}$ containing the $k_{\check{j}} \in \mathcal{K}_{\check{j}}$ source users' data may be expressed as

$$\boldsymbol{s}_j^{\mathrm{R,t}} = \sum_{k \in \mathcal{K}} \rho_{k,j} \boldsymbol{s}_{k,j}^{\mathrm{R,t}} = \sum_{k_{\check{j}} \in \mathcal{K}_{\check{j}}} \boldsymbol{s}_{k_{\check{j}}}^{\mathrm{R,t}}, \tag{5.8}$$

where $\rho_{k,j}$ is the S-R pairing factor of the k-th source and the j-th relay defined as follows

$$\rho_{k,j} = \begin{cases} 1, & \text{if } k = k_j, j = \check{j}, \\ 0, & \text{otherwise.} \end{cases} \tag{5.9}$$

Observe in Eq. (5.8) and Eq. (5.9) that from the set of J relays, only the relays $\check{j}$ selected for the set $\check{\mathcal{J}}$ are activated to forward the source data of user $k_{\check{j}}$ in the set $\mathcal{K}_{\check{j}}$, while the remaining candidate relays are not allowed to transmit.

Additionally, the technique of generating the signal transmitted from the relays depends on the specific choice of relaying protocols in operation, i.e. whether we use AF or hard-/soft-DF relaying. We shall discuss the various protocols in the following sections.

5.2.3.3 Amplify-and-Forward Protocol

According to Section 3.3.2, when the relay employs the subband-based AF protocol of Figure 3.3(b), the FD signal $\boldsymbol{y}_{k_j}^{\mathrm{R,f}}$ may be amplified on a subband-by-subband basis. More specifically, the n-th entry of the $(N \times N)$-element diagonal matrix $\boldsymbol{\beta}_k^{\mathrm{f}}$ refers to a specific gain factor, which is given by

$$\beta_{k,n}^{\mathrm{f}} = \sqrt{1/\left(P_k^{\mathrm{S}} G_{\mathrm{SR}} |h_{k,n}^{\mathrm{SR,f}}|^2 + \sigma_{\mathrm{N}}^2\right)}. \tag{5.10}$$

Since only the $k_{\check{j}}$-th source user's signal can be forwarded, here we present the resultant TD signal transmitted on the $\check{j}$-th relay, which is formulated as

$$\boldsymbol{s}_{k_{\check{j}}}^{\mathrm{R,t}} = \sqrt{P_{k_{\check{j}}}^{\mathrm{R}} G_{\mathrm{SR}}} \boldsymbol{\mathcal{F}}_U^H \boldsymbol{\mathcal{P}}_{k_{\check{j}}}^{\mathrm{R}} \boldsymbol{\beta}_{k_{\check{j}}} \boldsymbol{H}_{k,\check{j}}^{\mathrm{SR,f}} \boldsymbol{x}_{k_{\check{j}}}^{\mathrm{S,f}} + \bar{\boldsymbol{n}}_{k_{\check{j}}}^{\mathrm{R,t}}, \tag{5.11}$$

where $\bar{\boldsymbol{n}}_{k_{\check{j}}}^{\mathrm{S,t}}$ denotes the noise contribution imposed on the $k_{\check{j}}$-th user's signal at the relay, which is expressed as $\bar{\boldsymbol{n}}_{k_{\check{j}}}^{\mathrm{S,t}} = \boldsymbol{\mathcal{F}}_U^H \boldsymbol{\mathcal{P}}_{k_{\check{j}}}^{\mathrm{R}} \boldsymbol{\beta}_{k_{\check{j}}} (\boldsymbol{\mathcal{P}}_{k_{\check{j}}}^{\mathrm{S}})^T \boldsymbol{\mathcal{F}}_U \tilde{\boldsymbol{n}}_{\check{j}}^{\mathrm{R,t}}$. Furthermore, $\boldsymbol{\mathcal{P}}_{k_{\check{j}}}^{\mathrm{R}}$ refers to the $k_{\check{j}}$-th user's subband mapping matrix at the $\check{j}$-th relay according to the specific subband allocation strategy, which will be presented in Section 5.3.

5.2.3.4 Decode-and-Forward Protocol

The receiver of the DF relay invokes the MMSE based turbo FD-LE of Figure 5.4(a) in the principle of turbo equalisation algorithm in [88–90]. As shown in Figure 5.4(a), the k_j-th user's first-hop FD received signal vectors $\boldsymbol{y}_{k_j}^{\mathrm{R,f}}[n_{\mathrm{s}}]$ at the j-th relay, for $(n_{\mathrm{v}} = 0, 1, \cdots, N_{\mathrm{v}} - 1)$ and $(N_{\mathrm{v}} = N_{\mathrm{s}}/N)$, are equalised by the *a-posteriori* probability based MMSE FD-LE combined with the symbol-to-bits demapper. All signals are represented in terms of their *logarithmic-likelihood-ratio* (LLR), as seen in the iterative structure of Figure 5.4(c), which is based on the BICM concept using *iterative decoding* (ID), which was detailed in Section 2.3.2.

***Hard*-Decisions:** In order to recover the original bit sequence at the relay, during the last

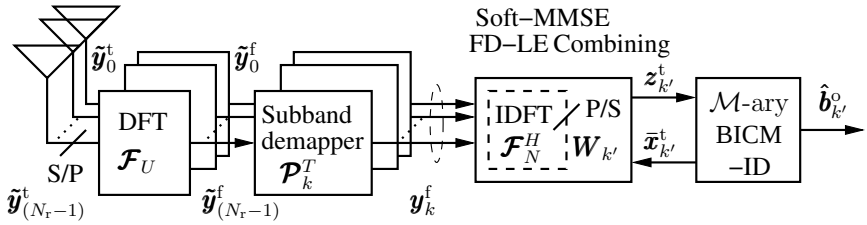

(a) Turbo FD-LE for SC-FDMA.

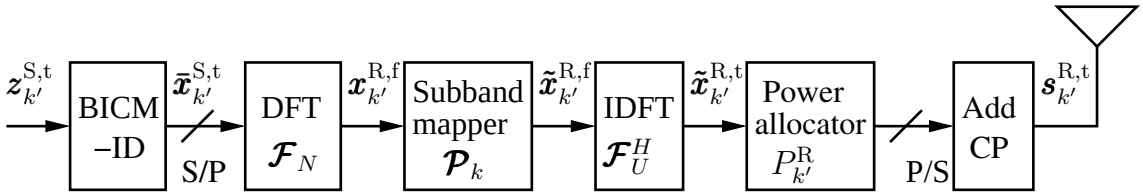

(b) Soft-DF transceiver for SC-FDMA.

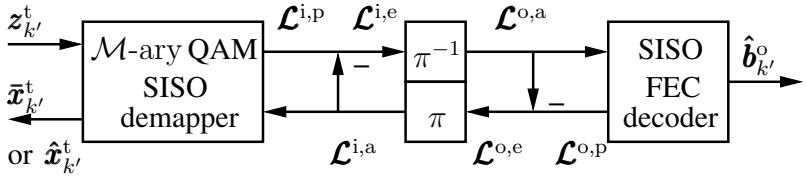

(c) The $\mathcal{M}$-ary BICM-ID decoder block of Figure 5.4(a) using iterative decoding (ID).

FIGURE 5.4: The identical turbo receiver schematics of the DF relay and of the BS relying on BICM-aided SC-FDMA, where the DF relay's receiver employs single antenna, while the BS's receiver may employ multiple antennas as seen in Figure 5.4(a). This schematic of Figure 5.4(c) was repeated from Figure 2.15 for convenience. The corresponding TD/FD plots were shown in Figures 2.10(a) and 2.11(a). Particularly, the schematic of soft-DF relay's transceiver is portrayed in Figure 5.4(b) invoking the soft symbol input from the BICM-ID of Figure 5.4(c).

iteration we make a *hard*-decision as to the original source bits. This process only requires the *extrinsic* LLRs $\boldsymbol{\mathcal{L}}^{\mathrm{o,e}}(\boldsymbol{b}^{\mathrm{o}}_{k_{\tilde{j}}})$ related to the source bit stream $\boldsymbol{b}^{\mathrm{o}}_{k_{\tilde{j}}}$ at the output of the channel decoder, but not those of the parity bits. Hence we generate the hard-decision vector $\hat{\boldsymbol{b}}^{\mathrm{R}}_{k_{\tilde{j}}}$, whose ι-th element may be expressed as

$$\hat{b}^{\mathrm{R}}_{k_{\tilde{j}},\iota} = 0.5 \left| \mathrm{round} \left\{ \mathrm{sgn}[-\mathcal{L}^{\mathrm{o,e}}(b^{\mathrm{o}}_{k_{\tilde{j}},\iota}) + 0.5] \right\} \right|, \tag{5.12}$$

where we have $\iota = 0, 1, \cdots, (N_{\mathrm{b}} - 1)$. Before regenerating the SC-FDMA symbol at the relay's transmitter, the bit sequence $\hat{b}^{\mathrm{R}}_{k_{\tilde{j}},\iota}$ is encoded and passed to the channel interleaver π_{R} in order to form the inner-encoded bit stream for modulation, as seen in Fig 5.4(c).

***Soft*-Decisions:** By contrast, in order to reduce the detrimental effects of error propagation, *soft*-decisions may be invoked [49,210], as shown in Figure 5.4(b). Specifically, instead of using *extrinsic* LLRs $\boldsymbol{\mathcal{L}}^{\mathrm{o,e}}(\boldsymbol{b}^{\mathrm{o}}_{k_{\tilde{j}}})$, the *extrinsic* LLRs related to the encoded bit stream $\boldsymbol{c}^{\mathrm{o}}_{k_{\tilde{j}}}$ of Figure 5.2 may be used as the relevant soft-decision variables. Following the appropriate

reordering of the bits in the sequence by the soft-bit interleaver π_{R} of Fig 5.4(c), the resultant LLRs $\boldsymbol{\mathcal{L}}^{\mathrm{o,e}}(\boldsymbol{c}^{\mathrm{o}}_{k_{\check{j}}})$ become the *a-priori* information $\boldsymbol{\mathcal{L}}^{\mathrm{i,a}}(\boldsymbol{b}^{\mathrm{i}}_{k_{\check{j}}})$ of Fig 5.4(c), which allows us to calculate the bit probability $P(b_{k_{\check{j}},n_{\mathrm{s}},q} = \mathsf{b}_{i,q})$, for $q = 0, 1, \cdots, Q-1$. Then we further derive the probability of the transmitted symbols of the $k_{\check{j}}$-th source MT, which are given by [88]

$$P(x^{\mathrm{S,t}}_{k_{\check{j}},n_{\mathrm{s}}} = \mathsf{s}_i) = \prod_{q=0}^{Q-1} \frac{1}{2} \left(1 + \mathring{\mathsf{b}}_{i,q} \tanh \frac{\mathcal{L}^{\mathrm{i,a}}_{k_{\check{j}},(n_{\mathrm{s}}Q+q)}}{2} \right), \tag{5.13}$$

where we have $n_{\mathrm{s}} = n_{\mathrm{v}}N + n$ for $n_{\mathrm{s}} = 0, 1, \cdots, (N_{\mathrm{s}} - 1)$, $n = 0, 1, \cdots, (N-1)$ and $q = 0, 1, \cdots, (Q-1)$. Additionally, the symbols of the k-th user forwarded by the $\check{j}$-th DF relay may be defined by the corresponding soft-decision aided complex symbol $\bar{x}^{\mathrm{S,t}}_{k_{\check{j}},n_{\mathrm{s}}}$, which can be expressed in terms of the expected value of the transmitted symbol $x^{\mathrm{S,t}}_{k_{\check{j}},n_{\mathrm{s}}}$ as

$$x^{\mathrm{R,t}}_{k_{\check{j}},n_{\mathrm{s}}} = \bar{x}^{\mathrm{S,t}}_{k_{\check{j}},n_{\mathrm{s}}} = \mathrm{E}[x^{\mathrm{S,t}}_{k_{\check{j}},n_{\mathrm{s}}}] = \sum_{\mathsf{s}_i \in \mathbb{S}} \mathsf{s}_i \cdot P(x^{\mathrm{S,t}}_{k_{\check{j}},n_{\mathrm{s}}} = \mathsf{s}_i). \tag{5.14}$$

Finally, the n_{v}-th N-element DF symbol vector $\boldsymbol{x}^{\mathrm{R,t}}_{k_{\check{j}}}[n_{\mathrm{v}}] = [x^{\mathrm{R,t}}_{k_{\check{j}},1}, x^{\mathrm{R,t}}_{k_{\check{j}},1}, \cdots, x^{\mathrm{R,t}}_{k_{\check{j}},(N-1)}]^T$ is used for generating the k-th user's U-element transmitted DFT-spread OFDMA symbol $\boldsymbol{s}^{\mathrm{R,t}}_{k_{\check{j}}}$ at the $\check{j}$-th relay, before attaching the CP, yielding

$$\boldsymbol{s}^{\mathrm{R,t}}_{k_{\check{j}}} = \sqrt{P^{\mathrm{R}}_{k_{\check{j}}}} \boldsymbol{\mathcal{F}}^H_U \boldsymbol{\mathcal{P}}^{\mathrm{R}}_{k_{\check{j}}} \boldsymbol{\mathcal{F}}_N \boldsymbol{x}^{\mathrm{R,t}}_{k_{\check{j}}}, \tag{5.15}$$

where the subband allocation process of the corresponding S-R pair is carried out by the matrix $\boldsymbol{\mathcal{P}}^{\mathrm{R}}_{k_{\check{j}}}$.

5.2.4 Signal Representation at the Multi-Antenna Aided BS Receiver

Since we assume that the BS's receiver seen in Figure 5.4(a) or Figure 5.5(a) invokes N_{r} antennas, the U-element TD signal vector holding the K user's data received at the n_{r}-th BS antenna from the selected relays in the set $\check{\mathcal{J}}$ may be expressed as:

$$\begin{aligned} \tilde{\boldsymbol{y}}^{\mathrm{D,t}}_{n_{\mathrm{r}}} &= \sum_{\check{j} \in \check{\mathcal{J}}} \sqrt{G_{\mathrm{RD}}} \tilde{\boldsymbol{H}}^{\mathrm{RD,t}}_{\check{j},n_{\mathrm{r}}} \boldsymbol{s}^{\mathrm{R,t}}_{\check{j}} + \tilde{\boldsymbol{n}}^{\mathrm{D,t}}_{n_{\mathrm{r}}} \\ &= \sum_{\check{j} \in \check{\mathcal{J}}} \sqrt{G_{\mathrm{RD}}} \tilde{\boldsymbol{H}}^{\mathrm{RD,t}}_{\check{j},n_{\mathrm{r}}} \sum_{k_{\check{j}} \in \mathcal{K}_{\check{j}}} \boldsymbol{s}^{\mathrm{R,t}}_{k_{\check{j}}} + \tilde{\boldsymbol{n}}^{\mathrm{D,t}}_{n_{\mathrm{r}}}, \end{aligned} \tag{5.16}$$

where the $\tilde{\boldsymbol{H}}^{\mathrm{RD,t}}_{\check{j},n_{\mathrm{r}}}$ denotes the $(U \times U)$-element TD circulant channel coefficient matrix between relay $\check{j}$ and the n_{r}-th antenna. Next, the U-point FFT carried out at each antenna of Figure 5.4(a) or Figure 5.5(a) transforms the TD signal $\tilde{\boldsymbol{y}}^{\mathrm{D,t}}_{n_{\mathrm{r}}}$ into the FD, where the signal of user $k_{\check{j}}$ is then demapped into the appropriate subband group according to the subband

allocation matrix by $\boldsymbol{\mathcal{P}}^{\mathrm{R}}_{k^{\check{}}_{\check{j}}}$ at the relay, where we have

$$\begin{aligned}\boldsymbol{y}^{\mathrm{D,f}}_{n_{\mathrm{r}},k^{\check{}}_{\check{j}}} &= (\boldsymbol{\mathcal{P}}^{\mathrm{R}}_{k^{\check{}}_{\check{j}}})^T \boldsymbol{\mathcal{F}}_U \tilde{\boldsymbol{y}}^{\mathrm{D,t}}_{n_{\mathrm{r}}} \\ &= (\boldsymbol{\mathcal{P}}^{\mathrm{R}}_{k^{\check{}}_{\check{j}}})^T \boldsymbol{\mathcal{F}}_U (\sqrt{G_{\mathrm{RD}}} \tilde{\boldsymbol{H}}^{\mathrm{RD,t}}_{\check{j},n_{\mathrm{r}}} \boldsymbol{s}^{\mathrm{R,t}}_{k^{\check{}}_{\check{j}}} + \tilde{\boldsymbol{n}}^{\mathrm{D,t}}_{n_{\mathrm{r}},k^{\check{}}_{\check{j}}}).\end{aligned} \tag{5.17}$$

5.2.4.1 AF Signal Received at the BS

Specifically, for the AF scenario of Figure 3.3(b), both the two hop's channel knowledge is available at the BS's receiver, when aiming for detecting the original signal transmitted by the source MTs. Hence, the received signal of user $k^{\check{}}_{\check{k}}$ at the n_{r}-th antenna of Figure 5.4(a) or Figure 5.5(a) may be formulated as

$$\begin{aligned}\boldsymbol{y}^{\mathrm{D,f}}_{n_{\mathrm{r}},k^{\check{}}_{\check{j}}} &= \sqrt{P^{\mathrm{R}}_{k^{\check{}}_{\check{j}}} G_{\mathrm{RD}} G_{\mathrm{SR}}} \boldsymbol{H}^{\mathrm{RD,f}}_{k^{\check{}}_{\check{j}},n_{\mathrm{r}}} \boldsymbol{\beta}_{k^{\check{}}_{\check{j}}} \boldsymbol{H}^{\mathrm{SR,f}}_{k,\check{j}} \boldsymbol{\mathcal{F}}_N \boldsymbol{x}^{\mathrm{S,t}}_{k^{\check{}}_{\check{j}}} \\ &\quad + \sqrt{G_{\mathrm{RD}}} (\boldsymbol{\mathcal{P}}^{\mathrm{R}}_{k^{\check{}}_{\check{j}}})^T \boldsymbol{\mathcal{F}}_U \tilde{\boldsymbol{H}}^{\mathrm{RD,t}}_{\check{j},n_{\mathrm{r}}} \bar{\boldsymbol{n}}^{\mathrm{R,t}}_{k^{\check{}}_{\check{j}}} + (\boldsymbol{\mathcal{P}}^{\mathrm{R}}_{k^{\check{}}_{\check{j}}})^T \boldsymbol{\mathcal{F}}_U \tilde{\boldsymbol{n}}^{\mathrm{D,t}}_{n_{\mathrm{r}},k^{\check{}}_{\check{j}}} \\ &= \sqrt{P^{\mathrm{R}}_{k^{\check{}}_{\check{j}}}} \boldsymbol{H}^{\mathrm{AF,f}}_{k^{\check{}}_{\check{j}},n_{\mathrm{r}}} \boldsymbol{\mathcal{F}}_N \boldsymbol{x}^{\mathrm{S,t}}_{k} + \boldsymbol{n}^{\text{AF-D,f}}_{n_{\mathrm{r}},k^{\check{}}_{\check{j}}},\end{aligned} \tag{5.18a}$$

where $\boldsymbol{H}^{\mathrm{RD,f}}_{k^{\check{}}_{\check{j}},n_{\mathrm{r}}} = (\boldsymbol{\mathcal{P}}^{\mathrm{R}}_{k^{\check{}}_{\check{j}}})^T \boldsymbol{\mathcal{F}}_U \tilde{\boldsymbol{H}}^{\mathrm{RD,t}}_{\check{j},n_{\mathrm{r}}} \boldsymbol{\mathcal{F}}^H_U \boldsymbol{\mathcal{P}}^{\mathrm{R}}_{k^{\check{}}_{\check{j}}}$ represents the equivalent FD R-D channel coefficient matrix. Furthermore, we express the equivalent FD two-hop channel matrix related to the n_{r}-th antenna as $\boldsymbol{H}^{\mathrm{AF,f}}_{k^{\check{}}_{\check{j}},n_{\mathrm{r}}} = \sqrt{G_{\mathrm{RD}} G_{\mathrm{SR}}} \boldsymbol{H}^{\mathrm{RD,f}}_{k^{\check{}}_{\check{j}},n_{\mathrm{r}}} \boldsymbol{\beta}_{k^{\check{}}_{\check{j}}} \boldsymbol{H}^{\mathrm{SR,f}}_{k,\check{j}}$. Additionally, the equivalent noise imposed at the n_{r}-th antenna over the two-hop link is $\boldsymbol{n}^{\text{AF-D,f}}_{n_{\mathrm{r}},k^{\check{}}_{\check{j}}} = (\boldsymbol{\mathcal{P}}^{\mathrm{R}}_{k^{\check{}}_{\check{j}}})^T \boldsymbol{\mathcal{F}}_U (\sqrt{G_{\mathrm{RD}}} \tilde{\boldsymbol{H}}^{\mathrm{RD,t}}_{\check{j},n_{\mathrm{r}}} \bar{\boldsymbol{n}}^{\mathrm{R,t}}_{k^{\check{}}_{\check{j}}} + \tilde{\boldsymbol{n}}^{\mathrm{D,t}}_{n_{\mathrm{r}},k^{\check{}}_{\check{j}}})$, and the corresponding noise power of the n-th element may be estimated as $\mathcal{N}^{\mathrm{AF}}_{n_{\mathrm{r}},n} = \sigma^2_{\mathrm{N}} |h^{\mathrm{RD,f}}_{n_{\mathrm{r}},n}|^2 + \sigma^2_{\mathrm{N}} / \beta^2_{k^{\check{}}_{\check{j}}}$.

5.2.4.2 DF Signal Received at the BS

By contrast, in the DF scenario of Figure 5.4(a), the BS's receiver only detects the signal transmitted by the relay, which relies only on the CSI of the R-D link. Hence, we arrive at the received signal of user $k^{\check{}}_{\check{j}}$ at the n_{r}-th antenna of Figure 5.4(a) expressed as:

$$\begin{aligned}\boldsymbol{y}^{\mathrm{D,f}}_{n_{\mathrm{r}},k^{\check{}}_{\check{j}}} &= \sqrt{P^{\mathrm{R}}_{k^{\check{}}_{\check{j}}} G_{\mathrm{RD}}} \boldsymbol{H}^{\mathrm{RD,f}}_{k^{\check{}}_{\check{j}},n_{\mathrm{r}}} \boldsymbol{\mathcal{F}}_N \boldsymbol{x}^{\mathrm{R,t}}_{k^{\check{}}_{\check{j}}} + (\boldsymbol{\mathcal{P}}^{\mathrm{R}}_{k^{\check{}}_{\check{j}}})^T \boldsymbol{\mathcal{F}}_U \tilde{\boldsymbol{n}}^{\mathrm{D,t}}_{n_{\mathrm{r}},k^{\check{}}_{\check{j}}} \\ &= \sqrt{P^{\mathrm{R}}_{k^{\check{}}_{\check{j}}}} \boldsymbol{H}^{\mathrm{DF,f}}_{k^{\check{}}_{\check{j}},n_{\mathrm{r}}} \boldsymbol{\mathcal{F}}_N \boldsymbol{x}^{\mathrm{R,t}}_{k} + \boldsymbol{n}^{\text{DF-D,f}}_{n_{\mathrm{r}},k^{\check{}}_{\check{j}}},\end{aligned} \tag{5.18b}$$

where $\boldsymbol{H}^{\mathrm{DF,f}}_{k^{\check{}}_{\check{j}},n_{\mathrm{r}}} = \sqrt{G_{\mathrm{RD}}} \boldsymbol{H}^{\mathrm{RD,f}}_{k^{\check{}}_{\check{j}},n_{\mathrm{r}}}$ denotes the equivalent FD channel matrix for reception by the n_{r}-th antenna in the context of DF relaying, while the noise contribution $\boldsymbol{n}^{\text{DF-D,f}}_{n_{\mathrm{r}},k^{\check{}}_{\check{j}}} = (\boldsymbol{\mathcal{P}}^{\mathrm{R}}_{k^{\check{}}_{\check{j}}})^T \boldsymbol{\mathcal{F}}_U \tilde{\boldsymbol{n}}^{\mathrm{D,t}}_{n_{\mathrm{r}},k^{\check{}}_{\check{j}}}$ is imposed at the n_{r}-th antenna and the corresponding power of the n-th element is $\mathcal{N}^{\mathrm{DF}}_{n_{\mathrm{r}},n} = \sigma^2_{\mathrm{N}}$.

TABLE 5.1: BS's Received Signal Comparison of AF and DF relaying

	AF	DF
Signal Power	Transmitted power $P^{\mathrm{R}}_{k_{\tilde{j}}}$ at relay	Transmitted power $P^{\mathrm{R}}_{k_{\tilde{j}}}$ at relay
Data Symbols	Original symbol $\boldsymbol{x}^{\mathrm{S,t}}_{k_{\tilde{j}}}$ at the source	Regenerated symbol $\boldsymbol{x}^{\mathrm{R,t}}_{k_{\tilde{j}}}$ at the relay
DFT Spreading	N-point FFT $\boldsymbol{\mathcal{F}}_N$	N-point FFT $\boldsymbol{\mathcal{F}}_N$
Channel	$\sqrt{G_{\mathrm{RD}}G_{\mathrm{SR}}}\boldsymbol{H}^{\mathrm{RD,f}}_{k_{\tilde{j}},n_{\mathrm{r}}}\boldsymbol{\beta}_{k_{\tilde{j}}}\boldsymbol{H}^{\mathrm{SR,f}}_{k,\tilde{j}}$	$\sqrt{G_{\mathrm{RD}}}\boldsymbol{H}^{\mathrm{RD,f}}_{k_{\tilde{j}},n_{\mathrm{r}}}$
Noise Power	$\sigma^2_{\mathrm{N}}\lvert h^{\mathrm{RD,f}}_{n_{\mathrm{r}},n}\rvert^2+\sigma^2_{\mathrm{N}}/\beta^2_{k_{\tilde{j}}}$	σ^2_{N}
Reception	Multiple-access at the n_{r}-th antenna	Multiple-access at the n_{r}-th antenna

5.2.4.3 Receiver Diversity Combining

Based on Eqs. (5.18a) and (5.18b), we conclude by comparing the AF and DF signals received by the n_{r}-th BS antenna in Table 5.1. Hence, the similarities and differences stated in Table 5.1 allow us to arrive at the generalised multi-antenna aided received signal model. Specifically, the $N_{\mathrm{r}}N$-element power-normalised FD observation of user $k'=k_{\tilde{j}}$ received via N_{r} antennas is formulated as:

$$\boldsymbol{y}^{\mathrm{f}}_{k'}=\boldsymbol{H}_{k'}\boldsymbol{x}^{\mathrm{t}}_{k'}+\boldsymbol{n}^{\mathrm{f}}_{k'}, \tag{5.19}$$

where we have

$$\boldsymbol{y}^{\mathrm{f}}_{k'} = \sqrt{1/P^{(\cdot)}_{k_{\tilde{j}}}}\left[(\boldsymbol{y}^{\mathrm{D,f}}_{0,k_{\tilde{j}}})^T,(\boldsymbol{y}^{\mathrm{D,f}}_{1,k_{\tilde{j}}})^T,\cdots,(\boldsymbol{y}^{\mathrm{D,f}}_{(N_{\mathrm{r}}-1),k_{\tilde{j}}})^T\right]^T, \tag{5.20}$$

$$\boldsymbol{H}_{k'} = \boldsymbol{H}^{\mathrm{f}}_{k'}\boldsymbol{\mathcal{F}}_N=\left[\boldsymbol{h}_{k',0},\boldsymbol{h}_{k',1},\cdots,\boldsymbol{h}_{k',(N-1)}\right], \tag{5.21}$$

$$\boldsymbol{H}^{\mathrm{f}}_{k'} = \left[(\boldsymbol{H}^{(\cdot),\mathrm{f}}_{k_{\tilde{j}},0})^T,(\boldsymbol{H}^{(\cdot),\mathrm{f}}_{k_{\tilde{j}},1})^T,\cdots,(\boldsymbol{H}^{(\cdot),\mathrm{f}}_{k_{\tilde{j}},(N_{\mathrm{r}}-1)})^T\right]^T=\left[\boldsymbol{h}^{\mathrm{f}}_{k',0},\boldsymbol{h}^{\mathrm{f}}_{k',1},\cdots,\boldsymbol{h}^{\mathrm{f}}_{k',(N-1)}\right], \tag{5.22}$$

$$\boldsymbol{x}^{\mathrm{t}}_{k'} = \boldsymbol{x}^{\mathrm{S,t}}_{k_{\tilde{j}}}\text{ or }\boldsymbol{x}^{\mathrm{R,t}}_{k_{\tilde{j}}},\quad \boldsymbol{n}^{\mathrm{f}}_{k'}=\sqrt{1/P^{(\cdot)}_{k_{\tilde{j}}}}\left[(\boldsymbol{n}^{(\cdot)\text{-D,f}}_{0,k_{\tilde{j}}})^T,(\boldsymbol{n}^{(\cdot)\text{-D,f}}_{1,k_{\tilde{j}}})^T,\cdots,(\boldsymbol{n}^{(\cdot)\text{-D,f}}_{(N_{\mathrm{r}}-1),k_{\tilde{j}}})^T\right]^T \tag{5.23}$$

Specifically, $\boldsymbol{H}_{k'}$ denotes the $(N_{\mathrm{r}}N\times N)$-element equivalent interference channel coefficient matrix invoking N-point DFT spreading[4] of user k', where $\boldsymbol{n}^{\mathrm{f}}_{k'}$ holds the normalised noise imposed on the N_{r} antennas. Note that $P^{(\cdot)}_{k_{\tilde{j}}}$ represents the transmitted power of the source or the relay, depending on both $\boldsymbol{H}^{(\cdot)}_{k_{\tilde{j}},n_{\mathrm{r}}}$ and on the noise-component $\boldsymbol{n}^{(\cdot)\text{-D,f}}_{n_{\mathrm{r}},k_{\tilde{j}}}$ of AF or DF relaying, respectively. Let us introduce the vector $\boldsymbol{e}_n=[0_0,0_1,\cdots,1_n,\cdots,0_{N-1}]^T$. Then the n-th column of $\boldsymbol{H}_{k'}$ and $\boldsymbol{H}^{\mathrm{f}}_{k'}$ is given by $\boldsymbol{h}_{k',n}=\boldsymbol{H}_{k'}\boldsymbol{e}_n$ and $\boldsymbol{h}^{\mathrm{f}}_{k',n}=\boldsymbol{H}^{\mathrm{f}}_{k'}\boldsymbol{e}_n$, respectively. Additionally, the $[(n_{\mathrm{r}}N+n'),n]$-th entry of $\boldsymbol{H}_{k'}$ may be expressed as:

$$h_{k',(n_{\mathrm{r}}N+n'),n}=\frac{1}{\sqrt{N}}\sum_{n''=0}^{N-1}h^{\mathrm{f}}_{k',(n_{\mathrm{r}}N+n'),n''}\exp\left(-j\frac{2\pi nn''}{N}\right), \tag{5.24}$$

[4]As a result, the corresponding equaliser weight matrix $\boldsymbol{W}_{k'}$ of Figures 5.4(a) and 5.5 also invokes the N-point DFT operation $\boldsymbol{\mathcal{F}}_N$. Therefore, the N-point IDFT operation at the receiver is not necessary after applying $\boldsymbol{W}^H_{k'}$ and it is denoted as $(\boldsymbol{\mathcal{F}}^H_N)$ in Figures 5.4(a) and 5.5(a), which is also shown in the dashed block of Figure 5.5(b).

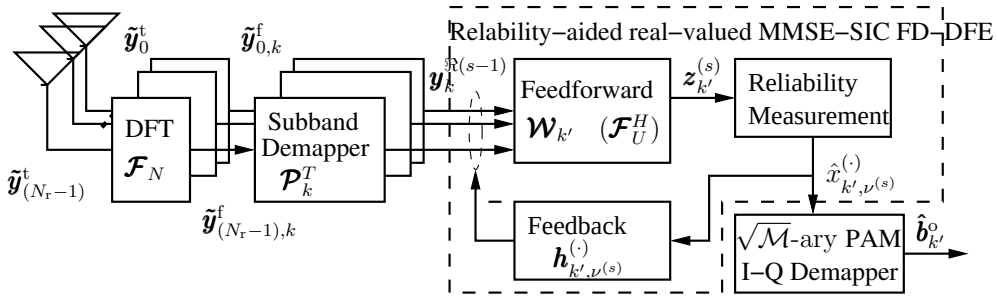

(a) SC-FDMA using MMSE-SIC FD-DFE

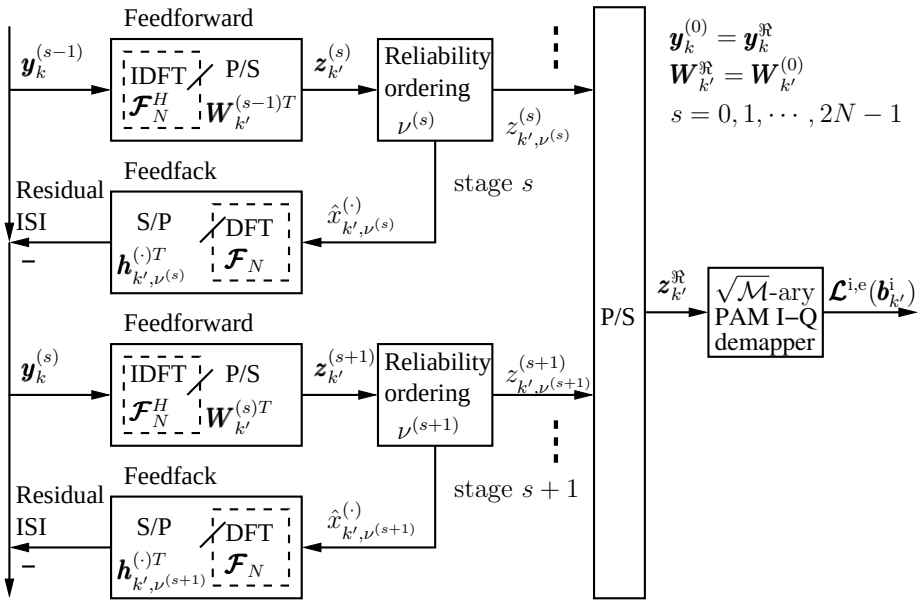

(b) Reliability-aided real-valued MMSE-SIC FD-DFE using soft-output

FIGURE 5.5: Receiver schematic of MMSE-SIC FD-DFE for the uncoded SC-FDMA uplink, which was derived from Figure 2.12. Their difference is the multi-antenna aided MMSE-SIC FD-DFE replaces the single-antenna aided MMSE FD-LE of Figure 2.12.

where $h^{\mathrm{f}}_{k',(n_{\mathrm{r}}N+n'),n''}$ is the $[(n_{\mathrm{r}}N+n'),n'']$-th entry of $\boldsymbol{H}^{\mathrm{f}}_{k'}$, and $h^{\mathrm{f}}_{k',(n_{\mathrm{r}}N+n'),n''}=0$, when $n'\neq n''$, $(n,n',n''=0,1,\cdots,N-1)$.

5.2.4.4 Frequency-Domain Equalisation

The BS's receiver of uncoded SC-FDMA seen in Figure 5.5(a) may then invoke the MMSE based real-valued FD-DFE relying on the principle of SIC as described in [86, 87], which is hence denoted as the MMSE-SIC FD-DFE scheme. The related so-called reliability-aided MMSE-SIC detection philosophy of Figure 5.5(b), was originally applied for multi-user detection (MUD) in CDMA and SDMA systems [86,87,213]. Unlike the conventional MMSE assisted SIC based DFE of [55,102], which quantifies the reliabilities of the detected symbols in terms of the SINR, the SIC based real-valued FD-DFE of Figure 5.5(b) determines the SIC-ordering based on the maximum *a-posteriori* probability (MAP) criterion. Therefore,

TABLE 5.2: Examples to contrast the resource allocation schemes in the following broadband systems: (a) Subcarrier-pairing based multi-relay assisted single-user OFDM [75], (b) Scheduling of SC-FDMA [91], (c) DRA-OR assisted SC-FDMA.

(a)

User	Relay	1st-,2nd-hop
1	1	1, 3
1	2	3, 5
1	3	4, 1
1	4	2, 2
1	5	5, 4

(b)

User	DT
1	3
6 (1)	5
5	1
4	2
3	4

(c)

User	Relay	1st-,2nd-hop
1	1	1, 3
2	6 (1)	2, 5
3	5	3, 1
4	4	4, 2
5	3	5, 4

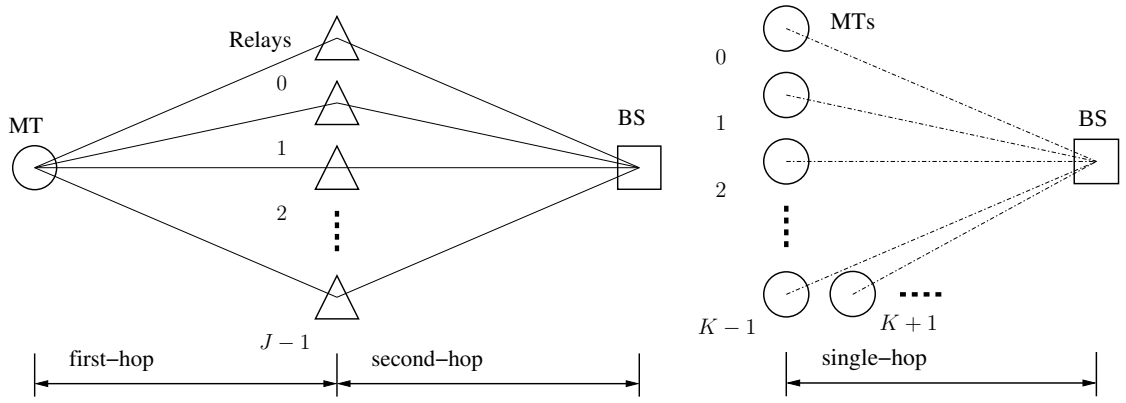

(a) Multi-relay assisted single-user OFDM (b) Multi-user scheduling of SC-FDMA

FIGURE 5.6: The topologies of two broadband systems. The regime seen in Figure 5.6(b) exploits the independent fading of the K S-D links, while that of Figure 5.6(a) has a potentially higher grade of freedom by exploiting the independent fading of the J S-R and R-D links.

the impact of both the fading and that of random noise are taken into account during the SIC process. In a SC-FDE system, the power of the residual ISI mainly depends on the time-dispersion imposed by multi-path fading channels. By incorporating the real-valued MMSE-SIC algorithm of Figure 5.5(b) detailed in [86, 87] into the FD-DFE receiver of uncoded SC-FDMA, we are capable of removing the residual ISI.

By contrast, the BS's receiver conceived for channel coded SC-FDMA systems may be designed by invoking the complex-valued MMSE turbo FD-LE of Figure 5.4(a). The design philosophy of the turbo FD-LE receiver was detailed in [88–90], based on the BICM-ID scheme of Figure 5.4(c) reviewed in Section 2.3.2.

5.3 Dynamic Resource Allocation for Opportunistic Relay

In the OR channels we considered, both the spatial- and spectral-domain resources offered by multiple relays may be explored for the sake of power reduction. In order to achieve a selec-

tion diversity gain, the *dynamic resource allocation* (DRS) allows each user to benefit from exploring both J different S-R channels and J R-D channels. The corresponding complex-valued fading envelope may be deemed to be independent and identically distributed (i.i.d) for each of these links of the resultant virtual *multiple-input multiple-output* MIMO scheme created from the single antennas of the MTs. Furthermore, the DSA beneficially rearranges the multi-user signals for transmission over the most appropriate subband groups for second-hop relaying. Furthermore, experiencing frequency-selective fading in the DRA assisted OR scheme may provide an additional multi-user diversity gain for the system. To elaborate a little further, we provide an example to describe the evolutionary development of our proposed DRA aided OR assisted SC-FDMA regime from two different systems in Table 5.2[5], namely from the subband pairing aided multi-relay assisted single-user OFDM of Figure 5.6(a) and from the multi-user scheduling assisted SC-FDMA uplink of Figure 5.6(b). The DRA conceived for OR assisted SC-FDMA may be regarded as an extended version of the single-user subband pairing regime of Table 5.2(a) considered for our multi-user system, as briefly mentioned in Section 5.1. Observe that, this regime is also reminiscent of the multi-user scheduling invoked in the DT scenario, as shown in Table 5.2(b). To expound a little further, multi-user scheduling allows specific subbands of multiple consecutive time slots to be allocated to more than $K = M$ dynamically assigned users, although only K or less users associated with the best channels were activated for simultaneous transmissions. By contrast, in the context of DRA aided OR, a beneficial diversity gain is attained by scheduling the multi-user signals of appropriate subband groups, when relying on multiple parallel relays within a single time slot. Therefore, the beneficial combination of DRS and DSA is capable of assigning appropriate desired subband groups for conveying the multiple users' signals regenerated at the appropriate relays, each of which may dynamically serve multiple users.

***First-Hop-Quality-Aware* Joint Dynamic Resource Allocation:** Although the conventional combination of DRS and DSA achieves a diversity gain with the aid of beneficial subband allocation and relay selection, the grade-of-freedom associated with beneficially allocating the multi-user signals across the entire set of $(M \times J)$ subband groups of the J relays has not been fully exploited. Unless near-error-free decoding is possible at the DF relays, the multi-user signals received and forwarded by the AF or DF relays may result in error-propagation at the BS, due to the first-hop transmissions in terms of the S-R CQI. This phenomenon motivates us to design and investigate attractive FHQA JDRA schemes conceived for OR assisted SC-FDMA. We assume that the CSIs of the K S-R links and of

[5]In Table 5.2, the columns representing the 1st-, 2nd-hop and the DT lists the index of subcarriers in Table 5.2(a), and the index of subband groups in Table 5.2(b) and Table 5.2(c). Notation 6 (1) in the second line of Table 5.2(b) and Table 5.2(c) indicates that instead of allowing User 6 of Table 5.2(b) or Relay 6 Table 5.2(c) to transmit, User 1 of Table 5.2(b) or Relay 1 of Table 5.2(c) may be scheduled for transmission, provided that the multiplexing is enabled in the context of Table 5.2(b) or Table 5.2(c), respectively.

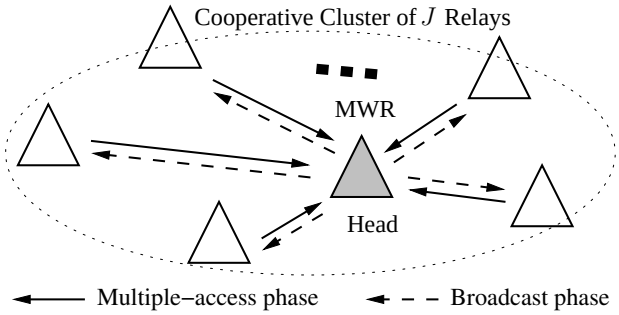

FIGURE 5.7: An example to illustrate the pilot-aided CQI exchange in the cooperative cluster of J relays by assuming *multi-way relaying* (MWR).

the $(M \times J \times N_{\mathrm{r}})$ R-D links are estimated perfectly at each relay's receiver. We also assume that these cooperating relays are capable of exchanging their CQIs. More specifically, as mentioned in Section 5.1, the $(J-1)$ relays of Figure 5.7 [211] transmit their CQI to an appropriately selected relay that acts as a *cluster-head*, which then broadcasts the CQI back to the $(J-1)$ relays. Let us now embark on designing two JDRA schemes, where the relevant decision are made at the relay rather than at the BS. This implies that the BS's receiver does not require the CQI of the first hop. [6]

In this section, five schemes are investigated:

1. *Random relay selection* (RRS) combined with SSA, denoted as 'RRS-SSA';
2. DRS Combined with SSA, denoted as 'DRS-SSA';
3. Conventional DRS approach combined with DSA, denoted as 'DRS-DSA';
4. FHQA JDRA approach-1, denoted as 'JDRA-1', a modified version of DRS-DSA invoking CQI exchange;
5. FHQA JDRA approach-2, denoted as 'JDRA-2', a design alternative of JDRA-1.

Their scenarios are summarised in Table 5.3 [7]. Specifically, the extent of S-R and R-D channel-quality dependence may vary with the relay strategies in terms of the different modes. When the controller of the OR-aided resource allocation is located at the BS's

[6] Let us define the notations as follows. The notations $\mathcal{K}$, $\mathcal{J}$, $\mathcal{M}$, $\mathcal{G}^{\mathrm{SR}}$ and $\mathcal{G}^{\mathrm{RD}}$, denote the set of users $k = 0, 1, 2, \cdots, K-1$, $(\forall k \in \mathcal{K})$, the relays $j = 0, 1, 2, \cdots, J-1$, $(\forall j \in \mathcal{J})$, the subband groups $m = 0, 1, 2, \cdots, M-1$, $(\forall m \in \mathcal{M})$, S-R channel gains $\forall g_{k,j}^{\mathrm{SR}} \in \mathcal{G}^{\mathrm{SR}}$ and R-D channel gains $\forall g_{j,m}^{\mathrm{RD}} \in \mathcal{G}^{\mathrm{RD}}$, respectively. Given the elements in the set $\mathcal{A}$, $(\forall a \in \mathcal{A})$, the notation $\check{a}$ represents the selected element of a and is collected in the set $\check{\mathcal{A}}$; the notation $\mathring{a}_i$ denotes the element a with ordering index i in the ordered version $\mathring{\mathcal{A}}$ of the original set $\mathcal{A}$. The notation $\varnothing$ represents the 'clear' operation. The notation $\cup$, $\setminus$ indicates that the element in $\{a\}$ is incorporated or excluded from the set $\mathcal{A}$, respectively.

[7] Note that, the channel dependence of each scheme may be characterised as being low or high over the S-R or R-D channels; The options for the relaying strategy are distributed or localised using non-cooperative relays (non-coop.) or cooperative relays (coop.); The controller may be located at the BS or relay cluster-head.

TABLE 5.3: Assumptions in OR-aided Resource Allocation

Mode	Channel dependence	Relay strategy	Controller
RRS-SSA	None	Distributed non-coop.	None
DRS-SSA	R-D, low	Distributed non-coop.	BS
DRS-DSA	R-D, high	Localised non-coop.	BS
JDRA-1	S-R & R-D, high	Localised coop.	Relay cluster-head
JDRA-2	S-R & R-D, high	Localised coop.	Relay cluster-head

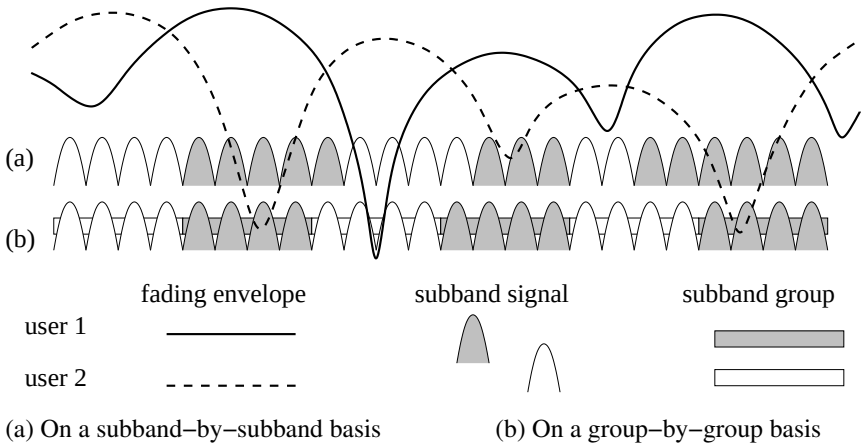

FIGURE 5.8: An example of illustrating the allocation of $K = 2$ users' signals to prospective subbands for $N = 4$ subband per user and bandwidth expansion of $M = 6$. The corresponding localised subband mapping scheme was portrayed in Figure 5.3.

receiver, no cooperation is required among the relays. By contrast, the JDRA modes benefit from the cooperation-aided interaction among the relays, in which case the optimisation tasks are solved by the cooperative cluster-head of Figure 5.7.

5.3.1 Channel Quality Information

There are several reasons for grouping the N subbands of each user together for relaying. The first one is related to the relevant complexity considerations, since searching for the optimal solution on a group-by-group rather than subband-by-subband basis is significantly less complex. For instance, Figure 5.8 illustrates the prospective subband assignment of the signals of $K = 2$ users both on a *subband-by-subband* basis in Figure 5.8(a) and on a group-by-group basis in Figure 5.8(b). Explicitly, observe in Figure 5.8(a) that the subband-by-subband based allocation is more flexible and hence it is capable of better exploiting the channel quality differences of the users than the more rigid, but less complex group-by-group regime. Another reason for grouping the N subbands of each user together is because each user's TD symbol generated after first-hop channel equalisation at the relay is related to all the N elements in $\boldsymbol{y}_{k_j}^{\mathrm{R,f}}$ due to the well-understood nature of the IDFT employed at the SC-FDMA receiver. Therefore, the subband-by-subband allocation is not permitted in

SC-FDMA systems.

Therefore, we use the average S-R channel attenuation of the N subbands of the k-th user's signal received by the j-th relay for quantifying the corresponding channel quality, which may be expressed as

$$g_{k,j}^{\mathrm{SR}} = \frac{1}{N} \sum_{n=0}^{N-1} |h_{k,j,n}^{\mathrm{SR,f}}|^2. \tag{5.25}$$

We also assume that the BS invokes N_{r} receiver antennas, where the sum of channel attenuations averaged over multiple antennas may be considered as a relevant quality metric for the overall channel effects. The average attenuation of the m-th group of N subbands in the channel spanning from the j-th relay to the BS is given by

$$g_{j,m}^{\mathrm{RD}} = \frac{1}{N} \sum_{u=mN}^{mN+N-1} \sum_{n_{\mathrm{r}}=0}^{N_{\mathrm{r}}-1} |h_{j,u,n_{\mathrm{r}}}^{\mathrm{RD,f}}|^2. \tag{5.26}$$

5.3.2 Relaying Frame Structure

Observe in Figure 5.9 that in our DRA aided OR system, each SC-FDMA symbol in the FD is referred to as a *resource vector* (RV), where the components of the RV are the original symbols modulating each of the subbands. Furthermore, N_{rv} consecutive RVs in the TD constitute a *resource block* (RB) in the uplink during a single time slot as the basic unit of resource allocation. The first RV may be regarded as the reference, which is known to both the transmitter as well as the receiver and hence may be used for channel quality estimation. Then, both the subband allocation and the relay selection valid for the corresponding time slot is optimised for the channel quality determined with the aid of this pilot RV. Hence we have a total of $N_{\mathrm{rb}} = N_{\mathrm{v}}/N_{\mathrm{rv}}$ RBs within a frame of N_{s} QAM symbols. Specifically, the number of RVs N_{rv} per RB determines the transmission overhead required, including the synchronisation sequences, the pilot RVs invoked for the estimation of the S-R and R-D links as well as the duration of the CQI exchange of Fig. 5.7 for the FHQA JDRA schemes[8]. Naturally, increasing the overhead provides more accurate channel estimation in support of the CQI exchange, hence it may result in an increased energy-efficiency, albeit it may reduce the system's throughput. The N_{rb} RBs of each user are allocated by conventional static localised subband mapping during the first-hop transmissions from the source MTs. However, during the second-hop, each RB or prossibly several consecutive RBs of a specific user may be rearranged at the appropriate relays, depending on the specific resource allocation schemes employed. Moreover, in the channel coded system the signal is interleaved

[8]For the sake of simplicity, we assume that the transmissions of two-hop relaying and of the CQI exchange are perfectly synchronised, hence the practical synchronisation issue is ignored. However, we evaluate the energy consumption expended in the relatively short duration of the pilots-based CQI exchange compared to that of the two-hop relaying.

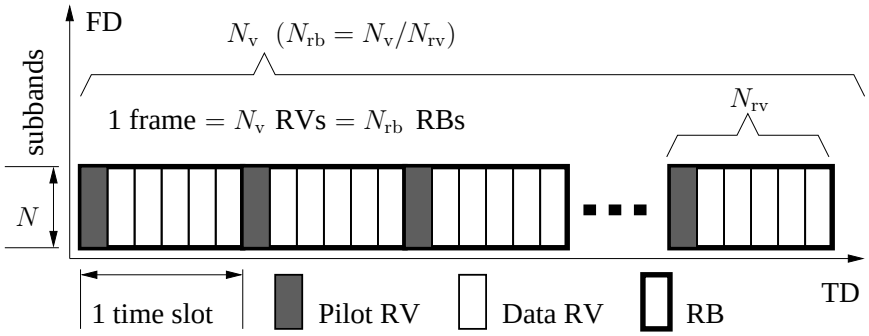

FIGURE 5.9: The resource allocation frame structure in the SC-FDMA uplink scheme of Figure 5.1. The frame structure of BICM aided SC-FDMA transmission was portrayed in Figure 2.14, where the N-element TD symbol vector is transformed by DFT into the FD represented by a resource vector (RV) in Figure 5.9.

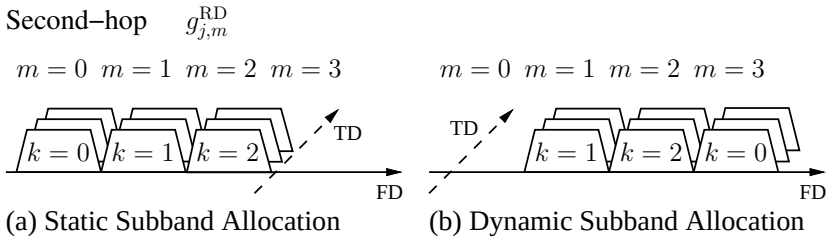

FIGURE 5.10: The snapshot of subband allocation schemes for single-relay assisted SC-FDMA.

and decoded on a *frame-by-frame* basis. Hence, an interleaver-length-dependent buffering delay is introduced, when using iterative decoding at the DF relay. Additionally, the specific number of consecutive RBs scheduled for concomitant transmission is typically determined by the normalised Doppler frequency $f_{\rm nd}$, which is usually carried out without changing the subband group and relay.

5.3.3 Static Subband Allocation Combined with Dynamic Relay Selection

When the relay allocates the same subbands for forwarding the k-th user's signal as the one that was used for receiving over the S-R link, we referred to this scenario as SSA in Figure 5.10(a), where a single-relay is involved. Specifically, each user's RB occupies a subband group in the FD and a time slot in the TD. Since the S-R and R-D channels typically experience i.i.d. fading, the specific SSA used for the R-D channel will never be optimal, regardless, whether the source MT does or does not invoke conventional localised SSA or DSA for transmission to the relay. By assuming that the localised subband mapping regime of Figure 5.3 is adopted for S-R transmissions, the m-th subband group may be allocated to the k-th user's signal, when we have $m = k$, which is transmitted by the specific relay having the index of $\breve{j}_m$ in the context of OR. We refer to this scenario as SSA for OR in Figure 5.11, where both the associated topology and resource allocation are characterised.

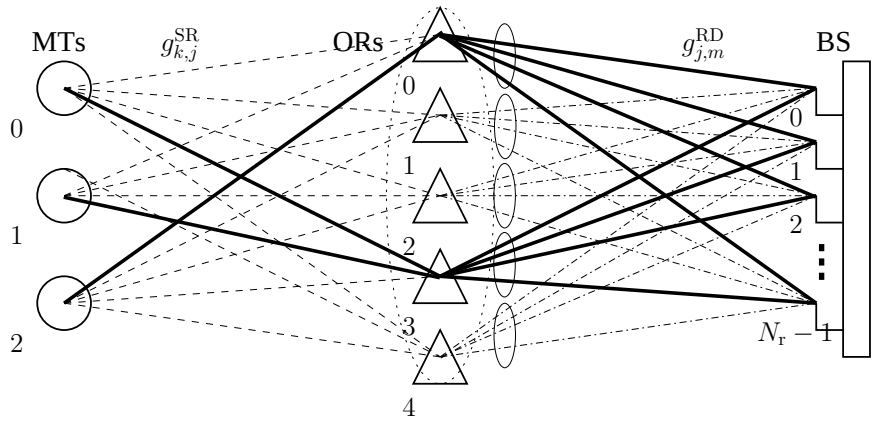

(a) Snapshot of topology in Figure 5.1 derived from Figure 5.6(a).

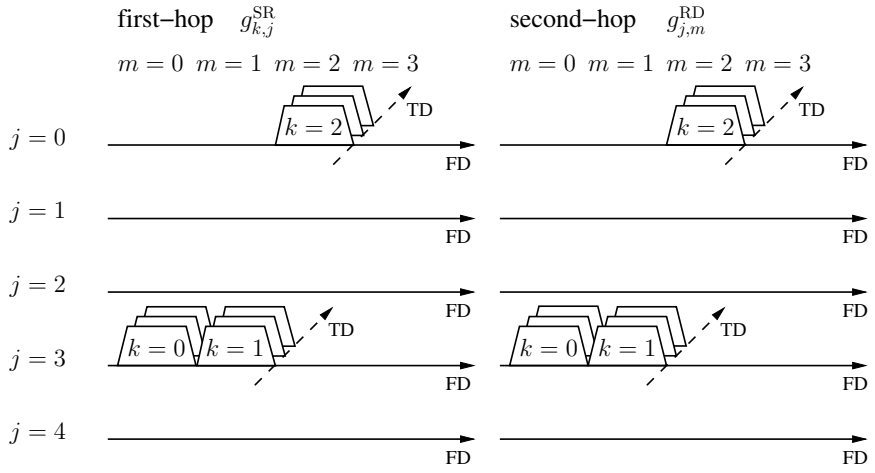

(b) Snapshot of resource block allocation

FIGURE 5.11: Illustration of *static subband allocation combined with dynamic relay selection* (DRS-SSA) for $K=3$, $M=4$ and $J=5$, which may be contrasted to the single-relay aided scheme of Figure 5.10(a).

5.3.3.1 DRS-SSA Algorithm

Second-Hop DRS: Apart from RRS, the DRS philosophy of Figure 5.11(a) may be invoked, which provides the maximum R-D gain of $g_{j,m}^{\mathrm{RD}}$ amongst all the m-th subband groups of the other relays, i.e. we have

$$\begin{aligned} \check{j}_m &= \arg\max_{j\in\mathcal{J}}\{g_{j,m}^{\mathrm{RD}}\} \\ \text{s. t.} &: m=k, m\in\mathcal{M}, k\in\mathcal{K}. \end{aligned} \tag{5.27}$$

Additionally, the initial set of desired relays is empty, i.e. we have $\check{\mathcal{J}}=\varnothing$. Then, at the m-th subband group, for $m\in\mathcal{M}$, $m=0,1,\cdots,M-1$, we update the set $\check{\mathcal{J}}$ by incorporating

the relay having the index $\check{j}_m$, which is formulated as:

$$\check{\mathcal{J}} = \check{\mathcal{J}} \cup \{\check{j}_m\}. \tag{5.28}$$

We note that the RB allocation scheme of the different users may be deemed to be fair even without any particular ordering, since each user will be assigned to orthogonal subband groups at their best relay and this assignment is carried out independently of the other users' assignments.

5.3.3.2 An Example of DRS-SSA

Additionally, Table 5.4 illustrates an example of the SSA regime of Figure 5.11(b) combined with the DRS scheme. The same parameters are adopted also in Tables 5.6 - 5.10 for all the DRA schemes of Figures 5.12(b) - 5.15(b). The RBs having numbers printed in boldface denote the highest R-D gain $g_{j,m}^{\mathrm{RD}}$ in each column for a specific subband group index m, where we have the corresponding relay of index j in the rows. The assigned RBs of each user is marked by underlining them. Moreover, the specific assignment of the relay j and subband group m to each user k is given by $(\check{j}, \check{m})$, where the subband groups assigned for the second-hop remain the same as during the first-hop.

To elaborate on Table 5.4 a little further, let us consider the S-R and R-D channel gains of all the $K = 3$ users, $M = 4$ subband groups and $J = 5$ relays. In the S-R link user $k = 0$ has the highest gain of $g_{0,4}^{\mathrm{SR}} = 1.42$ via relay $j = 4$, user $k = 1$ has $g_{1,2}^{\mathrm{SR}} = 3.07$ relying on relay $j = 2$, while user $k = 2$ has $g_{2,0}^{\mathrm{SR}} = 2.26$ with the assistance of relay $j = 0$. As for $g_{j,m}^{\mathrm{RD}}$, we arrive at $(j, m) = (3, 0)$, $(3, 1)$ and $(0, 2)$ associated with $g_{j,m}^{\mathrm{RD}}$ of **1.75**, **2.50** and **1.90**, as seen in Table 5.4. Nevertheless, a limitation of the DRS-SSA regime of Figure 5.11(b) is revealed for the scenario of $K < M$. For instance, we have $g_{1,3}^{\mathrm{RD}} =$ **4.41**, which is the highest R-D gain in the column of the subband group of $m = 3$, but since we only have $K = 3$ users, owing to the rigidity of the SSA of Figure 5.11(b) only the subband groups of $m = 0$, 1 and 2 may be used. In order to circumvent the SSA's rigidity, the combination of the DSA of Figure 5.12(b) with the DRS scheme is motivated and will be invoked in Section 5.3.4.

5.3.4 Conventional Dynamic Subband Allocation Combined with Dynamic Relay Selection

The original DSA concept invoked for a single-relay system is demonstrated in Figure 5.10(b), where a diversity gain may be attained in the FD. In parallel, in the OR assisted system of Figure 5.12(a), the conventional combination of DSA and DRS allows the multiple users' received signals to be adaptively transmitted in the most appropriate subband groups

TABLE 5.4: An example of *static subband allocation combined with the dynamic relay selection* (DRS-SSA) for $K = 3$, $M = 4$ and $J = 5$. Specifically, the RBs indicated by the numbers printed in boldface denote the highest R-D gain $g^{\mathrm{RD}}_{j,m}$ in each column for a specific subband group index m, where we have the corresponding relay index j in the rows. The assigned RBs of each user are marked by underlining them. Moreover, the specific assignment of relay j and subband group m to each user k is given by $(\check{j}, \check{m})$, where the subband groups assigned for the second-hop remain the same as during the first-hop.

	First-hop $g^{\mathrm{SR}}_{k,j}$			Second-hop $g^{\mathrm{RD}}_{j,m}$			
	$k=0$	$k=1$	$k=2$	$m=0$	$m=1$	$m=2$	$m=3$
$j=0$	0.05	0.53	2.26	0.04	0.33	**1.90**	0.56
$j=1$	0.16	0.20	0.57	0.70	1.91	0.84	**4.41**
$j=2$	0.90	3.07	0.70	0.45	0.26	0.28	0.90
$j=3$	0.18	0.09	0.21	**1.75**	**2.50**	0.02	0.09
$j=4$	1.42	1.44	0.81	0.29	1.36	0.17	0.05
Target $(\check{j}, \check{m})$	$(3,0)$	$(3,1)$	$(0,2)$				

at dynamically selected relays, by taking into account the $(M \times J)$ possible subband groups of the J relays. Figure 5.12(b) and Table 5.6 demonstrate the differences between the DSA and SSA combined with the DRS scheme in the context of OR, which may be contrasted to Figure 5.11(b) and Table 5.4, respectively.

5.3.4.1 DRS-DSA Algorithm

Let us now describe the DRS-DSA algorithm in more detail.

Second-Hop DRS: Firstly, we carry out the DRS procedure discussed in Section 5.3.3. Furthermore, we also update the set $\check{\mathcal{G}}^{\mathrm{RD}}$ by incorporating the R-D channel gain of $g^{\mathrm{RD}}_{\check{j},m}$ for all $m \in \mathcal{M}$, $m = 0, 1, \cdots, M-1$.

Second-Hop DSA: Furthermore, we then initialise the ordered set of desired subband groups $\mathring{\mathcal{M}}$ to be empty. The i-th desired subband group $\mathring{m}_i$ in the set $\mathring{\mathcal{M}}$ having the highest R-D channel gain can be obtained by maximising the R-D channel gain $g^{\mathrm{RD}}_{\check{j},m}$ among all the M groups from the relays in set $\check{\mathcal{J}}$. Additionally, the corresponding channel gain $g^{\mathrm{RD}}_{\check{j},\check{m}_i}$ should be removed from $\check{\mathcal{G}}^{\mathrm{RD}}$ for finding the next, i.e. the $(i+1)$-st user to be given resources. Therefore, we obtain the i-th user's assignment of subband group $\mathring{m}_i$ and relay $\check{j}_{\mathring{m}_i}$, as discussed in more detail below.

User Assignment: We note that the i-th user to be granted resource for his/her transmissions from the subband groups associated with the current $(M-i+1)$-element R-D channel gain set $\check{\mathcal{G}}^{\mathrm{RD}}$ benefits from a total selection diversity order of $J \times (M-i+1)$, which may be gleaned from both the frequency domain (subband groups) and from the spatial domain (relays). In order to guarantee for all users to be fairly treated and supported, the subband groups associated with the set $\check{\mathcal{G}}^{\mathrm{RD}}$ are randomly assigned to each user within each time

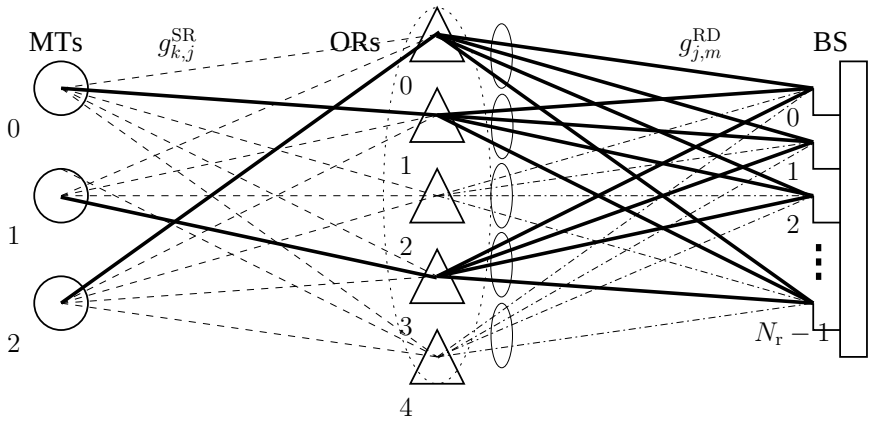

(a) Snapshot of topology, which may be contrasted to Figure 5.11(a).

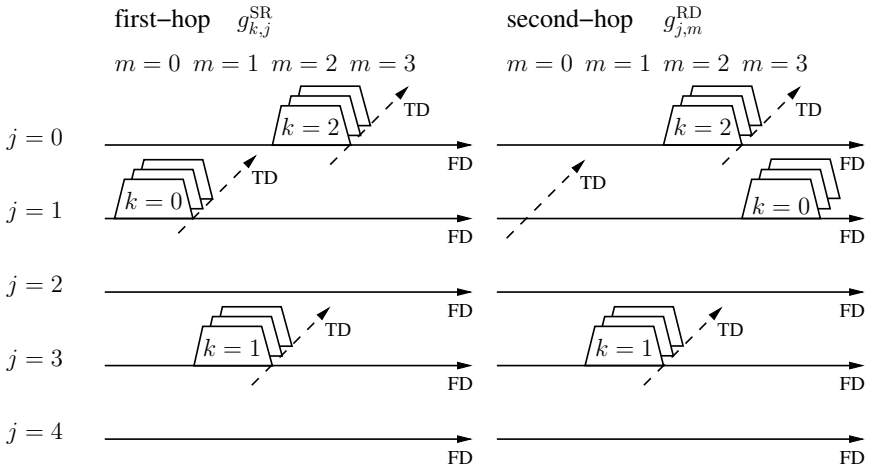

(b) Snapshot of resource block allocation

FIGURE 5.12: The illustration of *dynamic subband allocation combined with the dynamic relay selection* (DRS-DSA) for $K=3$, $M=4$ and $J=5$, which may be contrasted to the corresponding *static subband allocation* (DRS-SSA) of Figure 5.11. Their main difference is that the DRS-DSA scheme assigns K users to the K best RBs associated with the highest R-D channel gains over the M subband groups among the J relays. By contrast, the second hop RB of $(j,m)=(1,3)$ may not be allocated when using the DRS-SSA scheme of Figure 5.11(b). Additionally, this difference is also similar to that between DSA and SSA schemes in the single-relay scenario in Figure 5.10.

slot. Specifically, we store the indices of the users waiting for resource assignment in the set $\underline{\mathcal{K}}$. Hence, the index associated with those users waiting for resource assignment $\underline{k} \in \underline{\mathcal{K}}$, $(\underline{k}=0,1,\cdots,K-1)$ is given by

$$i = \mathrm{randi}(0, \underline{K}-1). \tag{5.29}$$

As a result, the signal of user $\underline{k}_i$ is assigned to the $\mathring{m}_i$-th subband group at the $\check{j}_{\mathring{m}_i}$-th relay, where we have $\check{j}_{\mathring{m}_i} \in \check{\mathcal{J}}$ when $m=\mathring{m}_i$. Additionally, we remove the most recently assigned user $\underline{k}_i$ from the set $\underline{\mathcal{K}}$ and return to Eq. (5.29) in order to allocate the subband group $\check{m}_{(i+1)}$ associated with $g^{\mathrm{RD}}_{\check{j},\check{m}_{(i+1)}}$ to the $(i+1)$-st user, i.e. we have $\underline{\mathcal{K}} = \underline{\mathcal{K}} \setminus \{\underline{k}_i\}$.

TABLE 5.5: Conventional *dynamic subband allocation combined with the dynamic relay selection* (DRS-DSA) algorithm

1. Initialisation:	Set $\check{\mathcal{J}} = \varnothing$, $\mathring{\mathcal{M}} = \varnothing$.
2. 2nd-Hop DRS:	At the m-th subband group, $\forall m \in \mathcal{M}$: (a) Obtain $\check{j}_m = \arg\max_{j\in\mathcal{J}}\{g^{\mathrm{RD}}_{j,m}\}$; (b) Update $\check{\mathcal{J}} = \check{\mathcal{J}} \cup \{\check{j}_m\}$ and $\check{\mathcal{G}}^{\mathrm{RD}} = \check{\mathcal{G}}^{\mathrm{RD}} \cup \{g^{\mathrm{RD}}_{\check{j},m}\}$.
3. 2nd-Hop DSA:	For $i = 0, 1, \cdots, M-1$: (a) Obtain $\mathring{m}_i = \arg\max_{m\in\mathcal{M}}\{g^{\mathrm{RD}}_{\check{j},m}\}$; (b) Update $\mathring{\mathcal{M}} = \mathring{\mathcal{M}} \cup \{\mathring{m}_i\}$, $\check{\mathcal{G}}^{\mathrm{RD}} = \check{\mathcal{G}}^{\mathrm{RD}} \setminus \{g^{\mathrm{RD}}_{\check{j},\mathring{m}_i}\}$, $\forall \check{j}_m \in \check{\mathcal{J}}$.
4. Fair User Assignment:	For $i = 0, 1, \cdots, K-1$: Assign the user $\mathring{k}_i$ with the resource pair $(\mathring{m}_i, \check{j}_{\mathring{m}_i})$ randomly.

TABLE 5.6: An example of *dynamic subband allocation combined with the dynamic relay selection* (DRS-DSA) for $K = 3$, $M = 4$ and $J = 5$, which may be readily contrasted to the corresponding static subband allocation of Table 5.4. Briefly, the difference between them is that upon invoking the DRS-DSA scheme the assigned RBs associated with the underlined R-D channel gain $g^{\mathrm{RD}}_{j,m}$ of Table 5.6 are chosen from the K highest $g^{\mathrm{RD}}_{j,m}$ values printed in boldface over the M subband groups among J relays. For instance, the second-hop RB of $(j, m) = (1, 3)$ having the highest gain of $g^{\mathrm{RD}}_{1,3} = 4.41$ in Table 5.6, may be chosen instead of the RBs of $(j, m) = (3, 0)$ having a gain of $g^{\mathrm{RD}}_{3,0} = 1.75$, when invoking the DRS-SSA scheme characterised in Table 5.4.

	First-hop $g^{\mathrm{SR}}_{k,j}$			Second-hop $g^{\mathrm{RD}}_{j,m}$			
	$k=0$	$k=1$	$k=2$	$m=0$	$m=1$	$m=2$	$m=3$
$j=0$	0.05	0.53	<u>2.26</u>	0.04	0.33	**<u>1.90</u>**$^{(3rd)}$	0.56
$j=1$	<u>0.16</u>	0.20	0.57	0.70	1.91	0.84	**<u>4.41</u>**$^{(1st)}$
$j=2$	0.90	3.07	0.70	0.45	0.26	0.28	0.90
$j=3$	0.18	<u>0.09</u>	0.21	**1.75**$^{(4th)}$	**<u>2.50</u>**$^{(2nd)}$	0.02	0.09
$j=4$	1.42	1.44	0.81	0.29	1.36	0.17	0.05
Target $(\check{j}, \check{m})$	$(1, 3)$	$(3, 1)$	$(0, 2)$				

Ultimately, this DRS-DSA algorithm is summarised in Table 5.5.

5.3.4.2 An Example of DRS-DSA

To elaborate on Table 5.6 a little further, let us consider the S-R and R-D channel gains of all the $K = 3$ users, $M = 4$ subband groups and $J = 5$ relays. In the S-R link user $k = 0$ has the highest gain of $g^{\mathrm{SR}}_{0,4} = 1.42$ with the aid of relay $j = 4$, user $k = 1$ has $g^{\mathrm{SR}}_{1,2} = 3.07$ via relay $j = 2$, while user $k = 2$ has $g^{\mathrm{SR}}_{2,0} = 2.26$, when invoking relay $j = 0$. By observing the R-D channel gains $g^{\mathrm{RD}}_{j,m}$ in Table 5.6, we can see that the RBs with the highest $g^{\mathrm{RD}}_{j,m}$ values are in boldface in each column for a specific subband group index m. They are further sorted by the superscripts of $(1st)$, $(2nd)$, etc. Hence, the RBs having the first K assignments of relay j and subband group m, such as $(1, 3)$, $(3, 1)$ and $(0, 2)$ associated with $g^{\mathrm{RD}}_{j,m}$ of $\mathbf{4.41}^{(1st)}$, $\mathbf{2.50}^{(2nd)}$ and $\mathbf{1.90}^{3rd}$, respectively, may be allocated to the users in the set $\mathcal{K}$, which are marked by underlining in Table 5.6. Compared to the DRS-SSA scheme of

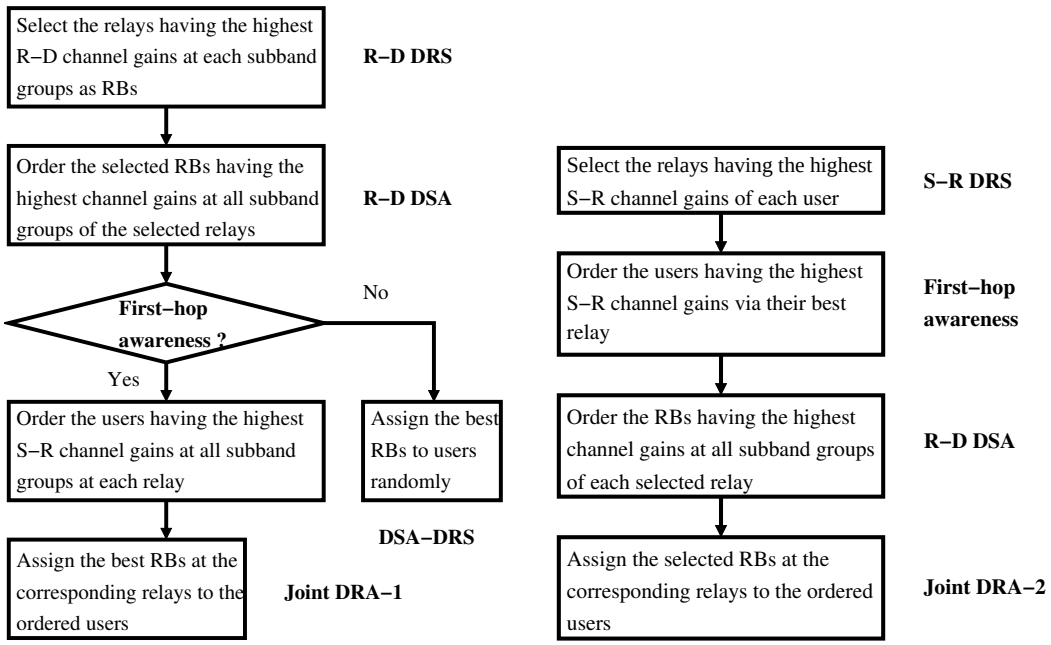

FIGURE 5.13: Flow charts of the *first-hop-quality-aware* (FHQA) joint *dynamic resource allocation* (DRA) schemes. Observe the differences of procedures in Figure 5.13(a) with respect to the DSA-DRS of Section 5.3.4 and JDRA-1 scheme in Section 5.3.5 are exploited. Meanwhile, the main differences between two kinds of JDRA approaches are also characterised by contrasting Figure 5.13(b) to Figure 5.13(a).

Table 5.4, the RB having $g_{3,0}^{\mathrm{RD}} = \mathbf{1.75}^{(4th)}$ is abandoned by the DRS-DSA approach of Table 5.6. Consequently, we arrive at the solution illustrated in Figure 5.12(b) for a specific time slot.

5.3.5 FHQA Joint Dynamic Resource Allocation Approach-1

The first JDRA-1 approach optimises the conventional DRA scheme of Figure 5.12 by allocating the RBs having the highest channel gain for the R-D links to the appropriate users, which are stored in an ordered user set at each relay in terms of their first-hop CQI. We assume that each relay stores and labels a sorted CQI set of the S-R links, while receiving from K users. The resultant J appropriately ordered CQI sets of the S-R links and the CQI sets of the R-D links are then exchanged among the J relays via the relays' cluster-head, as shown in Fig. 5.7.

A flow chart of the proposed JDRA-1 algorithm is presented in Figure 5.13(a), where the processing blocks inherited from the conventional methods are highlighted using bold acronyms. Furthermore, compared to the conventional combination of DSA and DRS as portrayed in Figure 5.12, the differences in both the snapshots of topology and RB allocation using JDRA-1 are illustrated in Figure 5.14 in the same channel quality scenario as used in Fig-

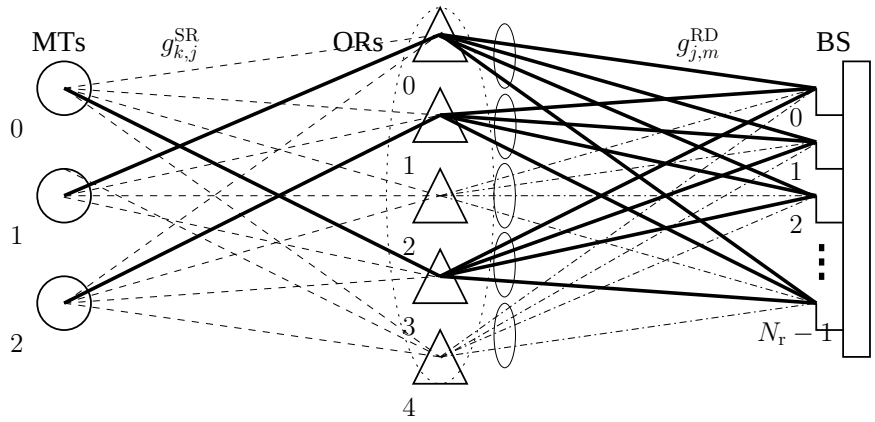

(a) Snapshot of Topology, which may be contrasted to Figures 5.12(a) and 5.11(a).

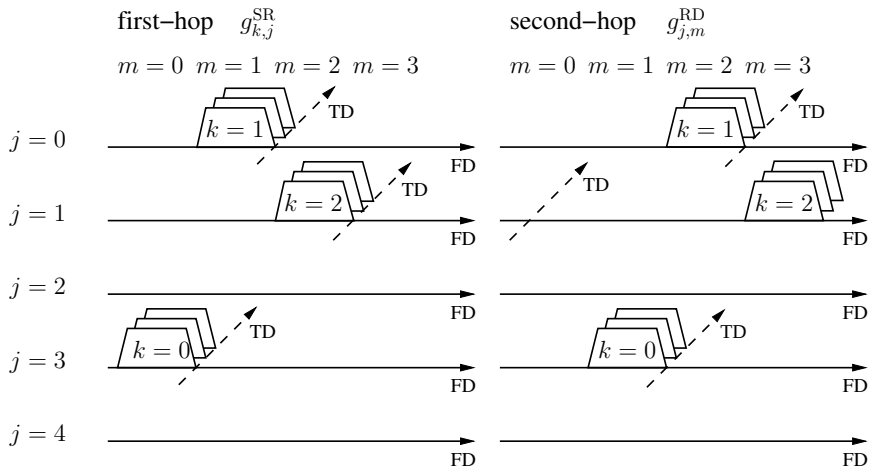

(b) Snapshot of Resource Block Allocation

FIGURE 5.14: The illustration of *first-hop-quality-aware* (FHQA) *joint dynamic resource allocation: approach 1* (JDRA-1) for $K = 3$, $M = 4$ and $J = 5$, which may be contrasted to the separate static and dynamic resource allocation schemes (DRS-SSA and DRS-DSA) of Figures 5.11 and 5.12. Their main difference is that the JDRA-1 scheme optimises the conventional DRA scheme of Figure 5.12 by allocating the RBs having the highest channel gains for the R-D links to the appropriate users, which are stored in an ordered user set at each relay in terms of their first-hop CQI.

ures 5.11 and 5.12. For example, Table 5.8 characterises the allocation strategy based on the conventional DSA combined with the DRS procedure of Table 5.6.

5.3.5.1 FHQA JDRA-1 Algorithm

To elaborate on the FHQA JDRA-1 scheme a little further, we describe the associated procedures step by step as follows:

Second-Hop DRS and DSA: Initially, we adopt the second-hop DSA combined with DRS, as detailed in Sections 5.3.3 and 5.3.4.

TABLE 5.7: *First-hop-quality-aware* (FHQA) *joint dynamic resource allocation: approach-1* (JDRA-1) algorithm

1. 2nd-Hop DRS-DSA:	Detailed in Section 5.3.4.
2. FHQA Ordering:	At the j-th relay, $\forall j \in \mathcal{J}$: (a) Set $\mathring{\mathcal{G}}_j^{\mathrm{SR}} = \varnothing$, $\mathring{\mathcal{K}}_j = \varnothing$; (b) Collect $\mathcal{G}_j^{\mathrm{SR}} = \{g_{0,j}^{\mathrm{SR}}, g_{1,j}^{\mathrm{SR}}, \cdots, g_{K-1,j}^{\mathrm{SR}}\}$; (c) For $i = 0, 1, \cdots, K-1$: (i) Obtain the i-th ordered user index in the set $\mathring{\mathcal{K}}_j$: $\mathring{k}_{i,j} = \arg\max_{k \in \mathcal{K}} \{g_{k,j}^{\mathrm{SR}}\}$; (ii) Update $\mathring{\mathcal{K}}_j = \mathring{\mathcal{K}}_j \cup \{\mathring{k}_{i,j}\}$, $\mathring{\mathcal{G}}_j^{\mathrm{SR}} = \mathring{\mathcal{G}}_j^{\mathrm{SR}} \cup \{g_{\mathring{k}_{i,j},j}^{\mathrm{SR}}\}$, and $\mathcal{G}_j^{\mathrm{SR}} = \mathcal{G}_j^{\mathrm{SR}} \setminus \{g_{\mathring{k}_{i,j},j}^{\mathrm{SR}}\}$.
3. User Assignment:	Set $\mathring{\mathcal{K}} = \varnothing$; For the $\imath$-th user to be given resources, $(\imath = 0, 1, \cdots, K-1)$, $\forall \mathring{k}_{i,\check{j}_{\mathring{m}_\imath}} \in \mathcal{K}_{\check{j}_{\mathring{m}_\imath}}$, $\forall \check{j}_{\mathring{m}_\imath} \in \check{\mathcal{J}}$: (a) Let $i = 0$; (b) If $\mathring{k}_{i,\check{j}_{\mathring{m}_\imath}} \notin \mathring{\mathcal{K}}$: (i) Collect the user $\mathring{k}_{i,\check{j}_{\mathring{m}_\imath}}$ to the $\imath$-th element of $\mathring{\mathcal{K}}$, $\mathring{\mathcal{K}} = \mathring{\mathcal{K}} \cup \{\mathring{k}_{i,\check{j}_{\mathring{m}_\imath}}\}$; (ii) Update $\mathring{\mathcal{K}}_{\check{j}_{\mathring{m}_\imath}} = \mathring{\mathcal{K}}_{\check{j}_{\mathring{m}_\imath}} \setminus \{\mathring{k}_{i,\check{j}_{\mathring{m}_\imath}}\}$; (iii) Assign the user $\mathring{k}_{i,\check{j}_{\mathring{m}_\imath}}$ with the resource pair $(\mathring{m}_\imath, \check{j}_{\mathring{m}_\imath})$. Else if $\mathring{k}_{i,\check{j}_{\mathring{m}_\imath}} \in \mathring{\mathcal{K}}$, we apply $i := i + 1$, return to step 3-(a);

First-Hop Consideration: At the j-th relay, we obtain the S-R channel gains $g_{k,j}^{\mathrm{SR}}$ of the k-th user, which we would like to optimise. The gains of all users are contained in the set $\mathcal{G}_j^{\mathrm{SR}}$. Meanwhile, the ordered set $\mathring{\mathcal{G}}_j^{\mathrm{SR}}$ of the S-R channel qualities recorded for the links spanning from the K users to the j-th relay and the ordered user set $\mathring{\mathcal{K}}_j$ regarding the j-th relay are initialised to be empty. Furthermore, by maximising $g_{k,j}^{\mathrm{SR}}$ for the j-th relay among all users, we obtain the i-th ordered user index $(i = 0, 1, \cdots, K-1)$ as the i-th element in the set $\mathring{\mathcal{K}}_j$ at the j-th relay. The corresponding channel gain $g_{\mathring{k}_{i,j},j}^{\mathrm{SR}}$ is then fed into the S-R channel quality based ordered set $\mathring{\mathcal{G}}_j^{\mathrm{SR}}$ with respect to the j-th relay, and it is also removed from the set $\mathcal{G}_j^{\mathrm{SR}}$ for the next allocation.

User Assignment: After clearing the ordered set $\mathring{\mathcal{K}}$, the index of the $\imath$-th user about to be given resources is denoted by $\mathring{k}_{i,\check{j}_{\mathring{m}_\imath}}$ if $\mathring{k}_{i,\check{j}_{\mathring{m}_\imath}} \notin \mathring{\mathcal{K}}$. In other words, the user $\mathring{k}_{i,\check{j}_{\mathring{m}_\imath}}$ may be assigned to the $\imath$-th element of $\mathring{\mathcal{K}}$. Meanwhile, for the sake of avoiding the repeated allocation of the subband group and that of a specific relay to the users to be given resources, the assigned user should be removed from the S-R link's ordered user set $\mathring{\mathcal{K}}_{\check{j}_{\mathring{m}_\imath}}$ regarding the $\check{j}_{\mathring{m}_\imath}$-th relay. Otherwise, in case of $\mathring{k}_{i,\check{j}_{\mathring{m}_\imath}} \in \mathring{\mathcal{K}}$, we apply $i := i + 1$ for the sake of providing the next user with communication resources in the ordered set $\mathring{\mathcal{K}}_{\check{j}_{\mathring{m}_\imath}}$.

Consequently, the associated algorithm may be summarised in Table 5.7.

TABLE 5.8: An example of *first-hop-quality-aware* (FHQA) *joint dynamic resource allocation: approach 1* (JDRA-1) for $K = 3$, $M = 4$ and $J = 5$, which may be contrasted to the separate static and dynamic resource allocation schemes (DRS-SSA and DRS-DSA) of Tables 5.4 and 5.6. Explicitly, their main difference is that the user assignment of the JDRA-1 scheme is dependent on the first-hop quality, namely on the $g^{\mathrm{SR}}_{k,j}$-based ordered user set at the specific relays, which were allocated the second-hop RBs associated with the K highest gains $g^{\mathrm{RD}}_{j,m}$. For instance, the second-hop RB associated with $g^{\mathrm{RD}}_{1,3} = 4.41$ at the subband group $m = 3$ and the relay $j = 1$ is assigned to user $k = 2$, since the first-hop RB of user $k = 2$ has the highest hirst-hop gain of $g^{\mathrm{SR}}_{2,1} = 0.57$ amongst the users at relay $j = 1$.

	First-hop $g^{\mathrm{SR}}_{k,j}$			Second-hop $g^{\mathrm{RD}}_{j,m}$			
	$k=0$	$k=1$	$k=2$	$m=0$	$m=1$	$m=2$	$m=3$
$j=0$	$0.05^{(3rd)}$	$\underline{0.53}^{(2nd)}$	$\mathbf{2.26}^{(1st)}$	0.04	0.33	$\underline{\mathbf{1.90}}^{(3rd)}$	0.56
$j=1$	$0.16^{(3rd)}$	$0.20^{(2nd)}$	$\underline{\mathbf{0.57}}^{(1st)}$	0.70	1.91	0.84	$\underline{\mathbf{4.41}}^{(1st)}$
$j=2$	0.90	**3.07**	0.70	0.45	0.26	0.28	0.90
$j=3$	$\underline{0.18}^{(2nd)}$	$0.09^{(3rd)}$	$\mathbf{0.21}^{(1st)}$	$\mathbf{1.75}^{(4th)}$	$\underline{\mathbf{2.50}}^{(2nd)}$	0.02	0.09
$j=4$	1.42	**1.44**	0.81	0.29	1.36	0.17	0.05
Target $(\check{j}, \check{m})$	$(3,1)$	$(0,2)$	$(1,3)$				

5.3.5.2 An Example of FHQA JDRA-1

To elaborate on Table 5.8 a little further, which should be contrasted to Table 5.6, let us consider the S-R and R-D channel gains of all the $K = 3$ users, $M = 4$ subband groups and $J = 5$ relays. In the S-R links user $k = 0$ benefits from the highest gain of $g^{\mathrm{SR}}_{0,4} = 1.42$ via relay $j = 4$, user $k = 1$ attains the gain of $g^{\mathrm{SR}}_{1,2} = 3.07$ using relay $j = 2$, while user $k = 2$ has $g^{\mathrm{SR}}_{2,0} = 2.26$ using relay $j = 0$. Specifically, the sorted CQI set of each S-R channel may be obtained by ordering the $g^{\mathrm{SR}}_{k,j}$ values in each row of Table 5.8 marked with $(1st)$, $(2nd)$ and $(3rd)$. After choosing the RBs having the best K combination of relays in the rows and the best subband groups in the columns of Table 5.8 for transmission over the R-D channels, the user waiting for resource assignment is determined by the corresponding relay, where the specific ordering of $g^{\mathrm{SR}}_{k,j}$ is considered. As a result, compared to the random user assignment of the DRS-DSA scheme characterised in Table 5.6, we arrive at the second-hop RBs having indices of $(j, m) = (1, 3)$. More explicitly, these RBs are associated with a first-hop quality $g^{\mathrm{SR}}_{2,1} = \mathbf{0.57}$ for user $k = 2$ and with the second-hop RB of $(j, m) = (3, 1)$ associated with the first-hop quality of $g^{\mathrm{SR}}_{0,3} = 0.18$ for user $k = 0$ and finally with the second-hop RB of $(j, m) = (0, 2)$ associated with the first-hop quality of $g^{\mathrm{SR}}_{1,0} = 0.53$ for user $k = 1$.

5.3.6 FHQA Joint Dynamic Resource Allocation Approach-2

The best first-hop channel quality may be determined form either the user's or the relay's perspective. This distinction leads to the definition of our JDRA-2 scheme. More specifically, rather than finding the best link of a specific user to a relay in JDRA-2, we find the specific user, which can be supported by a particular relay with the best possible channel quality.

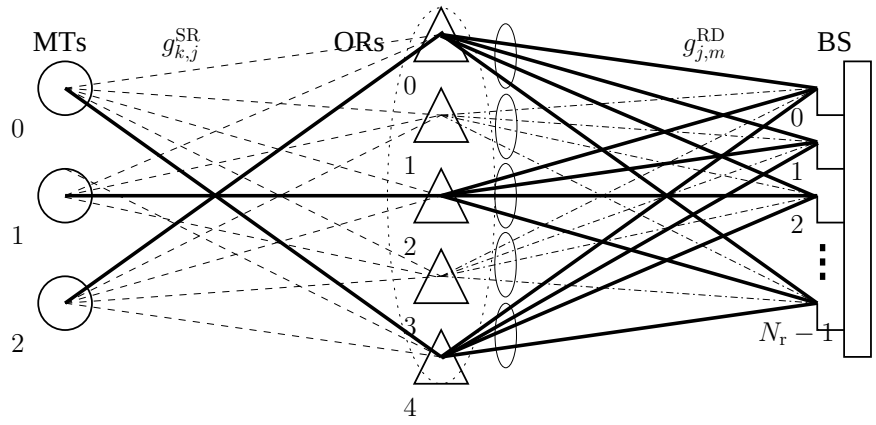

(a) Snapshot of topology

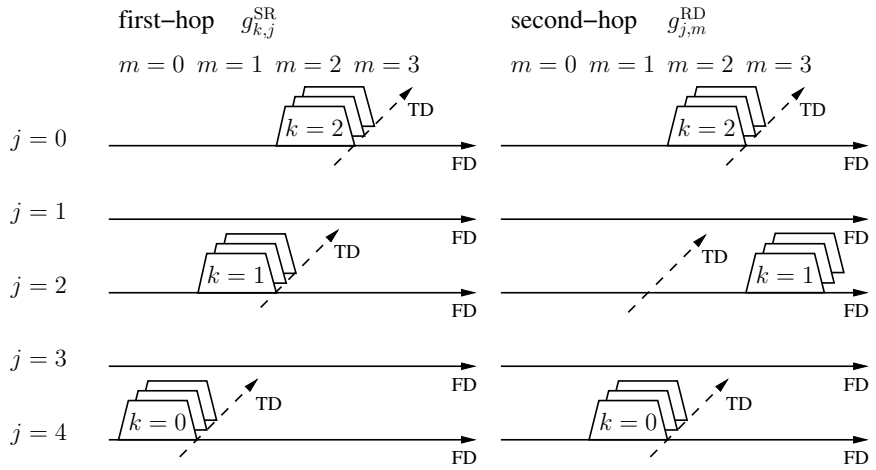

(b) Snapshot of resource block allocation

FIGURE 5.15: The illustration of *first-hop-quality-aware* (FHQA) *joint dynamic resource allocation: approach-2* (JDRA-2) for $K = 3$, $M = 4$ and $J = 5$, which may be contrasted to JDRA-1 of Figure 5.14. Briefly, their main difference is that rather than finding the best link of a specific user to a relay, in JDRA-2 we find the specific user, which can be supported by a particular relay at the best possible S-R channel quality of $g^{\mathrm{SR}}_{k,j}$. The relay selection and the user assignment of JDRA-2 are based on the first-hop quality while that of JDRA-1 are depended on the second-hop quality. By contrast, both two JDRA schemes allocate the subband groups in terms of the second-hop channel gains. The more explicit contrast is made in Figure 5.13.

The relay selection and user assignment regimes of JDRA-2 are based on the first-hop quality, while those of JDRA-1 are dependent on the second-hop quality. By contrast, both Joint DRA schemes allocate the subband groups based on the second-hop channel gains. We assume that each cooperative relay forwards its S-R CQI recorded for each of the K users to the cooperative relays' cluster-head of Figure 5.7. This head cluster relay is capable of determining, which are the K best S-R links from the entire set of (KJ) CQIs and it feeds back this information to the $(J-1)$ relays.

The flow chart of the proposed JDRA-2 algorithm is presented in Figure 5.13(b), where the

differences with respect to the previously introduced methods, such as the JDRA-1 method of Section 5.3.6, are made explicit. The differences between JDRA-1 and JDRA-2 may be further contrasted by comparing Figures 5.14 and 5.15 as well as Tables 5.8 and 5.10. Specifically, Table 5.10 provides an example of using the JDRA-2 approach, while relying on the same channel qualities as in Table 5.8. Again, the resultant snapshots of the topology as well as RB allocation are portrayed in Figure 5.15.

5.3.6.1 FHQA JDRA-2 Algorithm

Let us now elaborate on this scheme in more detail below.

First-Hop DRS: At the beginning, the best relay set $\check{\mathcal{J}}$ of the K users in set $\mathcal{K}$ and the first-hop channel gain set $\check{\mathcal{G}}^{\mathrm{SR}}$ are initialised to be empty, i.e. we have $\check{\mathcal{J}} = \varnothing$ and $\check{\mathcal{G}}^{\mathrm{SR}} = \varnothing$. By maximising the S-R channel gain $g^{\mathrm{SR}}_{k,j}$ over all relays in the set $\mathcal{J}$ for the k-th user, the best relays and the corresponding channel gains can be stored in the sets $\check{\mathcal{J}}$ and $\check{\mathcal{G}}^{\mathrm{SR}}$.

First-Hop Consideration: Furthermore, we have the ordered user set $\mathring{\mathcal{K}}$ based on the first-hop channel gains in the set $\check{\mathcal{G}}^{\mathrm{SR}}$ at the best relays in $\check{\mathcal{J}}$. Again, we initialise both the set $\mathring{\mathcal{K}}$ and the set $\mathring{\mathcal{G}}^{\mathrm{SR}}$ to be empty. Then, we obtain the i-th element in $\mathring{\mathcal{K}}$, $(i = 0, 1, \cdots, K-1)$, by seeking the maximum S-R channel gain $g^{\mathrm{SR}}_{k,\check{j}}$ among the channels spanning between all the K users and the specific relays in the set $\check{\mathcal{J}}$. Additionally, the maximum gain $g^{\mathrm{SR}}_{k,\check{j}}$ found during each iteration may be held in the ordered set $\mathring{\mathcal{G}}^{\mathrm{SR}}$, while the element $g^{\mathrm{SR}}_{\mathring{k}_i,\check{j}}$ in the set $\check{\mathcal{G}}^{\mathrm{SR}}$ is removed for the next iteration.

Second-Hop DSA: After initialisation of the ordered set of allocated subband groups $\mathring{\mathcal{M}}$ to be empty, the i-th element $\mathring{m}_i$ in the set $\mathring{\mathcal{M}}$ may be found by maximising the R-D channel gain $g^{\mathrm{RD}}_{m,\check{j}_{\mathring{k}_i}}$ in the set $\mathcal{G}^{\mathrm{RD}}_{\check{j}_{\mathring{k}_i}}$ at the $\check{j}_{\mathring{k}_i}$-th relay. We also update the contents of the sets $\mathring{\mathcal{M}}$ and $\mathcal{G}^{\mathrm{RD}}_{\check{j}_{\mathring{k}_i}}$.

User Assignment: Finally, we allocate the $\mathring{m}_i$-th subband group at relay $\check{j}_{\mathring{k}_i}$ to the $\mathring{k}_i$-th user's signal for transmission from this relay to the BS.

Therefore, the associated algorithm is summarised in Table 5.9.

5.3.6.2 An Example of FHQA JDRA-2

To elaborate on Table 5.10 a little further, let us consider again the S-R and R-D channel gains of all the $K = 3$ users, $M = 4$ subband groups and $J = 5$ relays. In the S-R link the highest gain of $g^{\mathrm{SR}}_{0,4} = 1.42$ for user $k = 0$, was found via relay $j = 4$, user $k = 1$ has $g^{\mathrm{SR}}_{1,2} = 3.07$ when relying on relay $j = 2$, while user $k = 2$ has $g^{\mathrm{SR}}_{2,0} = 2.26$ with the aid of

TABLE 5.9: *First-hop-quality-aware* (FHQA) *joint dynamic resource allocation: approach-2* (JDRA-2) algorithm

1. Initialisation:	Set $\check{\mathcal{J}} = \varnothing$, $\check{\mathcal{K}} = \varnothing$, $\check{\mathcal{G}}^{\mathrm{SR}} = \varnothing$, $\mathring{\mathcal{G}}^{\mathrm{SR}} = \varnothing$ and $\mathring{\mathcal{M}} = \varnothing$;
2. 1st-hop DRS:	For the k-th user, $\forall k \in \mathcal{K}$: (a) Obtain $\check{j}_k = \arg\max_{j\in\mathcal{J}}\{g^{\mathrm{SR}}_{k,j}\}$, (b) Update $\check{\mathcal{J}} = \check{\mathcal{J}} \cup \{\check{j}_k\}$ and $\check{\mathcal{G}}^{\mathrm{SR}} = \check{\mathcal{G}}^{\mathrm{SR}} \cup \{g^{\mathrm{SR}}_{k,\check{j}}\}$;
3. FHQA Ordering:	For $i = 0, 1, \cdots, K-1$, $\forall \check{j}_k \in \check{\mathcal{J}}$: (a) Obtain $\mathring{k}_i = \arg\max_{k\in\mathcal{K}}\{g^{\mathrm{SR}}_{k,\check{j}}\}$; (b) Update $\mathring{\mathcal{K}} = \mathring{\mathcal{K}} \cup \{\mathring{k}_i\}$, $\mathring{\mathcal{G}}^{\mathrm{SR}} = \mathring{\mathcal{G}}^{\mathrm{SR}} \cup \{g^{\mathrm{SR}}_{\mathring{k}_i,\check{j}}\}$, $\check{\mathcal{G}}^{\mathrm{SR}} = \check{\mathcal{G}}^{\mathrm{SR}} \setminus \{g^{\mathrm{SR}}_{\mathring{k}_i,\check{j}}\}$.
4. 2nd-hop DSA:	For $i = 0, 1, \cdots, K-1$, $\forall \check{j}_{\mathring{k}_i} \in \check{\mathcal{J}}$: (a) Collect $\mathcal{G}^{\mathrm{RD}}_{\check{j}_{\mathring{k}_i}} = \{g^{\mathrm{RD}}_{0,\check{j}_{\mathring{k}_i}}, g^{\mathrm{RD}}_{1,\check{j}_{\mathring{k}_i}}, \cdots, g^{\mathrm{RD}}_{M-1,\check{j}_{\mathring{k}_i}}\}$; (b) Obtain $\mathring{m}_i = \arg\max_{m\in\mathcal{M}, m\notin\mathring{\mathcal{M}}}\{g^{\mathrm{RD}}_{m,\check{j}_{\mathring{k}_i}}\}$; (c) Update $\mathring{\mathcal{M}} = \mathring{\mathcal{M}} \cup \{\mathring{m}_i\}$, $\mathcal{G}^{\mathrm{RD}}_{\check{j}_{\mathring{k}_i}} = \mathcal{G}^{\mathrm{RD}}_{\check{j}_{\mathring{k}_i}} \setminus \{g^{\mathrm{RD}}_{\mathring{m}_i,\check{j}_{\mathring{k}_i}}\}$.
5. User Assignment:	For $i = 0, 1, \cdots, K-1$: Allocate the resource pair $(\mathring{m}_i, \check{j}_{\mathring{k}_i})$ to the user $\mathring{k}_i$.

TABLE 5.10: An example of *first-hop-quality-aware* (FHQA) *joint dynamic resource allocation: approach-2* (JDRA-2) for $K = 3$, $M = 4$ and $J = 5$, which may be contrasted to JDRA-1 of Table 5.8. Explicitly, the highest S-R channel gain $g^{\mathrm{SR}}_{k,j}$ of each user in the columns of Table 5.10 are marked by underlining. Thus, by ordering the underlined values of $g^{\mathrm{SR}}_{j,k}$, JDRA-2 assigns the appropriately ordered users $k = 1$, $k = 2$ and $k = 0$ to the above-mentioned relays of $j = 2$, $j = 0$ and $j = 4$, respectively. However, the first-hop quality $g^{\mathrm{SR}}_{k,j}$ of JDRA-1 determines the order of users separately at each relay in the rows of Table 5.8. By contrast, the ordering of users in JDRA-2 allocates the RB having the highest R-D channel gain $g^{\mathrm{RD}}_{j,m}$ to the specific user at the corresponding relay. These RBs are distinguished by underlining in all subband groups observe that some RBs having the highest R-D gains in fact may not be considered, such as $g^{\mathrm{RD}}_{1,3} = \mathbf{4.41}$ and $g^{\mathrm{RD}}_{3,1} = \mathbf{2.50}$, because the DRS carried in JDRA-2 is based on the first-hop CQI.

	First-hop $g^{\mathrm{SR}}_{k,j}$			Second-hop $g^{\mathrm{RD}}_{j,m}$			
	$k=0$	$k=1$	$k=2$	$m=0$	$m=1$	$m=2$	$m=3$
$j=0$	0.05	0.53	**2.26**$^{(2nd)}$	0.04$^{(4th)}$	0.33$^{(3rd)}$	**1.90**$^{(1st)}$	0.56$^{(2nd)}$
$j=1$	0.16	0.20	0.57	0.70	1.91	0.84	**4.41**
$j=2$	0.90	**3.07**$^{(1st)}$	0.70	0.45$^{(2nd)}$	0.26$^{(4th)}$	0.28$^{(3rd)}$	**0.90**$^{(1st)}$
$j=3$	0.18	0.09	0.21	1.75	**2.50**	0.02	0.09
$j=4$	**1.42**$^{(3rd)}$	1.44	0.81	0.29$^{(2nd)}$	**1.36**$^{(1st)}$	0.17$^{(3rd)}$	0.05$^{(4th)}$
Target $(\check{j}, \check{m})$	$(4,1)$	$(2,3)$	$(0,2)$				

relay $j = 0$. The highest S-R channel gain $g^{\mathrm{SR}}_{k,j}$ of each user in the columns of Table 5.10 is marked by underlining. Thus, using ordering based on the underlined values of $g^{\mathrm{SR}}_{j,k}$, the JDRA-2 algorithm assigns the appropriately ordered users $k = 1$, $k = 2$ and $k = 0$ to the above-mentioned relays of $j = 2$, $j = 0$ and $j = 4$, respectively. However, the first-hop quality $g^{\mathrm{SR}}_{k,j}$ of JDRA-1 determines the order of the users separately at each relay in the rows of Table 5.8. By contrast, the ordering of users in JDRA-2 allocates the RB having the highest R-D channel gain to the specific user at the corresponding relay. These RBs are distinguished by underlining in all subband groups. Observe that some RBs having

the highest R-D gains in fact may not be considered, such as for example $g_{1,3}^{\mathrm{RD}} = \mathbf{4.41}$ and $g_{3,1}^{\mathrm{RD}} = \mathbf{2.50}$ of Table 5.10, because the DRS carried in JDRA-2 is based on the first-hop CQI. For instance, in Table 5.10 we have $g_{1,2}^{\mathrm{SR}} = \mathbf{3.07}^{(1st)}$ at relay $j = 2$, hence the RB of $(j, m) = (2, 1)$ having $g_{2,1}^{\mathrm{RD}} = \mathbf{0.90}$ may be allocated to user $k = 1$. Then we obtain the RBs having the gains of $g_{0,2}^{\mathrm{RD}} = \mathbf{1.90}^{(1st)}$ and $g_{4,0}^{\mathrm{RD}} = \mathbf{1.36}^{(1st)}$, which are available at the rest of the relays, namely at $j = 0$ and $j = 4$. Finally, we allocate these RBs to users $k = 2$ and $k = 0$, respectively.

5.3.7 Comparison of Resource Allocation for Opportunistic Relaying

Having described the principles of the above-mentioned OR-aided resource allocation schemes, let us now embank on a comparative discussion.

Firstly, Table 5.11 summarises the information to be exchanged among the relays relying on the MWR principle of Figure 5.7. It is clear that the differences are related to the amount of the knowledge required concerning the S-R links. Specifically, the JDRA-1 scheme only requires each relay's ordered set of K users, as determined by their S-R channel gains. The JDRA-1 aided relays' cluster-head determines the ordering of user assignment depending on the R-D channel quality. By contrast, the JDRA-2 mode considers the pilot-based CQI of all S-R links gleaned from each relay, in order to find the optimal relay for each user with respect to the associated first-hop quality. In other words, the ordering of users is also determined by the JDRA-2 assisted relays' cluster-head based on their S-R channel quality.

Secondly, the benefits of exploiting the best RBs indicated by boldfaced values and the actually allocated RBs marked by the underlined values of $g_{k,j}^{\mathrm{SR}}$ and $g_{j,m}^{\mathrm{RD}}$ in both Table 5.8 and Table 5.10 will be investigated. We found that the JDRA-1 scheme allocates most subband groups to the R-D channels associated with the values printed in boldface, while the JDRA-2 approach assigns the highest-quality S-R channels.

As described in Section 5.3.5 and 5.3.6, both FHQA JDRA schemes have three main functions, namely the relay selection, subband allocation and user assignment. Explicitly, for both JDRA schemes, the subband allocation is based on the second-hop quality, while the user assignment depends on the first-hop quality. The relay selection of JDRA-1 is based on the second-hop quality, while that of JDRA-2 relies on the first-hop quality. Therefore, the JDRA-1 method predominantly relies on the second-hop quality, while JDRA-2 on the first-hop quality. As a result, the attainable performance of both JDRA-1 and JDRA-2 is limited by the quality of its dominant channels.

Additionally, the computational complexity of a single-user system, of a lightly loaded system associated with $K < M$, and finally, of a fully loaded system having $K = M$ and

TABLE 5.11: Information Exchange Amongst Joint DRA aided Cooperative Relays

Mode	Strategy	Exchanged Information
JDRA-1	MWR	$\breve{\mathcal{K}}_j$ or $\breve{\mathcal{G}}_j^{\mathrm{SR}}$, and $g_{j,m}^{\mathrm{RD}}$, $(m \in \mathcal{M})$
JDRA-2	MWR	$g_{k,j}^{\mathrm{SR}}$, $(k \in \mathcal{K})$ and $g_{j,m}^{\mathrm{RD}}$, $(m \in \mathcal{M})$

TABLE 5.12: Complexity comparison of single-user systems ($K = 1$)

Mode	Proposed Solution	Exhaustive Search
RRS-SSA	$\mathcal{O}\{0\}$	$\mathcal{O}\{0\}$
DRS-SSA	$\mathcal{O}\{J-1\}$	$\mathcal{O}\{J!\}$
DRS-DSA	$< \mathcal{O}\{M(J-1) + M\log M\}$	$\mathcal{O}\{MJ! + M\}$
JDRA-1	$< \mathcal{O}\{M(J-1) + M\log M\}$	$\mathcal{O}\{J + MJ! + M\}$
JDRA-2	$< \mathcal{O}\{J-1+JM\log M\}$	$\mathcal{O}\{J! + 1 + JM\}$

TABLE 5.13: Complexity comparison of lightly-loaded multi-user systems ($K < M$)

Mode	Proposed Solution	Exhaustive Search
RRS-SSA	$\mathcal{O}\{0\}$	$\mathcal{O}\{0\}$
DRS-SSA	$\mathcal{O}\{K(J-1)\}$	$\mathcal{O}\{KJ!\}$
DRS-DSA	$\leq \mathcal{O}\{M(J-1) + M\log M\}$	$\mathcal{O}\{MJ! + \mathrm{P}_K^M\}$
JDRA-1	$\leq \mathcal{O}\{JK\log K + M(J-1) + M\log M\}$	$\mathcal{O}\{JK! + MJ! + \mathrm{P}_K^M\}$
JDRA-2	$\leq \mathcal{O}\{K(J-1) + K\log K + JM\log M\}$	$\mathcal{O}\{KJ! + K! + J\mathrm{P}_K^M\}$

TABLE 5.14: Complexity comparison of full-Load multi-user systems ($K = M$)

Mode	Proposed Solution	Exhaustive Search
RRS-SSA	$\mathcal{O}\{0\}$	$\mathcal{O}\{0\}$
DRS-SSA	$\mathcal{O}\{M(J-1)\}$	$\mathcal{O}\{MJ!\}$
DRS-DSA	$\mathcal{O}\{M(J-1) + M\log M\}$	$\mathcal{O}\{MJ! + M!\}$
JDRA-1, 2	$\mathcal{O}\{M(J-1) + (J+1)M\log M\}$	$\mathcal{O}\{MJ! + (J+1)M!\}$

employing various OR-aided resource allocation schemes is presented in Tables 5.13, 5.12 and 5.14, respectively. Specifically, the complexity of our proposed JDRA schemes is linearly increased upon increasing J. By contrast, for a given J, we infer from Tables 5.12, 5.13 and 5.14 that the order of complexity $\mathcal{O}$ versus M relationship is linear.

5.4 Simulation Results and Discussions

In this section, the performance achieved by the various resource allocation schemes relying on both AF and DF aided OR is characterised in the context of both uncoded and channel-coded SC-FDMA systems upon varying the fading channel conditions. The basic assumptions of our channel model are summarised in Table 5.15, where diverse multi-path

TABLE 5.15: Channel Model of Opportunistic Relaying

S-D fading	No S-D link
S-R, R-D fading	Frequency-selective Rayleigh
Power delay spread	Uniform
Shadowing	Not considered ($\sigma_\xi^2 = 0$ dB)
Path-loss	$G_{\mathrm{SR}} = G_{\mathrm{RD}} = 0.5^{-4}$

TABLE 5.16: Modulation and Coding Parameters

	Uncoded system	Coded system
Modulation	4-QAM	4-QAM
Labelling	Gray	Set-partitioning (SP)
FEC coding	Non	RSC (2,1,3), $R_{\mathrm{c}} = 1/2$

fading channels are considered along with various system configurations. We analyse the attainable performance in terms of the *bit error rate* (BER) of the modulation and coding schemes summarised in Table 5.16. When the system operated at a given BER and information rate, the energy-efficiency may be quantified in terms of the associated energy consumption metrics [1, 199] of Section 5.4.1 by comparing the total transmit energy per bit, i.e. E_b/N_0, required by the reference system to that of the system under test.

5.4.1 Energy Efficiency Evaluation

Let us now evaluate the *energy efficiency* of both the DT and of the proposed OR schemes at the physical layer, when considering the energy consumption due to CQI exchange among relays[9]. Let $r_k^{(\cdot)}, r_\Sigma^{(\cdot)}$ denote the coding and modulation rate of the $(\cdot)$-type transmissions, i.e. that of DT or OR, for the SU and MU scenarios, respectively.

Since we have a block duration of T_{v} for each RV as seen in Figure 5.9, T_{v} pilot RV overhead per RB duration of $N_{\mathrm{rv}}T_{\mathrm{v}}$ may be used for channel estimation for each first-hop and second-hop transmissions. Hence, we have an *overhead-to-data ratio* expressed as

$$\frac{2T_{\mathrm{v}}}{(2N_{\mathrm{rv}} - 2)T_{\mathrm{v}}} = \frac{1}{N_{\mathrm{rv}} - 1}. \tag{5.30}$$

[9]When evaluating the achievable energy-efficiency, the half-rate difference imposed by two-hop relaying was indeed taken into account in terms of the Eq. (5.33). Therefore, we arrived at a fair comparison between the OR and DT scenarios in terms of the ECG formulated in Eq. (5.34).

Furthermore, the *energy consumption per bit* of the DT scheme may be expressed as

$$\begin{aligned}\varepsilon_{\mathrm{DT}} &= \frac{\sum_{k=0}^{K-1} P_k T}{\sum_{k=0}^{K-1} r_k^{\mathrm{DT}}(T - N_{\mathrm{rb}} T_{\mathrm{v}})} \\ &= \frac{P_{\Sigma}^{\mathrm{DT}} N_{\mathrm{rv}}}{r_{\Sigma}^{\mathrm{DT}}(N_{\mathrm{rv}} - 1)} \quad (J/bit),\end{aligned} \tag{5.31}$$

where $T = N_{\mathrm{rb}} N_{\mathrm{rv}} T_{\mathrm{v}}$ denotes the time duration per hop within a frame, including the channel estimation overheads.

By contrast, in addition to the channel estimation overhead, our proposed two-hop FHQA JDRA based OR scheme requires a further $2T_{\mathrm{v}}$ RVs for exchanging the CQI per RB. Hence, we have a total overhead-to-data ratio expressed as

$$\frac{4T_{\mathrm{v}}}{(2N_{\mathrm{rv}} - 4)T_{\mathrm{v}}} = \frac{2}{N_{\mathrm{rv}} - 2}. \tag{5.32}$$

Moreover, the corresponding energy consumption per bit of the two-hop OR scheme including the above-mentioned total overheads may be expressed as

$$\begin{aligned}\varepsilon_{\mathrm{OR}} &= \frac{\sum_{k=0}^{K-1}(P_k^{\mathrm{S}} + P_k^{\mathrm{R}})T + \sum_{k=0}^{K-1} P_k^{\mathrm{R}}(2N_{\mathrm{rb}} T_{\mathrm{v}})}{\sum_{k=0}^{K-1} 2r_k^{\mathrm{OR}}(T - N_{\mathrm{rb}} T_{\mathrm{v}})} \\ &= \frac{P_{\Sigma}^{\mathrm{OR}}(N_{\mathrm{rv}} + 1)}{r_{\Sigma}^{\mathrm{DT}}(N_{\mathrm{rv}} - 1)} \quad (J/bit),\end{aligned} \tag{5.33}$$

where we have $P_k^{\mathrm{S}} = P_k^{\mathrm{R}} = 0.5P_{\Sigma}/K$, and $r_k^{\mathrm{OR}} = r_k^{\mathrm{DT}}/2 = R_c Q/2$.

We define the power reduction $\gamma_{\mathrm{b}}^{\Delta}$ per bit as the *SNR reduction per bit*, i.e. we have $\gamma_{\mathrm{b}}^{\Delta} = \gamma_{\mathrm{b}}^{\mathrm{DT}} - \gamma_{\mathrm{b}}^{\mathrm{OR}}$ dB, where $\gamma_{\mathrm{b}}^{(\cdot)}$ denotes the E_b/N_0 of the $(\cdot)$-type scheme at a given BER[10]. Moreover, by using the DT as a reference as defined in [1], the relative ECG of our proposed OR may be expressed as

$$ECG = \frac{\varepsilon_{\mathrm{DT}}}{\varepsilon_{\mathrm{OR}}} = \frac{P_{\Sigma}^{\mathrm{DT}} N_{\mathrm{rv}}}{P_{\Sigma}^{\mathrm{OR}}(N_{\mathrm{rv}} + 1)} = \frac{10^{\gamma_{\mathrm{b}}^{\Delta}/10} N_{\mathrm{rv}}}{N_{\mathrm{rv}} + 1}. \tag{5.34}$$

5.4.2 Performance of DRA aided AF Opportunistic Relaying over Uncorrelated Fading Channels

In this section, we consider the various resource allocation schemes of Section 5.3 that are applied by the AF OR based uncoded SC-FDMA uplink, while using the simulation parameters of Table 5.17.

[10] E_{b} denotes the total energy per bit transmitted by the source and the relay per user-signal, which is normalised to unity, while N_0 is the noise power spectral density at the receiver, which is assumed to be the same for all the relays and the BS receivers. Hence, E_{b}/N_0 represents the *average SNR per bit*.

TABLE 5.17: Resource Allocation for OR

Channel model	Uncorrelated
Relaying protocol	AF or DF
Relay selection	Static or dynamic
Subband mapping	Localised
Subband allocation	Static or dynamic
Number of subbands per user	$N = 12$
Bandwidth expansion factor	$M = 6$
Total number of subbands	$U = 72$
Number of source users	$K = 6$
Number of relay candidates	$J = 6$
Number of paths	$L = 4$
Number of RV per RB	$N_{\text{rv}} = 1$
Transmit power	$P_k^{\text{S}} = P_k^{\text{R}} = 0.5$
Number of BS receiver antennas	$N_{\text{r}} = 1, 8$

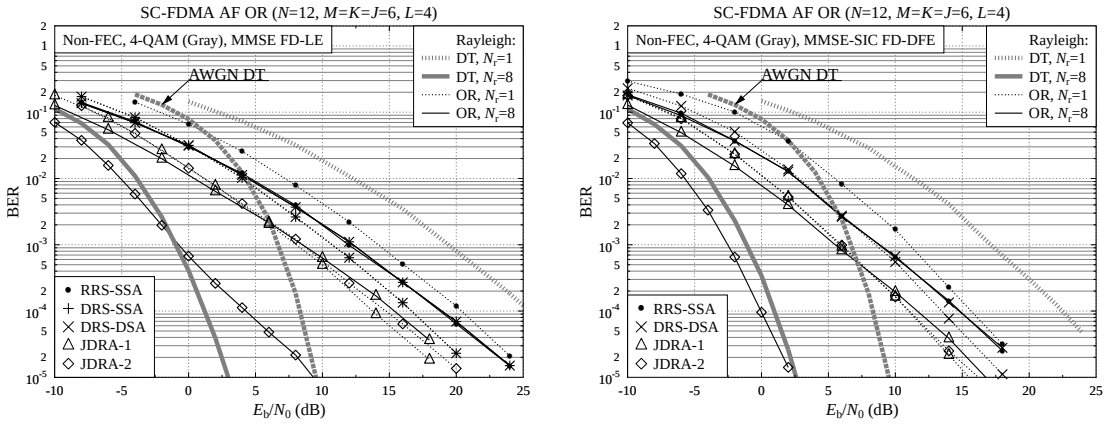

(a) Classic MMSE FD-LE (b) MMSE-SIC FD-DFE

FIGURE 5.16: BER versus E_b/N_0 performance of the AF OR based uncoded SC-FDMA uplink for $N_{\text{r}} = 1$ and 8 upon varying the resource allocation schemes compared to its DT benchmark, where the BS's receiver invokes (a) the classic MMSE FD-LE of Figure 2.12 or (b) the MMSE-SIC FD-DFE of Figure 5.5. The channel and system parameters are summarised in Tables 5.15, 5.16 and 5.17.

Figure 5.16 depicts the performance of the SC-FDMA uplink using the receiver of Figure 5.5 [86,87] in the context of the uncoded AF OR system of Figure 5.1 upon varying the resource allocation schemes compared to its DT benchmark, for $N_{\text{r}} = 1$ and 8 at the BS[11]. When a low-complexity single-stage MMSE receiver is invoked, the FD-DFE receiver degenerates to the classic single-tap MMSE FD-LE of Figure 2.12 and its performance is characterised in Figure 5.16(a), while the performance of the MMSE-SIC FD-DFE scheme is characterised

[11]According to [23], when coherent combining is invoked at the receiver, the multiple receive antennas spaced sufficiently far apart may actually provide both a power gain and a diversity gain. Specifically, the effective power gain of the received signal is increased linearly with the number of receive antennas N_{r}. Furthermore, the diversity gain of a diversity order of N_{r} is reflected by converging the combination of the N_{r}-branch channel gains to 1 with increasing N_{r}, where the fading variance of each channel is normalised to unity. For example, when $N_{\text{r}} = 8$, the DT system is capable of achieving a power gain of 9 dB and a diversity gain of upto 15 dB, as shown in Figure 5.16.

in Figure 5.16(b).

When the number of dispersive paths is $L = 4$, the system suffers from residual ISI, which cannot be entirely eliminated by a classic FD-LE receiver. By observing Figure 5.16(b) to 5.16(a), we observe that the proposed MMSE-SIC FD-DFE enhances the OR system's performance by up to 5 dB at the BER of 10^{-4} compared to the conventional MMSE FD-LE. Specifically, when the multi-user system operates at full user load, i.e. we have $K = M$, the SSA of Section 5.3.3 achieves the same performance as the DSA arrangement of Section 5.3.4 combined with DRS. By invoking a single-antenna BS receiver, the DRS-SSA scheme of Figure 5.11 in Section 5.3.3 and DRS-DSA scheme of Figure 5.12 detailed in Section 5.3.4 attain a power gain of about 2.5 dB over the RRS benchmark at a BER of 10^{-4}, while both of our proposed JDRA schemes perform similarly and attain an approximately 2.5 dB additional power gain compared to the DRS scheme of Sections 5.3.3 and 5.3.4.

By contrast, the multiple-antenna BS invoked in our system offers receive diversity gains. The fading-induced variation of $g_{j,m}^{\mathrm{RD}}$ is beneficially reduced, when assuming an increased number of N_{r} independent channel attenuations averaged over the m-th subband group for the multi-path channel between the j-th relay and the BS. Therefore, the achievable selection diversity gain of using J R-D channels is reduced in the absence of shadowing. As a result, the DRS-SSA and DRS-DSA schemes detailed in Section 5.3.3 and 5.3.4 have more-or-less the same performance as the RRS-SSA mentioned in Section 5.3.3, which implies that the gain gleaned from selection diversity over the R-D channels cannot be attained in the multi-antenna scenario. However, the proposed FHQA JDRA methods of Section 5.3.5 and Section 5.3.6 are capable of achieving an additional gain by rearranging the resources at the ORs by appropriately exploiting the S-R link quality. Importantly, by invoking the JDRA-2 of Section 5.3.6, the first-hop quality becomes the dominant factor in determining the achievable performance benefits of exchanging CQI between the cooperating relays, as we discussed in Section 5.3.7. At a BER of 10^{-4}, we note that JDRA-2 and JDRA-1 attain gains of 14 dB and 3 dB compared to their conventional counterparts, respectively.

By contrast, Figure 5.17 characterises the half-rate RSC coded AF OR based BICM SC-FDMA using the turbo FD-LE of Figure 5.4 [88–90] combined with BICM-ID, where '0-iteration' refers to the classic non-iterative FD-LE of Figure 5.17(a). Note that, in the context of BICM aided SC-FDMA system using $N_{\mathrm{r}} = 8$, the JDRA-2 scheme offers an additional 3 dB gain over the JDRA-1 approach and also saves up to 2 dB transmit power compared to the DT benchmark.

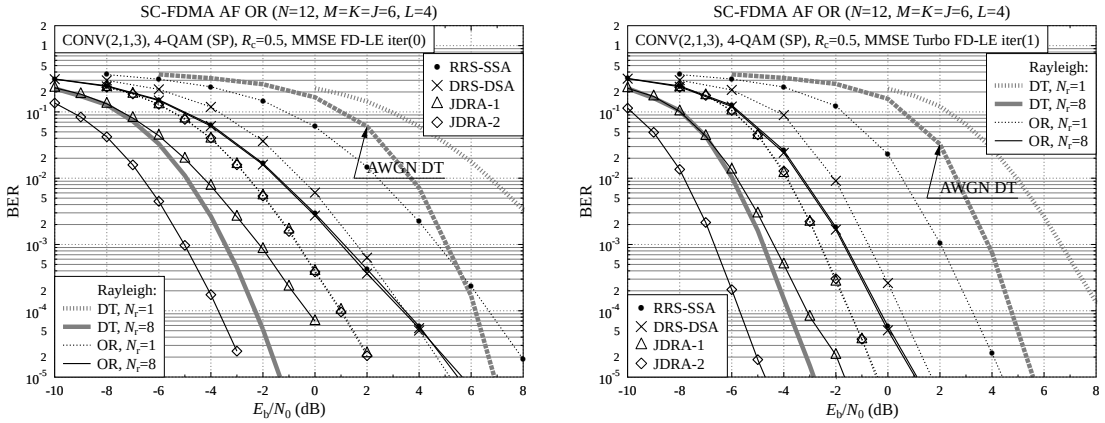

(a) Classic MMSE FD-LE (0-iteration) (b) MMSE turbo FD-LE (1-iteration)

FIGURE 5.17: BER versus E_b/N_0 performance of the AF OR based BICM SC-FDMA uplink for $N_r = 1$ and 8 upon varying the resource allocation schemes compared to its DT benchmark, where the BS's receiver invokes (a) the classic MMSE FD-LE of Figure 2.12 or (b) the MMSE turbo FD-LE of Figure 5.4. The channel and system parameters are summarised in Tables 5.15, 5.16 and 5.17.

TABLE 5.18: MMSE Turbo FD-LE modes

	Relay	BS
0-iteration	Figure 5.18(a), Figure 5.18(b)	Figure 5.18(a), Figure 5.19(a)
1-iteration	Figure 5.19(a), Figure 5.19(b)	Figure 5.18(b), Figure 5.19(b)

5.4.3 BER Performance of DRA aided DF Opportunistic Relaying over Uncorrelated Fading Channels

In this section, we evaluate the performance of the resource allocation approaches of Section 5.3 that are employed by the DF OR based SC-FDMA uplink. The half-rate RSC-coded SC-FDMA scheme of Figure 5.2 invokes the MMSE turbo FD-LE relying on the BICM-ID scheme discussed in Section 2.3.2 which is used both at the relay's and the BS's receivers, where '0-iteration' refers to the classic non-iterative FD-LE. The MMSE turbo FD-LE configurations employed are summarised in Table 5.18, while their parameters are summarised in Table 5.17.

Firstly, let us consider the BS's receiver using a single antenna. Figures 5.18 and 5.19 characterise the DF-relay of Section 5.2.3.4 operating with aid of either hard-decision or soft-decision and denoted as 'hard-DF' and 'soft-DF', respectively. As expected, the hard-DF has a lower BER performance compared to soft-DF, since hard-DF typically introduces more dramatic error propagation at the relay. Furthermore, the attainable performance of the hard-DF or of the soft-DF schemes seen in Figure 5.18 may remain the same, when using a non-iterative FD-LE at the relay, regardless of the number of iterations used at

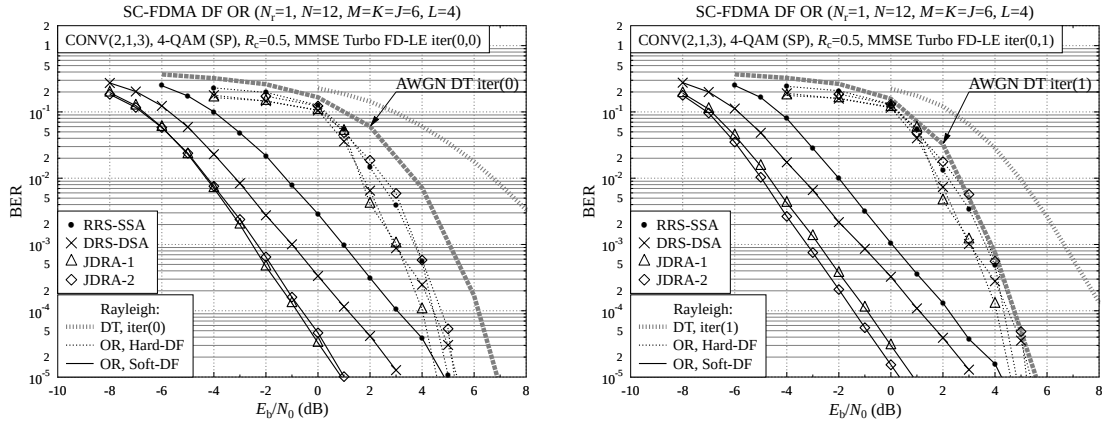

(a) Classic MMSE FD-LE (0 iteration) (b) MMSE turbo FD-LE (1 iteration)

FIGURE 5.18: BER versus E_b/N_0 performance of the soft-decision aided DF OR based BICM SC-FDMA uplink for $N_r = 1$ upon varying the resource allocation schemes compared to its hard-decision based DF benchmark, when the relay's receiver uses the classic MMSE FD-LE (0-iteration) of Figure 5.4, while the BS's receiver invokes (a) the classic MMSE FD-LE of Figure 2.12 or (b) the MMSE turbo FD-LE (1-iteration) of Figure 5.4. The channel and system parameters are summarised in Tables 5.15, 5.16 and 5.17.

the BS's receiver. By contrast, observe in Figure 5.19 that the substantial performance enhancements may be attained by the turbo FD-LE upon increasing the number of iterations at the relay. This is because carrying out iterative joint equalisation and decoding at the relay mitigates the ISI and eliminates the potential error propagation during relaying. Additionally, observe in Figure 5.19(a) that the JDRA-1 scheme of Section 5.3.5 outperforms the JDRA-2 approach of Section 5.3.6, when the residual ISI inflicted upon the R-D links cannot be removed by the non-iterative FD-LE at the BS's receiver. The reason for this phenomenon is that the JDRA-2 scheme selects the best relays in terms of the S-R channel quality, albeit these relays may not provide the best resources associated with high channel gains for the R-D links.

By contrast, when invoking a multi-antenna aided BS, Figure 5.20 characterises the BER versus E_b/N_0 performance of the various resource allocation schemes for the soft-DF based OR systems using the turbo FD-LE. Similar to the single-antenna scenario for $N_r = 1$ of Figure 5.19, a substantial performance enhancement is provided by the turbo FD-LE with aid of iterative detection at the relay, which prevents the introduction of residual ISI-induced error propagation during the second hop. Specifically, when we have $N_r = 8$ as in Figure 5.20(b), the proposed JDRA-1 and JDRA-2 schemes invoking the turbo FD-LE of Figure 5.4 at both the relay and the BS attain a 1.5 and 3 dB gain over the conventional schemes at a BER of 10^{-4}, respectively.

Additionally, Figure 5.21 characterises the performance of the various resource allocation schemes that are applied to the soft-DF based OR SC-FDMA using the turbo FD-LE of

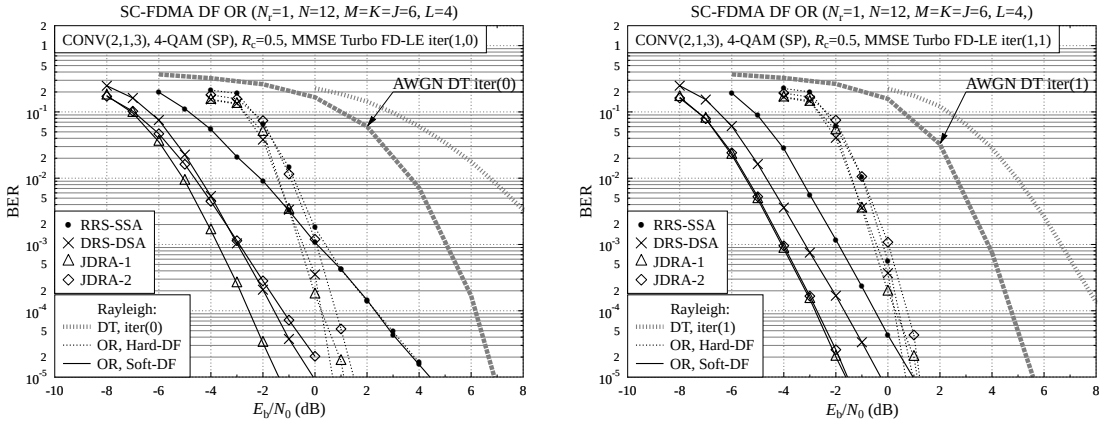

(a) Classic MMSE FD-LE (0 iteration) (b) MMSE turbo FD-LE (1 iteration)

FIGURE 5.19: BER versus E_b/N_0 performance of the soft-decision aided DF OR based BICM SC-FDMA uplink for $N_r = 1$ upon varying the resource allocation schemes compared to its hard-decision based DF benchmark, when the relay's receiver uses the MMSE turbo FD-LE (1-iteration) of Figure 5.4 relying on the BICM-ID, while the BS's receiver invokes (a) the classic MMSE FD-LE (0-iteration) of Figure 2.12 or (b) the MMSE turbo FD-LE of Figure 5.4. The channel and system parameters are summarised in Tables 5.15, 5.16 and 5.17.

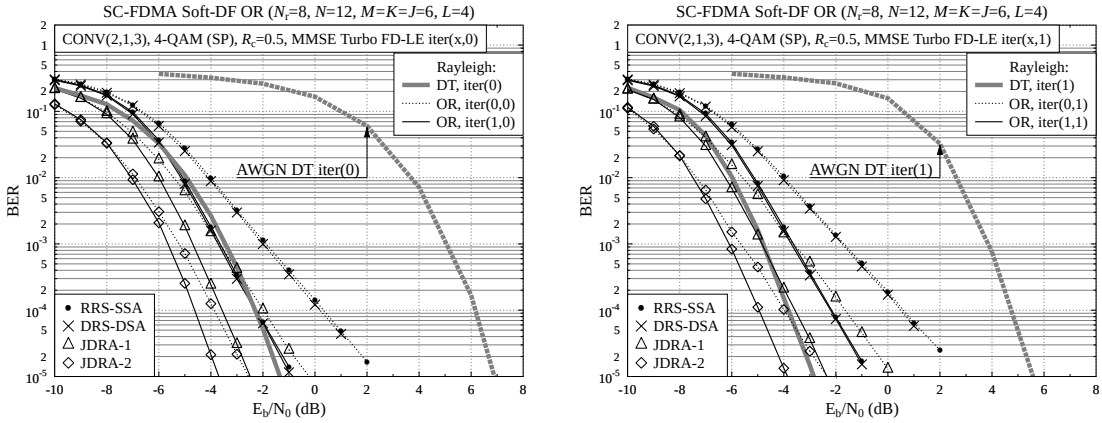

(a) Classic MMSE FD-LE (0-iteration) (b) MMSE turbo FD-LE (1 iteration)

FIGURE 5.20: BER versus E_b/N_0 performance of the soft-decision aided DF based BICM OR SC-FDMA uplink for $N_r = 8$ upon varying the resource allocation schemes, when the BS's receiver invokes (a) the classic MMSE FD-LE (0-iteration) of Figure 2.12 compared to (b) the MMSE turbo FD-LE (1-iteration) of Figure 5.4, where the relay's receiver invokes either the classic MMSE FD-LE of Figure 2.12 or the MMSE turbo FD-LE of Figure 5.4. The channel and system parameters are summarised in Tables 5.15, 5.16 and 5.17.

Figure 5.4 at both the relay's and the BS's receivers, compared to their channel-coded DT benchmark for $N_r = 1$ and 8. The achievable transmit power reductions per bit γ_b^{Δ} recorded at the BER of 10^{-4} are summarised in Table 5.20.

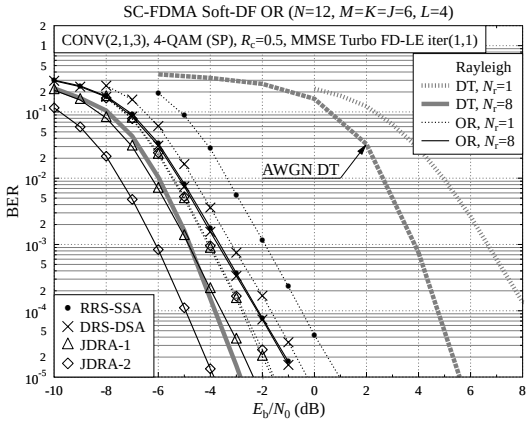

FIGURE 5.21: BER versus E_b/N_0 performance of the soft-decision aided DF based BICM OR SC-FDMA uplink for $N_\mathrm{r} = 1$ and 8 upon varying the resource allocation schemes compared to its DT benchmark, where both the relay's and the BS's receiver invoke the MMSE turbo FD-LE (1-iteration) of Figure 5.4. The channel and system parameters are summarised in Tables 5.15, 5.16 and 5.17.

TABLE 5.19: Energy-efficiency comparison of OR based uncoded SC-FDMA

		γ_b^Δ (dB)		*ECG*	
	N_r	1	8	1	8
DT	-	0	0	0	0
RRS-SSA	AF	6.5	−14	4.47	0.04
DRS-DSA	AF	8.5	−14	7.08	0.04
JDRA-1	AF	11.5	−11	14.13	0.08
JDRA-2	AF	11.5	1	14.13	1.26

5.4.4 Energy-Efficiency of DRA Aided OR based SC-FDMA over Uncorrelated Fading Channels

Let us now discuss the energy consumption metrics, namely the ECG of Section 5.4.1. The attainable power reductions per bit γ_b^Δ are summarised in Table 5.19 and 5.20. In Table 5.20, we ignore the energy dissipated by the relatively short duration of the pilot-aided channel estimation and CQI exchange. Specifically, for $N_\mathrm{r} = 1$, the proposed JDRA schemes are capable of achieving an ECG of upto 14.1 compared to the DT benchmark. By contrast, for $N_\mathrm{r} = 8$, our proposed JDRA-2 aided OR scheme attained an ECG of 1.6, while the other methods may not succeed in reducing the transmit power compared to DT. Furthermore, in Table 5.21, we take the energy consumption during the pilots-based CQI exchange into account, hence we have a ECG of upto 12.6 for $N_\mathrm{r} = 1$ and a ECG of upto 1.6 for $N_\mathrm{r} = 8$. The reason for this is that multiple-antenna aided reception provides a substantial receive diversity gain by exploiting the independent fading of N_r antennas. Therefore, the DRS-DSA method's benefits of assigning the most appropriate resources to multiple users erode and hence it results in a similar performance to that of the RRS-SSA scheme of Section 5.3.3.

TABLE 5.20: Energy-efficiency comparison of OR based BICM SC-FDMA using turbo receiver for $N_{\mathrm{rv}} = 1$, when ignoring the energy dissipated by the pilots-based CQI exchange.

		$\gamma_{\mathrm{b}}^{\Delta}$ (dB)		*ECG*	
	N_{r}	1	8	1	8
DT	-	0	0	0	0
RRS-SSA	AF	5	−3.5	3.16	0.45
	DF	8.75	−1.5	7.5	0.71
DRS-DSA	AF	7.5	−3.5	5.62	0.45
	DF	10	−1.5	10	0.71
JDRA-1	AF	9.5	−1	8.91	0.79
	DF	11	−0.25	12.6	0.94
JDRA-2	AF	9.5	2	8.91	1.58
	DF	11	1	12.6	1.26

TABLE 5.21: Energy-efficiency comparison of OR based BICM SC-FDMA using turbo receiver for $N_{\mathrm{rv}} = 6$, when considering on the energy dissipated by the pilots-based CQI exchange.

		$\gamma_{\mathrm{b}}^{\Delta}$ (dB)	*ECG*		
	N_{r}	1	8	1	8
DT		0	0	1	1
JDRA-1	AF	9.5	−1	7.63	0.68
	DF	11	−0.25	10.79	0.80
JDRA-2	AF	9.5	2	7.63	1.35
	DF	11	1	10.79	1.08

TABLE 5.22: Resource Allocation of RRS-RSA aided Soft-DF-OR

Common	$N = 12, M = K = N_{\mathrm{rv}} = 6$, L=4, $J = 1, 2, 4$ and 8
Figure 5.22(a)	$N_{\mathrm{r}} = 1, N_{\mathrm{c}} = 720$
Figure 5.22(b)	$N_{\mathrm{r}} = 1, N_{\mathrm{c}} = 7200$

Additionally, as discussed in Section 5.4.2, the second-hop quality becomes the dominant factor in determining the performance by invoking the JDRA-1 approach.

5.4.5 BER Performance of DF Based OR versus the Interleaver Length over Correlated Fading Channels

Let us initially consider the effects of varying the number of candidate relays J and the normalised Doppler frequency of f_{nd} for $N_{\mathrm{rv}} = 6$. Figures 5.22(a) and 5.22(b) depict the BER versus E_b/N_0 performance of soft-DF based BICM OR SC-FDMA operating with the aid of the RRS-SSA scheme for the interleaver lengths of $N_{\mathrm{c}} = 720$ and 7200 coded bits per frame, respectively. Since both DRS and DSA offer selection diversity gains, we adopted a low-complexity RRS scheme for OR in order to characterise the advantages of OR and the impact of the interleaver depth N_{c} on SC-FDMA employing the turbo FD-LE of Figure 5.4.

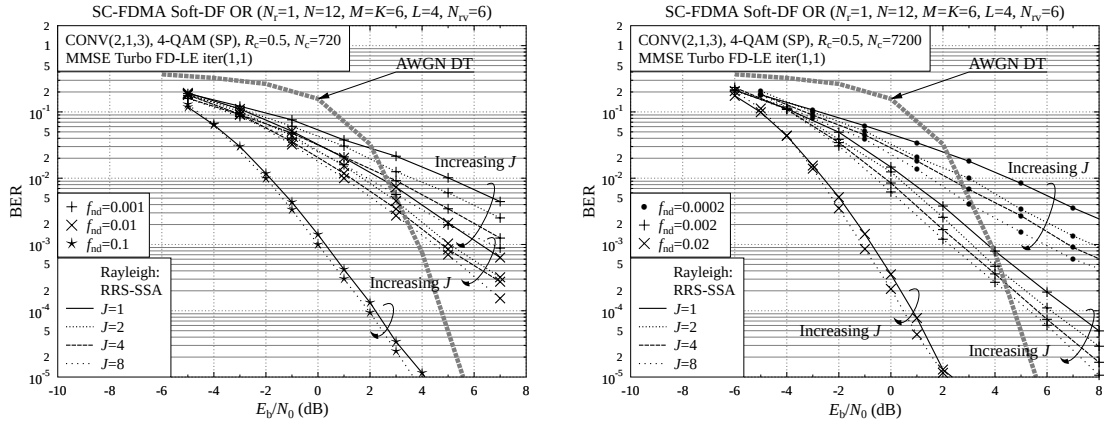

(a) $N_c = 720$ and $f_{nd} = 0.001, 0.01, 0.1$ (b) $N_c = 7200$ and $f_{nd} = 0.0002, 0.002, 0.02$

FIGURE 5.22: BER versus E_b/N_0 performance of RRS-SSA aided Soft-DF based BICM OR SC-FDMA uplink upon varying the number of relays $J = 1, 2, 4$ and 8 subject to various normalised Doppler frequency f_{nd}, where we have the number of RV of $N_{rv} = 6$ and the interleaver length of $N_c = 720$ and 7200 coded bits per frame, respectively. The channel and system parameters are summarised in Tables 5.15, 5.16 and 5.22.

TABLE 5.23: Resource Allocation of Section 5.4.6

Common	$N_r = 1, N = 12, L = 4, N_{rv} = 6, N_c = 7200, f_{nd=0.02}$
Figure 5.24(a)	$M = 12, J = 6$, varying K and DRAs
Figure 5.24(b)	$M = K = 6$, JDRA-1, varying J

Specifically, the performance of single-relay aided RSC-coded SC-FDMA for $J = 1$ degrades, when the fading channel suffers from an increased TD correlation associated with a reduced normalised Doppler frequency f_{nd}. This scenario may result in a burst of errors within a coded bit stream associated with a length of N_c over prolonged fades, where the interleaver having a limited depth is no longer effective. However, when increasing J at a given f_{nd} and N_c, the fading of OR channels becomes more spatially independent, leading to an improved BER performance. Hence, the transmit energy per bit may be reduced. Therefore, rather than using a long interleaver having a large buffering delay, the shorter interleaver based DF-OR may be considered, particularly for real-time inter-active lip-synchronised video applications subject to limited buffering delay [214].

5.4.6 BER Performance of DRA aided OR versus the Number of Users and Relays

In this section, we quantify the impact of the number of source MTs K and that of the candidate relays J involved in the various resource allocation schemes on the achievable BER performance, when communicating over both uncorrelated and correlated fading channels in Figure 5.23 and Figure 5.24, respectively. The simulation parameters are given in Table

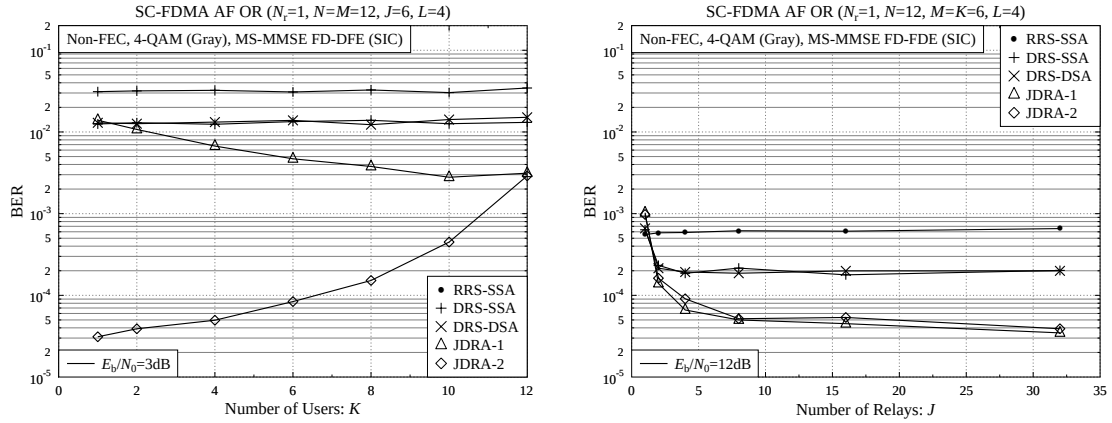

(a) Effects of the number of source users K at $E_b/N_0 = 3$ dB

(b) Effects of the number of candidate relays J at $E_b/N_0 = 12$ dB

FIGURE 5.23: BER performance comparison of the various resource allocation schemes of Section 5.3 over uncorrelated fading channels. The system schematic of Figure 5.5 and the parameters of Tables 5.15, 5.16 and 5.23 were used.

5.23.

Since the design of the JDRA-1 scheme was further developed in Section 5.3.5 from the DRS-DSA by invoking user ordering based on their first-hop quality, observe by comparing Figure 5.23(a) that its single-user BER performance remains the same as that of DRS-DSA. However, the BER performance of JDRA-1 was found to be better in Figure 5.23(a) than that of DRS-DSA, when the multi-user system operated at its full user load. In contrast to JDRA-1, observe in Figure 5.23(a) that the JDRA-2 scheme guarantees that the best relay is assigned to each user before DSA, which results in a significantly reduced BER for the single-user scenario, while exhibiting the same performance for the full-load multi-user scenario. Furthermore, as evidenced by Figure 5.23(b), both JDRA schemes maximise the benefits of all the candidate relays involved in DRA, hence providing a better performance than the conventional schemes, upon increasing J.

5.4.7 Complexity of DRA aided OR versus the Number of Relays and the Bandwidth Expansion Factor

Last but not least, Figure 5.25 characterises the computational complexity in terms of the number of comparisons $\mathcal{O}$ within each resource allocation scheme for both single-user and full-load multi-user systems according to Tables 5.12 and 5.14. The complexity of our proposed JDRA schemes is linearly increased upon increasing J, as shown in Figure 5.25(a). By contrast, upon observing Figure 5.25(b) for a given J, we infer that the $\mathcal{O}$ versus M relationship is linear. Practically, by taking into account the results of Figures 5.23 and 5.24, we can strike an attractive trade-off between the performance achieved and the complexity

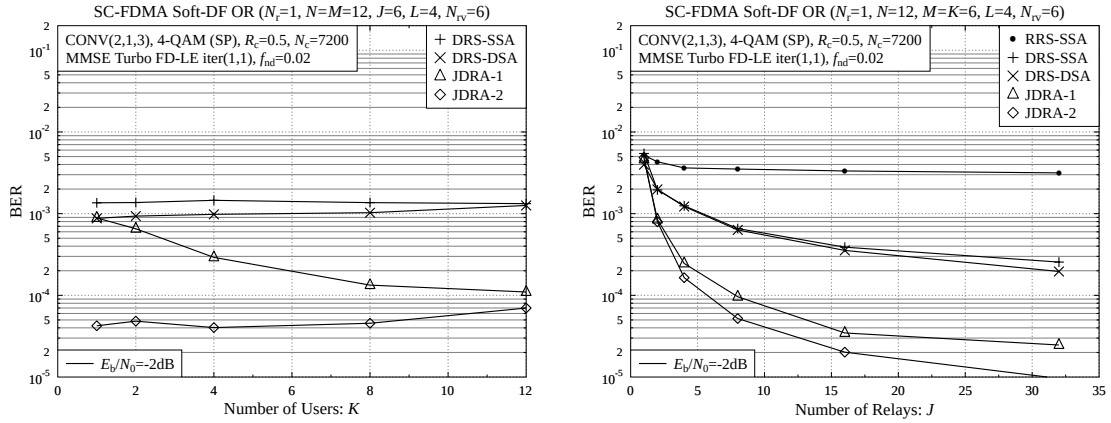

(a) Effects of the number of source users K at $E_b/N_0 = -2$ dB

(b) Effects of the number of candidate relays J at $E_b/N_0 = -2$ dB

FIGURE 5.24: BER performance of the various resource allocation schemes of Section 5.3 over correlated fading channel for $f_{nd} = 0.02$, $N_{rv} = 6$. The system schematic of Figure 5.4 and the parameters of Tables 5.15, 5.16 and 5.23 were used.

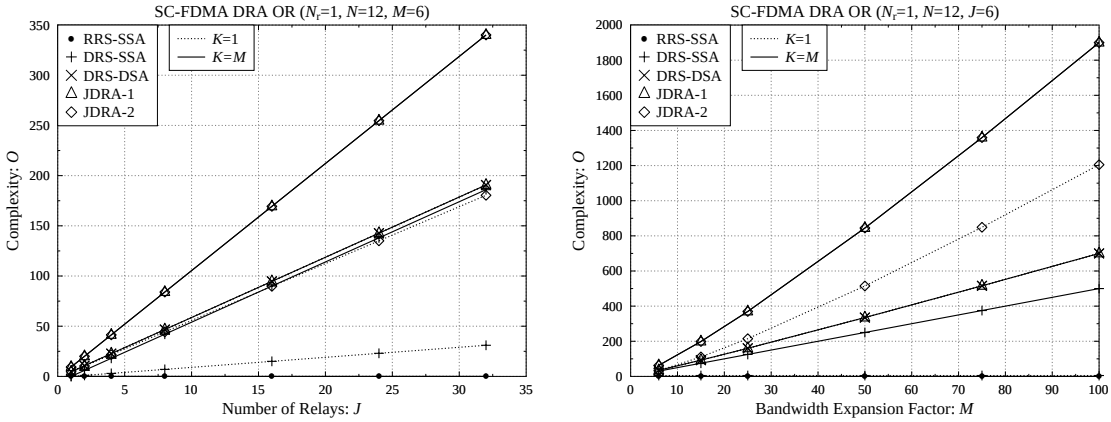

(a) Effects of the number of candidate relays J

(b) Effects of the number of bandwidth expansion factor M

FIGURE 5.25: Complexity comparison of the various resource allocation schemes of Section 5.3 for the single-user ($K = 1$) and the full-load multi-user ($K = M$) scenarios in terms of Tables 5.12 and 5.14.

imposed by the JDRA schemes for $J < 15$ and $M = 6, 15$.

5.5 Summary

In this chapter, we investigated dynamic resource allocation aided opportunistic relaying conceived for the SC-FDMA uplink, in order to improve the attainable reliability and energy-efficiency. We assumed that the relays were in each other's vicinity, and either the subband-based AF scheme of Figure 3.3(b) or the turbo FD-LE aided DF relay scheme of Figure 5.4 was employed. We studied the conventional schemes, such as the DRS combined with either

TABLE 5.24: Power reduction in terms of the SNR gain per bit γ_b^{Δ} (dB) recorded at the BER of 10^{-4} of various resource allocation schemes for the OR based SC-FDMA uplink compared to the DT benchmark using $N = 12$, $M = K = J = 6$, $L = 4$, when the BS's receiver employs single- or multiple antennas for communicating over frequency-selective fading channels. The schemes are listed in descending order of complexity.

γ_b^{Δ} (dB)		Non-FEC		BICM	
	N_r	1	8	1	8
JDRA-2	AF	11.5	1	9.5	2
	DF	-	-	11	1
JDRA-1	AF	11.5	−11	9.5	−1
	DF	-	-	11	−0.25
DRS-DSA	AF	8.5	−14	7.5	−3.5
	DF	-	-	10	−1.5
RRS-SSA	AF	6.5	−14	5	−3.5
	DF	-	-	8.75	−1.5

SSA or DSA for two-hop relaying transmissions. By assuming that the cooperative relays can exchange their CQIs, we proposed the novel FHQA-aided JDRA schemes of Figure 5.13, which exploit the first-hop quality for the joint design of DRS and DSA at the relays. Furthermore, the FHQA aided JDRA-1 and JDRA-2 schemes of Figures 5.14 and 5.15 were activated depending on whether the second-hop or the first-hop channel quality dominates the attainable performance.

Our studies and performance results demonstrated that the proposed FHQA aided JDRA algorithms of Sections 5.3.5 and 5.3.6 outperform the conventional DRS-DSA of Figure 5.3.4 and achieve up to 2 dB power reduction in channel coded systems. Furthermore, by invoking a multi-antenna aided BS, the JDRA-2 scheme of Subsection 5.3.6 outperforms the JDRA-1 method of Subsection 5.3.5. When compared to a SC-FDMA DT benchmark, both of the JDRA schemes are capable of attaining an ECG of 14.1, when invoking a single-antenna BS, while an ERG of up to 1.6 was offered by the JDRA-2 scheme in the multi-antenna aided scenario. Therefore, by employing a multi-antenna BS, the proposed JDRA schemes are capable of achieving a superior performance in comparison to the DT benchmark, while its counterparts consume significantly more power. Furthermore, channel coded OR systems were found to be capable of reducing the transmit power as a benefit of its spatial interleaving gain owing to increasing the number of relays, when communicating over highly correlated fading channels. Hence, for the sake of decreasing the buffering delay and increasing the energy-efficiency, the interleaver depth of the proposed systems may be shortened, when the relays invoke the soft-DF protocol of Section 5.2.3.4. Finally, Table 5.24 summarises the achievable power reduction in terms of the SNR gain per bit γ_b^{Δ} (dB) of various resource allocation schemes for the OR based SC-FDMA uplink compared to the DT benchmark using $N = 12$, $M = K = J = 6$, $L = 4$, when the BS's receiver employs single- or multiple antennas for communicating over frequency-selective fading channels. The schemes are listed

in descending order of complexity.

Chapter 6

Conclusions and Future Work

In this concluding chapter, we summarise the findings for our investigations. Furthermore, suggestions for future research will be presented at the end of this chapter.

6.1 Summary of Findings

In this thesis, we have investigated a variety of cooperative relaying schemes designed for the SC-FDMA uplink, when communicating over broadband wireless channels, for the sake of increasing the achievable energy-efficiency. We have assumed that there are a number of inactive MTs acting as potential relays, which have either fixed or time-variant positions in a cell. Our investigation have been focused on the optimum exploitation of the resources, when considering relay selection, power allocation and subband allocation, as well as novel FDE and diversity combining approaches. In comparison to the benchmark schemes considered in the literature, the reliability and energy-efficiency of our proposed systems was significantly improved. Below we first summarise our main findings obtained in each of the chapters.

6.1.1 Chapter 1

In this chapter, an overview of cooperative communications was presented. Our research was motivated by aiming for energy saving. The user cooperation concept relying on relaying techniques was introduced in Section 1.2.2, which is capable of forming a virtual MIMO among the cooperating single-antenna-aided MTs in order to achieve a cooperative diversity gain with the aid of the cooperative relaying protocols reviewed in Section 1.2.3. As discussed in Section 1.2.4, cooperative networks may rely on either serial or parallel multi-relay assisted regimes, as well as on a generalised model combining both of them. We then considered the

signal processing techniques applied at the relays in Section 1.2.5. The AF relays benefit from low-complexity implementation, while the DF relays are capable of achieving higher power reduction with the aid of FEC coding. The resource allocation schemes introduced in Section 1.2.6 for the relays may consider the issues of relay selection, power allocation and subband allocation, for the sake of achieving a selection diversity gain in both the frequency- and spatial-domains as well as for reducing the transmitted power. Specifically, the dynamic approaches of relay selection, power allocation and subband allocation require the knowledge of instantaneous CSI. Finally, we detailed the thesis outline and highlighted our novel contributions in Section 1.3.2. Let us now elaborate on these contributions a little further.

6.1.2 Chapter 2

In Sections 2.1, 2.2 and 2.3 we have reviewed the basic principles of the OFDM, SC-FDMA and BICM-ID techniques, respectively.

We have shown that OFDM is capable of reducing the effects of ISI with the aid of the CP. However, as argued in Section 2.1.4, multi-carrier modulation results in a high PAPR. Furthermore, OFDM is in general unable to attain frequency-diversity and time-diversity in the absence of FEC coding and inter-subcarrier interleaving or subcarrier-repetition, which reduces the throughput.

By contrast, SC-FDMA schemes are capable of eliminating the PAPR problem, hence they are suitable for high-rate uplink transmissions. As argued in Section 2.2.1, the implementation complexity of the TD SC-FDMA transmitter of Figure 2.5 is lower than that of the TFD SC-FDMA transmitter, which invokes the DFT-spread OFDMA structure of Figure 2.8(a). The receiver complexity of both the TD and TFD SC-FDMA of Figure 2.4(b) and 2.12 is the similar. The TFD SC-FDMA arrangement benefits from the flexibility of transceiver reconfiguration. Both the LFDMA and IFDMA versions of the TFD SC-FDMA systems discussed in Section 2.2.2 may achieve some diversity gain in the presence of frequency-selective fading. Indeed, IFDMA is capable of achieving the maximum attainable frequency-diversity in dispersive multi-path fading channels. By contrast, the LFDMA has a modest frequency diversity in comparison to IFDMA. However, the LFDMA scheme has to invoke either intelligent symbol-to-subband allocation schemes or multi-user scheduling in order to achieve multi-user diversity. Nevertheless, as argued in Section 2.2.5, the above-mentioned frequency-diversity gain is only achievable for both the LFDMA and IFDMA, when the residual ISI was efficiently mitigated. At the receiver of both SC-FDE and SC-FDMA of Figure 2.4(b) and 2.12, invoking DFT and IDFT allows low-complexity single-tap FDE to be carried out. Therefore, the joint complexity of the equaliser, DFT and

IDFT may become lower than that of the conventional TD equaliser having a high number of taps. However, the residual ISI may persist, when non-ZF types of FD equalisers are employed.

The combination of BICM with OFDM and SC-FDMA, etc exhibits various benefits, since BICM was designed for increasing the time-diversity gain of coded modulation in order to mitigate the effects of fading. It was shown in [92] that given a total complexity of 64 trellis states, BICM-ID outperforms BICM in both AWGN and uncorrelated fading channels. It was also shown in [92] that as expected, the performance of BICM is dependent on the interleaver length in correlated fading channels, albeit not in uncorrelated fading, which models an infinite-interleaver scenario. By contrast, the BER performance of BICM-ID is highly dependent on the interleaver length in both AWGN and correlated fading channels.

6.1.3 Chapter 3

In this chapter, we investigated the AF fixed-relay assisted cooperative SC-FDMA scheme using IFDMA signalling. Both the SDR and SSR topologies were considered, when the multi-user systems either have a sufficiently high number of relays, so that each of them is dedicated to a single user, or have insufficient relays, hence they have to be shared by multiple users. In this chapter, two types of AF relaying schemes were conceived for both the SDR and SSR topologies of Figure 3.1, which include the conventional AF and the proposed subband-based AF schemes of Figure 3.3. Specifically, the proposed subband-based AF relaying scheme was designed for the sake of noise suppression at relays. Furthermore, the MMSE based FD-LE was employed separately, i.e. in isolation for the direct and the relaying channels. Then the decision variables generated were combined by the simple TD-EGC of Figure 3.4.

Our performance results of this chapter show that the proposed single-relay assisted cooperative SC-FDMA schemes are free from MUI at the relays, when communicating over frequency-selective fading channels. The IFDMA signalling scheme of Figure 2.10(b) is capable of providing a significant frequency diversity gain in cooperative systems, where cooperative diversity may be achieved for both SDR and SSR topologies in both single-path and multi-path fading channels. As a result, the subband-based AF scheme of Figure 3.3(b) is capable of achieving a multi-user performance, which is better than that of the conventional single-user AF protocol operated in a multi-path environment, which is an exploit benefit of the subband-based AF regime as well as of the noise suppression capability of the relay. It can be shown that the achievable power reduction may be up to 6 dB at a BER of 10^{-4}, when compared to the conventional DT benchmark. Finally, Table 3.3 summarises the power reduction in terms of the SNR gain per bit $\gamma_{\Delta}^{\mathrm{b}}$ recorded at the BER of 10^{-4} of the

various single-relay assisted AF schemes for the cooperative SC-FDMA uplink compared to the DT benchmark, when experiencing frequency-selective fading. The schemes are listed in descending order of complexity.

6.1.4 Chapter 4

In this chapter, we assumed that the relays were roamed in a geographically distributed scenario. The performance benefits of the energy-efficient opportunistic cooperation conceived for the multi-user SC-FDMA uplink were evaluated, when communicating over frequency-selective fading channels in large-scale fading environments. In order to maintain MUI free conditions at the relays, each relay was assumed to employ the subband-based AF scheme of Figure 3.3(b). Furthermore, since the noise imposed at BS's receiver both by the direct- and relaying links has a coloured spectral density, the MMSE FD-LE based JFDEC solution of Figure 4.4 was proposed, which jointly optimised the equalisation and receiver diversity combining at the BS's receiver, in order to maximise the cooperative diversity gain. Moreover, a number of energy consumption metrics were adopted for evaluating the energy-efficiency of the proposed schemes. In this chapter, we proposed three different types of channel-dependent relay selection schemes designed for opportunistic cooperation, which relied on specifically designed source/relay power allocation in the presence of both pass-loss and shadowing, while subjected to imperfect power control. Firstly, the SU-RS scheme of Figure 4.5(a) was designed, when assuming that the number of available relays is sufficient for each cluster of relays serving a single source MT. Secondly, assuming that the number of available relays is insufficient, the proposed MU-RS scheme of Figure 4.5(b) allows multiple users to share the same cluster of relays. Finally, the MA-RS scheme dynamically assigns a single relay to serve all the source MTs, when the number of relays is lower than the number of source MTs.

Our performance results demonstrated that at a BER of 10^{-4}, the proposed JFDEC aided BS's receiver of Figure 4.4 is capable of saving 2 dB power by achieving a higher cooperative diversity gain than the conventional receiver of Figure 3.4. Furthermore, as shown in Figure 4.8(a), the optimal location of the AF relay is close to the BS and the AF relay requires a lower transmit power than the source MT. When the relays are dynamically distributed, the proposed SU-RS, MU-RS and MA-RS schemes of Figure 4.5 benefit from substantial selection diversity gains in diverse shadowing scenarios. For instance, when the channel exhibits as high shadowing variance as 8 dB at $E_b/N_0 = -10$ dB, an ECG of $2.5 - 4.5$ is attainable by invoking the proposed SU-RS, MU-RS and MA-RS schemes in comparison to the conventional DT scenario. Most importantly, the ECG gleaned from our MU-RS and MA-RS schemes may increase to $4 - 8$, when the shadowing variance is increased from 4 to 8 dB, compared to the DT in the absence of shadowing at $E_b/N_0 = -10$ dB. Finally, Table

4.10 summarises the power reduction in terms of SNR gain per bit γ_b^{Δ} recorded at the BER of 10^{-4} of the various relay selection schemes using OPA for the AF based OC SC-FDMA uplink compared to the DT benchmark using $N = L = M = 8$, when communicating over frequency-selective fading channels. The schemes are listed in descending order of complexity.

6.1.5 Chapter 5

In this chapter, we investigated dynamic resource allocation aided opportunistic relaying conceived for the SC-FDMA uplink, in order to improve the attainable reliability and energy-efficiency. We assumed that the relays were in each other's vicinity, and either the subband-based AF scheme of Figure 3.3(b) or the turbo FD-LE aided DF relay scheme of Figure 5.4 was employed. We studied the conventional schemes, such as the DRS combined with either SSA or DSA for two-hop relaying transmissions. By assuming that the cooperative relays can exchange their CQIs, we proposed the novel FHQA-aided JDRA schemes of Figure 5.13, which exploit the first-hop quality for the joint design of DRS and DSA at the relays. Furthermore, the FHQA aided JDRA-1 and JDRA-2 schemes of Figures 5.14 and 5.15 were activated depending on whether the second-hop or the first-hop channel quality dominates the attainable performance.

Our studies and performance results demonstrated that the proposed FHQA aided JDRA algorithms of Sections 5.3.5 and 5.3.6 outperform the conventional DRS-DSA of Figure 5.3.4 and achieve up to 2 dB power reduction in channel coded systems. Furthermore, by invoking a multi-antenna aided BS, the JDRA-2 scheme of Subsection 5.3.6 outperforms the JDRA-1 method of Subsection 5.3.5. When compared to a SC-FDMA DT benchmark, both of the JDRA schemes are capable of attaining an ECG of 14.1, when invoking a single-antenna BS, while an ECG of up to 1.6 was offered by the joint DRA-2 scheme in the multi-antenna aided scenario. Therefore, by employing a multi-antenna BS, the proposed joint DRA schemes are capable of achieving a superior performance in comparison to the DT benchmark, while its counterparts consume significantly more power. Furthermore, channel coded OR systems were found to be capable of reducing the transmit power as a benefit of its spatial interleaving gain owing to increasing the number of relays, when communicating over highly correlated fading channels. Hence, for the sake of decreasing the buffering delay and increasing the energy-efficiency, the interleaver depth of the proposed systems may be shortened, when the relays invoke the soft-DF protocol of Section 5.2.3.4. Finally, Table 5.24 summarises the power reduction in terms of SNR gain per bit γ_b^{Δ} (dB) of various resource allocation schemes for OR SC-FDMA compared to the DT benchmark for $N = 12$, $M = K = J = 6$, $L = 4$, when the BS's receiver employs single- or multiple antennas communicating over frequency-selective fading channels. The schemes are listed

in descending order of complexity.

6.2 Suggestions for Future Work

In this thesis, we mainly considered the user cooperation in a *single-cell* scenario. However, in a *multi-cell* network [215], substantial *inter-cell interference* (ICI) may be imposed on the received signals at the MT, at the BS as well as at the relays [216]. In [217], various architectures of stationary relay deployment have been designed for LTE-Advanced systems by taking into account the MT location, BS sectoring and frequency-reuse in interference-limited scenarios. In order to mitigate the ICI and reduce the energy per bit, a trade-off has to be struck between the energy-efficiency and bandwidth-efficiency. In this section, several suggestions are made for energy-efficient cooperative cellular systems, which may be considered as in our future work.

6.2.1 Relay-Assisted Multi-Cell Resource Allocation

In a single-cell scenario resource allocation may be carried out either in a centralised fashion or in a distributed fashion, where the latter regime leads to the concept of *distributed antenna systems* (DAS). However, the resource allocation of multi-cell network has to be appropriately designed for coordinating the ICI. In [218], a variety of solutions operating in both single-cell and multi-cell OFDMA networks were reviewed in the absence of relays. When invoking the relays, the increased ICI may be mitigated by *multi-cell processing* (MCP) [219]. However, MCP requires a joint signal processing capability across multiple BSs, which relies on real-time information exchange amongst the BSs over the backhaul [220]. Therefore, relay-assisted multi-cell resource allocation may be a promising solution, which allows the relays to have the capability of dynamic scheduling [221]. In this case, having low-complexity resource allocation algorithms is attractive and the signal processing workload at the BSs may be reduced for the sake of energy reduction in SC-FDMA/OFDMA Networks.

In Chapter 5, we introduced the multi-way relaying (MWR) [211,222] philosophy for the sake of exchanging CQI among a cluster of dynamic relays in a single-cell. Naturally, extending this CQI-oriented MWR regime to the multi-cell network allows the relays to carry out MUD and resource allocation in order to mitigate the ICI for the S-R channels and to avoid the ICI for R-D channels in the uplink, particularly when encountering a good channel quality among the multiple relays. For instance, wireless backhauls associated with a low path-loss and a line-of-sight (LOS) component may be available, when the distributed relays are stationary or the co-located relays are inactive MTs.

TABLE 6.1: An example of non-identical propagation channels in uplink and downlink

Link Channel	Path-loss η	Shadowing ξ	Multi-path fading
S-D uplink/downlink	4	8 dB	Non-LOS (Rayleigh)
S-R uplink	2	2 dB	Non-LOS (Rayleigh)
R-D uplink/S-R downlink	2	0 dB	LOS (Rician)
R-D downlink	2	2 dB	Non-LOS (Rayleigh)

Moreover, in [223–231], queueing based scheduling has been conceived for fair resource allocation in wireless cellular networks. By introducing cooperative relaying as well as BS cooperation, the source MTs at the cell-edge require access both to multiple relays and to multiple BSs. Therefore, the queueing and multi-user scheduling issues of both the source and the relays may be investigated. It is also possible to jointly consider the associated hand-over issues, where the relays and BSs may be regarded as multiple servers in the queueing models [232].

However, the optimisation of the above-mentioned resource allocation crossing different layers of multi-cell networks remains an open problem at the time of writing.

6.2.2 Link-Quality-Aware Relay-Assisted Network Optimisation

In conventional network optimisation the QoS may be guaranteed by appropriate cell planing and power control relying on a simplified propagation model, which is essentially based on path-loss. In relay-assisted networks, when assuming that the S-D, S-R and R-D links experience identical fading distribution as well as the same path-loss exponent, multi-hop relaying and cooperative relaying are capable of extending cellular coverage and increasing the system's throughput, respectively. However, in realistic propagation channels, both the fading distributions and path-loss exponents of the S-D channel, of the S-R channels, as well as of the R-D channels may be non-identical. For example, as shown in Table 6.1, we may assume that a wireless backhaul may be set up between the BS and the J relays associated with strong LOS components. In this case, the S-D channel quality is much lower than that of the S-R and R-D channels, which results in a low SINR for the S-D link at the receiver. In this case, the maximal ratio combining of the direct link and of the J relaying links may have non-central chi-squared distributed channel gains, which implies having a diversity order lower than $(J + 1)$ compared to the previously assumed identical channel scenario. However, the signal received from direct link and form the relay may assist the each other at the destination by improving the FEC decoding capability.

Glossary

2G	second generation.
3G	third generation.
3GPP	Third Generation Partnership Project.
4G	fourth generation.
AF	amplify-and-forward.
AWGN	additive white Gaussian noise.
BCJR	Bahl-Cocke-Jelinek-Raviv.
BER	bit-error rate.
BICM	bit-interleaved coded modulation.
BLAST	Bell Laboratories Layered Space-Time.
BLER	block-error rate.
BPSK	binary phase-shift keying.
BS	base station.
CCMC	continuous-input continuous-output memoryless channel.
CDF	cumulative density function.
CDMA	code-division multiple-access.
CIR	channel impulse response.
CP	cyclic prefixing.
CQI	channel quality information.
CSI	channel state information.
CSIR	channel state information at the receiver.
CSIT	channel state information at the transmitter.
DAS	distributed antenna systems.

DF	decode-and-forward.
DFT	discrete Fourier transform.
DPA	default power allocation.
DRA	dynamic resource allocation.
DRS	dynamic relay selection.
DS-CDMA	direct-sequence code-division multiple-access.
DSA	dynamic subband/subcarrier allocation.
DT	direct transmission.
ECG	energy consumption gain.
EGC	equal-gain combiner.
EPA	equal power allocation.
FD	frequency-domain.
FD-DFE	frequency-domain decision-feedback equalisation.
FD-LE	frequency-domain linear equalisation.
FDCHTF	frequency-domain channel transfer function.
FDE	frequency-domain equalisation.
FDMA	frequency-division multiple-access.
FEC	forward-error-correction.
FHQA	first-hop quality awareness.
ICT	information and communication technology.
ID	iterative decoding.
IDFT	inverse discrete Fourier transform.
IFDMA	interleaved frequency-division multiple-access.
ISI	inter-symbol interference.
JDRA	joint dynamic resource allocation.
JFDEC	joint frequency-domain equalisation and combining.
LFDMA	localised frequency-division multiple-access.
LLR	logarithmic-likelihood ratio.
Log-MAP	logarithmic maximum a-posteriori probability.
LTE	Long Term Evolution.
LTI	linear time invariant.
MA-RS	multiple-access relay selection.

MAP	maximum a-posteriori probability.
MCP	multi-cell processing.
MF	matched-filtering.
MIMO	multiple-input multiple-output.
MISO	multiple-input single-output.
MMSE	minimum mean-square error.
MRC	maximum ratio combiner.
MT	mobile terminal.
MU-RS	multi-user relay selection.
MUD	multi-user detection.
MUI	multi-user interference.
MWR	multi-way relaying.
NSC	non-systematic convolutional.
OC	opportunistic cooperation.
OFDM	orthogonal frequency-division multiplexing.
OFDMA	orthogonal frequency-division multiple-access.
OPA	optimal power allocation.
OPEX	operating expenditure.
OR	opportunistic relaying.
P/S	parallel-to-serial.
PAPR	peak-to-average power ratio.
PCE	power control error.
PDF	probability density function.
QAM	quadrature amplitude modulation.
QoS	quality-of-service.
R-D	relay-to-destination.
RB	resource block.
RF	radio frequency.
RRS	random relay selection.
RSC	recursive systematic convolutional.
RV	resource vector.
S-D	source-to-destination.
S-R	source-to-relay.

S/P	serial-to-parallel.
SC-FDE	single-carrier frequency-domain equalisation.
SC-FDMA	single-carrier frequency-division multiple-access.
SDR	single-dedicated-relaying.
SIC	successive interference cancellation.
SIMO	single-input multiple-output.
SINR	signal-to-interference-plus-noise-ratio.
SISO	soft-input soft-output.
SNR	signal-to-noise-ratio.
SP	set-partitioning.
SRS	static relay selection.
SSA	static subband allocation.
SSR	single-shared-relaying.
SU-RS	single-user relay selection.
TCM	trellis-coded modulation.
TD	time-domain.
TD-EGC	time-domain equal-gain combiner.
TDD	time-division-duplex.
TFD	time-frequency-domain.
TS	time-slot.
TTCM	turbo trellis-coded modulation.
ZF	zero-forcing.
ZP	zero-padding.

Bibliography

[1] C. Han, T. Harrold, S. Armour, I. Krikidis, S. Videv, P. M. Grant, H. Haas, J. S. Thompson, I. Ku, C.-X. Wang, T. A. Le, M. R. Nakhai, J. Zhang, and L. Hanzo, "Green radio: radio techniques to enable energy-efficient wireless networks," *IEEE Communications Magazine*, vol. 49, no. 6, pp. 46–54, Jun. 2011.

[2] *Evolved Universal Terrestrial Radio Access (E-UTRA); LTE physical layer; General description (Release-8)*, 3GPP Std. TS 36.201 (V8.3.0), 2009.

[3] S. Fletcher, "Energy efficient wireless communications - green radio access networks," Digital Communications Knowledge Transfer Network, Tech. Rep., Mar. 2011.

[4] G. Y. Li, Z. Xu, C. Xiong, C. Yang, S. Zhang, Y. Chen, and S. Xu, "Energy-efficient wireless communications: tutorial, survey, and open issues," *IEEE Wireless Communications Magazine*, vol. 18, no. 6, pp. 28–35, Dec. 2011.

[5] Y. Chen, S. Zhang, S. Xu, and G. Y. Li, "Fundamental trade-offs on green wireless networks," *IEEE Communications Magazine*, vol. 49, no. 6, pp. 30–37, Jun. 2011.

[6] P. Xia, S. Zhou, and G. B. Giannakis, "Bandwidth- and power-efficient multicarrier multiple access," *IEEE Transactions on Communications*, vol. 51, no. 11, pp. 1828–1837, Nov. 2003.

[7] P. Limpaphayom and K. A. Winick, "Power- and bandwidth-efficient communications using LDPC codes," *IEEE Transactions on Communications*, vol. 52, no. 3, pp. 350– 354, Mar. 2004.

[8] S. Cui, A. J. Goldsmith, and A. Bahai, "Energy-constrained modulation optimization," *IEEE Transactions on Wireless Communications*, vol. 4, no. 5, pp. 2349–2360, Sep. 2005.

[9] H. B. Peek, "Multirate modulation: a bandwidth- and power-efficient modulation scheme," *IEEE Transactions on Communications*, vol. 53, no. 10, pp. 1679–1687, Oct. 2005.

[10] F. Meshkati, H. V. Poor, and S. C. Schwartz, "Energy-efficient resource allocation in wireless networks," *IEEE Signal Processing Magazine*, vol. 24, no. 3, pp. 58–68, May 2007.

[11] S. Buzzi and H. Poor, "Joint receiver and transmitter optimization for energy-efficient CDMA communications," *IEEE Journal on Selected Areas in Communications*, vol. 26, no. 3, pp. 459–472, Apr. 2008.

[12] A.-M. Silvester, L. Lampe, and R. Schober, "Distributed space-time continuous phase modulation code design," *IEEE Transactions on Wireless Communications*, vol. 7, no. 11, pp. 4455–4461, Nov. 2008.

[13] H. Moon and D. Cox, "Efficient power allocation for coded OFDM systems," *IEEE Transactions on Communications*, vol. 57, no. 4, pp. 943–947, Apr. 2009.

[14] M. P. Wylie-Green, E. Perrins, and T. Svensson, "Introduction to CPM-SC-FDMA: A novel multiple-access power-efficient transmission scheme," *IEEE Transactions on Communications*, vol. 59, no. 7, pp. 1904–1915, Jul. 2011.

[15] S. Zhou, M. Zhao, X. Xu, J. Wang, and Y. Yao, "Distributed wireless communication system: a new architecture for future public wireless access," *IEEE Communications Magazine*, vol. 41, no. 3, pp. 108–113, Mar. 2003.

[16] R. Madan, N. Mehta, A. Molisch, and J. Zhang, "Energy-efficient cooperative relaying over fading channels with simple relay selection," *IEEE Transactions on Wireless Communications*, vol. 7, no. 8, pp. 3013–3025, Aug. 2008.

[17] Y. Yang, H. Hu, J. Xu, and G. Mao, "Relay technologies for WiMax and LTE-advanced mobile systems," *IEEE Communications Magazine*, vol. 47, no. 10, pp. 100–105, Oct. 2009.

[18] X.-H. You, D.-M. Wang, B. Sheng, X.-Q. Gao, X.-S. Zhao, and M. Chen, "Cooperative distributed antenna systems for mobile communications," *IEEE Wireless Communications Magazine*, vol. 17, no. 3, pp. 35–43, Jun. 2010.

[19] K. Loa, C.-C. Wu, S.-T. Sheu, Y. Yuan, M. Chion, D. Huo, and L. Xu, "IMT-advanced relay standards," *IEEE Communications Magazine*, vol. 48, no. 8, pp. 40–48, Aug. 2010.

[20] A. Attar, H. Li, and V. C. M. Leung, "Green last mile: how fiber-connected massively distributed antenna systems can save energy," *IEEE Wireless Communications Magazine*, vol. 18, no. 5, pp. 66–74, Oct. 2011.

[21] C. E. Shannon, "A mathematical theory of communication," *Bell System Technical Journal*, vol. 27, pp. 379–423, 623–656, Jul. 1948.

[22] A. Paulraj, R. Nabar, and D. Gore, *Introduction to Space-Time Wireless Communications*. Cambridge University Press, 2003.

[23] D. N. C. Tse and P. Viswanath, *Fundamentals of Wireless Communications*. Cambridge University Press, 2005.

[24] A. Wittneben, "A new bandwidth efficient transmit antenna modulation diversity scheme for linear digital modulation," in *Proceedings of the IEEE International Conference of Communications, 1993, (ICC 1993)*, May 1993, pp. 1630–1634.

[25] G. J. Foschini, "Layered space-time architecture for wireless communication in a fading environment when using multi-element antennas," *Bell Labs Technical Journal*, vol. 1, no. 2, pp. 41–59, Aut. 1996.

[26] S. M. Alamouti, "A simple transmit diversity technique for wireless communications," *IEEE Journal on Selected Areas in Communications*, vol. 16, no. 8, pp. 1451–1458, Oct. 1998.

[27] V. Tarokh, H. Jafarkhani, and A. R. Calderbank, "Space-time block codes from orthogonal designs," *IEEE Transactions on Information Theory*, vol. 45, no. 5, pp. 1456–1467, Jul. 1999.

[28] P. Vandenameele, L. Van Der Perre, M. G. E. Engels, B. Gyselinckx, and H. J. De Man, "A combined OFDM/SDMA approach," *IEEE Journal on Selected Areas in Communications*, vol. 18, no. 11, pp. 2312–2321, Nov. 2000.

[29] B. Hassibi and B. M. Hochwald, "High-rate codes that are linear in space and time," *IEEE Transactions on Information Theory*, vol. 48, no. 7, pp. 1804–1824, Jul. 2002.

[30] W. Su, Z. Safar, M. Olfat, and K. J. R. Liu, "Obtaining full-diversity space-frequency codes from space-time codes via mapping," *IEEE Transactions on Signal Processing*, vol. 51, no. 11, pp. 2905–2916, Nov. 2003.

[31] L. Hanzo, O. Alamri, M. El-Hajjar, and N. Wu, *Near-capacity Multi-functional MIMO Systems: Sphere-packing, Iterative Detection and Cooperation.* Wiley, 2009.

[32] *Evolved Universal Terrestrial Radio Access (E-UTRA); User Equipment (UE) radio transmission and reception (Release-10)*, 3GPP Std. TS 36.101 (V10.5.0), 2011.

[33] E. C. van der Meulen, "Three-terminal communication channels," *Advances in Applied Probability*, vol. 3, no. 1, pp. 120–154, 1971.

[34] ——, "A survey of multi-way channels in information theory: 1961-1976," *IEEE Transactions on Information Theory*, vol. 23, no. 1, pp. 1–37, Jan. 1977.

[35] *Evolved Universal Terrestrial Radio Access (E-UTRA); LTE physical layer; General description (Release-10)*, 3GPP Std. TS 36.201 (V10.0.0), 2011.

[36] *Evolved Universal Terrestrial Radio Access (E-UTRA); Physical layer for relaying operation (Release-10)*, 3GPP Std. TS 36.216 (V10.3.1), 2011.

[37] A. Sendonaris, E. Erkip, and B. Aazhang, "Increasing uplink capacity via user cooperation diversity," in *Proceedings of IEEE International Symposium on Information Theory 1998 (ISIT 1998)*, Aug. 1998, p. 156.

[38] J. N. Laneman and G. W. Wornell, "Energy-efficient antenna sharing and relaying for wireless networks," in *Proceedings of IEEE Wireless Communications and Networking Conference 2000 (WCNC2000)*, vol. 1, Sep. 2000, pp. 7–12.

[39] A. Sendonaris, E. Erkip, and B. Aazhang, "User cooperation diversity- Part I and II," *IEEE Transactions on Communications*, vol. 51, no. 11, pp. 1927–1948, Nov. 2003.

[40] R. U. Nabar, H. Bölcskei, and F. W. Kneubühler, "Fading relay channels: Performance limits and space-time signal design," *IEEE Journal on Selected Areas in Communications*, vol. 22, no. 6, pp. 1099–1109, Aug. 2004.

[41] J. N. Laneman and G. W. Wornell, "Distributed space-time-coded protocols for exploiting cooperative diversity in wireless networks," *IEEE Transactions on Information Theory*, vol. 49, no. 10, pp. 2415–2425, Oct. 2003.

[42] J. Boyer, D. D. Falconer, and H. Yanikomeroglu, "Multihop diversity in wireless relaying channels," *IEEE Transactions on Communications*, vol. 52, no. 10, pp. 1820–1830, Oct. 2004.

[43] P. A. Anghel and M. Kaveh, "Exact symbol error probability of a cooperative network in a Rayleigh-fading environment," *IEEE Transactions on Wireless Communications*, vol. 3, no. 5, pp. 1416–1421, Sep. 2004.

[44] L.-L. Yang and H.-H. Chen, "Error probability of digital communications using relay diversity over Nakagami-m fading channels," *IEEE Transactions on Wireless Communications*, vol. 7, no. 5, pp. 1806–1811, May 2008.

[45] A. Ribeiro, X. Cai, and G. B. Giannakis, "Symbol error probabilities for general cooperative links," *IEEE Transactions on Wireless Communications*, vol. 4, no. 3, pp. 1264–1273, May 2005.

[46] J. N. Laneman, D. N. C. Tse, and G. W. Wornell, "Cooperative diversity in wireless networks: Efficient protocols and outage behavior," *IEEE Transactions on Information Theory*, vol. 50, no. 12, pp. 3062–3080, Dec. 2004.

[47] S. Simoens, O. Muoz-Medina, J. Vidal, and A. Del Coso, "Compress-and-forward cooperative MIMO relaying with full channel state information," *IEEE Transactions on Signal Processing*, vol. 58, no. 2, pp. 781–791, Feb. 2010.

[48] J. Yuan, Y. Li, and L. Chu, "Differential modulation and relay selection with detect-and-forward cooperative relaying," *IEEE Transactions on Vehicular Technology*, vol. 59, no. 1, pp. 261–268, Jan. 2010.

[49] Y. Li, B. Vucetic, T. F. Wong, and M. Dohler, "Distributed turbo coding with soft information relaying in multihop relay networks," *IEEE Journal on Selected Areas in Communications*, vol. 24, no. 11, pp. 2040–2050, Nov. 2006.

[50] M. Janani, A. Hedayat, T. E. Hunter, and A. Nosratinia, "Coded cooperation in wireless communications: space-time transmission and iterative decoding," *IEEE Transactions on Signal Processing*, vol. 52, no. 2, pp. 362–371, Feb. 2004.

[51] A. Nosratinia, T. E. Hunter, and A. Hedayat, "Cooperative communication in wireless networks," *IEEE Communications Magazine*, vol. 42, no. 10, pp. 74–80, Oct. 2004.

[52] T. E. Hunter and A. Nosratinia, "Diversity through coded cooperation," *IEEE Transactions on Wireless Communications*, vol. 5, no. 2, pp. 283–289, Feb. 2006.

[53] Y. Li, "Distributed coding for cooperative wireless networks: An overview and recent advances," *IEEE Communications Magazine*, vol. 47, no. 8, pp. 71–77, Aug. 2009.

[54] L. Kong, S. X. Ng, R. G. Maunder, and L. Hanzo, "Maximum-throughput irregular distributed space-time code for near-capacity cooperative communications," *IEEE Transactions on Vehicular Technology*, vol. 59, no. 3, pp. 1511–1517, Mar. 2010.

[55] L. Hanzo, M. Münster, B.-J. Choi, and T. Keller, *OFDM and MC-CDMA for Broadband Multi-User Communications, WLANs and Broadcasting*. Wiley, 2003.

[56] C. Y. Wong, R. S. Cheng, K. B. Letaief, and R. D. Murch, "Multiuser OFDM with adaptive subcarrier, bit and power allocation," *IEEE Journal on Selected Areas in Communications*, vol. 17, no. 10, pp. 1747–1758, Oct. 1999.

[57] T. Keller and L. Hanzo, "Adaptive multicarrier modulation: a convenient framework for time-frequency processing in wireless communications," *Proceedings of the IEEE*, vol. 88, no. 5, pp. 611–640, May 2000.

[58] K. B. Letaief and Y. J. Zhang, "Dynamic multiuser resource allocation and adaptation for wireless systems," *IEEE Wireless Communications Magazine*, vol. 13, no. 4, pp. 38–47, Aug. 2006.

[59] X. Wang, G. B. Giannakis, and A. G. Marques, "A unified approach to qos-guaranteed scheduling for channel-adaptive wireless networks," *Proceedings of the IEEE*, vol. 95, no. 12, pp. 2410–2431, Dec. 2007.

[60] G. Song and G. Y. Li, "Cross-layer optimization for OFDM wireless networks- Part I: Theoretical framework," *IEEE Transactions on Wireless Communications*, vol. 4, no. 2, pp. 614–624, Mar. 2005.

[61] ——, "Cross-layer optimization for OFDM wireless networks- Part II: Algorithm development," *IEEE Transactions on Wireless Communications*, vol. 4, no. 2, pp. 625– 634, Mar. 2005.

[62] G. Miao, N. Himayat, G. Y. Li, and A. Swami, "Cross-layer optimization for energy-efficient wireless communications: a survey," *Wireless Communications and Mobile Computing*, vol. 9, no. 4, p. 529542, Apr. 2009.

[63] W. Fang, L.-L. Yang, and L. Hanzo, "Single-user performance of direct-sequence code-division multiple-access using relay diversity and power allocation," *IET Proceedings on Communications*, vol. 2, no. 3, pp. 462–472, Mar. 2008.

[64] L. Wang and L. Hanzo, "The resource-optimized differentially modulated hybrid AF/DF cooperative cellular uplink using multiple-symbol differential sphere detection," *IEEE Signal Processing Letters*, vol. 16, no. 11, pp. 965–968, Nov. 2009.

[65] A. Bletsas, A. Khisti, D. P. Reed, and A. Lippman, "A simple cooperative diversity method based on network path selection," *IEEE Journal on Selected Areas in Communications*, vol. 24, no. 3, pp. 659–672, Mar. 2006.

[66] A. Bletsas, H. Shin, and M. Z. Win, "Cooperative communications with outage-optimal opportunistic relaying," *IEEE Transactions on Wireless Communications*, vol. 6, no. 9, pp. 3450–3460, Sep. 2007.

[67] Y. Jing and H. Jafarkhani, "Single and multiple relay selection schemes and their achievable diversity orders," *IEEE Transactions on Wireless Communications*, vol. 8, no. 3, pp. 1414–1423, Mar. 2009.

[68] Y. Peng, S. Armour, and J. McGeehan, "An investigation of dynamic subcarrier allocation in MIMO-OFDMA systems," *IEEE Transactions on Vehicular Technology*, vol. 56, no. 5, pp. 2990–3005, Sep. 2007.

[69] Y.-F. Chen and J.-W. Chen, "A fast subcarrier, bit, and power allocation algorithm for multiuser OFDM-based systems," *IEEE Transactions on Vehicular Technology*, vol. 57, no. 2, pp. 873–881, Mar. 2008.

[70] I. C. Wong, O. Oteri, and W. Mccoy, "Optimal resource allocation in uplink SC-FDMA systems," *IEEE Transactions on Wireless Communications*, vol. 8, no. 5, pp. 2161–2165, May 2009.

[71] W.-C. Pao and Y.-F. Chen, "Reduced complexity subcarrier allocation schemes for DFT-precoded OFDMA uplink systems," *IEEE Transactions on Wireless Communications*, vol. 9, no. 9, pp. 2701–2706, Sep. 2010.

[72] O. Nwamadi, X. Zhu, and A. K. Nandi, "Dynamic physical resource block allocation algorithms for uplink Long Term Evolution," *Communications, IET*, vol. 5, no. 7, pp. 1020–1027, May 2011.

[73] Y. Li, W. Wang, J. Kong, and M. Peng, "Subcarrier pairing for amplify-and-forward and decode-and-forward OFDM relay links," *IEEE Communications Letters*, vol. 13, no. 4, pp. 209–211, Apr. 2009.

[74] O. Duval, Z. Hasan, E. Hossain, F. Gagnon, and V. Bhargava, "Subcarrier selection and power allocation for amplify-and-forward relaying over OFDM links," *IEEE Transactions on Wireless Communications*, vol. 9, no. 4, pp. 1293–1297, Apr. 2010.

[75] W. Dang, M. Tao, H. Mu, and J. Huang, "Subcarrier-pair based resource allocation for cooperative multi-relay OFDM systems," *IEEE Transactions on Wireless Communications*, vol. 9, no. 5, pp. 1640–1649, May 2010.

[76] C.-N. Hsu, H.-J. Su, and P.-H. Lin, "Joint subcarrier pairing and power allocation for OFDM transmission with decode-and-forward relaying," *IEEE Transactions on Signal Processing*, vol. 59, no. 1, pp. 399–414, Jan. 2011.

[77] H. Boostanimehr and V. K. Bhargava, "Selective subcarrier pairing and power allocation for DF OFDM relay systems with perfect and partial CSI," *IEEE Transactions on Wireless Communications*, vol. 10, no. 12, pp. 4057 –4067, Dec. 2011.

[78] Y. Liu and M. Tao, "Optimal channel and relay assignment in OFDM-based multi-relay multi-pair two-way communication networks," *IEEE Transactions on Communications*, vol. 60, no. 2, pp. 317–321, Feb. 2012.

[79] H. Zhang, Y. Liu, and M. Tao, "Resource allocation with subcarrier pairing in OFDMA two-way relay networks," *IEEE Wireless Communications Letters*, vol. 1, no. 2, pp. 61–64, Apr. 2012.

[80] Y. Li, B. Vucetic, Z. Zhou, and M. Dohler, "Distributed adaptive power allocation for wireless relay networks," *IEEE Transactions on Wireless Communications*, vol. 6, no. 3, pp. 948–958, Mar. 2007.

[81] Y. Zhao, R. Adve, and T. J. Lim, "Improving amplify-and-forward relay networks: Optimal power allocation versus selection," *IEEE Transactions on Wireless Communications*, vol. 6, no. 8, pp. 3114–3123, Aug. 2007.

[82] K. Bakanoglu, S. Tomasin, and E. Erkip, "Resource allocation for the parallel relay channel with multiple relays," *IEEE Transactions on Wireless Communications*, vol. 10, no. 3, pp. 792–802, Mar. 2011.

[83] A. Ghosh, R. Ratasuk, B. Mondal, N. Mangalvedhe, and T. Thomas, "LTE-advanced: next-generation wireless broadband technology," *IEEE Wireless Communications Magazine*, vol. 17, no. 3, pp. 10–22, Jun. 2010.

[84] R. Dinis, D. Falconer, T. Matsumoto, M. Ran, A. Springer, and P. Zhu, "A mixed OFDM plus single-carrier mode air interface," WWRF, Tech. Rep., Aug. 2003.

[85] M. Schnell, I. D. Broeck, and U. Sorger, "A promising new wideband multiple-access scheme for future mobile communications systems," *European Transactions on Telecommunications*, vol. 10, no. 4, pp. 417–427, Jul. 1999.

[86] L.-L. Yang, "Receiver multiuser diversity aided multi-stage MMSE multiuser detection for DS-CDMA and SDMA systems employing I-Q modulation," in *Proceedings of the 2010 IEEE 72nd Vehicular Technology Conference, Fall (VTC 2010-Fall)*, Sep. 2010, pp. 1–5.

[87] ——, "Receiver multiuser diversity aided multi-stage minimum mean-square error detection for heavily loaded DS-CDMA and SDMA systems," *IEEE Transactions on Communications*, vol. 58, no. 12, pp. 3397–3404, Dec. 2010.

[88] M. Tüchler, A. C. Singer, and R. Koetter, "Minimum mean squared error equalization using a priori information," *IEEE Transactions on Signal Processing*, vol. 50, no. 3, pp. 673–683, Mar. 2002.

[89] M. Tüchler, R. Koetter, and A. C. Singer, "Turbo equalization: principles and new results," *IEEE Transactions on Communications*, vol. 50, no. 5, pp. 754–767, May 2002.

[90] M. Tüchler and A. C. Singer, "Turbo equalization: An overview," *IEEE Transactions on Information Theory*, vol. 57, no. 2, pp. 920–952, Feb. 2011.

[91] H. G. Myung and D. J. Goodman, *Single Carrier FDMA: A New Air Interface for Long Term Evolution.* Wiley, 2008.

[92] L. Hanzo, T. Liew, B. Yeap, R. Tee, and S. X. Ng, *Turbo Coding, Turbo Equalisation and Space-Time Coding (EXIT-Chart-Aided Near-Capacity Designs for Wireless Channels).* Wiley (IEEE Press), 2011.

[93] H. Sari, G. Karam, and I. Jeanclaude, "Transmission techniques for digital terrestrial TV broadcasting," *IEEE Communications Magazine*, vol. 33, no. 2, pp. 100–109, Feb. 1995.

[94] D. D. Falconer, S. L. Ariyavisitakul, A. Benyamin-Seeyar, and B. Eidson, "Frequency domain equalization for single-carrier broadband wireless systems," *IEEE Communications Magazine*, vol. 40, no. 4, pp. 58–66, Apr. 2002, white paper.

[95] U. Sorger, I. De Broeck, and M. Schnell, "Interleaved FDMA- A new spread-spectrum multiple-access scheme," in *Proceedings of IEEE International Conference on Communications, 1998. (ICC 1998)*, vol. 2, Jun. 1998, pp. 1013–1017 vol.2.

[96] D. Galda and H. Rohling, "A low complexity transmitter structure for ofdm-fdma uplink systems," in *Proceedings of IEEE 55th Vehicular Technology Conference, 2002. (VTC 2002 Spring)*, vol. 4, 2002, pp. 1737–1741.

[97] X. Li and J. A. Ritcey, "Bit-interleaved coded modulation with iterative decoding," *IEEE Communications Letters*, vol. 1, no. 6, pp. 169–171, Nov. 1997.

[98] ——, "Bit-interleaved coded modulation with iterative decoding using soft feedback," *Electronics Letters*, vol. 34, no. 10, pp. 942–943, May 1998.

[99] R. W. Chang, "Synthesis of band-limited orthogonal signals for multichannel data transmission," *Bell System Technical Journal*, vol. 46, pp. 1775–1796, Dec. 1966.

[100] A. J. Goldsmith, *Wireless Communications*. Cambridge University Press, 2005.

[101] S. Weinstein and P. Ebert, "Data transmission by frequency-division multiplexing using the discrete fourier transform," *IEEE Transactions on Communication Technology*, vol. 19, no. 5, pp. 628–634, Oct. 1971.

[102] L.-L. Yang, *Multicarrier Communications*. Wiley, 2009.

[103] B. Muquet, Z. Wang, G. B. Giannakis, M. de Courville, and P. Duhamel, "Cyclic prefixing or zero padding for wireless multicarrier transmissions?" *IEEE Transactions on Communications*, vol. 50, no. 12, pp. 2136–2148, Dec. 2002.

[104] R. Steele and L. Hanzo, *Mobile Radio Communications, 2th Edition*. IEEE Press and John Wiley, 1999.

[105] L. Hanzo, Y. Akhtman, L. Wang, and M. Jiang, *MIMO-OFDM for LTE, WIFI and WIMAX: Coherent Versus Non-Coherent and Cooperative Turbo-Transceivers*. Wiley (IEEE Press), Oct. 2010.

[106] D. Huang, K. B. Letaief, and J. Lu, "Bit-interleaved time-frequency coded modulation for OFDM systems over time-varying channels," *IEEE Transactions on Communications*, vol. 53, no. 7, pp. 1191–1199, Jul. 2005.

[107] X. Li and J. Cimini, L. J., "Effects of clipping and filtering on the performance of OFDM," *Communications Letters, IEEE*, vol. 2, no. 5, pp. 131–133, may 1998.

[108] J. Cimini, L. J. and N. R. Sollenberger, "Peak-to-average power ratio reduction of an OFDM signal using partial transmit sequences," *IEEE Communications Letters*, vol. 4, no. 3, pp. 86–88, Mar. 2000.

[109] A. D. S. Jayalath and C. R. N. Athaudage, "On the PAR reduction of OFDM signals using multiple signal representation," *IEEE Communications Letters*, vol. 8, no. 7, pp. 425–427, Jul. 2004.

[110] X. Huang, J. Lu, J. Zheng, K. B. Letaief, and J. Gu, "Companding transform for reduction in peak-to-average power ratio of OFDM signals," *IEEE Transactions on Wireless Communications*, vol. 3, no. 6, pp. 2030–2039, Nov. 2004.

[111] T. Jiang and G. Zhu, "Complement block coding for reduction in peak-to-average power ratio of OFDM signals," *IEEE Communications Magazine*, vol. 43, no. 9, pp. S17–S22, Sep. 2005.

[112] M. Sharif, V. Tarokh, and B. Hassibi, "Peak power reduction of OFDM signals with sign adjustment," *IEEE Transactions on Communications*, vol. 57, no. 7, pp. 2160–2166, Jul. 2009.

[113] A. E. Jones, T. A. Wilkinson, and S. K. Barton, "Block coding scheme for reduction of peak to mean envelope power ratio of multicarrier transmission schemes," *Electronics Letters*, vol. 30, no. 25, pp. 2098–2099, Dec. 1994.

[114] N. Benvenuto, R. Dinis, D. D. Falconer, and S. Tomasin, "Single carrier modulation with nonlinear frequency domain equalization: An idea whose time has come-again," *Proceedings of the IEEE*, vol. 98, no. 1, pp. 69–96, Jan. 2010.

[115] Ericsson, "Some aspects of single-carrier transmission for E-UTRA, (TSG-RAN WG1 #42)," 3GPP, Tech. Rep. R1-050251, Aug. 2005.

[116] *Evolved Universal Terrestrial Radio Access (E-UTRA); Physical channels and modulation (Release-10)*, 3GPP Std. TS 36.211 (V10.4.0), 2011.

[117] D. Bai, C. Park, J. Lee, H. Nguyen, J. Singh, A. Gupta, Z. Pi, T. Kim, C. Lim, M.-G. Kim, and I. Kang, "LTE-advanced modem design: challenges and perspectives," *IEEE Communications Magazine*, vol. 50, no. 2, pp. 178–186, Feb. 2012.

[118] M. V. Clark, "Adaptive frequency-domain equalization and diversity combining for broadband wireless communications," *IEEE Journal on Selected Areas in Communications*, vol. 16, no. 8, pp. 1385–1395, Oct. 1998.

[119] N. Benvenuto and S. Tomasin, "On the comparison between OFDM and single carrier modulation with a DFE using a frequency-domain feedforward filter," *IEEE Transactions on Communications*, vol. 50, no. 6, pp. 947–955, Jun. 2002.

[120] A. Gusmao, R. Dinis, and N. Esteves, "On frequency-domain equalization and diversity combining for broadband wireless communications," *IEEE Transactions on Communications*, vol. 51, no. 7, pp. 1029–1033, Jul. 2003.

[121] Z. Wang, X. Ma, and G. B. Giannakis, "OFDM or single-carrier block transmissions?" *IEEE Transactions on Communications*, vol. 52, no. 3, pp. 380–394, Mar. 2004.

[122] R. Dinis, D. D. Falconer, C. T. Lam, and M. Sabbaghian, "A multiple access scheme for the uplink of broadband wireless systems," in *Proceedings of IEEE Global Telecommunications Conference, 2004. (GLOBECOM 2004)*, vol. 6, Nov. 2004, pp. 3808–3812.

[123] N. Benvenuto and S. Tomasin, "Block iterative DFE for single carrier modulation," *Electronics Letters*, vol. 38, no. 19, pp. 1144– 1145, Sep. 2002.

[124] ——, "Iterative design and detection of a DFE in the frequency domain," *IEEE Transactions on Communications*, vol. 53, no. 11, pp. 1867– 1875, Nov. 2005.

[125] H. G. Myung, J. Lim, and D. J. Goodman, "Single carrier FDMA for uplink wireless transmission," *IEEE Vehicular Technology Magazine*, pp. 30–38, Sep. 2006.

[126] ——, "Peak-to-average power ratio of single carrier FDMA signals with pulse shaping," in *Proceedings of IEEE 17th International Symposium on Personal, Indoor and Mobile Radio Communications, 2006 (PIMRC 2006)*, Sep. 2006, pp. 1–5.

[127] J. Lim, H. G. Myung, K. Oh, and D. J. Goodman, "Proportional fair scheduling of uplink single-carrier FDMA systems," in *Proceedings of IEEE 17th International Symposium on Personal, Indoor and Mobile Radio Communications, 2006 (PIMRC 2006)*, Sep. 2006, pp. 1–6.

[128] ——, "Channel-dependent scheduling of uplink single carrier FDMA systems," in *Proceedings of 2006 IEEE 64th Vehicular Technology Conference, 2006. (VTC-2006 Fall)*, Sep. 2006, pp. 1–5.

[129] T. Frank, A. Klein, and E. Costa, "IFDMA: A scheme combining the advantages of OFDMA and CDMA," *IEEE Wireless Communications*, pp. 9–10, Jun. 2007.

[130] G. Berardinelli, B. Priyanto, T. B. Sorensen, and P. Mogensen, "Improving SC-FDMA performance by turbo equalization in utra lte uplink," in *Proceedings of the 2008 IEEE Vehicular Technology Conference, Spring. (VTC 2008-Spring)*, May 2008, pp. 2557–2561.

[131] L. Ruiz de Temino, G. Berardinelli, S. Frattasi, and P. Mogensen, "Channel-aware scheduling algorithms for SC-FDMA in LTE uplink," in *Proceedings of IEEE 19th International Symposium on Personal, Indoor and Mobile Radio Communications, 2008. (PIMRC 2008)*, Sep. 2008, pp. 1–6.

[132] G. Berardinelli, L. Ruiz de Temino, S. Frattasi, M. Rahman, and P. Mogensen, "OFDMA vs. SC-FDMA: Performance comparison in local area IMT-A scenarios," *IEEE Wireless Communications Magazine*, vol. 15, no. 5, pp. 64–72, Oct. 2008.

[133] F. Adachi, K. Takeda, and H. Tomeba, "Frequency-domain equalization for boradband single-carrier multiple access," *IEICE Transactions on Communications*, vol. E92-B, no. 5, pp. 1441–1456, May 2009.

[134] ——, "Introduction of frequency-domain signal processing to boradband single-carrier transmissions in a wireless channel," *IEICE Transactions on Communications*, vol. E92-B, no. 9, pp. 2789–2808, Sep. 2009.

[135] C.-H. Choi and G.-H. Im, "Bit-interleaved coded multilevel modulation for single-carrier frequency-domain equalization," *IEEE Communications Letters*, vol. 14, no. 3, pp. 193–195, Mar. 2010.

[136] T.-W. Yune, C.-H. Choi, G.-H. Im, J.-B. Lim, E.-S. Kim, Y.-C. Cheong, and K.-H. Kim, "SC-FDMA with iterative multiuser detection: improvements on power/spectral efficiency," *IEEE Communications Magazine*, vol. 48, no. 3, pp. 164–171, Mar. 2010.

[137] C. Zhang, Z. Wang, C. Pan, S. Chen, and L. Hanzo, "Low-complexity iterative frequency domain decision feedback equalization," *IEEE Transactions on Vehicular Technology*, vol. 60, no. 3, pp. 1295–1301, Mar. 2011.

[138] C. Zhang, Z. Wang, Z. Yang, J. Wang, and J. Song, "Frequency domain decision feedback equalization for uplink SC-FDMA," *IEEE Transactions on Broadcasting*, vol. 56, no. 2, pp. 253–257, Jun. 2010.

[139] Nokia, "Uplink considerations for UTRAN LTE, (TSG-RAN WG1 #40bis)," 3GPP, Tech. Rep. R1-050251, Mar. 2005.

[140] Motorola, "Uplink multiple access for E-UTRA, (TSG-RAN WG1 #40bis)," 3GPP, Tech. Rep. R1-050245, Apr. 2005.

[141] J. Zhang, L.-L. Yang, and L. Hanzo, "First-hop-quality-aware dynamic resource allocation for amplify-and-forward opportunistic relaying assisted SC-FDMA," in *Proceedings of the 2012 IEEE International Conference on Communications (ICC 2012)*, Jun. 2012, pp. 1–5.

[142] D. Z. Filho, L. Féty, and M. Terré, "A hybird single-carrier/multicarrier transmission scheme with power allocation," *EURASIP Journal on Wireless Communications and Networking*, vol. 2008, pp. 1–11, 2008.

[143] H. G. Myung, K. Oh, J. Lim, and D. J. Goodman, "Channel-dependent scheduling of an uplink SC-FDMA system with imperfect channel information," in *Proceedings of IEEE Wireless Communications and Networking Conference, 2008. (WCNC 2008)*, Mar. 2008, pp. 1860–1864.

[144] J. Lim, "Adaptive radio resource management for uplink wireless networks," Ph.D. dissertation, Polytechnic University, 2006.

[145] U. Madhow and M. L. Honig, "MMSE interference suppression for direct-sequence spread-spectrum CDMA," *IEEE Transactions on Communications*, vol. 42, pp. 3178–3188, Dec. 1994.

[146] L. Electronics, "Performance of localised and distributed SC-FDMA, (TSG-RAN WG1 #44)," 3GPP, Tech. Rep. R1-060540, Feb. 2006.

[147] G. Ungerboeck, "Channel coding with multilevel/phase signals," *IEEE Transactions on Information Theory*, vol. 28, no. 1, pp. 55– 67, Jan. 1982.

[148] D. Divsalar and M. K. Simon, "Multiple trellis coded modulation (MTCM)," *IEEE Transactions on Communications*, vol. 36, no. 4, pp. 410–419, Apr. 1988.

[149] ——, "The design of trellis coded MPSK for fading channels: performance criteria," *IEEE Transactions on Communications*, vol. 36, no. 9, pp. 1004–1012, Sep. 1988.

[150] ——, "The design of trellis coded MPSK for fading channels: set partitioning for optimum code design," *IEEE Transactions on Communications*, vol. 36, no. 9, pp. 1013–1021, Sep. 1988.

[151] P. Robertson and T. Worz, "Bandwidth-efficient turbo trellis-coded modulation using punctured component codes," *IEEE Journal on Selected Areas in Communications*, vol. 16, no. 2, pp. 206–218, Feb. 1998.

[152] E. Zehavi, "8-PSK trellis codes for a Rayleigh channel," *IEEE Transactions on Communications*, vol. 40, no. 5, pp. 873–884, May 1992.

[153] G. Caire, G. Taricco, and E. Biglieri, "Bit-interleaved coded modulation," in *Proceedings of 1997 IEEE International Symposium on Information Theory. 1997. (ISIT 1997)*, Jun. 1997, p. 96.

[154] ——, "Bit-interleaved coded modulation," in *Proceedings of 1997 IEEE International Conference on Communications, 1997. (ICC 1997)*, vol. 3, Jun. 1997, pp. 1463–1467 vol.3.

[155] ——, "Bit-interleaved coded modulation," *IEEE Transactions on Information Theory*, vol. 44, no. 3, pp. 927–946, May 1998.

[156] X. Li, A. Chindapol, and J. A. Ritcey, "Bit-interleaved coded modulation with iterative decoding and 8 PSK signaling," *IEEE Transactions on Communications*, vol. 50, no. 8, pp. 1250–1257, Aug. 2002.

[157] E. Akay and E. Ayanoglu, "Low complexity decoding of bit-interleaved coded modulation for M-ary QAM," in *Proceedings of IEEE International Conference on Communications, 2004 (ICC 2004)*, vol. 2, Jun. 2004, pp. 901–905.

[158] P.-C. Yeh, S. A. Zummo, and W. E. Stark, "Error probability of bit-interleaved coded modulation in wireless environments," *IEEE Transactions on Vehicular Technology*, vol. 55, no. 2, pp. 722–728, Mar. 2006.

[159] A. Martinez, A. Guillen i Fabregas, and G. Caire, "Error probability analysis of bit-interleaved coded modulation," *IEEE Transactions on Information Theory*, vol. 52, no. 1, pp. 262– 271, Jan. 2006.

[160] A. Martinez, A. Guillen i Fabregas, G. Caire, and F. Willems, "Bit-interleaved coded modulation in the wideband regime," *IEEE Transactions on Information Theory*, vol. 54, no. 12, pp. 5447–5455, Dec. 2008.

[161] ——, "Bit-interleaved coded modulation revisited: A mismatched decoding perspective," *IEEE Transactions on Information Theory*, vol. 55, no. 6, pp. 2756–2765, Jun. 2009.

[162] R. Tee, R. G. Maunder, and L. Hanzo, "EXIT-chart aided near-capacity irregular bit-interleaved coded modulation design," *IEEE Transactions on Wireless Communications*, vol. 8, no. 1, pp. 32–37, Jan. 2009.

[163] A. Nasri and R. Schober, "Performance of BICM-SC and BICM-OFDM systems with diversity reception in non-gaussian noise and interference," *IEEE Transactions on Communications*, vol. 57, no. 11, pp. 3316–3327, nov. 2009.

[164] T. Matsumoto, S. Ibi, S. Sampei, and R. Thoma, "Adaptive transmission with single-carrier multilevel BICM," *Proceedings of the IEEE*, vol. 95, no. 12, pp. 2354–2367, Dec. 2007.

[165] H. V. Poor and S. Verdu, "Probability of error in MMSE multiuser detection," *IEEE Transactions on Information Theory*, vol. 43, no. 3, pp. 858–871, May 1997.

[166] L. Bahl, J. Cocke, F. Jelinek, and J. Raviv, "Optimal decoding of linear codes for minimizing symbol error rate," *IEEE Transactions on Information Theory*, vol. 20, no. 2, pp. 284– 287, Mar. 1974.

[167] P. Robertson, E. Villebrun, and P. Hoeher, "A comparison of optimal and sub-optimal map decoding algorithms operating in the log domain," in *Proceedings of 1995 IEEE International Conference on Communications, (ICC 1995)*, vol. 2, Jun. 1995, pp. 1009–1013 vol.2.

[168] D. Chen, K. Azarian, and J. N. Laneman, "A case for amplify-forward relaying in the block-fading multiple-access channel," *IEEE Transactions on Information Theory*, vol. 54, no. 8, pp. 3728–3733, Aug. 2008.

[169] W. Fang, L.-L. Yang, and L. Hanzo, "Performance of DS-CDMA downlink using transmitter preprocessing and relay diversity over Nakagami-m fading channels," *IEEE Transactions on Wireless Communications*, vol. 8, no. 2, pp. 678–682, Feb. 2009.

[170] ——, "Transmitter preprocessing assisted cooperative downlink transmission in DS-CDMA systems experiencing propagation pathloss and Nakagami-m fading," *IEEE Transactions on Vehicular Technology*, vol. 58, no. 8, pp. 4182–4192, Oct. 2009.

[171] F. Pancaldi, G. M. Vitetta, R. Kalbasi, N. Al-Dhahir, M. Uysal, and H. Mheidat, "Single-carrier frequency domain equalization," *IEEE Signal Processing Magazine*, pp. 37–56, Sep. 2008.

[172] T.-W. Yune, J.-B. Lim, Y.-C. Cheong, and G.-H. Im, "Iterative multiuser detection with spectral efficient protocol for relay-assisted SC-FDE," *IEEE Communications Letters*, vol. 12, no. 3, pp. 182–184, Mar. 2008.

[173] T.-W. Yune, J.-B. Lim, and G.-H. Im, "Iterative multiuser detection with spectral efficient relaying protocols for single-carrier transmission," *IEEE Transactions on Wireless Communications*, vol. 8, no. 7, pp. 3789–3797, Jul. 2009.

[174] R. Zhang and L. Hanzo, "Coding schemes for energy efficient multi-source cooperation aided uplink transmission," *IEEE Signal Processing Letters*, vol. 16, no. 5, pp. 438–441, May 2009.

[175] M. Kaneko, K. Hayashi, P. Popovski, K. Ikeda, H. Sakai, and R. Prasad, "Amplify-and-forward cooperative diversity schemes for multi-carrier systems," *IEEE Transactions on Wireless Communications*, vol. 7, no. 5, pp. 1845–1850, May 2008.

[176] D. Gunduz and E. Erkip, "Opportunistic cooperation by dynamic resource allocation," *IEEE Transactions on Wireless Communications*, vol. 6, no. 4, pp. 1446–1454, Apr. 2007.

[177] Y. Zou, B. Zheng, and J. Zhu, "Outage analysis of opportunistic cooperation over rayleigh fading channels," *IEEE Transactions on Wireless Communications*, vol. 8, no. 6, pp. 3077–3085, Jun. 2009.

[178] Y. Zou, B. Zheng, and W.-P. Zhu, "An opportunistic cooperation scheme and its BER analysis," *IEEE Transactions on Wireless Communications*, vol. 8, no. 9, pp. 4492–4497, Sep. 2009.

[179] R. Yuan, T. Zhang, J. Huang, and L. Sun, "Opportunistic cooperation and optimal power allocation for wireless sensor networks," *IEEE Transactions on Consumer Electronics*, vol. 56, no. 3, pp. 1898–1904, Aug. 2010.

[180] W. Zeng, C. Xiao, Y. Wang, and J. Lu, "Opportunistic cooperation for multi-antenna multi-relay networks," *IEEE Transactions on Wireless Communications*, vol. 9, no. 10, pp. 3189–3199, Oct. 2010.

[181] H. Wang, S. Ma, T.-S. Ng, and H. V. Poor, "A general analytical approach for opportunistic cooperative systems with spatially random relays," *IEEE Transactions on Wireless Communications*, vol. 10, no. 12, pp. 4122–4129, Dec. 2011.

[182] J. Zhang, L.-L. Yang, and L. Hanzo, "Multi-user performance of the amplify-and-forward single-relay assisted SC-FDMA uplink," in *Proceedings of the 2009 IEEE 70th Vehicular Technology Conference, Fall (VTC 2009-Fall)*, Sep. 2009, pp. 1–5.

[183] H. Gacanin and F. Adachi, "A performance of cooperative relay network based on OFDM/TDM using MMSE-FDE in a wireless channel," in *Proceedings of the 2009 IEEE 70th Vehicular Technology Conference, Fall (VTC 2009-Fall)*, Sep. 2009, pp. 1–5.

[184] G. Kadel, "Diversity and equalization in frequency domain a robust and flexible receiver technology for broadband mobile communication systems," in *Proceedings of 1997 IEEE Vehicular Technology Conference, (VTC 1997)*, vol. 2, May 1997, pp. 894–898.

[185] J. Coon, S. Armour, M. Beach, and J. McGeehan, "Adaptive frequency-domain equalization for single-carrier multiple-input multiple-output wireless transmissions," *IEEE Transactions on Signal Processing*, vol. 53, no. 8, pp. 3247–3256, Aug. 2005.

[186] J.-S. Baek and J.-S. Seo, "Efficient design of block adaptive equalization and diversity combining for space-time block-coded single-carrier systems," *IEEE Transactions on Wireless Communications*, vol. 7, no. 7, pp. 2608–2611, Jul. 2008.

[187] H. Xiong, J. Xu, and P. Wang, "Frequency-domain equalization and diversity combining for demodulate-and-forward cooperative systems," in *Proceedings of the IEEE International Conference on Acoustics, Speech and Signal Processing, 2008 (ICASSP 2008)*, Mar. 2008, pp. 3245–3248.

[188] K. S. Woo, Y. J. Kim, H. I. Yoo, J. Kim, S. Yun, and Y. S. Cho, "An improved receive diversity combining technique for SC-FDMA-based cooperative relays," in *Proceedings of the 2009 IEEE 70th Vehicular Technology Conference, Fall (VTC 2009-Fall)*, Sep. 2009, pp. 1–5.

[189] K. S. Woo, H. Yim, Y. J. Kim, H. I. Yoo, and Y. S. Cho, "An efficient receive-diversity-combining technique for SC-FDMA-based cooperative relays," *IEEE Transactions on Vehicular Technology*, vol. 59, no. 8, pp. 4187–4191, Oct. 2010.

[190] N. Kong and L. B. Milstein, "Error probability of multicell CDMA over frequency selective fading channels with power control error," *IEEE Transactions on Communications*, vol. 47, no. 4, pp. 608–617, Apr. 1999.

[191] Z. Han, T. Himsoon, W. P. Siriwongpairat, and K. J. R. Liu, "Resource allocation for multiuser cooperative OFDM networks: Who helps whom and how to cooperate," *IEEE Transactions on Vehicular Technology*, vol. 58, no. 5, pp. 2378–2391, Jun. 2009.

[192] Y. Ding and M. Uysal, "Amplify-and-forward cooperative ofdm with multiple-relays: performance analysis and relay selection methods," *IEEE Transactions on Wireless Communications*, vol. 8, no. 10, pp. 4963–4968, Oct. 2009.

[193] K. Vardhe, D. Reynolds, and B. D. Woerner, "Joint power allocation and relay selection for multiuser cooperative communication," *IEEE Transactions on Wireless Communications*, vol. 9, no. 4, pp. 1255–1260, Apr. 2010.

[194] J. Zhang, L.-L. Yang, and L. Hanzo, "Power-efficient opportunistic amplify-and-forward single-relay aided multi-user SC-FDMA uplink," in *Proceedings of the 2010 IEEE Vehicular Technology Conference, Spring (VTC 2010-Spring)*, May 2010, pp. 1–5.

[195] T. S. Rappaport, *Wireless Communications, 2nd Edition*. Prentice Hall PTR, 2002.

[196] J. G. Proakis, *Digital Communications, 4th Edition*. McGraw Hill, 2000.

[197] K. J. R. Liu, A. K. Sadek, W. Su, and A. Kwasinski, *Cooperative Communications and Networking*. Cambridge University Press, 2008.

[198] R. Pabst, B. H. Walke, D. C. Schultz, P. Herhold, H. Yanikomeroglu, S. Mukherjee, H. Viswanathan, M. Lott, W. Zirwas, M. Dohler, H. Aghvami, D. D. Falconer, and G. P. Fettweis, "Relay-based deployment concepts for wireless and mobile broadband radio," *IEEE Communications Magazine*, vol. 42, no. 9, pp. 80– 89, Sep. 2004.

[199] J. Zhang, L.-L. Yang, and L. Hanzo, "Energy-efficient channel-dependent cooperative relaying for the multiuser SC-FDMA uplink," *IEEE Transactions on Vehicular Technology*, vol. 60, no. 3, pp. 992–1004, Mar. 2011.

[200] M. Jiang and L. Hanzo, "Multiuser MIMO-OFDM for next-generation wireless systems," *Proceedings of the IEEE*, vol. 95, no. 7, pp. 1430–1469, Jul. 2007.

[201] F. Khan, *LTE for 4G Mobile Broadband: Air Interface Technologies and Performance.* Cambridge University Press, 2009.

[202] K. Kim, Y. Han, and S.-L. Kim, "Joint subcarrier and power allocation in uplink OFDMA systems," *IEEE Communications Letters*, vol. 9, no. 6, pp. 526– 528, Jun. 2005.

[203] L. Hanzo and B.-J. Choi, "Near-instantaneously adaptive HSDPA-style OFDM versus MC-CDMA transceivers for WIFI, WIMAX, and next-generation cellular systems," *Proceedings of the IEEE*, vol. 95, no. 12, pp. 2368–2392, Dec. 2007.

[204] C. Y. Ng and C. W. Sung, "Low complexity subcarrier and power allocation for utility maximization in uplink OFDMA systems," *IEEE Transactions on Wireless Communications*, vol. 7, no. 5, pp. 1667–1675, May 2008.

[205] T. Liu, C. Yang, and L.-L. Yang, "A low-complexity subcarrier-power allocation scheme for frequency-division multiple-access systems," *IEEE Transactions on Wireless Communications*, vol. 9, no. 5, pp. 1564–1570, May 2010.

[206] T. Wang and L. Vandendorpe, "WSR maximized resource allocation in multiple DF relays aided OFDMA downlink transmission," *IEEE Transactions on Signal Processing*, vol. 59, no. 8, pp. 3964–3976, Aug. 2011.

[207] ——, "Sum rate maximized resource allocation in multiple DF relays aided OFDM transmission," *IEEE Journal on Selected Areas in Communications*, vol. 29, no. 8, pp. 1559–1571, Sep. 2011.

[208] C.-H. Yu and O. Tirkkonen, "Opportunistic multiple relay selection with diverse mean channel gains," *IEEE Transactions on Wireless Communications*, vol. 11, no. 3, pp. 885–891, Mar. 2012.

[209] M. Chen, T. C.-K. Liu, and X. Dong, "Opportunistic multiple relay selection with outdated channel state information," *IEEE Transactions on Vehicular Technology*, vol. 61, no. 3, pp. 1333–1345, Mar. 2012.

[210] K. C. Lee and L. Hanzo, "MIMO-assisted hard versus soft decoding-and-forwarding for network coding aided relaying systems," *IEEE Transactions on Wireless Communications*, vol. 8, no. 1, pp. 376–385, Jan. 2009.

[211] D. Gunduz, A. Yener, A. J. Goldsmith, and H. V. Poor, "The multi-way relay channel," in *Proceedings of the IEEE International Symposium on Information Theory, 2009 (ISIT 2009)*, Jul. 2009, pp. 339–343.

[212] L. Hanzo, L.-L. Yang, E.-L. Kuan, and K. Yen, *Single- and Multi-Carrier DS-CDMA: Multi-User Detection, Space-Time Spreading, Synchronisation, Networking and Standards.* Wiley, 2003.

[213] L.-L. Yang, "Receiver multiuser diversity aided multi-stage MMSE multiuser detection: A low-complexity detector fast-converging to the optimum," in *Proceedings of the 2010 IEEE 71st Vehicular Technology Conference, Spring(VTC 2010-Spring)*, May 2010, pp. 1–5.

[214] T. Chen and R. R. Rao, "Audio-visual integration in multimodal communication," *Proceedings of the IEEE*, vol. 86, no. 5, pp. 837–852, May 1998.

[215] R. Zhang and L. Hanzo, "Wireless cellular networks," *IEEE Vehicular Technology Magazine*, vol. 5, no. 4, pp. 31–39, Dec. 2010.

[216] G. Boudreau, J. Panicker, N. Guo, R. Chang, N. Wang, and S. Vrzic, "Interference coordination and cancellation for 4G networks," *IEEE Communications Magazine*, vol. 47, no. 4, pp. 74–81, Apr. 2009.

[217] S. W. Peters, A. Y. Panah, K. T. Truong, and R. W. Heath, "Relay architectures for 3GPP LTE-advanced," *EURASIP Journal on Wireless Communications and Networking*, vol. 2009, pp. 1–14, Mar. 2009. [Online]. Available: http://dx.doi.org/10.1155/2009/618787

[218] E. Yaacoub and Z. Dawy, "A survey on uplink resource allocation in OFDMA wireless networks," *IEEE Communications Surveys and Tutorials*, vol. PP, no. 99, pp. 1–16, 2011.

[219] D. Gesbert, S. Hanly, H. Huang, S. Shamai Shitz, O. Simeone, and W. Yu, "Multi-cell MIMO cooperative networks: A new look at interference," *IEEE Journal on Selected Areas in Communications*, vol. 28, no. 9, pp. 1380–1408, Dec. 2010.

[220] A. Tajer and X. Wang, "Information exchange limits in cooperative MIMO networks," *IEEE Transactions on Signal Processing*, vol. 59, no. 6, pp. 2927–2942, Jun. 2011.

[221] D. W. K. Ng and R. Schober, "Resource allocation and scheduling in multi-cell OFDMA systems with decode-and-forward relaying," *IEEE Transactions on Wireless Communications*, vol. 10, no. 7, pp. 2246–2258, july 2011.

[222] Z. Zhao, Z. Ding, M. Peng, W. Wang, and K. Leung, "A special case of multi-way relay channel: When beamforming is not applicable," *IEEE Transactions on Wireless Communications*, vol. 10, no. 7, pp. 2046–2051, Jul. 2011.

[223] A. Eryilmaz and R. Srikant, "Joint congestion control, routing, and MAC for stability and fairness in wireless networks," *IEEE Journal on Selected Areas in Communications*, vol. 24, no. 8, pp. 1514–1524, Aug. 2006.

[224] L. Ying, R. Srikant, A. Eryilmaz, and G. E. Dullerud, "Distributed fair resource allocation in cellular networks in the presence of heterogeneous delays," *IEEE Transactions on Automatic Control*, vol. 52, no. 1, pp. 129–134, Jan. 2007.

[225] C. Mohanram and S. Bhashyam, "Joint subcarrier and power allocation in channel-aware queue-aware scheduling for multiuser OFDM," *IEEE Transactions on Wireless Communications*, vol. 6, no. 9, pp. 3208–3213, Sep. 2007.

[226] A. Eryilmaz and R. Srikant, "Fair resource allocation in wireless networks using queue-length-based scheduling and congestion control," *IEEE/ACM Transactions on Networking*, vol. 15, no. 6, pp. 1333–1344, Dec. 2007.

[227] G. Song, G. Y. Li, and L. Cimini, "Joint channel- and queue-aware scheduling for multiuser diversity in wireless OFDMA networks," *IEEE Transactions on Communications*, vol. 57, no. 7, pp. 2109–2121, Jul. 2009.

[228] M. Torabzadeh and W. Ajib, "Packet scheduling and fairness for multiuser MIMO systems," *Vehicular Technology, IEEE Transactions on*, vol. 59, no. 3, pp. 1330–1340, Mar. 2010.

[229] M. Fathi and H. Taheri, "Utility-based resource allocation in orthogonal frequency division multiple access networks," *IET Communications*, vol. 4, no. 12, pp. 1463–1470, 13 2010.

[230] M. Salem, A. Adinoyi, H. Yanikomeroglu, and D. D. Falconer, "Fair resource allocation toward ubiquitous coverage in OFDMA-based cellular relay networks with asymmetric traffic," *IEEE Transactions on Vehicular Technology*, vol. 60, no. 5, pp. 2280–2292, Jun. 2011.

[231] M. Fathi, H. Taheri, and M. Mehrjoo, "Utility maximisation in channel-aware and queue-aware orthogonal frequency division multiple access scheduling based on arrival rate control," *IET Communications*, vol. 6, no. 2, pp. 235–241, 24 2012.

[232] P. V. Mieghem, *Performance Analysis of Communications Networks and Systems*. Cambridge University Press, 2006.

Author Index

Index